Clinical Significance and Regulation of Cohesin Depletion in Mammalian Oocytes

Daniel Cooney

Supervisor: Professor Mary Herbert

Doctor of Philosophy

Newcastle University
Institute of Genetic Medicine

September 2018

Abstract

The likelihood of chromosome segregation errors in human oocytes increases dramatically from the age of 35. This results in an increased chance of pregnancies from older women ending in miscarriage. Oocytes are particularly vulnerable to ageing, as it can take five decades for them to undergo growth, from their formation during embryogenesis as prophase arrested primordial-stage oocytes.

Chromosomal stability in oocytes is provided by cohesin. This is loaded onto oocyte chromosomes during embryogenesis and removed during anaphase after oocyte growth. Recent work in our laboratory indicates that cohesin is predominantly lost at the primordial stage. However, questions remain around the timing and mechanism of loss. I will seek to address this as well as investigate whether loss of cohesin can explain age-related segregation errors in human oocytes.

My findings indicate that cohesin loss occurs gradually during ageing, and that the meiosis-specific cohesin subunit REC8 appears more affected by age than the universal sub-unit SMC3. I find that RAD21 is expressed at the primordial-oocyte stage, suggesting a potential turnover of RAD21-containing complexes could explain this difference. The protease separase, which cleaves cohesin during anaphase, is also detectable in the oocyte cytoplasm at the primordial stage. Using an oocyte-specific separase null mouse, I find that cohesin depletion occurs in the absence of separase. Finally, I use human oocytes to test the clinical significance of cohesin depletion. My findings indicate that ageing is associated with loss of REC8 from between chromatids. However, due to diffuse association of cohesin with chromatin in oocytes from older women, no overall reduction in chromosome-associated REC8 occurs. Thus, in contrast to mice, ageing in human oocytes appears to manifest as mislocalisation, rather than reduction of REC8. These findings indicate that ageing impacts on cohesin in both mouse and human oocytes but that the outcome manifests differently between organisms.

Acknowledgements

I would first like to thank my supervisor Mary Herbert, for her support and guidance during my PhD and for giving me the opportunity to study meiosis in her group. I would like to thank all the current and previous members of Mary's group. In particular Lisa Lister (for her collaboration on the human oocytes), Randy Ballesteros-Meija (for his work preceding mine on the primordial-stage oocytes) and Mahdi Lamb (for developing the linescan macro). Thanks must also go to my very good friends Chris, Dimitri and Mag as well as Yuko, Raveen, Linlin, Jess and Lilly for their support and friendship during my PhD. Also, I would like to thank the undergraduate and masters students who helped me with my work. In particular Stephanie Myszkowski for her help with primordial oocyte analysis. I would also like to thank the NHS fertility centre team at the Centre for Life for providing me with ICSI reject oocytes.

I would like to thank my lunch crew, Emily, Lillia, Lauren, Kate and Catherine, for being such helpful and supportive friends during my write-up. Also, thanks to John Munro, James Kinkead and Marcus Price for their help in proof reading and for their encouragement.

I would especially like to thank my parents and brother, for always encouraging me to pursuit my interest in science and supporting me in every possible way, even if it was just a chat about football.

Most importantly of all I would like to thank my wife, Madeleine. Who has endured every failed experiment, late night and working weekend over the past three years, responding only with support, encouragement and love. Without her I would not have completed this work.

Finally, I would like to thank all the women who have donated their eggs to this research. Without them this work would not have been possible.

Table of Contents

Table of Figures

vii

viii

List of Tables

Abbreviations

μl	Micro litre
A.U	arbitrary units
Ab	antibody
ACA	anti-centromere antibody
AcSMC3	acetylated-Smc3
ALDH1	Aldehyde dehydrogenase 1
AMA1	Activator of meiotic anaphase complex
AMH	anti-mullerian hormone
APC/C	Anaphase promoting complex/cyclosome
ART	Assisted reproduction techniques
Bub1	Budding uninhibited by benzimadoles 1
BubR1	Budding uninhibited by benzimadole-related 1
cAMP	cyclic adenosine monophosphate
CDC20	cell-division cycle protein 20
cdc7	cell-division cycle protein 7
Cdk1	cyclin-dependent kinase 1
CENP	centromeric protein
CGH	comparative genome hybridisation
cGMP	cyclic guanosine monophosphate
CK1	casein kinase 1
COC	cumulus-oocyte-complex
DAPI	4′,6-diamidino-2-phenylindole
D-box	destruction box
ddH20	double-distilled H20
dHJ	Double Holliday junctions.
DMSO	Dimethyl sulfoxide
DNA	Deoxyribonucleic acid
dpc	days post coitum
DSBs	double strand breaks
DTT	Dithiotheritol
E7.5	Embryonic Day 7.5
EDTA	ethylenediamineteraacetic acid

ESCO1/2	establishment of sister chromatid cohesion N-acetyltransferase 1/2
EtOH	Ethanol
EU	European union
F.I	flourescence intensity
f/f	flox-flox
FACS	Fluorescence-activated cell sorting
FISH	fluorescence in situ hybridisation
FSH	Follicle Stimulating hormone
GAPDH	Glyceraldehyde 3-phosphate dehydrogenase
GDF9	growth differentiation factor-9
GV	Germinal Vesicle
GVBD	Germinal Vesicle Breakdown
H3K9me3	trimethylation of H3-lysine 9
hCG	human chorionic gonadotrophan
HFEA	human fertilisation and embryology authority
I2PP2A	inhibitor of PP2A
IBMX	isobutylmethylxanthine
ICSI	Intracytoplasmic sperm injection
I.F	Immunoflourescence
IVF	In-vitro fertilisation
LH	luteinising hormone
M.F	Mouse fibroblasts
Mad1/2	Mitotic-arrest deficient 1/2
Max.	Maximum
mg/ml	milligram per millitre
MI	meiosis I
MII	meiosis II
MLH1	MutL homologue
M-phase	meiosis phase
MYC	Myelocytomatosis viral oncogene
nm	nanometre
no.	number
OCT	optimum cutting temperature

OECD	organisation for economic co-operation
PB	polar body
PBS	phosphate buffered saline
pc	post coitum
pDS5	precocious dissociation of sisters
PFA	parafomaldehyde
PGC	primordial germ cell
PI3K	phosphoinsitide 3-kinase
PLK1	Polo-like kinase 1
pmol/L	picomole per litre
PP2A	Protein phosphatase 2A
PTEN	Phosphatase and tense homolog ten
rcf	relative centrifugal force
Rpm	Revolutions per minute
RNA	ribonucleic acid
ROI	region of interest
ROS	Reactive oxygen species
s.d	standard deviation
SA	Stromal antigen
SAC	Spindle assembly checkpoint
SC	synaptonemeal complex
SCC	sister chromatid cohesion
SDS	sodium dodecyl sulfate
SGO1	Shugoshin 1
SGOL2	Shugoshin-like 2
SMC	Strucutral maintenance of chromosome
TBS	tris-buffered saline solution
Tev	Tobacco etch virus
TGF-β	Transforming growth factor-β
TOPO II	Topoisomerase II
WAPL	Wings-apart like

Chapter 1. Introduction

1.1   Meiosis and the maternal age effect

The predominant way that genetic diversity is introduced in to an animal population is via sexual reproduction. This is when a female and a male organism produce haploid gametes (oocytes and sperm respectively) which then fuse together during fertilisation, creating a new life. To produce these haploid gametes, organisms rely on a specialised form of cell division called meiosis (Petronczki et al., 2003, Herbert et al., 2015, MacLennan et al., 2015). This involves one round of DNA replication followed by two rounds of division. This is distinct from mitosis, which involves just one round of DNA replication followed by one round of division and is used by all other cells in the body (Petronczki et al., 2003).

For meiosis to be completed accurately, paternal and maternal homologues must undergo a reciprocal exchange of DNA after replication to ensure they are physically linked together (Kleckner, 2006, Baudat et al., 2013). During the first meiotic division (MI), these homologues separate in a reductional division before separating again during meiosis II (MII) in an equational division. In mammals, the male and female single copy genomes generated during meiosis become separately packaged in pronuclei and do not come together in the same nucleus until the resulting embryo divides to the two cell stage (Petronczki et al., 2003, Herbert et al., 2015).

While the accurate completion of the two meiotic divisions is fundamental to producing healthy offspring, human oocytes are highly prone to chromosome segregation errors (Hassold and Hunt, 2001). This can occur during both divisions with too few or too many chromatids remaining in the oocyte. This leads the oocyte to be in a state termed as aneuploidy. The consequences of aneuploidy during pregnancy are serious as it is the leading cause of miscarriage and stillbirths (Hassold and Hunt, 2001). Even in the few cases of aneuploidy where the pregnancy can be carried to term, the most likely outcome is for the child to be born with developmental or intellectual disabilities (Fragouli et al., 2011, Hassold and Hunt, 2001).

While there are several factors that make some chromosomes more susceptible to aneuploidy than others (such as their size, with smaller chromosomes more at risk

1

than larger ones), all chromosomes have an increased risk of aneuploidy with advancing maternal age (Risch et al., 1986, Hassold and Hunt, 2001)(Figure 1.1). This risk is thought to rise to as high as 60% by the time a woman is in her mid-40's, up from an already relatively high chance of 20% at the age of 35 (Kuliev et al., 2011). By comparison, sperm have an error rate of around 1–2% (Hassold and Hunt, 2001). Proof that reduced fertility in older women is a consequence of defects in the egg comes from In vitro fertilisation (IVF) cycles in which donor eggs from women aged <35 years completely rescue the age-related decline in fertility (Sauer, 1998)
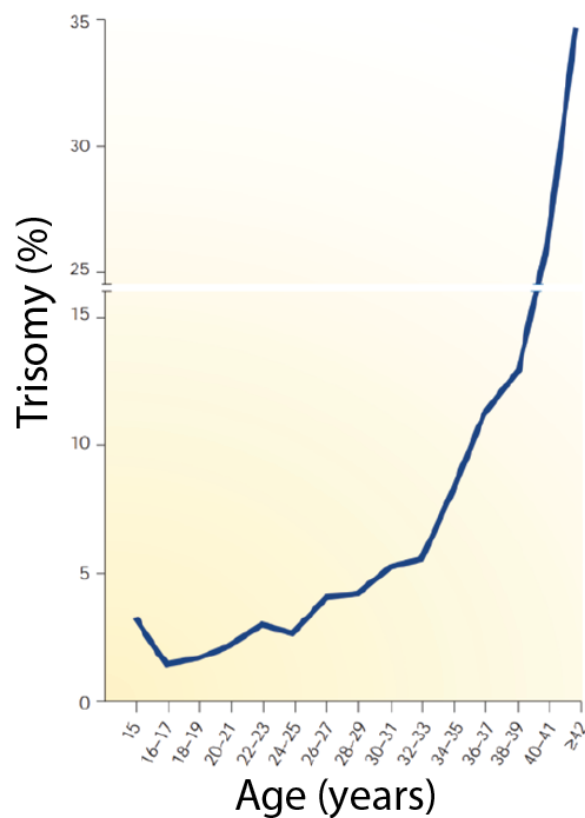
Figure 1.1 Incidence of trisomy increases with age in human oocytes. *Graph showing incidence of trisomy against age of the mother at the time of pregnancy. The chances of trisomy occurring increases drastically from the age of 35 onwards (Hassold and Hunt, 2001).*

Recent demographic trends have led to an increased interest in the relationship between maternal age and prevalence of aneuploidy. A study looking at the average age of first time mothers from western, southern and northern Europe as well as Japan, saw an increase from 24 to 28 years of age between 1970 and 2008 (Schmidt

et al., 2012). In the UK over the same time, the number of births to women over 30 has risen, while those to women under 30 has fallen (Figure 1.2).
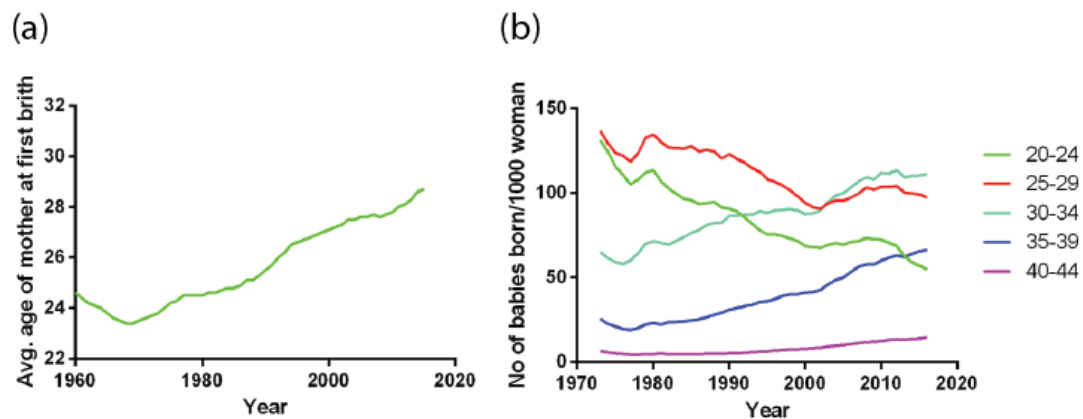
Figure 1.2 More women are delaying pregnancy into their 30s. *(a) Graph showing the average age of first time mothers in the UK from 1960 to present. The average age has steadily increased from the 1970s onwards. (b) Graph showing number of babies born/1000 women by age. Since the mid-1970s the number of babies born to women under 30 has decreased while those born to women over 30 has increased (eurostat, 2015).*

This delay has had real consequences in terms of pregnancy outcomes. The clearest example of this is the increase in the number of Down's syndrome pregnancies over the past 30 years. Down's syndrome occurs due to trisomy of chromosome 21, causing the child to suffer from a spectrum of learning difficulties (Hassold and Hunt, 2001). While the link between maternal age and Down's syndrome has been understood for several decades (Penrose, 1933), the growing trend for women to delay pregnancy until later in life has resulted in a 71% increase between 1989 and 2008 in Down's syndrome pregnancies (Morris and Alberman, 2009).

The demographic trends towards later age of pregnancy also have important social and economic ramifications. The delay in motherhood, combined with the increase in life expectancy and growing number of pensioners, presents a demographic crisis in the developed world (Schmidt et al., 2012). This is highlighted by the fact that by 2080, it is projected that the percentage of the population in the EU-28 aged over 65 will have risen from 18.5% in 2014 to 28.7%. This will occur along with a fall in those aged between 15–65 from 65.9% to 56.2% (eurostat, 2015).

3

To understand and develop potential solutions to the age-related loss of fertility, it is essential to determine why oocytes are so susceptible to aneuploidy. To do this, it is necessary to understand the unique and protracted way in which oocytes are formed and maintained before they can help create a life.

1.2   Oogenesis – formation and maturation of oocytes

A key aspect of oocyte biology, distinguishing it from all other cells, is the prolonged quiescent state in which oocytes exist before resuming meiosis. Unlike sperm or somatic cells, oocytes do not appear to be formed during adult life (Adhikari and Liu, 2009). Instead, a stockpile of oocytes formed during embryo development provide the source of all oocytes ovulated during each woman's reproductive lifespan. In humans, this can be up to five decades, leaving oocytes particularly susceptible to age-related problems (Herbert et al., 2015).

The initial steps in the formation of an oocyte occur several days after conception with the production of primordial germ cells (PGCs)(Richardson and Lehmann, 2010). These form around E7.25 in the yolk sac of mouse embryos (around 3–5 weeks in human embryos (Floros et al., 2018)) and were initially identified due to their high alkaline phosphatase activity (Nikolic et al., 2016). To establish a sex-specific embryonic gonad the PGCs must enter the genital ridge by migrating from the primitive streak to the endoderm, and then into the gonad (E7.5–E10.5). (Richardson and Lehmann, 2010).

After reaching the gonad, the PGCs undergo multiple rounds of mitotic cell division. At this point these cells (termed oogonia) do not complete cytokinesis and instead form cysts with the oogonia physically linked together through ring canals (E11–E13) (Pepling and Spradling, 1998, Pepling and Spradling, 2001). Once they undergo the pre-meiotic S phase, these cells enter prophase of meiosis I and undergo reciprocal exchange of DNA between the paternal and maternal homologues to form crossovers. This results in the formation of a structure called the bivalent chromosome which consists of four chromatids (two each from the paternal and maternal homologues) (Kleckner, 2006, Lam and Keeney, 2014). The cytological manifestations of the sites of crossover formation are known as chiasmata (Kleckner, 2006, Baudat et al., 2013) (Figure 1.3).

4
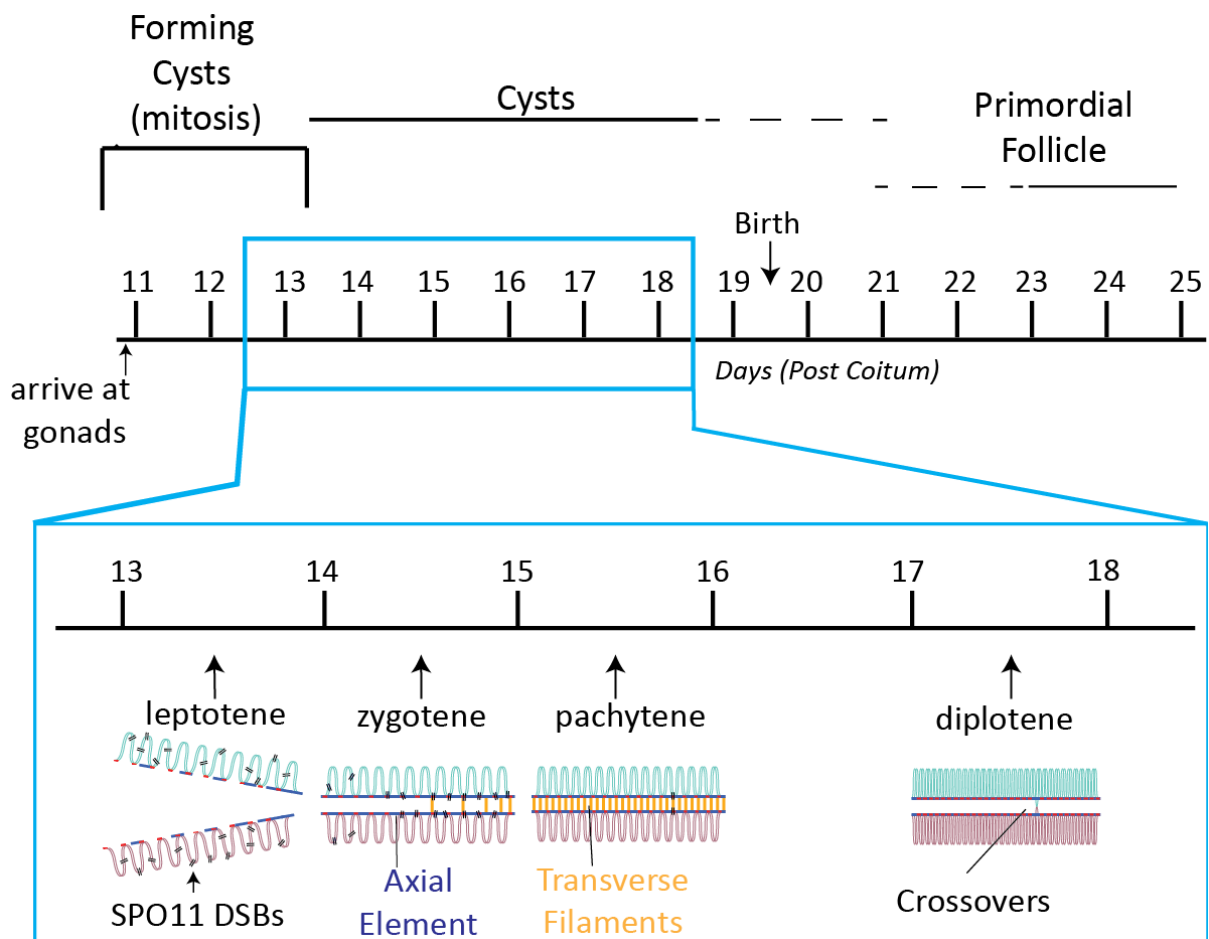
Figure 1.3 primordial oocyte and bivalent chromosome formation during mouse embryogenesis. *Schematic diagram showing the stages in a female mouse in the formation of primordial follicles. PGCs infiltrate the gonads at E10.5 forming mitotic cysts. The chromosomes in the PGCs then undergo a reciprocal exchange of DNA leading to the formation of bivalent chromosomes. Cells in the cyst then separate and 3 days after birth primordial follicles are formed. In humans PGCs are present 3-5 weeks after conception with primordial follicles fully formed around 18-20 weeks after conception. Blue box shows the four stages of prophase that occur to create bivalent chromosomes. Green and red DNA strands represent the homolgous chromosomes. SPO11 causes DSBs in the paternal and maternal homologues. This is followed by formation of the synaptonemal complex constructed of the axial element and transverse filaments. This is then resolved with the formation of crossovers from double Holliday junction (dHJ) in diplotene causing homologous chromosomes to be physically linked (Pepling and Spradling, 2001, Maheshwari and Fowler, 2008, Herbert et al., 2015, Floros et al., 2018).*

The process of recombination starts with the meiotic topoisomerase-like SPO11 being targeted by PRDM9 to induce double strand breaks (DSBs) at recombination hotspots along the DNA (Baudat et al., 2013). These DSBs are either resolved as crossovers or non-crossovers. Non-crossovers are necessary as SPO11 causes significantly more DSBs than crossovers. This process is essential, as evidenced by the fact that *Spo 11$^{-/-}$* mice are infertile, with defects seen 15 days post coitum (dpc) (Romanienko and Camerini-Otero, 2000).

In leptotene, the DNA condenses and forms loops organised along the axial element (Lam and Keeney, 2014).The cell enters zygotene, forming transverse filaments leading to construction of the synaptonemal complex (SC) in pachytene (Page and Hawley, 2004). The SC "zips" the two homologous chromosomes together, using the axial element on the DNA and the transverse filaments between them (Heyting, 1996, Kleckner, 2006, Lam and Keeney, 2014). The DNA DSBs are then repaired between homologues leaving double-Holliday junctions (dHJs) that resolve to become crossovers in diplotene (Page and Hawley, 2004). The supporting SC is removed and the DNA can decondense entering the cell into dictate arrest. The establishment of these crossovers is essential for completion of meiosis. Knockout mice of the mismatch repair protein MLH1 (which are therefore unable to establish crossover) are unable to properly align during the first meiotic division causing them to arrest at metaphase (Woods et al., 1999). Crossover location, as well as their frequency, is important for bivalent chromosome stability. Crossovers that are close to the telomeres or pericentromeres are more likely to result in segregation errors during meiotic division than those located further along the chromosome arm (Lamb et al., 2005, Oliver et al., 2008).

Around the time of bivalent chromosome formation, the oocytes in the cyst separate, becoming enclosed within a single layer of granulosa cells and can now be termed as primordial follicles. They will then remain in this state until either undergoing atresia – a process of follicle breakdown - or maturation (Pepling and Spradling, 2001). In mice and rats, this process is completed a couple of days after birth (Pepling and Spradling, 2001). In primates and ruminants, however, it occurs during foetal development (Maheshwari and Fowler, 2008, Adhikari and Liu, 2009).

It has been widely accepted for many decades that the pool of primordial oocytes formed during embryogenesis is the sole source of oocytes in a female's life (Zuckerman, 1951). However, the past 15 years has seen the emergence of the

controversial claim that a population of ovarian germline stem cells exist within the ovary (Johnson et al., 2004). It was postulated that these so-called oogonial stem cells could give rise to primordial oocytes in the adult ovary. This pool could potentially be stimulated later in a woman's life, to extend the duration of fertility. While exploitation of such a pool would be a potential solution to loss of fertility with age, studies looking at in-vivo cell lineage tracing suggested that there is no new production (Zhang et al., 2014). Much of the difficulty in defining whether these stem cells exist has related to finding a reproducible way of extracting them from the ovary. Extraction using fluorescence-activated cell sorting (FACS) based on expression of DDX4 (a germ cell marker) have suggested that the cells being extracted are not in fact stem cells (Kerr et al., 2012, Zhang et al., 2015). However, Clarkson et al. have recently suggested a DDX4 positive population also expressing the stem cell marker ALDH1 in human adult ovarian tissue (Clarkson et al., 2018). It was suggested that this population is capable of forming early follicles however this will need further investigation before the existence of ovarian stem cells is accepted.

Once primordial follicles have been established in the ovary in foetal life, they are recruited for growth throughout a woman's life until the pool becomes exhausted around the time of menopause. Both inhibition and initiation of growth in primordial oocytes is mediated through the PI3K-PTEN-AKT pathway (Makker et al., 2014). Prevention of growth is controlled by FOXO3A (a transcription factor), with PTEN inhibiting the FOXO3A suppressor AKT (John et al., 2008). Once AKT is activated, FOXO3A is shuttled out of the nucleus, allowing for growth. Uncontrolled recruitment of primordial-stage oocytes into the growing pool is observed in $Pten^{loxP/loxP};GCre^+$ and $Foxo3a^{-/-}$ mice, showing their essential role in maintaining the primordial pool (Castrillon et al., 2003, Reddy et al., 2008). Simultaneously with FOXO3A suppression, primordial oocytes undergo growth with AKT activation causing suppression of mTORC1 inhibitors TSC1 and 2 (Makker et al., 2014). Once mTORC1 is released the primordial stage oocyte is then able to grow from having a diameter of ~10 μm in size to ~100 μm, making it the largest cell in the body (Griffin et al., 2006).

While there are important changes going on within the oocyte during oogenesis, the process leading to an ovulated egg relies on signalling between the oocyte and its surrounding cells. Primordial follicles consist of the primordial stage oocyte and a single layer of surrounding flattened granulosa cells which help maintain its quiescent status (Da Silva-Buttkus et al., 2008). When it is selected for growth, not only does

the oocyte increase in size, but the granulosa cells that surround it change as well. These go from a flattened structure to becoming cuboidal while undergoing multiple rounds of division (Adhikari and Liu, 2009). Once surrounded by a single layer of cuboidal cells, it is classed as a primary follicle then becoming a secondary follicle after the granulosa cell multiply to form several layers around the oocyte (Orisaka et al., 2009) (Figure 1.4). At the primary follicle stage, the oocyte forms a glycoprotein layer called the zona pellucida. The interaction between the oocyte and the granulosa cells is maintained through the zona pellucida by transzonal processes (Albertini et al., 2001). A thecal layer also forms on the outside of the basement membrane (Campbell et al., 2013). The follicle then forms a fluid filled antrum, with the antral (also known as Graafian) follicle now ready for ovulation.
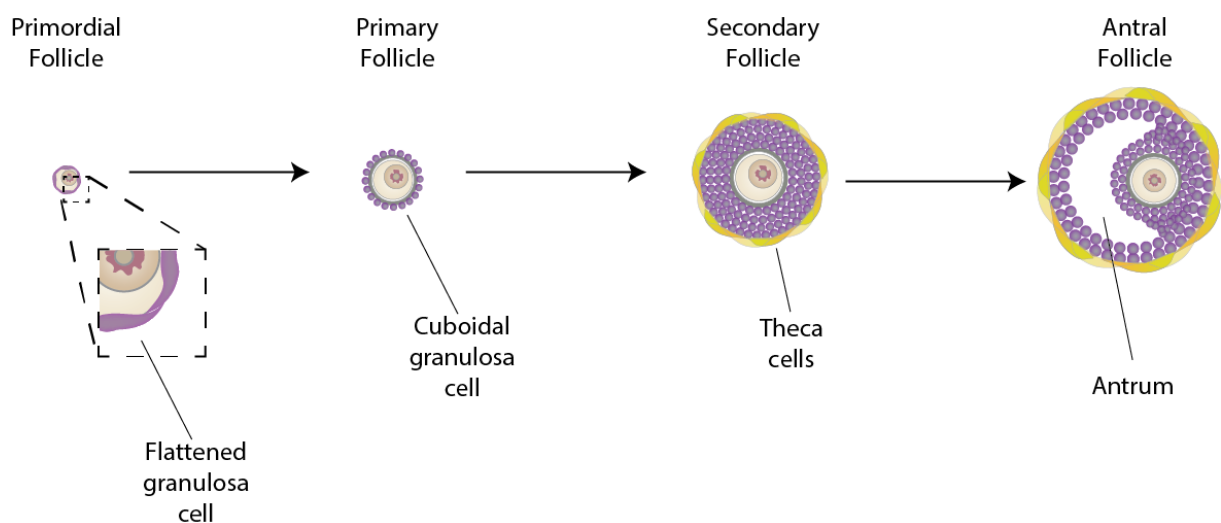
Figure 1.4 Primordial to antral follicle formation. *Schematic diagram of primordial to antral follicle formation. Primordial stage oocytes are surrounded by flattened granulosa cells. Once primordial follicles are signalled to initiate growth they undergo a transition in to primary follicles and the oocyte is surrounded by a single layer of cuboidal granulosa cells. This is followed by more replication of granulosa cells to form several layers of granulosa cells and a thecal cell layer. Finally, a fluid filled antrum is formed to create the antral follicle (Herbert et al., 2015).*

Primordial-stage oocytes are recruited for growth, developing to the secondary follicle stage of development before puberty; however, the follicles are unable to progress

8

any further towards ovulation until after puberty (Hsueh et al., 2015). This is due to further progression requiring release of follicle stimulating hormone (FSH) and luteinising hormone (LH) (Adhikari and Liu, 2009). This can only happen after puberty, with changes to the hypothalmo-pituitary-gonadal axis. Because of this, the process towards ovulation can be divided into two broad stages: the initial recruitment to growth, which happens before puberty and takes the primordial follicle to secondary follicle stage (Hsueh et al., 2015), and the cyclic recruitment stage, which occur after puberty and takes primordial follicles through antral formation and to ovulation (Figure 1.5). While there will be several antral follicles present during each cycle, in mono-ovulatory species such as humans one will become dominant and capable of developing to the pre-ovulatory stage (McGee and Hsueh, 2000). This is due to receptivity to a small window of FSH, which only the largest, most dominant follicle will be. The other follicles (which are considered subordinate) will succumb to atresia (Hsueh et al., 2015). This is surpassed during IVF treatment when administration of FSH for 10-12 days prevents atresia, allowing multiple follicles to develop the preovulatory stage.

After puberty, granulosa cell proliferation past secondary follicle stage is FSH dependent, as is estradiol production. This in turn drives release of LH from the pituitary (Edson et al., 2009). This LH surge causes a breakdown in the junctions between granulosa cells and the associated oocyte, resulting in a reduction of cyclic adenosine monophosphate (cAMP) within the oocyte and increased levels of CDK1 and cyclin B1 (Von Stetina and Orr-Weaver, 2011). The breakdown of junctions is essential for this function, as it is the granulosa cells that provide the cyclic guanosine monophosphate (cGMP) that inhibits PDE3A removal of cAMP (Norris et al., 2009). This drives the transition of the oocyte from prolonged arrest in prophase of meiosis I into M-phase of the first meiotic divisions. This transition is marked by breakdown of the germinal vesicle (GV) membrane, formation of the metaphase I spindle and completion of the first meiotic division, marked by formation of the 1st polar body. Finally the follicle ruptures and the egg, now arrested at metaphase of meiosis II, and surrounded by a cloud of cumulus cells is released into the oviduct (Gook et al., 2003).

9
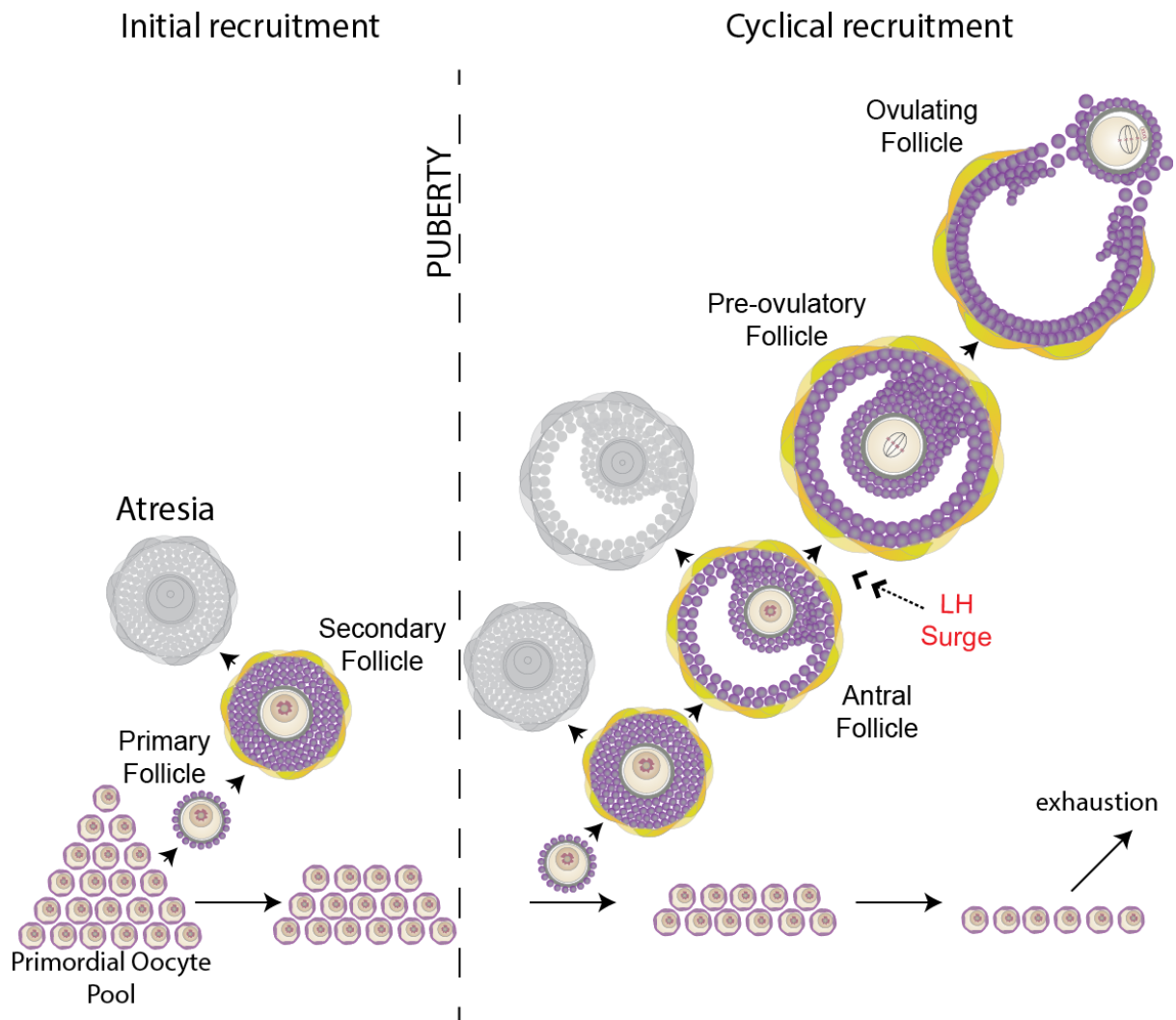
Figure 1.5 Recruitment of ovarian follicles during oogenesis. *Schematic diagram showing recruitment of oocytes during ovulation. Prior to puberty primordial oocytes are able to undergo growth but die of atresia. It is only after puberty and with the LH surge that the dominant follicle is able to undergo ovulation. The process of recruitment stops with exhaustion of the available pool of oocytes (McGee and Hsueh, 2000)*

After ovulation, the cells within the follicle differentiate to become progesterone-secreting luteal cells and the structure is then called the corpus luteum. This is formed from the remaining theca and granulosa cells and is necessary to help maintain pregnancy. If a pregnancy does not occur the corpus luteum regresses and menstrual bleeding occurs (Reed and Carr, 2000).

Though the process of primordial oocyte growth and ovulation is necessary for fertility, the chances of an individual primordial oocyte completing it is in fact very low. While prior to birth the ovary contains several million oocytes, only around 500 will

ever be ovulated in adult life, with the vast majority instead becoming atretic (Adhikari et al., 2016, Broekmans et al., 2007). This is borne out by the fact that in humans, of the around 7 million oocytes formed during foetal development, only 1 million are present after birth. Due to continued recruitment for growth or atresia, the number of primordial follicles is estimated to be around 400,000–600,000 at puberty with 50–1,000 remaining at the time of menopause (Figure 1.6) (Adhikari and Liu, 2009, Broekmans et al., 2007, te Velde et al., 1998). After birth, the rate of primordial oocyte loss is thought to occur at around 1000 oocytes per year until the age of 37. After 37 this rate then rapidly increases until the time of menopause (Faddy and Gosden, 1996, Faddy, 2000). The biological basis for this high level of oocyte loss by atresia is unclear. Fertility is maintained following irradiation of knockout mice for *Puma* and *Noxa,* which mediate cell death following oocyte cell damage (Kerr et al., 2012). The decline in available oocytes represents one of the pressures exerted by ageing on female fertility.
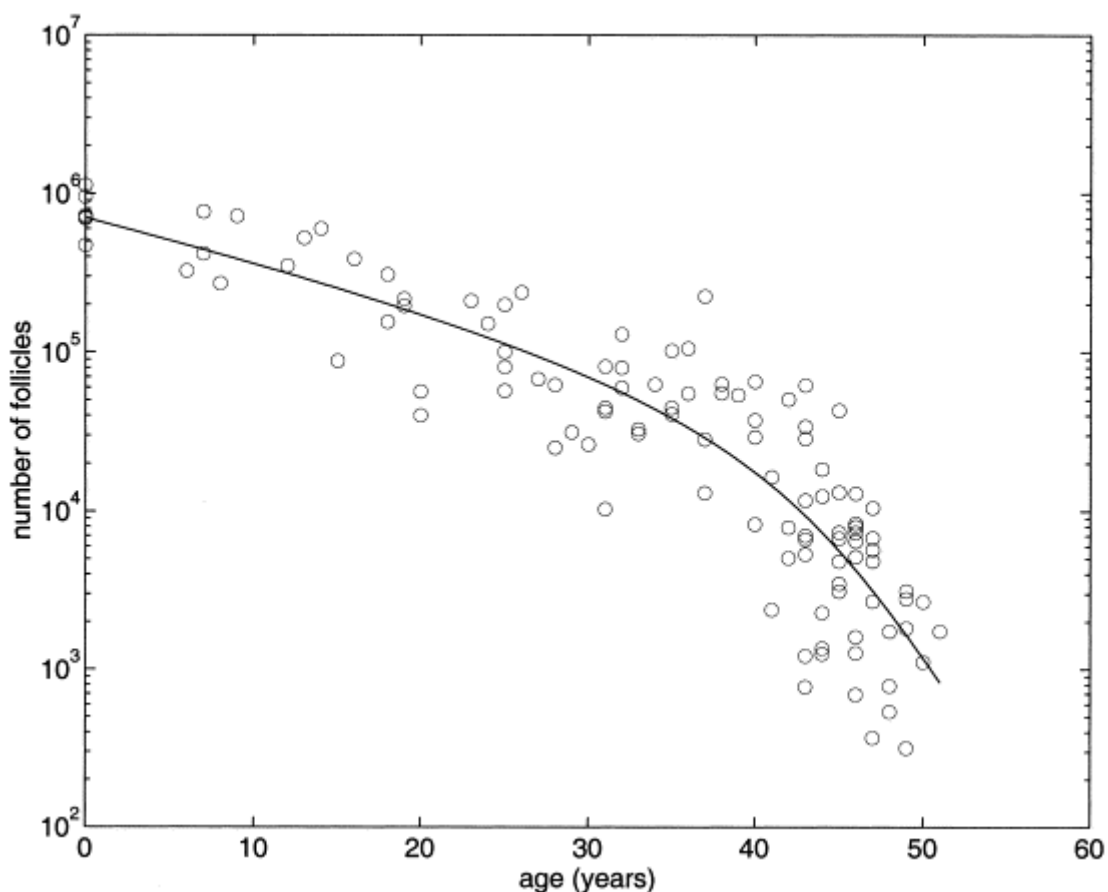
Figure 1.6 Ovarian follicle reserve declines with age. *Graph shows number of oocyte follicles (y- axis) plotted against age in human ovaries. Rate of the decline increases from the mid-30's onwards until menopause in the 50s (Faddy, 2000).*

1.3 Oocyte Meiosis: From Germinal Vesicle break-down to fertilisation

The process of meiosis is required to produce haploid gametes (which contain one chromatid) from diploid precursors (which contain four chromatids) for the purpose of sexual reproduction. While male spermatagonial stem cells produce four individual sperm from each round of meiosis, females only produce one egg (Petronczki et al., 2003). This may seem inefficient, but oocytes must provide all the cytoplasmic material necessary for early embryogenesis (such as mitochondria) as well as the necessary maternal DNA complement (Schon et al., 2012).

Prior to resuming meiosis the DNA in oocytes is contained within a large nuclear structure called a germinal vesicle. Once CDK1 and cyclin B1 levels have increased, resumption of meiosis occurs (Herbert et al., 2015). This manifests itself through two distinct processes in the oocyte. The first is germinal vesicle breakdown (GVBD) which allows for the DNA contained within to condense and become visible as discrete bivalent chromosome structures. The stability of these bivalent chromosomes is provided by the cohesin complex, which binds sister chromatids together (Nasmyth, 2011, Nasmyth and Haering, 2009, Peters and Nishiyama, 2012). The second key feature is the assembly of the MI spindle which is necessary for segregation of homologues between the oocyte and the 1st PB (Petronczki et al., 2003).

During MI, bivalent chromosomes biorient so that sister centromeres can be bound to by microtubules emanating from the same pole (Figure 1.7). This monopolar spindle attachment is unique to the first division of meiosis (Watanabe, 2012). The mechanism which controls this process in higher eukaryotes is not well understood. However, recent work suggests the presence of a meiosis-specific protein called MEIKIN that is highly conserved throughout eukaryotes (Kim et al., 2015). This is an orthologue of budding yeast monopolin and fission yeast Moa1, which are necessary to facilitate monopolar spindle attachment in these organisms (Toth et al., 2000, Yokobayashi and Watanabe, 2005).
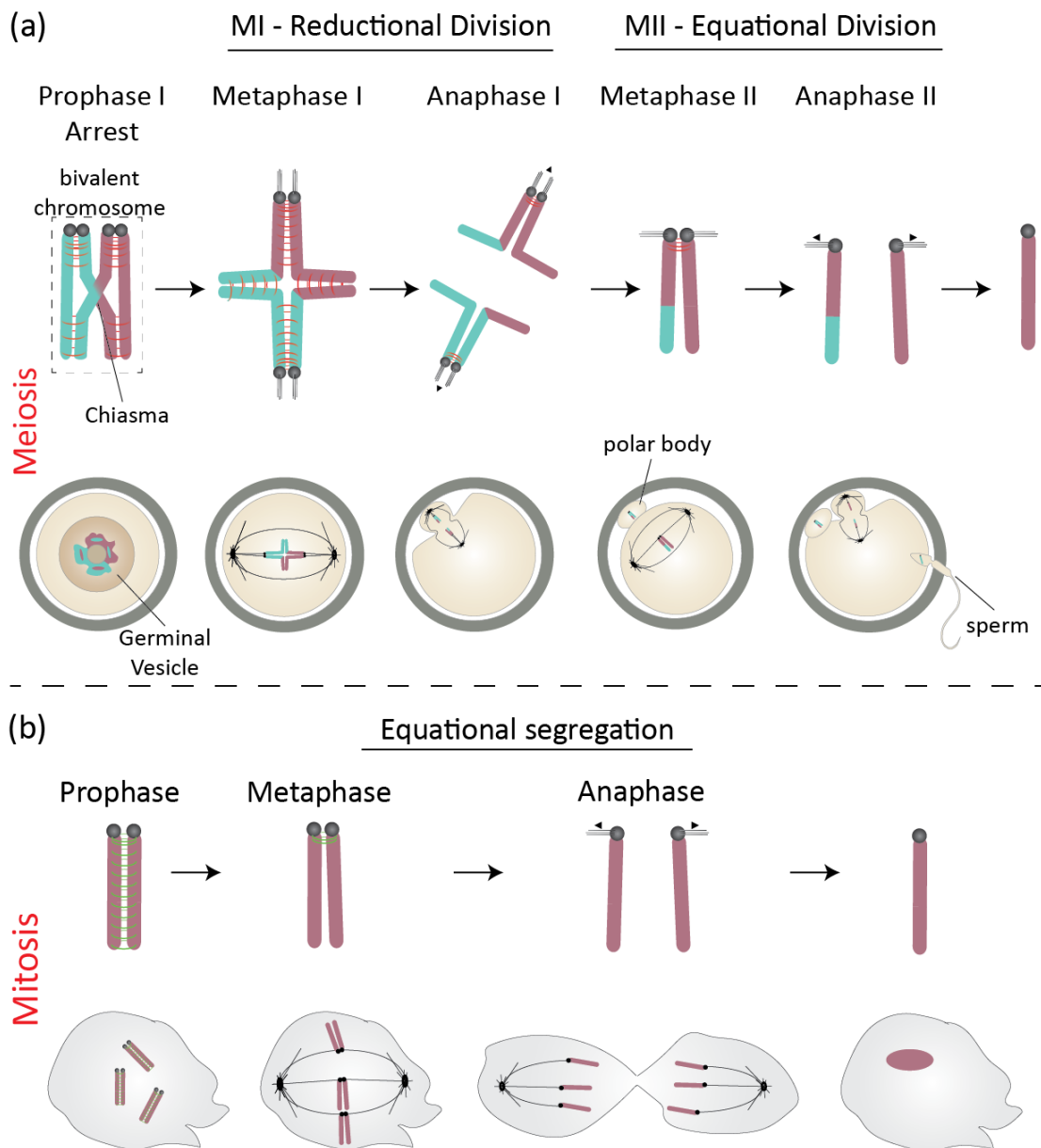
Figure 1.7 Chromosome segregation in meiosis and mitosis. *(a) Schematic diagram showing the segregation of chromosomes during meiosis. Oocytes are maintained at prophase arrest until GVBD when they enter into metaphase of MI. At this stage, bivalent chromosomes must biorientate to allow for monopolar spindle attachment to occur. Upon anaphase the reductional division occurs and one set of chromosomes are taken into the polar body while the other remains in the oocyte. The remaining chromosomes in the oocyte will then undergo bipolar spindle attachment and upon fertilisation by the sperm undergo the second round of meiotic division which is a reductional division. (b) Schematic diagram showing chromosome segregation during mitosis. After prophase mitotic chromosomes biorientate on the mitotic spindle. Upon anaphase the chromosomes divide and two new cells are formed (this is a diagram based on Herbert et al., 2015).*

13

During this period, the microtubules bind to the centromeres and re-adjust until monopolar attachment has occurred for each set of homologous chromosomes. This has been suggested to take at least one or more rounds of error correction in oocytes for the vast majority of chromosomes (Kitajima et al., 2011). Lack of microtubule binding and error correction is mediated by the spindle assembly checkpoint (SAC), which recognises aberrant spindle binding and signals for correction (Lara-Gonzalez et al., 2012). Importantly, the cohesin loaded onto the chromosomes during S-phase keeps the homologues of the bivalent chromosomes together in spite of the tension which arises from monopolar spindle attachment (Peters and Nishiyama, 2012, Herbert et al., 2015). After the kinetochores have established stable microtubule attachments, the anaphase-promoting complex (APC/C) is activated (Lara-Gonzalez et al., 2012). This causes the paternal and maternal homologues to be pulled apart to opposite poles with the cohesin on the chromosome arms being cleaved. One set of chromosomes is sent to the polar body for degradation while the other set of dyads remains in the oocyte (Figure 1.7) (Herbert et al., 2015).

The remaining dyads then biorient their centromeres on the MII spindle (Hauf and Watanabe, 2004). These dyads are maintained through centromeric cohesin which is protected during MI. This holds dyad sister centromeres together during anaphase I. The oocyte remains arrested at metaphase of meiosis II until it is fertilised by the sperm. After fertilisation, the second division happens with one set of chromatids being pulled to the second polar body and the other remaining in the oocyte with the chromatids from the sperm (Herbert et al., 2015) (Figure 1.7).

Many of the features of meiosis can in some ways be distinguished in mitosis. Cohesin stabilises chromosomes and is first removed from the chromosome arms before it is removed at the centromeres. Alignment defects are corrected by the SAC before segregation can occur. To understand what mechanisms may be responsible for the age-related increase in chromosome segregation errors, it is necessary to understand the mechanisms behind how chromosomes are stabilised and segregated in both mitosis and meiosis.

1.4 Chromosome stability in meiosis and mitosis

1.4.1 Cohesin structure

Chromosomal stability during prophase and metaphase is mediated by the cohesin complex. This is a highly conserved ring structure formed of two structural maintenance of chromosome (SMC) subunits (called SMC3 and SMC1) and two non-SMC subunits (Nasmyth and Haering, 2009). These components combine to create a ring structure capable of entrapping DNA strands. SMC3 and SMC1 are both large proteins of over 1000 amino acids in size that contain a central hinge domain, flanked either side by coiled-coil domains (Hirano and Hirano, 2002). The N- and C- terminals have nucleotide-binding motifs which associate with one another when the protein folds (Peters and Nishiyama, 2012). This happens at the hinge region, with the coiled-coil domains forming in an anti-parallel structure. SMC3 and SMC1 interact with one another through their hinge domains (Haering et al., 2002). The two remaining subunits consist of an α-kleisin subunit, that binds the nucleotide-binding regions of the SMC proteins, and a stromal antigen subunit, which directly binds the α-kleisin subunit to create the core complex (Figure 1.8). The most widely accepted model for how cohesin provides cohesion and stability is that one cohesin ring entraps two sister DNAs when the genome is replicated during S phase. This maintains cohesion between sister chromatids until anaphase when the cohesin ring is opened by separase-mediated cleavage of the α-kleisin subunit (Nasmyth and Haering, 2009, Nasmyth, 2011, Peters and Nishiyama, 2012). Recent work looking at entrapment of mini-chromosomes by cohesin has also reported this to be the case. Using mutations of the cohesin ring Srinivasan *et al.* were able to show that cohesin entraps two strands of DNA within one ring to provide cohesion (Srinivasan et al., 2018).

The composite parts of the cohesin ring differ between mitosis and meiosis with only SMC3 conserved in both (Nasmyth and Haering, 2009). In mitosis, the variant of SMC1 is SMC1α, the α-kleisin subunit is SCC1 (also known as RAD21) and the stromal antigen subunit is SCC3 (also known as SA1 and SA2). In meiosis, these elements are replaced by SMC1β, REC8 and STAG3 respectively (Nasmyth and Haering, 2009) (Figure 1.7). More recently another meiosis specific α-kleisin subunit called RAD21L has been described in mammalian germ cells. This is necessary for recombination during prophase (Lee and Hirano, 2011).

15
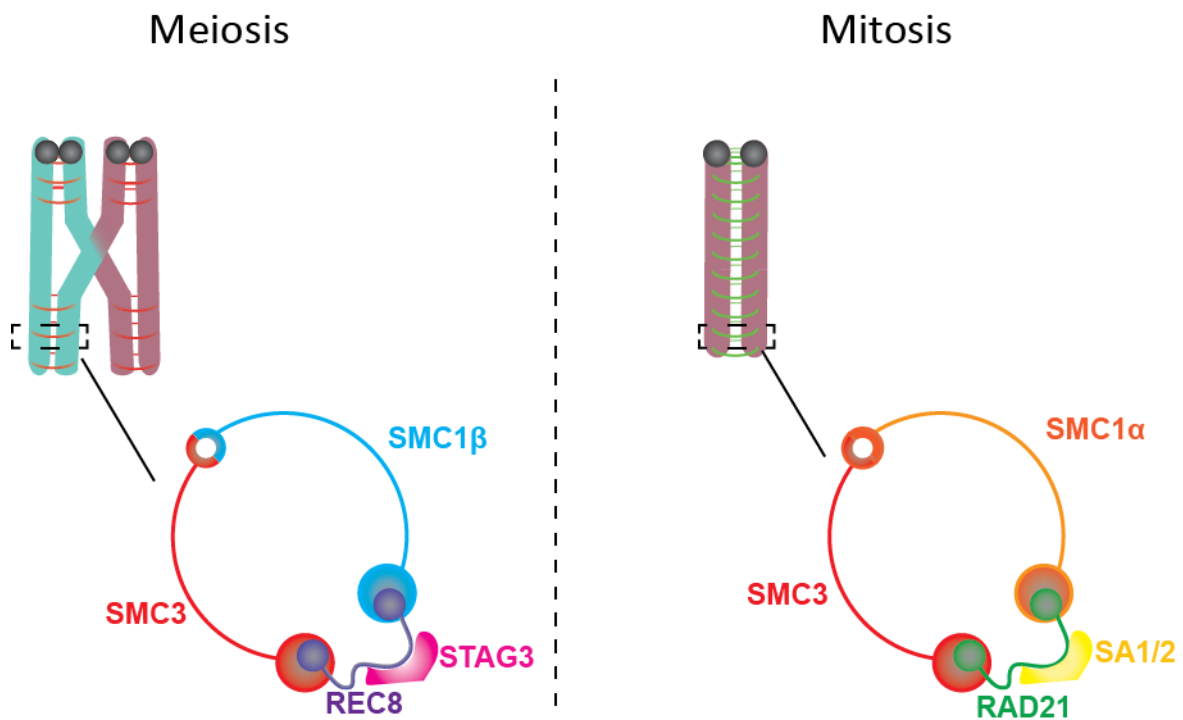
Figure 1.8 Cohesin structure in meiosis and mitosis. *Schematic diagram showing the core components of the cohesin ring in meiosis and mitosis. In meiosis, SMC3 and SMC1β bind to each other at their hinge domain and interact with the α-kleisin subunit REC8 at the nucleotide binding domain. STAG3 then interacts with REC8 to complete the core complex. Only SMC3 is conserved between both meiosis and mitosis. In mitosis SMC1β is replaced with SMC1α and REC8 is replaced by RAD21. STAG3 is replaced by SA1/2.*

While RAD21 containing cohesin is expressed in mouse oocytes, it is the REC8 containing cohesin that confers cohesion. This was reported in a study that artificially cleaved REC8 in fully grown mouse oocytes during metaphase I (Tachibana-Konwalski et al., 2010). This resulted in complete resolution of bivalent chromosomes to their four constituent chromatids. By contrast, artificial cleavage of RAD21 had no effect on the integrity of bivalents. This changes completely, however, after fertilisation, where there is a complete switch to RAD21 for chromosomal cohesion (Tachibana-Konwalski et al., 2010). SMC1β is also essential for cohesion in germ cells with *SMC1β^-/-* mice showing separation of chromosomes during metaphase (Revenkova et al., 2004, Hodges et al., 2005). Interestingly however, the oocytes from *SMC1β^-/-* mice displayed progressive loss of bivalent integrity resulting in their resolution to individual chromatids after 4 months of age (Hodges et al., 2005). This

16

suggests the presence of non-SMC1β containing cohesin complexes, which may be vulnerable to progressive removal during female ageing.

1.4.2 Cohesin loading and maintenance

The loading of cohesin is mediated by the Kollerin complex which is composed of NIPBL (SCC2) and MAU-2 (SCC4) (Ciosk et al., 2000, Peters and Nishiyama, 2012). Our current understanding of cohesin loading suggests that it occurs through the opening of the SMC1 and SMC3 hinge-region gate (Gruber et al., 2006, Buheitel and Stemmann, 2013). This was reported in yeast and later in HeLa cells by artificially locking the cohesin ring at specific interfaces. They found that cohesin could not be loaded when the SMC1-SMC3 hinge link was closed but could when the SMC and α-kleisin ones were.

Cohesin is loaded onto chromosomes during telophase but only become cohesive during S-phase after DNA replication (Gerlich et al., 2006). This is when ESCO1 and ESCO2 acetylate 2 lysine residues on SMC3 (K105 and K106 in humans) to make the cohesin ring cohesive (Zhang et al., 2008) (Figure 1.9). Prior to SMC3 acetylation (AcSMC3), cohesin in mitotic cells can be removed by the prophase pathway protein WAPL. This interacts with PDS5 (PDS5a/b in higher eukaryotes) to open the SMC3/α-kleisin gate, removing the cohesin ring from the DNA (Kueng et al., 2006, Chan et al., 2012) . After SMC3 acetylation WAPL is prevented from removing cohesin by sororin, which prevents WAPL from interacting with PDS5 (Nishiyama et al., 2010, Peters and Nishiyama, 2012)

17
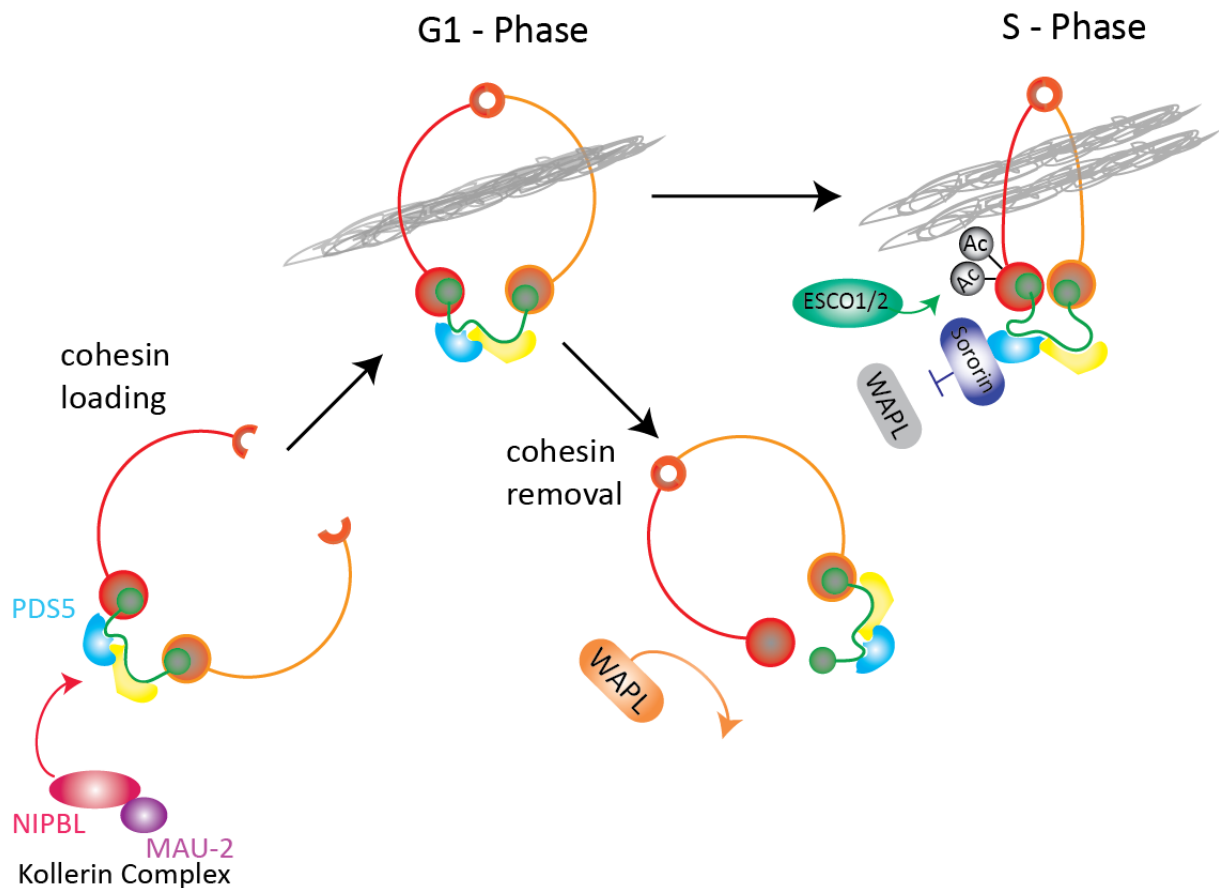
Figure 1.9 Cohesin loading and establishment. *During mitotis G1-phase the cohesin complex is loaded onto chromosomes (grey lines) by the Kollerin complex comprised of NIPBL and MAU2. This interacts with PDS5 to open the SMC3/SMC1 interface. Cohesin can be removed by Wapl during this period but once ESCO1/2 acetylates SMC3 in S-phase, sororin is recruited to PDS5. This prevents any more WAPL-mediated removal. Based on a figure from (Haarhuis et al., 2014).*

In mitosis cohesin is renewed after each division. In meiosis, however, it is not removed from chromosome arms until anaphase I and from centromeres until anaphase II. Crucially, studies in mice indicate that there appears to be no replenishment of cohesive cohesin during subsequent stages of oogenesis (Tachibana-Konwalski et al., 2010). This was further indicated in a recent study were REC8 containing TEV cleavage sites were expressed prior to cohesin establishment at S-phase. After this, REC8-MYC was expressed so that if cohesin is turned over during meiosis, REC8-MYC should be detected on the DNA. As REC8-MYC cannot be cleaved by TEV, this would result in reduced separation when *Tev* mRNA was injected into the oocyte and transcribed. This did not occur, suggesting that there is no turnover in REC8 during the prolonged period of prophase arrest (Burkhardt et al., 2016).

It should be noted that while providing cohesion between sister chromatids is a primary function, cohesin also has numerous additional functions. A growing body of work has focussed on the role cohesin, WAPL and the Kollerin complex plays in chromatin organisation. Cohesin associates with the CCCTC binding factor CTCF on DNA and is necessary for the transcriptional control and organisation of DNA (Parelho et al., 2008, Wendt et al., 2008). Knockout of WAPL results in extension of DNA loops in to discrete structures called vermicelli chromosomes (due to the visual similarity to the pasta). This phenotype is rescued by knockout of SCC4 (Haarhuis et al., 2017). A recent study in to the chromatin organisation of the zygotic genome found that cohesin was necessary for organisation of chromatin in to topologically associating domains (TADs) and chromatin loops (Gassler et al., 2017) Knockout of WAPL resulted in vermicelli formation in the pro-nuclei of these embryos. Cohesin is also necessary for helping in the repair of DNA double-strand breaks in both mitosis and meiosis (Nasmyth, 2011).

1.5   Cohesin removal in meiosis and mitosis

1.5.1 prophase pathway

The removal of cohesin in mitotic cells occurs by two independent mechanisms, with cohesin on the arm removed first through the APC/C-independent prophase pathway (Waizenegger et al., 2000). This involves WAPL opening the cohesin ring at the SMC3 and α-kleisin interface and removing it from the DNA (Chan et al., 2012). For WAPL to interact with PDS5 during the prophase pathway, sororin must be removed by CDK1 and Aurora B phosphorylation, and SA2 must be phosphorylated by PLK1 (Hauf et al., 2005, Nishiyama et al., 2013)(Figure 1.10). This allows for WAPL to then bind to PDS5 and initiate opening of the SMC3/RAD21 interface.
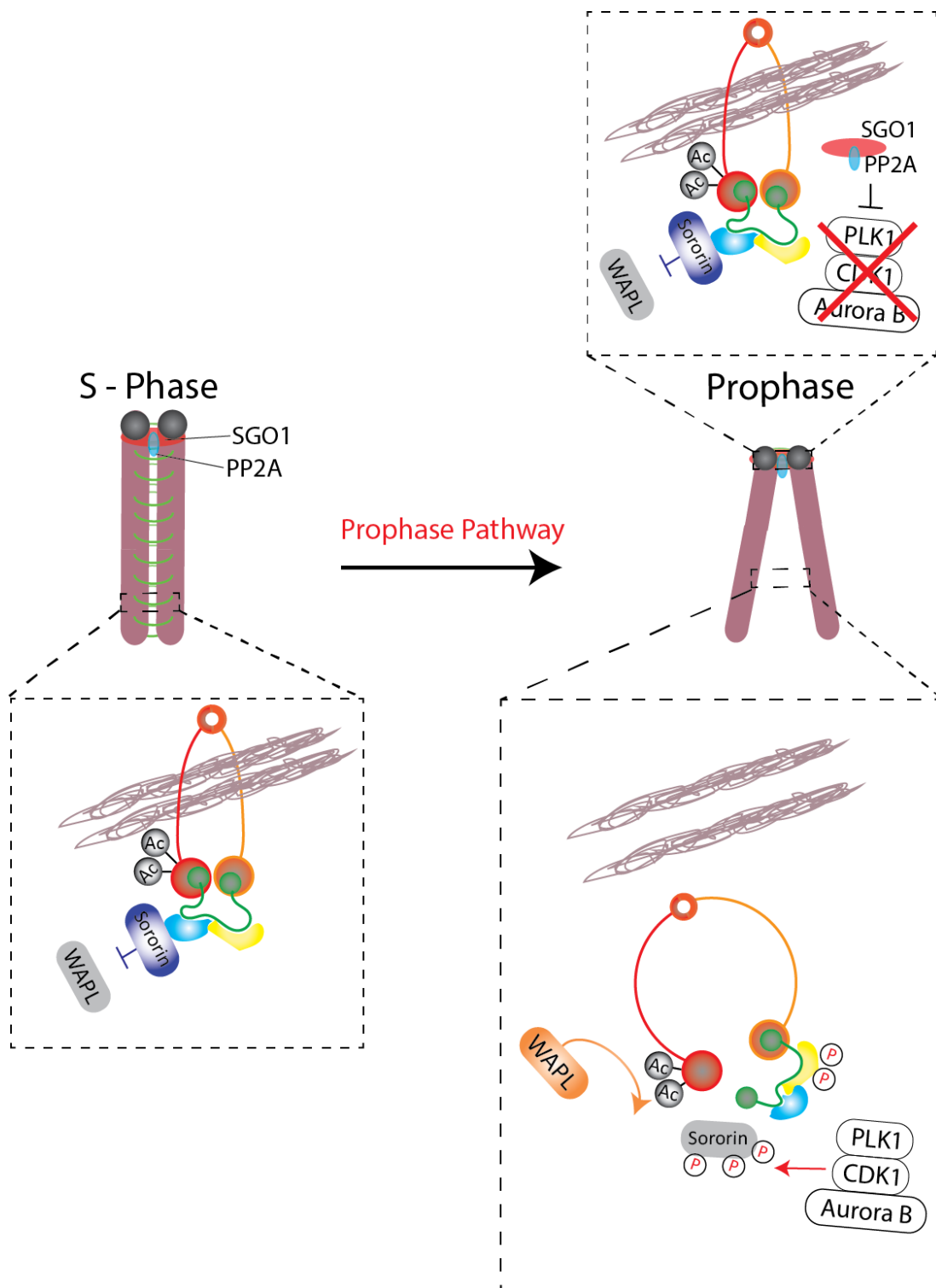
Figure 1.10 Prophase pathway removal of cohesin on chromosome arms during mitosis. *During S-phase SMC3 is acetylated by ESCO1/2 and sororin is recruited to PDS5. This antagonises WAPL and prevents it from opening the SMC3/Rad21 interface. Phosphorylation of sororin and SA2 by PLK1, CDK1 and Aurora B are necessary for sororin removal and openings of the RAD21/SMC3 interface. Centromeric cohesin is protected from this by the SGO1-PP2A complex which prevents phosphorylation (Haarhuis et al., 2014).*

To ensure only cohesin on the chromosome arm is removed during the prophase pathway, cohesin at the centromeres is protected from removal by the SGO1-PP2A complex (Kitajima et al., 2006, Riedel et al., 2006). SGO1 is localised to the pericentromere via BUB1 mediated phosphorylation of histone H2A on threonine 120 (H2A-pT120) and acts to prevent sororin phosphorylation (Kawashima 2010). SGO1 is essential for accurate completion of chromosome segregation in mitosis. Experiments using RNA depletion in HeLa cells reported mitotic arrest due to an inability to maintain cohesion (McGuinness et al., 2005, Salic et al., 2004). SGO1 is also necessary for microtubule stability during mitosis (Salic et al., 2004).

The role of WAPL and sororin in mitosis has been well characterised but not in meiosis. A recent study which expressed REC8 and STAG3 in somatic cells found that as long as STAG3 was expressed, Rec8 could confer cohesion in mitotic cells. Also, this REC8 containing cohesin could have its ring opened by WAPL and was protected by sororin (Wolf et al., 2018) . However, recent work in *C. elegans* indicated that while WAPL-1 promotes the removal of COH-3/4 kleisins, it does not with REC-8 containing cohesin (Crawley et al., 2016).

At first, the prophase pathway might seem unnecessary, especially as the remaining mitotic cohesin is cleaved by APC/C mediated separase release (Gandhi et al., 2006, Nakajima et al., 2007). The prophase pathway is necessary, however, as it offers the possibility of recycling cohesin rings for reloading in G1/S phase of the next cell cycle, a process that would not be required during meiosis (Haarhuis et al., 2014).

1.5.2 Spindle assembly checkpoint and the anaphase promoting complex

For anaphase to occur in both mitosis and meiosis, the cysteine protease separase must be released from its inhibitor securin to cleave cohesin (Ciosk et al., 1998, Zou et al., 1999, Kudo et al., 2006, Wirth et al., 2006). This release is mediated by the APC^{cdc20} which degrades M phase substrates, including securin and cyclin B1 (Figure 1.11). However, for accurate chromosome segregation to occur, it is necessary for the cell to ensure that all chromosomes are orientated correctly and bound by microtubules emanating from different poles. This requires centromeric cohesin during MII and mitosis and arm cohesin during MI to be maintained until this has occurred. To carry out this error correction the cell employs the SAC (Lara-Gonzalez

et al., 2012). This is comprised of several checkpoint proteins including MAD1, MAD2, BUB1, BUBR1 and MPS1. Upon registering the presence of an incorrectly bound centromere MAD1 binds to the kinetochore and recruits MAD2. This forms a closed conformation around CDC20 leading to its inhibition along with recruitment of BUB1 and BUBR1 inhibiting the APC/C (Lara-Gonzalez et al., 2012).
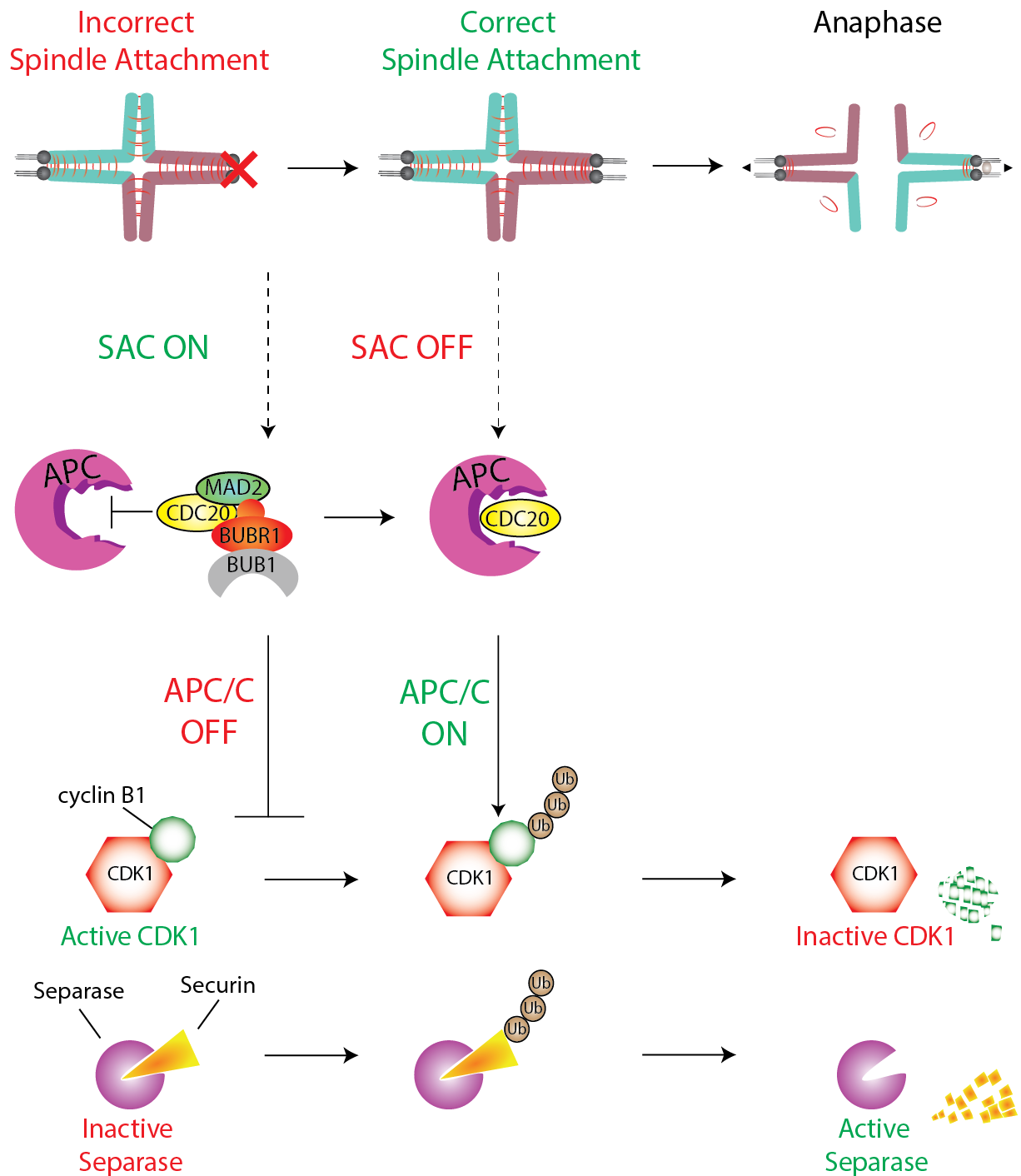
Figure 1.11 spindle assembly checkpoint control of the anaphase-promoting complex in oocytes. *Incorrect spindle attachment during metaphase triggers recruitment of the spindle assembly checkpoint which inhibits CDC20. This keeps CDK1 active through its interaction with cyclin B1 and separase inactive through its interaction with securin. Once correct spindle attachment has occurred the APC is able to polyubiquitinate cyclin B1 and securin. This inactivates CDK1 and activates separase leading to anaphase. Figure based on (Lara-Gonzalez et al., 2012)*

Oocytes do contain a functioning SAC. The spindle inhibitor nocodazole arrests meiosis before anaphase while knockout of BUB1 and depletion of key SAC proteins such as MAD2 and BUB1 results in a shortened time to anaphase (Wassmann et al., 2003, Homer et al., 2005, McGuinness et al., 2009). However, unlike in mitotic cells and in sperm where one misattachment activates the SAC, oocytes do not appear to be as sensitive (Musacchio and Salmon, 2007). This was initially reported on in XO mice, which only have a single univalent X chromosome. These escapes the SAC and do not inhibit anaphase (LeMaire-Adkins and Hunt, 2000). This was further supported by later work on oocytes from $Sycp3^{-/-}$ mice. These lack the SC protein SYCP3 resulting in a number of univalents. Rather than inhibiting anaphase, these univalent chromosomes evade the SAC by establishing bipolar kinetochore – microtubule attachments (Kouznetsova et al., 2007).

The satisfaction of the SAC allows for activation of the APC[cdc20]. This leads to anaphase allowing for separase mediated removal of cohesin. Prior to activation of the APC/C, separase is inhibited in two ways, firstly by its chaperone securin and secondly, by CDK1-mediated inhibitory phosphorylation (Zou et al., 1999, Stemmann et al., 2001, Chiang et al., 2011). Securin has been shown to inhibit the separase protease site by acting as a pseudo-substrate, preventing it from cleaving cohesin (Nagao and Yanagida, 2006, Boland et al., 2017). However, the relationship between securin and separase is more complicated than securin acting simply as an inhibitor. Securin is also necessary for separase function and stability. Indeed, securin-deficient HCT116 cell lines have a 4 four-fold reduction in separase levels (Jallepalli et al., 2001).

Activation of the APC/C results in the polyubiquitination and degradation of cyclin B1 and of securin by the 26S proteasome (Lara-Gonzalez et al., 2012, Musacchio and Salmon, 2007). Both these steps are necessary for anaphase (Herbert et al., 2003, Touati et al., 2012). This frees separase and allows it to cleave the α-kleisin subunit of cohesin. The degradation of both cyclin B1 and securin is mediated through the presence of conserved destruction-box (D-box) motifs. In contrast to finding in xenopus oocytes (Peter et al., 2001, Taieb et al., 2001) homologue disjunction in mouse oocytes was found to be dependent on APC/C-mediated degradation of cyclin B1 and securin (Herbert et al., 2003).

In mitosis after anaphase the cell can start the cycle again. However, in oocytes it must ensure it does not undergo another round of DNA replication or complete MII

24

before fertilisation (Schmidt et al., 2006). This is mediated by an activity known as cytostatic factor which involves inhibition of the APC/C by EMI2 ensuring that the remaining centromeric cohesin is not cleaved (Schmidt et al., 2005, Madgwick et al., 2006).

1.5.3 Separase mediated cohesin cleavage in meiosis and mitosis

Cohesin in meiosis is removed in a two-step process via separase cleavage (Kudo et al., 2009). The first step removes cohesin on chromosome arms before removing it at the centromeres in the second (Figure 1.12). Upon activation of the APC/C in MI, separase is liberated from securin and cleaves REC8 on chromosome arms. This resolves the two homologous chromosomes converting bivalent to dyad chromosomes (Herbert et al., 2015, MacLennan et al., 2015). Studies in budding yeast have reported that for Rec8 to be cleaved by separase it must first be phosphorylated by CK1 and Cdc7 (Ishiguro et al., 2010, Katis et al., 2010). This was recently reported to be Aurora B dependent in *C. elegans* (Ferrandiz et al., 2018). It is thought that this requirement for REC8 phosphorylation is conserved in mouse and human oocytes also.

Protection of centromeric cohesin from cleavage during anaphase I is essential for biorientation of sister centromeres in metaphase II. Because phosphorylation of Rec8 is required for its cleavage, it can be protected from separase by recruiting a phosphatase. In mouse oocytes, this function is fulfilled by an orthologue of SGO1 known as SGOL2 (Rattani et al., 2013, Llano et al., 2008, Lee et al., 2008). According to our current understanding, SGOL2-PP2A prevents phosphorylation of centromeric REC8 which in turn prevents any cleavage by separase (Riedel et al., 2006, Rattani et al., 2013)(Figure 1.12). The importance of SGOL2 in this role was shown through both knockdown and knockout experiments in mice (Lee et al., 2008, Llano et al., 2008). Deletion of SGOL2, or disruption of its ability to interact with PP2A results in significant chromosome segregation errors and infertility in mice (Lee et al., 2008, Llano et al., 2008, Rattani et al., 2013). SGO1 is also expressed during meiosis but appears to only result in a minor defect in MI chromosome segregation when it is knocked down in fully-grown GV stage oocytes (Lee et al., 2008).

The mechanisms responsible for SGOL2 localisation have remained elusive for some time. While BUB1 is important for recruiting SGO1 to centromeres, knockdown of

BUB1 in mouse oocytes resulted in a reductions in time to anaphase but, for the most part, only a minor defect in protection of centromeric cohesin (McGuinness et al., 2009). SGOL2 localisation has recently been suggested to be dependent upon not only BUB1 but also MPS1. This work indicated that knockdown of both MPS1 and BUB1 was required for total removal of SGOL2 (El Yakoubi 2017). Stabilisation of SGOL2 in MI is also thought to depend on MEIKIN (Kim et al., 2015).

Activation of the APC^{cdc20} following sperm entry results in a second round of securin degradation leading to activation of separase and cleavage of REC8 at centromeres (Nabti et al., 2008). It remains unclear exactly how SGOL2 is removed from the centromeres to allow for phosphorylation of centromeric REC8. One suggestion is that the pulling force exerted on centromeres during MII mechanically forces SGOL2 away from the centromeric cohesin (Gomez et al., 2007, Lee et al., 2008). Another suggested mechanism is that PP2A is inhibited from protecting REC8 phosphorylation by the action of a chaperone called I2PP2A (Chambon et al., 2013). It was reported that when I2PP2A is depleted, sister chromatid segregation is prevented. Recent work in yeast has suggested a highly integrated system in which removal of Sgo from centromeres to enable "deprotection" of centromeric Rec8 is orchestrated by the APC^{Cdc20}. This mechanism enables precise coordination of separase activation and deprotection of centromeric Rec8 (Arguello-Miranda et al., 2017). An implication of this finding is that protection is maintained up until the onset of anaphase II. This is particularly appealing in the case of mammalian oocytes, as it would offer additional protection against premature separation of sister centromeres during metaphase II arrest.
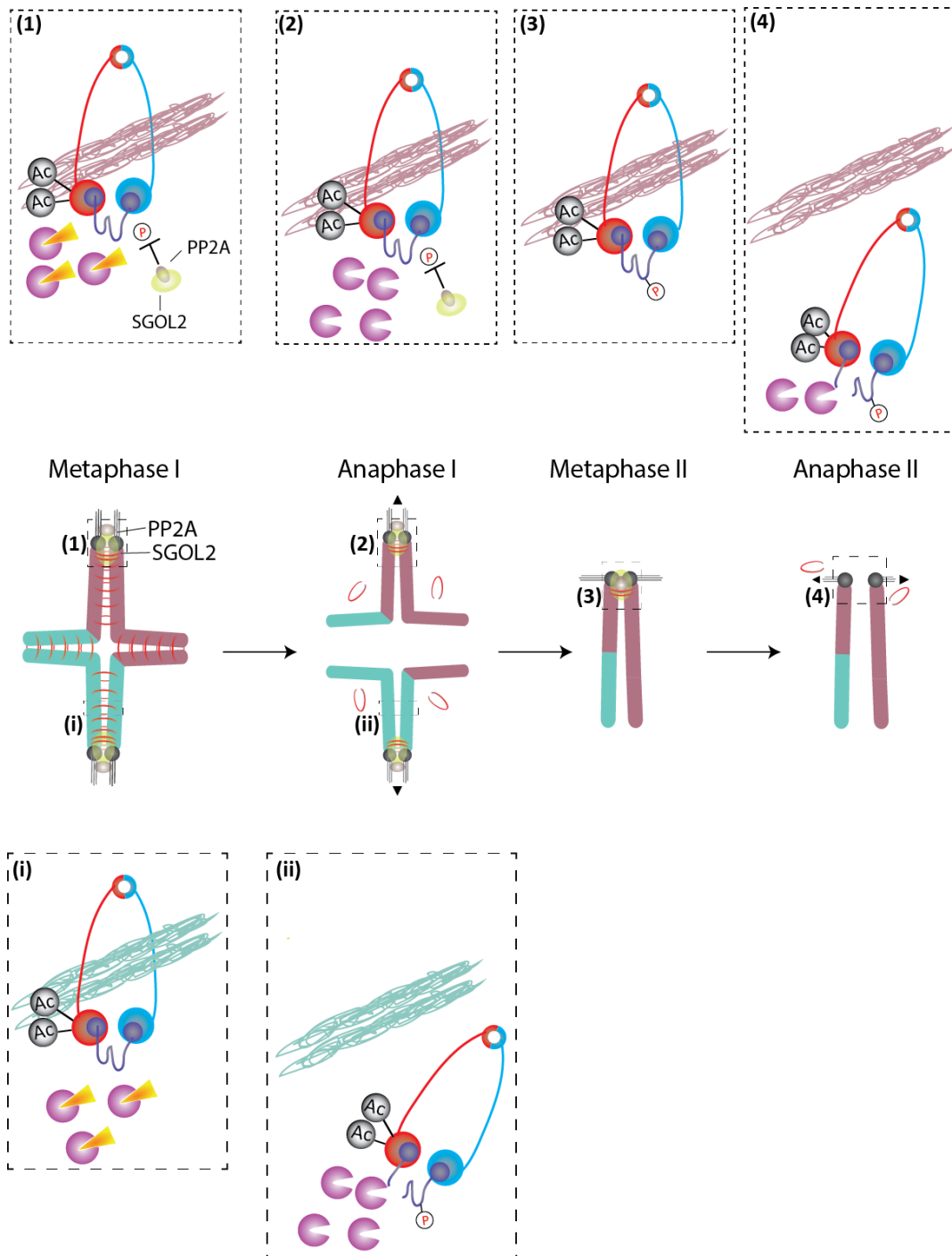
Figure 1.12 Separase-mediated removal of cohesin during meiosis. Schematic diagram showing the two step removal of cohesin in meiosis. *Arabic numbers indicate what occurs at the centromeres while roman numbers indicate what happens on the chromosome arms. (i) During metaphase I separase is inhibited by securin. (ii) After APC/C activation securin is degraded and separase is able to cleave phosphorylated REC8. (1) At the centromeres the SGOL2-PP2A complex prevents phosphorylation of REC8. (2) This protects it from cleavage by separase during anaphase I. (3) At metaphase II REC8 can be phosphorylated and (4) cleaved by separase allowing for anaphase II to occur (Herbert et al., 2015).*

27

Anaphase in mitotic cells also requires separase mediated cleavage of cohesin. After correct spindle attachment has been established and the SAC is satisfied, securin and cyclin B1 are degraded through polyubiquitination by the APC^{cdc20} (Lara-Gonzalez et al., 2012). This releases separase to cleave RAD21 and allows for anaphase to occur (Uhlmann et al., 1999, Uhlmann et al., 2000, Hauf et al., 2001).

1.6 Age-related decline in fertility and possibilities of clinical interventions

1.6.1 Molecular mechanisms of age-related chromosome segregation errors

The correlation between incidence of trisomy in oocytes and female age has been known for several decades. The initial appreciation of this came from population observations of how maternal and paternal age affected the likelihood of a child being born with Down's syndrome. This showed a strong correlation with maternal age but no correlation with paternal age (Penrose, 1933). Several potential mechanisms for why this occurs was suggested over the subsequent decades. These wrestled with the fact that smaller chromosomes seemed distinctly more susceptible to trisomy and that the number of crossovers between chromosomes was reduced with age (Hassold and Jacobs, 1984).Two of the strongest theories suggested were that the prolonged prophase arrest could be causing a deterioration in bivalent chromosome structure. Alternatively, there may be a gradient in terms of crossover number formation during oocyte production. This theory proposes that those oocytes produced, and therefore ovulated first, would have more chiasmata, while those produced and ovulated last would have fewer (Henderson and Edwards, 1968).

The theory of deterioration during prophase arrest gained significant traction due to ground-breaking work carried out by R. Angell in the early 90's (Figure 1.14) (Angell, 1991). In this work, she reported that the leading cause of age-related aneuploidy in human oocytes was as a result of premature separation of sister chromatids. This differed from the orthodoxy at the time that suggested it was from non-disjunction. She later showed that premature separation can occur in the first division with the oocyte still retaining the correct number of chromatids in a balanced pre-division (Angell, 1997) (Figure 1.13). This is then thought to become problematic during the

28

second round of division as the chromatids are no longer physically linked together. Her findings were later supported by fluorescence in situ hybridisation (FISH) and fixed oocyte imaging studies (Kuliev et al., 2011, Sakakibara et al., 2015).
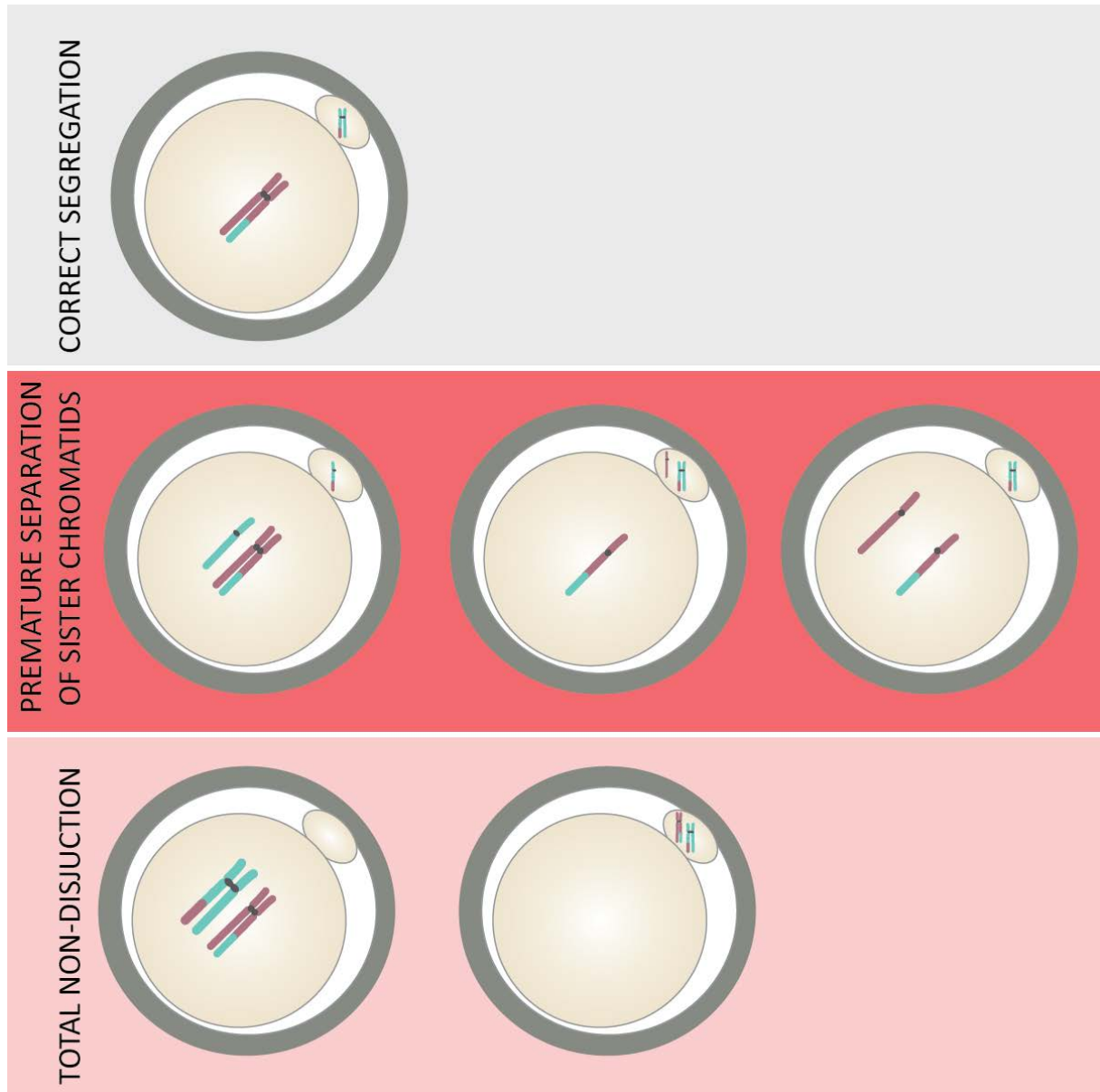
Figure 1.13 Segregation errors during the first meiotic division in oocytes. *DNA segregation during the first meiotic division requires a reductional division leading to one set of chromosomes in the polar body and one set in the oocyte. This can go wrong either by premature separation of sister chromatids or via total non-disjunction. The likelihood of premature separation occurring rather than total non-disjunction increases with age.*

The more recent studies to determine the frequency and distribution of chromosome errors in human oocytes have relied on whole genome amplification and array-based comparative genome hybridisation (CGH) of polar bodies (Fragouli et al., 2011, Fragouli et al., 2013, Handyside, 2013). These studies indicate that chromosome 15, 16, 21 and 22 are the most likely to suffer from segregation errors but that all chromosomes become susceptible to segregation errors during female ageing. Importantly, ageing is also associated with an increase in multiple chromosome segregation errors, occurring most often in women in their 40's (Franasiak et al., 2014, Handyside et al., 2012, Fragouli et al., 2013) .

Investigations by our lab and others have strongly suggested that the deterioration of oocyte quality during ageing best explains the increase in premature separation of sister centromeres. This has focused mostly on the cohesin complex, with REC8 found to be reduced substantially by 14 months in mouse oocytes (Chiang et al., 2010, Lister et al., 2010). This leads to a loss of bivalent chromosome stability as well as an increase in distance between centromeres (Chiang et al., 2010, Lister et al., 2010). This is supported by the fact that $SMC1\beta^{-/-}$ mice also show a loss of bivalent chromosome stability (Revenkova et al., 2004, Hodges et al., 2005). As it appears that there is no turnover or re-loading of cohesin after establishment during prophase arrest, any cohesin lost at this stage is not replaced (Tachibana-Konwalski et al., 2010, Burkhardt et al., 2016).

Loss of cohesin with age is also accompanied by loss of the centromeric cohesin protector SGOL2 (Lister et al., 2010). Immunofluorescence analysis of SGOL2-PP2A localisation suggested that it is loaded onto the MI centromeres after GVBD. This presents a model in which cohesion is reduced with age, leading to reduced recruitment of the protector SGOL2, leaving it particularly vulnerable to segregation errors at anaphase (Figure 1.14). Analysis by our group suggests that REC8 is lost during prophase arrest at the primordial oocyte stage of development, again, supporting the deterioration of cohesion hypothesis.

30
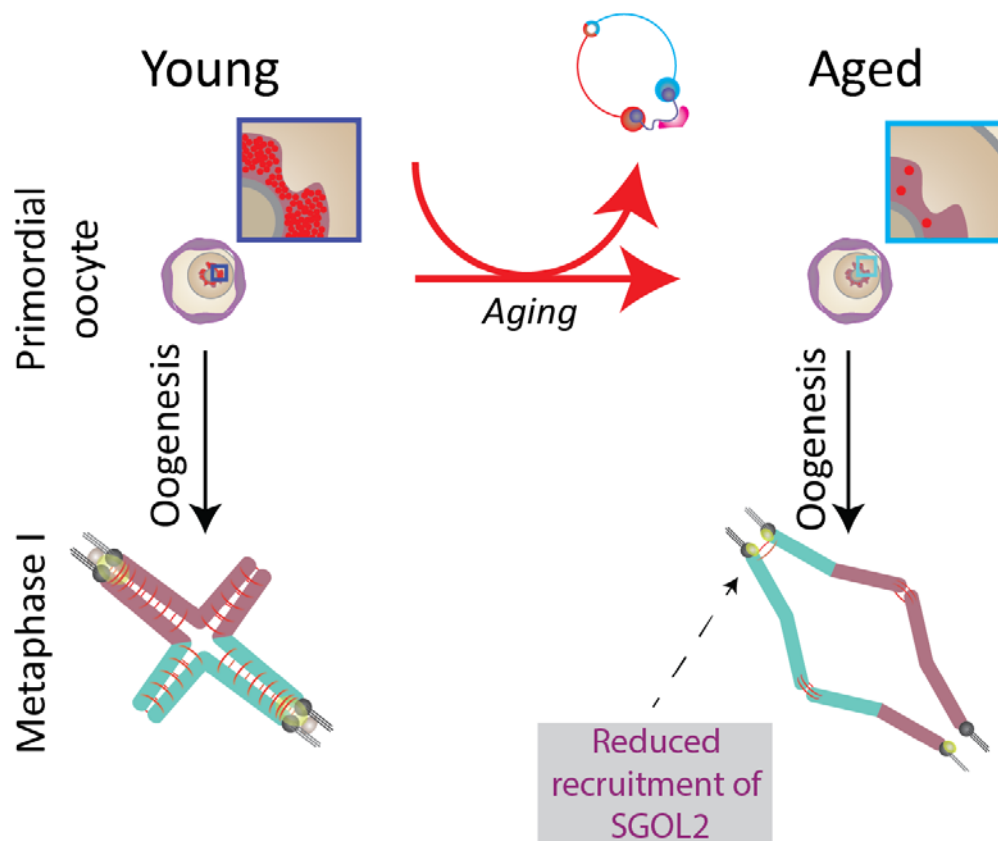
Figure 1.14. Current model for age-related increase in segregation errors in mouse oocytes. *Schematic diagram showing the current model for age-related segregation errors in mouse oocytes. In oocytes, cohesive cohesin is loaded onto DNA after S-phase and maintained throughout oogenesis. SGOL2 is then recruited to the centromeres after GVBD and meiosis occurs. However, as the mouse ages REC8 (red dots) becomes reduced in primordial-stage oocytes. After oogenesis has occurred, and the oocyte resumes meiosis, the bivalent chromosomes exhibit distal association of chromatids as well as an increase in centromeric distance. This also results in reduced recruitment of SGOL2 leaving the chromosomes susceptible to segregation errors.*

The findings in mice correlate with the phenotype seen in human oocytes. This involves an increase in centromeric distance between sister chromatids and a loss of chromosomal cohesion (Chiang et al., 2010, Lister et al., 2010, Duncan et al., 2012, Lagirand-Cantaloube et al., 2017, Zielinska et al., 2015, Sakakibara et al., 2015). How this physically manifests in aneuploidy has been the subject of recent investigation. Work using whole oocyte fixation and cold-stabilisation of microtubules

in human oocytes suggests uniquely high levels of separation between sister centromeres. This leads to hyper-twisted "inverted bivalent" or "half-inverted bivalent" conformation, with dyads biorientating instead of monoorientating during meiosis I. These then fail to segregate as dyads during anaphase, resulting in aneuploidy (Zielinska et al., 2015). Another study in fixed human oocytes suggests a different mechanism however, with bivalent chromosomes separating into univalent first, before biorientating and segregating like MII dyads during anaphase I (Sakakibara et al., 2015).

While loss of chromosomal cohesion is a common feature between humans and mice, and the presence of the three essential meiotic cohesin subunits (REC8, SMC1β and SMC3) have been identified in humans, it is not known whether a loss of these cohesin components is responsible for the increase in segregation errors in humans (Garcia-Cruz et al., 2010). Analysis in ovarian sections from women who have undergone hysterectomies did not show a significant difference in SMC3 and REC8 when analysed per woman (Tsutsumi et al., 2014). Observations of REC8 in chromosome spreads from another study seemed to suggest that there was no reduction with age (Garcia-Cruz et al., 2010). Importantly, these two sets of findings come with large caveats. The first study did not remove soluble cohesin which is present in the oocyte but – based on our current understanding of cohesin establishment – is not loaded onto the DNA. The second did not show any data and the oldest woman in their study was 34. Thus, there has so far been no systematic study of the effect of female ageing on chromosome-associated cohesin in human oocytes.

A large barrier to understanding the ageing effect in human oocytes is the current source of human oocytes available for use in research. Investigations into human oocyte mechanisms have used oocytes not suitable intracytoplasmic sperm injections (ICSI) (Webster and Schuh, 2017). These oocytes are not used for ICSI as they have not reached metaphase II following ovarian stimulation. These are thought to comprise around a fifth of oocytes extracted for ICSI (Reichman et al., 2010). While they have provided some key insight in to human meiosis, the fact that they failed to mature in vivo raises the possibility that they are not representative of a healthy population.

The "loss of cohesin" model is not the only mechanism that has been suggested as the prime-culprit of age-related segregation errors. An alternate theory suggests that

32

it may in fact be as a result of a defective SAC. Key components of the SAC have been reported to be reduced with age in mouse and human studies (Baker et al., 2004, Lagirand-Cantaloube et al., 2017). However, as mentioned previously, while the SAC has been reported to inhibit anaphase through inhibition of the APC/C when kinetochores are not attached to centromeres, it is unable to detect univalents even in younger mice, as the chromosomes biorientate on the MI spindle (Kouznetsova et al., 2007). A Study looking at timing of securin degradation and anaphase onset saw no difference between young and old mouse oocytes, suggesting no consequential loss of SAC proteins (Duncan et al., 2009, Lister et al., 2010, Sebestova et al., 2012). The existence of an age-related effect on cytoplasmic proteins affecting segregation is also questioned by studies looking at reciprocal GV transfers between young and old mice. Comparisons of naturally aged and senescence-accelerated mice produced no evidence of rescue of the ageing phenotype in old to young transfers (Liu and Keefe, 2004, Cui et al., 2005). This suggests that cohesin loss is a strong candidate to explain the age-related increase in premature separation.

With cohesin depletion being a plausible candidate to explain age-related segregation errors, the focus has turned to understanding the underlying mechanisms. Potential candidates include, aberrant cleavage of cohesin by the protease separase in the primordial-stage oocyte and/or protein damage occurring, for example as a consequence of increased reactive oxygen species over time.

Several factors point to "leaky inhibition" of separase as a candidate for cohesion removal. *Mnd2* yeast mutants which cannot inhibit the APC[AMA1] show premature destruction of securin and separase activity during prophase (Oelschlaegel et al., 2005, Penkner et al., 2005). Also, if separase is present in primordial-stage oocytes, CDK1 inhibition will be inactivated as at this stage CDK1 is inhibited by phosphorylation (Adhikari et al., 2016). This means that separase would only be inhibited by securin. This points to separase as a potential candidate for age-related loss of cohesion.

1.6.2 Clinical interventions to address age-related aneuploidy

Since the first child was born using IVF in 1978, assisted reproduction techniques (ART) have become well-established clinical procedures (Nagaoka et al., 2012).

33

While these techniques have helped previously infertile parents have their own genetically related children, IVF treatment does not overcome age-related dificulties in fertility if the woman uses her own eggs (Geraedts et al., 2011, Sauer, 1998). This is borne out clinically with Human Fertilisation and Embryology Authority (HFEA) data from 2016 showing that only 17% of own egg, partner sperm IVF cycles are from women over 40, while donor egg, partner sperm from over-40's make up 67% (HFEA, 2018).This has led to attempts to develop new techniques to detect aneuploidy so that the healthiest egg can be selected for fertilisation.

As mentioned previously, female fertility is shaped by two age-related factors. First is the decline in the ovarian reserve of primordial stage oocytes as women get older. Second is that the oocytes remaining in the ovary at advanced reproductive age are of a poorer quality (Broekmans et al., 2007). Ovarian reserves are currently assessed by measuring anti-Müllerian hormone (AMH) levels, which is produced by growing follicles (Visser et al., 2006, Grynnerup et al., 2012). Assessment of whether an oocyte is aneuploid has focused on the polar bodies which are biopsied before and after fertilisation. These are then analysed using CGH sequencing to quantify the number of chromosomes in the polar body, thus indicating how many should be in the oocyte (Handyside and Xu, 2012). While AMH measurements are readily available on the NHS, preimplantation genetic screening tests are only available in a small number of clinics.

These two methods give information on the state of the egg being analysed but do nothing to address the underlying problem. Currently, the most likely treatment to aid women in maintaining their fertility is to have their eggs vitrified for use at a later date. The freezing of oocytes for later use is currently used in the UK for women who are undergoing chemo- or radiotherapy but is only available privately for social reasons. Analysis of the use of frozen eggs in comparison to freshly extracted oocytes in a large scale study reported no significant difference in outcomes (Cobo et al., 2010). However, the overall success rate of IVF cycles is dependent on the number of oocytes retrieved from the woman as well as her age at the time of donating (Cobo et al., 2016). While it is possible to give older women higher doses of hormones to stimulate a greater number of oocytes and increase chances of finding a non-aneuploidy egg, it is thought that high levels of FSH may cause greater chromosomal abnormalities (Roberts et al., 2005). This means that women have to decide about freezing their eggs many years before they may have even found a partner.

34

From our current understanding of the mouse model there appears to be little scope for any other form of clinical intervention in human oocytes. However, whether the mouse model is in fact representative of human loss of fertility is currently unclear. Using both mouse and human biological material, a primary aim of my PhD project is to investigate the potential mechanisms for cohesin loss in primordial stage oocytes and to determine the clinical significance of age-related cohesin depletion by measuring cohesin levels in human oocytes. In view of the challenges associated with measurement of cohesin levels, I have explored a range of approaches for analysing chromosome-bound proteins by immunofluorescence of chromosome spreads.

Chapter 2. Aims

2.1 Overall Aim

The overall aim of this project is to establish the timing and mechanism around cohesin loss in primordial-stage mouse oocytes and to investigate the effects of ageing on cohesin in human oocyte.

2.2 Specific Aims

1) Develop improved methodology for quantification of chromosome associated proteins in oocyte ageing studies. This will be done by establishing an appropriate immunofluorescent marker to normalise proteins of interest to and developing a robust and easily reproducible methodology for carrying out analysis.

2) Investigate the effect of ageing on cohesin loss in primordial-stage oocytes. Investigate if the protease separase may be responsible for the loss of cohesin seen in primordial-stage oocytes through the use of an oocyte-specific *separase null* mouse. Investigate whether cohesin may be afforded any protection by the cohesin protectors SGO1 or SGOL2 in primordial-stage oocytes.

3) Investigate if the mouse model of cohesin loss during ageing can explain the increase in chromosome segregation errors and loss of bivalent stability in human oocytes. This will be done in part through establishing a new source of human oocytes not dependent upon those rejected from IVF cycles.

Chapter 3. Material and Methods

3.1 Mouse strains

In this project I utilised two genetically altered, without a harmful phenotype, mouse strains and one wild type mouse strain. Our collaborators in this project, Nobuaki Kudo and Kim Nasmyth provided us with a *Separase null* conditional knockout mouse. This mouse was generated with C57BL/6 background with iCre recombinase activity expressed from the *Gdf9* promoter. The Separase gene was replaced with a version that had the 8 COOH-terminal exon (exon 24 to exon 31) flanked by *loxP* sites (Kudo et al., 2006).

Our collaborators also provided us with a *TG Rec8-Myc* line. This mouse has a B6CBAF2 background. REC8 is expressed from a bacterial artificial chromosome which has nine tandem copies of human c-myc epitope at its C terminus (Kudo et al., 2009). CD1 wild type mice were used for non-aging experiments.

For ageing experiments that did not use the REC8-Myc mice I used the mice from the separase strain which did not express iCre ($Sep^{f/f}$ mice). These are referred to in this work as C57BL/6 mice.

The mice were housed and bred at the Institute of Genetic Medicine, Newcastle University. All CD1 mice used were purchased and imported from Charles River. All procedures were carried out in accordance with the regulations of the Home Office.

3.2 Mouse oocyte harvest

Mice were culled by cervical dislocation and ovaries were surgically removed using watchmaker forceps and bow string scissors. The ovaries were then transported to the laboratory in a 15ml falcon tube containing pre-warmed M2 medium (Sigma-Aldrich, M7167). On a heated stage in a laminar flow hood fitted with a stereoscope, fat surrounding the ovary and any remaining fallopian tube was removed from the ovary using 29G 1ml insulin needles (BD bioscience, VWR 613-4904) in the lid of a 60x15mm culture dish (BD bioscience, VWR-734-0007). The ovaries were then transferred to a 60x15mm culture dish using M2 supplemented with 200µM 3-isobutyl-1-methylxanthine (IBMX) (Sigma-aldrich, I7018). Oocytes were released from the ovary through maceration of the ovary using the insulin needles. The oocytes were collected using hand-held 127-129µm diameter glass denudation pipettes (BioTipp, Vitrolife, 14306) and stored at 37°C in 40µl M2+IBMX drops

covered in mineral oil (Sigma-Aldrich, M8410) in 35x10mm diameter culture dishes (BD bioscience, VWR-734-0005). The oocytes were kept like this until required to undergo germinal vesicle break down (GVBD).

3.3 Mouse oocyte culture

Prior to oocyte culture (minimum 4 hours but usually overnight) 5x40µl G-IVF (Vitrolife, 10136) drops were covered in filtered mineral oil in 35x10mm diameter culture dishes and equilibrated in a 5% CO_2 incubator at 37°C. To initiate GVBD the oocytes were washed repeatedly in each drop of G-IVF and left in the fifth drop. To attempt to synchronise GVBD as accurately as possible, GVBD was checked for at 1hr, 1.5hrs and 2hrs after being left in the final G-IVF drop. Anaphase was adjudged to have occurred if the oocyte undergone polar body extrusion. This was checked for at 7hrs, 7.5hrs, 8hrs and 8.5hrs after GVBD.

3.4 Mouse oocyte chromosome spreads

Prior to spreading 2x40µl drops of acid tyrodes (refer to 3.21), 4x40µl drops of M2 and 2x40µl drops of 0.5% sodium citrate were pipetted on to the lid of a 50x9mm petri dish (BD bioscience, VWR-391-1997) . The number of oocytes to be spread were transferred to the acid tyrodes from the culture dish using a stereoscope and a glass denudation pipette. After the zona pellucida was observed to have been removed, the oocytes were then washed through the 4 drops of M2 to remove any residual acid tyrodes. The oocytes were then placed in 0.5% sodium citrate for 2 minutes to allow swelling.

Approximately 30 seconds before the spread was carried out, 100µl of 1% PFA (refer to 3.21) solution was pipetted on to a pre-labelled polysine slide (Fisher Scientific, MNJ-800-010F) and the excess PFA was removed by dabbing on a sheet of blue roll. To guide where the oocytes were to be placed, a line was drawn on the back of the slide in permanent marker and the slide was placed inside a humidified chamber. A few seconds before the 2 minutes are up the oocytes are collected and expelled one by one on to the slide along the line and checked to see whether they have ruptured. The slide was then kept in the humidified chamber overnight. If spreads were being carried out with young and aged mouse oocytes on the same slide, the young mouse oocytes were put in sodium citrate first before the aged ones. The young mouse oocytes were then drawn up into the pipette first, then a barrier volume of sodium citrate was collected before the old mouse oocytes were collected. These were then expelled on to the slide so that the older mouse oocytes would be at the top and the
38

younger at the bottom. This allows for both sets to be spread simultaneously but still be separately distinguished on the slide.

The following day a hydrophobic barrier was drawn round the area where the oocytes were spread using an Immedge Hydrophobic Barrier Pap pen (Vector Laboratories, H-4000) and allowed to dry. The slides with the spreads were then washed 2x 2 minutes in H_2O+0.4% Photoflo (Silverprint, 90662), then 2x 2 minutes in 1xPBS (Melford Laboratories, P3206). Slides were stored in 1xPBS at 4°C until they were to be stained.

3.5 Human oocyte retrieval and recording

All oocytes were retrieved by the clinical team at the Newcastle fertility centre. Consent was provided by the women undergoing treatment. Each donation was assigned a specific sequential code and was recorded according to HFEA guidelines.

3.6 Human oocyte stripping and culture

Human oocytes were transported to the research lab from the clinical lab in G-IVF dishes and placed in the 5% CO_2 incubator. A 10x HYASE solution (Vitrolife, 10017) was diluted to 1x in G-MOPS plus (Vitrolife, 10130) and covered in Ovoil (Vitrolife, 10029) in an organ culture dish (Scientific laboratory supplies, 353037). The HYASE solution was allowed 15 minutes to reach 37°C. Cumulus-oocyte-complex's (COC) were collected using a 9" cotton plugged IVF Pasteur pipette (Origio, PP-9-90PL) and placed in HYASE solution and left for 30 seconds. HYASE solution was then washed off in G-MOPS and the cumulus cells were removed through pipetting up and down using the Pasteur pipette. The oocytes stage of maturation was judged based on whether a polar body had been extruded or a whether a GV was visible. The oocyte was then placed back in G-IVF for 1.5hrs before being prepared for spreading. If a polar body was observed the oocyte was placed back in the incubator for three further hours to allow for chromosomes to align on the MII spindle.

3.7 Human oocyte chromosome spreads

The procedure for human oocyte chromosome spreads followed a similar method to mouse oocyte chromosome spreads with some modifications (refer to 3.4). Rather than using acid tyrodes, M2 supplemented with pronase (1mg/ml) (Sigma Aldrich, P8811) was used to remove the zona pellucida. This was done on a 37°C heated stage. After being washed through 4 drops of M2 the oocytes were placed in 0.5% sodium citrate for 5 minutes to allow for swelling.

The 1% PFA solution was the same as used in mouse oocyte chromosome spreads, but supplemented with 3.4% sucrose (Sigma Aldrich, S1888). This was filtered through a 0.45µm syringe filter to remove any debris (VWR International, 514-0075). 1.5 hours after spreading, the sucrose/PFA solution was re-applied to the slide. The spreads were left overnight at room temperature in humidified chambers, and then stored at -20°C in a slide box for long term storage.

3.8 Genotyping

Ear clippings of recently weaned mice were incubated at 55°C overnight in 250µl of lysis buffer (refer to 3.21) supplemented with 2.5µl proteinase K (Roche Diagnostics Ltd, 3115887001). The next morning 250 µl of phenol:chloroform (Sigma Aldrich, P3803) was added and vortexed at max. speed for 1 minute until white. The cell lysate was centrifuged at max. speed (16.9 rcf) for 10 minutes and the supernatant moved to a separate tube. DNA precipitation of the supernatant was carried out using 250 µl of isopropanol and centrifuged at 4°C at max. speed for 30 minutes.

Without disturbing the pellet, the supernatant was discarded and the remaining pellet washed with 500 µl of 70% ethanol (RNase and DNase free) and centrifuged again at max. speed for 10 minutes. This step was repeated again before the eppendorf was placed in a hot block for 15 minutes, with the cap open to allow all of the ethanol to evaporate.

Once the evaporation step was complete, 20 µl of 1x TE buffer was added. To dissolve the pellet, the eppendorf was incubated at 50°C for 30 minutes.

PCR-primers used:

Table 1: Separase Primers

Primer Direction	Sequence	PCR product size
5' – 3'	ACT GAC CGT GAC ATT GAC CGT TAC	529bp
3' – 5'	TTCATCACCCAA GCTCCAAGCAG	

Table 2: Gdf9-iCre primers

Primer Direction	Sequence	PCR product size
5' – 3'	TCT GAT GAA GTC AGG AAG AAC C	~550bp *(band shows presence of Cre)*
3' – 5'	GAG ATG TCC TTC ACT CTG ATT C	

PCR reactants used: DEPC Nuclease free water (Fisher Scientific, 11597065), 10x buffer and Taq polymerase (New England Biolabs, M0267S) and dNTPs (New England Biolabs, N0447S). Primers purchased from eurofin genomics.

Table 3: PCR reactant volume

Reagent	Separase/Gdf9-iCRE (µl)
DEPC nuclease free water	19.88
10x Buffer	2.5
10mM dNTPs	0.5
5' – 3' Primer	0.5
3' – 5' Primer	0.5
Taq polymerase	0.13
Mouse Genomic DNA	1

Table 4: PCR settings

Step	Temperature °C	Time (min)	No. of Rpts.
1	94	2	1
2	94	1	30
3	58	2	30
4	72	2	30
5	72	5	1
6	4	∞	

3.9 Ovary embedding: OCT

After surgical removal of ovaries and fat removal, ovaries were briefly washed in PBS (Life Technologies Ltd, 10010015) and placed in a 10x10x5mm dispomoulds (cellpath, GAD-1000-10A) containing room temperature optimum cutting temperature matrix media (OCT) (Cellpath plc, KMA 0100-00A). To freeze the solution 2 metal blocks were placed in dry ice for 10 minutes to allow them to cool. The dipsomould containing the ovaries and OCT were then placed on one cooled metal block and the second pre-cooled metal block was placed on top. After the OCT had turned white and solid, (signifying that it had been frozen) the embedded ovaries were wrapped in tinfoil and stored at -80°C until the time of sectioning.

3.10 Cryosectioning

Prior to retrieving OCT embedded ovarian samples from the -80°C freezer, a blade (Fisher Scientific, SD3050822) was secured in the cryostat blade block using the blade clamp. The cryostat was set to -20°C (Leica CM1860). Two watchmaker forceps were also placed inside the machine and allowed to cool. Ovarian samples embedded in OCT were then retrieved from the -80°C freezer on dry ice and transported to the cryostat. A small amount of OCT was added to the chuck and the OCT embedded sample was placed on top. This was then placed inside the cryostat on the fast cooling block and left to freeze for at least 10 minutes. During this time polysine slides were labelled. After 10 minutes the chuck was loaded into its holder and manoeuvred so the sample was closeto the blade. Once the sample was brought close to the blade it was cut in a continuous motion to prevent folding of the tissue sections. After a pause of around 5 seconds, the glass anti-roll plate was removed and the sample was loaded onto the polysine slide, using a rolling motion starting from the bottom of the section. The section was allowed to then dry at room temperature before being stored at -20°C for short term storage, and -80°C for longer term storage. If there was remaining ovary left after sectioning, a small amount of OCT was applied over the sample and the chuck was placed back on the cooling block until the OCT went hard and white. It was then stored as required for future use. Sections in which the entire primordial nucleus needed to be accquired were cut at 30µm and those for investigating protein expression were cut at 15µm.

3.11 Ovary embedding: Paraffin Wax

After surgical removal of the ovaries and fat removal, ovaries were briefly washed in PBS and placed in 4% PFA (pH 7.4) overnight at 4°C. The following morning residual

42

PFA was washed off using PBS (Life Technologies Ltd, 10010015). This was followed by a process of increasing concentrations of ethanol, intended to dehydrate the ovary: 30 minutes in 50% ethanol; 30 minutes in 70% ethanol; 30 minutes in 90% ethanol; then 2x 30 minutes in 100% ethanol. The ovaries were then placed in 100% xylene (Sigma Aldrich, 534056) for 20 minutes inside a glass snap-top vial. While this happened a solution of 50% wax (VWR, 361077E) /50% xylene (Sigma-Aldrich, 534056) was heated to 60°C in a hot block. After the 100% xylene step the ovaries were placed in wax/xylene solution for 15 minutes. They were then incubated in 100% wax at 60°C 3x20 minutes each. Finally a 10x10x5 dispomould fitted with a system I embedding ring (Cellpath, GAB-902-10A) was partially filled with wax. The ovary was then placed in the dispomould and the dispomould was then filled completely with wax and left to solidify at room temperature.

3.12 Wax sectioning

Super frost slides (Fisher Scientific, 10149870) were labelled and a wax box was drawn round the outside of the glass. The slides were then placed on a heated platform at ~37°C and ddH$_2$0 was pipetted inside the box. After this, the wax embedded ovary was placed in the clamp of the microtome (Leica, RM2235) and locked in place while a microtome blade was inserted into the blade holder.

Using a fast, continuous motion, sections were cut in quick succession to form ribbons of sections. Using the wooden handle of a brush, ribbons were held up to prevent them from touching any surfaces before being placed on a black surfaced board. Sections were then loaded on to the water covered slides. The first section was loaded so that its outer edges would be in contact with the wax strip around the slide to hold it in place. The next section was then loaded to overlap with the previous to hold them all in place. The water was then allowed to evaporate overnight and slides were stored at room temperature in the dark.

3.13 Chromosome spread immunofluorescence

Slides with chromosome spreads were incubated for 1 hour at room temperature in a block solution of PBTT (1XPBS/0.25% Triton X-100 (Sigma Aldrich, T8787)/0.25% Tween-20 (Sigma Aldrich, P9416)) with 10% goat serum (Stratech Scientific, 005-000-121). The block was removed and the primary antibody was added, made up in the same block solution, and incubated overnight at 4°C.

43

The following morning the primary antibody was retrieved and the slides were washed at room temperature in a coplin jar on a shaking platform at 75–100 rpm. The washes consisted of 1x 10minutes PBS+0.4% Photo-flo; 2x10 minutes PBS+0.01% Triton X-100; 1x 10minutes PBS+0.4% Photo-flo and 1x2minutes PBS. After the washes the spreads were incubated in secondary antibody made up in the block solution for 1 hour in the dark. The washes were then repeated.

If the conjugated TOPO II antibody was used the spreads would be incubated overnight at 4°C in PBTT supplemented with non-immune rabbit IgG (1mg/ml) (Sigma Aldrich, I5006). Washes would be repeated the following day and then the spreads would be incubated in the dark overnight at 4°C with the conjugated TOPO II antibody in blocking solution. The following morning the washes were repeated and the chromosomes spreads mounted in Vectashield mounting media supplemented with DAPI for chromosome visualisation (Vector Laboratories, H-1200) using a No. 1.5 coverslip (Scientific Laboratory supplies, MIC3246), and sealed shut using a rubber solution .

3.14 Cryosection immunofluorescence

Slides with cryosections were removed from the -20°C or -80°C freezer and allowed to reach room temperature. They were then washed 2x5 minutes in PBS, 1x10 minutes PBS+1%-Triton, 1x5 minutes PBS at 50rpm on a platform shaker. The sections were then fixed for 15 minutes in 4% PFA (pH 7.4) (see 3.21) and then washed 2x10 minutes in PBS. Sections were then incubated for 1 hour at room temperature in cryobuffer (1xPBS/0.2% Triton X-100/1% DMSO (Sigma-Aldrich (D2650)) with 10% goat serum. The block was removed and the primary antibody (diluted in the blocking solution) was added. The sections were then stored overnight at 4°C.

The following morning the primary antibody was retrieved and the slides were washed 2x10 minutes PBS, 1x10 minutes PBS+1% Lipsol (Fisher Scientific, 12549965), 1x10 minutes PBS. Sections were incubated with secondary antibody in the blocking solution for 1 hr in the dark. After this they were washed 4x10 minutes in PBS. If TUNEL was being used, the solution would be applied and the sections incubated at 37°C for 1 hour followed by 4x10 minutes PBS washes. DNA was then labelled using TO-PRO-3 in PBS for 1 hour at room temperature. After this the sections were washed 3x5 minutes in PBS and then mounted in Vectashield

mounting media supplemented with DAPI using a No. 1.5 coverslip, and sealed shut using a rubber solution.

3.15 Wax section immunofluorescenece

Slides loaded with wax sections were incubated 2x10 minutes in xylene, followed by 2x5 minutes 100% EtOH, 1x5 minutes 70% EtOH, 1x5 minutes 50% EtOH and 1x5 minutes distilled H_20. While this was happening, citric acid buffer solution (see 3.21) was warmed in a pressure cooker using an electric hob. The slides were then loaded in to a metal rack and placed in the citric acid buffer solution. The lid of the pressure cooker was fitted and the temperature increased. When full pressure had be reached (signified by the whistling from the pressure cooker) the samples were steamed for an additional 8 minutes. After this the pressure cooker was cooled using cold water and ice. Slides were then washed in a coplin jar of 3x 5 minutes TBS. A hydrophobic barrier was drawn around the sections. A blocking solution of TBS+0.025% Triton supplemented with 10% goat serum was used for 1 hour. If a blocking peptide was being used then this was incubated with the primary antibody for 1 hour on a shaker in the blocking solution. After an hour the block was removed and the primary antibody was added and incubated overnight at 4°C. The following morning the primary antibody was retrieved and the slides were washed 3x10 minutes in TBS followed by 2x5 minutes TBS+0.025% Triton. Sections were then incubated in TBS-0.025% Triton with 10% goat serum with secondary antibody for 1 hour at room temperature. After this the slides were washed 3x10 minutes TBS and mounted in Vectashield mounting media supplemented with DAPI using a No. 1.5 coverslip and sealed using a rubber solution.

3.16 Microscope imaging

The following parameters were used for the imaging of immunofluorescence samples by confocal microscopy, both with and without airyscan post processing.

3.16.1 Nikon A1R confocal microscope

Immunofluorescence data was collected using a Nikon A1R confocal microscope with NIS elements software. Either a Plan Apo 60x/1.40 oil, or an S fluor 40x/1.30 oil objective was used. Sequential (Channel series ON)/Simultaneous (Channel series OFF) excitation at 405nm, 488nm, 561nm and 642nm was provided by the 405nm Cube laser (Coherent Inc., USA), 488nm Argon Laser (Melles Griot, USA), Sapphire 561nm Laser (Coherent Inc., USA) and Red Diode 642nm Laser (Melles Griot, USA), respectively. Emission filters BP 425-475nm, BP 525-555nm, 570-620nm and 662-

45

737nm for were used for detection of DAPI, Alexa 488, Alexa 555 and Alexa 647/Cy5/ TO-PRO-3 633 signal respectively.

Frame size: 1024x1024 pixels

Line average: 2x or 4x

Z-steps: 0.5μm

3.16.2 Zeiss LSM880

Airyscan: Immunofluorescence data was collected using a Zeiss LSM880 with Airyscan, a serial array of 32 GaAsP detectors. Images were acquired using either an oil Plan-apochromat 63x / 1.4NA or a 40x / 1.3NA objective, with Zen Black 2.3 SP1 software. Samples were either excited with visible light lasers (488nm, 561nm or 633nm), or a UV-laser (405nm) corrected with a collimator. Visible light lasers were cleaned up by a 488/561/633 beamsplitter and UV-light by a 405nm beamsplitter. Emission was collected using the Airyscan detector. Fluorescence was captured using multi-bandpass filters: for DAPI this was BP 420-480 + LP 605; Alexa-Fluor 488 was BP 420-480 + BP 495-550; Alexa-Fluor 555 and -TUNEL was BP 420-480 + BP 495-620; and Alexa-Fluor 647/TO-PRO-3 with BP 570-620 + LP 645. Data from the Airyscan detector was first processed in Zen Black to improve spatial resolution by applying a Wiener filter and pixel re-allocation. Further image processing was then performed on these data.

Confocal mode: Immunofourescence data was collected using a Zeiss LSM880 equipped with Zen Blue and Black software. Using either a Plan-Apochromat 63x / 1.4 oil or Plan-Apochromat 40x / 1.3 oil objective. Samples were either excited with visible light lasers (488nm, 561nm or 633nm), or a UV-laser (405nm) corrected with a collimator. Visible light lasers were cleaned up by a 488/561/633 beamsplitter and UV-light by a 405nm beamsplitter. Emission filters for BP 420-480, BP 495-550, BP560-620 and 645-754 were used for detection of DAPI, Alexa 488, Alexa 555/TUNEL, Alexa 647/TO-PRO-3 633 signal respectively.

3.17 Analysis

3.17.1 Imaris Surface segmentation

Surface segmentation using Imaris 9.0.2 (Bitplane AG) was carried out to determine TOPO II and ACA sum and peak fluorescent intensities. Images acquired by confocal

microscopy were loaded into the Imaris software. Chromosomes on the same slide were subject to the same thresholding and same surface detail size. The 'surface segmentation' function was selected and the surface detail size was selected based on measurements of the size of the region of interest. A fluorescence intensity threshold was set to include the region of interest being investigated. This was then maintained for all subsequent oocytes analysed on that slide. If regions of interest from two separate surfaces were touching, they could be cut using the 'cut surface' function under the edit tab on the surface menu. Data was exported as excel files using the *Statistics* tab with the *Detailed -> all values* drop down selected.

3.17.2 Volocity

Volocity Version 6.1.1 (PerkinElmer) was used for the purposes of calculating the sum fluorescence intensity within a primordial oocyte as well as the co-localisation between two markers in the primordial nucleus.

Sum Fluorescence Intensity Calculation

Images were loaded into the Volocity programme and the measurement tab selected. Regions of interest (ROI) were drawn free-hand around the primordial oocyte nucleus in the xy plane excluding (as best as possible) any surrounding granulosa cells. The region was then clipped in z-plane by selecting *Edit -> ROI -> Shrink.* To calculate the sum fluorescence intensity for each channel of interest the following parameters were selected:

- **Find Object**:

    Channel – *Primary channel of immunofluorescence marker being analysed. Threshold set per slide and kept consistent between primordial-stage oocytes analysed.*

    - **Clip to ROI** - *This ensures measurements are only for values within the region of interest.*
    - **Separate Touching objects** - *This allows for distinguishing of individual foci or structures in the image. Object size guide based on size of object of interest.*

This step is then repeated for TO-PRO-3. Finally the **Exclude Non-Touching** parameter was selected. This ensures that only the primary channel of interest touching the TO-PRO-3 signal is selected.

47

Co-localisation analysis

Regions of interest were drawn as in the previous section. The 'Colocalization' tab was selected. Channel 1 was set to TO-PRO-3 and Channel 2 the protein of interest. Thresholds using the same settings for each oocyte were then set to exclude background fluorescence and the "Pearson's Correlation" values under the "Threshold statistics" were recorded.

3.17.3 Linescan analysis

Confocal images were loaded in to ImageJ and the best focus on the Z-stack was selected. The line drawing tool was selected and set to a thickness of 20. This can vary but was kept consistent for each set of experiments. Lines were drawn straight across the region to be analysed and the graph of fluorescence intensity produced using an in house macro (M. Lamb, Institute of Genetic Medicine, Newcastle University). Unless specified, individual thresholds were set for each channel of interest and the area under the curve was calculated using the code

$$(A_1+A_2)/2*(D_1-D_2)$$

Were A is the fluorescence intensity value, and D is the distance value. The sum of the area under the curve values was calculated and this value was used for each linescan.

3.18.4 Inter-centromere distance measurement calculation

Lines were drawn through sister-centromeres using the line drawing ROI tool on ImageJ and the fluorescence intensity graph plotted. The values for the graph were then saved as .txt files. Distances were calculated using Extrema^{TM} software (V. Glenis; School of Civil Engineering and Geosciences, Newcastle University).

3.18 Western blotting

HeLa cells and mouse fibroblast pellets were treated with RIPA buffer (Life Technologies Limited, 89900) supplemented with Halt protease inhibitor to digest the cells (Life Technologies Limited, 78425). This was done by adding the RIPA buffer to the cell pellet on ice and pipetting the solution up and down to break up the cells before storing them at -80°C. Prior to running the lysate on a gel, samples were heated to 95ºC for 5 minutes in sample buffer to denature the proteins.

Cell lysate was then loaded in to a pre-cast Amersham ECL gel 4-12% (VWR international, 28-9898-06 *discontinued*) and ran on an Amersham ECL gel box for 95 minutes at 160V. After this the gel was sandwiched with 0.45µm PVDF transfer membrane (Thermo scientific, 88518), card, and sponges soaked in transfer buffer (see 3.21). Transfers were carried out at 100V for ~100 minutes in a transfer box inside a polystyrene box filled with ice. The success of the protein transfer was qualified using Ponceau S stain (Sigma Aldrich, 7170). This turned the protein bands on the transfer paper dark red if proteins had been transferred.

The tranfers were then blocked in a 5% milk solution, made up in wash buffer, for 1 hour before being incubated overnight in primary antibody at 4°C. Residual primary antibody was washed off using 3 x 5 minutes washes of PBS-T (PBS 0.1% Tween) and the transfers were incubated with secondary antibody for 1 hour. This was washed again using 3 x 5 minutes washes of PBS-T. Pierece ECL plus western blotting substrate (Thermo Fisher Scientific, 32132) was made up and added to the transfer membrane for 5 minutes. Any excess was dabbed off and the blot was then wrapped in plastic and kept in the dark.

To capture the results a single sheet of CL-XPosure™ film (Fisher Scientific, 10137683) was placed in a dark box along with the parafilm wrapped transfer. This was then developed through a tabletop processor (Konica Minolta, SRX-101A).

3.19 Statistics

Statistic were carried out using GraphPad prism software (GraphPad Software, Inc., USA). Normal distribution of data was assessed using either a D'agostino-Pearson omnibus normality test or a shapiro-Wilk tests depending on the number of samples. The significance of the difference in normally distributed data was then carried out using either an unpaired t-test or a one-way ANOVA with post hoc Tukey test. Non-normally distributed data was assessed through use of Mann-Whitney U test or a Kurskal-Wallis test with a post hoc Dunn's multiple comparison test.

3.20 Antibodies and dyes

Table 5: Antibodies

Primary	Source	Dilution	Secondary	Source	Dilution
Rabbit-anti-REC8	S Keeney (gift)	1:200	Goat-anti-rabbit Alexa Fluor 488	Fisher Scientific UK – 10729174	1:400
Rabbit-anti-human REC8	JL Barbero (gift)	1:50	Goat-anti-rabbit Alexa Fluor 488 or 555	Fisher Scientific UK – 10729174 Or Life Technologies Ltd - 21429	1:400
Rabbit-anti-Histone H3	Abcam Ab1791	1:200	Goat-anti-rabbit Alexa Fluor 488	Fisher Scientific UK – 10729174	1:800
Mouse-anti-Histone H2B	Abcam Ab52484	1:50 and 1:100	Goat-anti-mouse Alexa Fluor 488	Life Technologies Ltd – A11001	1:800
Mouse-anti-MYC Tag, clone 4A6, Alexa Fluor 488 conjugate	Millipore UK Ltd - 16-224	1:50	N/A	N/A	N/A
Rabbit-anti-SMC3 [EPR7984]	Abcam Plc - Ab201542	1:25	Goat-anti-rabbit Alexa Fluor 488 or 555	Fisher Scientific UK – 10729174 Or Life Technologies Ltd - 21429	1:400

Rabbit-anti-H3K9me3	Millipore UK Ltd – 07-442	1:50 (Cryosections) or 1:100 (chromosome spreads)	Goat-anti-rabbit Alexa Fluor 488	Fisher Scientific UK – 10729174	1:400 or 1:800
Human autoantibody against centromeres (CREST)	Cellon - HCT-0100	1:50	Goat-anti-human Cy5	Jackson Immuno 109-175-003	1:400
Purified Human-anti-centromere antibody (ACA)	Buck and Hickman – 15-235-0001	1:50	Goat-anti-human Alexa Fluor 555	Life Technologies Ltd - 21433	1:400 or 1:800
Rabbit-anti-Topoisomerase II [EPR5377] (Alexa Fluor® 647)	ABCAM Plc - ab200993	1:50	N/A	N/A	N/A
Rabbit-anti-RAD21	ABCAM Plc – ab992	1:200	Goat-anti-rabbit Alexa Fluor 488	Fisher Scientific UK – 10729174	1:800
Rabbit-anti-SGO1	JL Barbero (gift)	1:50	Goat-anti-rabbit Alexa Fluor 488	Fisher Scientific UK - 10729174	1:400
Rabbit-anti-Separase	Abcam Plc – ab52158	1:50 (paraffin wax Sections)	Goat-anti-rabbit Alexa Fluor 555	Life Technologies Ltd - 21429	1:800

		1:500 (Western Blotting)	goat-anti-rabbit IgG H+L (HRP)	Abcam Plc – ab6721	1:10000
Mouse-anti-DDX4	Abcam Plc – ab27591	1:50	Goat-anti-mouse Alexa Fluor 488	Life Technologies Ltd – A11001	1:800

Table 6: Blocking peptides, dyes and assays

Dye/Assay/Blocking peptide	Source	Dilution
TO-PRO-3	Thermo Fisher Scientific Ltd – T3605	1:1000 (diluted in 1xPBS)
Separase blocking peptide	Abbexa – abx161616	1:5 I.F staining 1:50 western blot
In situ cell death detection kit, TMR red	Roche Diagnostics Ltd – 12156792910	Instruction on kit (Diluted in PBS/0.02% Trition/0.02% Tween)

3.21 Reagents

Acid Tyrodes (100ml):

0.8g NaCl

0.02g KCl

0.024g CaCl.2H$_2$O

0.01g MgCl2.6H$_2$O

0.1g glucose

0.4g polyvinylpyrrolidone

Dissolve components in 90ml with MilliQ water. Adjust pH to 2.5 with 5M HCl and make to 100ml with autoclaved MilliQ water. Filter sterilise and make aliquots of 200µl.

Cell Lysis Buffer 200ml:

20ml 1M Tris-HCl (pH8.5)

100ml 10mM EDTA

2ml 20% SDS

0.234g NaCl

Make up to volume of 200ml with Milli-Q H2O

Citric acid buffer solution (11mM) (pH 6.0):

2.1g Citric Acid (Sigma Aldrich - C0759)

1L ddH$_2$O

pH using 5M NaOH

0.5ml of 20% Tween (if cytoplasm is needing removed)

1x PBS

100ml of 10x PBS solution (Melford Laboratories Ltd – P3206) diluted in 900ml of ddH$_2$O

1% PFA (25ml):

0.25g Parformaldehyde (Powder)

22.5ml of MilliQ ddH$_2$O

175µl 20% Triton X-100 (0.14% final concentration)

150µl 0.5M DTT (3mM final conc)

500µl Aliquoted into eppendorfs and frozen at -20°C for long term storage.

4% PFA (50ml)

2g PFA (powder)

0.5ml 1M NaOH

5ml PBS 10x (Melford Laboratories Ltd – P3206)

40ml ddH$_2$O

Adjust pH to 7.4 using 1M HCl. Make volume up to 50ml and filter through 0.45µm filter and freeze at -20°C in 1ml aliquots.

1xTBS

100ml 1M Tris-HCl pH 7.5

30ml 5M NaCl

870ml ddH$_2$O

5x Running Buffer (1 litre):

15.1g Tris

72g Glycine

5g SDS

Dilute to 1x in ddH$_2$O to use

1xTransfer Buffer (1 litre):

14.4g Glycine

3g   Tris

200ml Methanol (add last)

800ml dH$_2$O

30ul   10% SDS

1x Wash Buffer (1 litre):

5ml   1M Tris (pH 7.5)

2.92g NaCl

500ul Tween 20 (0.05% final conc)

Make up to 1L with ddH$_2$0

Chapter 4. Results: Quantification of chromosome associated proteins

Immunofluorescence imaging can be a highly effective tool in assessing cell state-dependent changes in protein expression and localisation. To ensure accurate representation of any differences in protein expression, it is important to minimise experimental variations that may obscure biological findings. There are various practical steps that can be taken to do this including having both the control and experimental samples on the same slide and imaging them on the same day to account for microscope laser power output.

While these steps can help minimise variation, ideally there would be a standard marker that could be used to compare between samples. The use of a standard for normalisation is common practice in western blotting and immunofluorescence analysis. However, finding a suitable standard for normalisation is not trivial as ageing is known to impact on many aspects of the cell (Lopez-Otin et al., 2013). This has made it difficult to find an appropriate standard for normalisation in my studies looking at oocyte chromosome spreads from young and aged mice. The most commonly used standards in these experiments are anticentromere antibodies (ACA). These were first discovered in the sera of patients suffering from a form of sclerosis called the CREST syndrome (Moroi et al., 1980). These antibodies predominantly mark the centromeric proteins CENP-A, CENP-B and CENP-C (Earnshaw and Cooke, 1989). However, it has been reported by our group and others that immunofluorescence for ACA declines significantly with age (Lister et al., 2010, Yun et al., 2014). This can mask any measurable changes in chromosome-associated proteins of interest. To address this long-standing issue I have sought to find an alternative marker for studying age-related changes in chromosome associated proteins in oocytes. A prime candidate for this is the decatenation enzyme topoisomerase II (TOPO II), which is necessary for DNA condensation and separation in meiosis (Lee et al., 2006, Li et al., 2013).

In this chapter I will establish an easy to use and reproducible method using TOPO II to help with quantification of chromosome bound proteins in aged mouse oocyte studies.

4.1 Defining criteria for a good standard.

Before determining if a marker is appropriate for ageing studies, it was important to establish criteria that would make it a useful tool for quantification. To address this I constructed a checklist to determine the suitability of potential candidates. The criteria included whether: (i) its localisation is static during meiosis, (ii) it allows for segmentation of the chromosome (distinguishing different structures on the chromosome), (iii) it can be used to determine chromosome architecture (number of crossovers, number of single sisters, separation of sister centromeres) and (iv) the marker is commercially available and compatible with multi-colour imaging with other antibodies.

Based on these criteria several potential candidates can be excluded. Table 7 shows candidates that were excluded and the reasons for their exclusion.

Table 7: Disqualified Candidates for immunofluorescence quantification

Candidate marker	Reasons excluded
Histone H3	Does not show staining to help distinguish different areas of chromosome. H3 is thought to reduce with aging (Lopez-Otin et al., 2013)
Histone H2B	Could not find suitable antibody
Condensin	Localisation on chromosome changes during meiosis (Lee et al., 2011)
TO-PRO-3	Does not stain in chromosome spreads
DAPI	Required for finding chromosomes on slide.

While the condensins would have been useful in determining aspects of chromosome architecture, they are dynamic during meiosis (Lee et al., 2011). This renders them inappropriate as their localisation will be altered depending on what stage of meiosis the oocyte is at.

While I have used the DNA label TO-PRO-3 (a monomeric cyanine stain which stoichiometrically labels DNA) for immunflourescence normalisation in ovarian

cryosections it does not label DNA in chromosomes spreads (Bink et al., 2001). DAPI cannot be used as it is required for recognition of chromosomes on the slide.

My search for an appropriate marker led me to the decatenation enzyme TOPO II. This antibody is raised against TOPO IIβ but was determined by the manufacturer to have some cross-reactivity with TOPO IIα during the course of my project. This antibody is commercially available from abcam and so will be easy to acquire for other researchers.

First I sought to investigate whether TOPO II localisation is dynamic, or remains constant during progression through the meiotic divisions. To determine whether TOPO II localisation changed between the two meiotic divisions, I prepared air-dried chromosome spreads of oocytes from CD1 mice at early and late MI and at MII. These spreads were immunolabelled with TOPO II and DNA was stained using DAPI. Imaging was carried out using confocal microscopy with airsyscan. This provides greater resolution of samples through the use of a serial array of 32 GaAsP detectors, which collects all emitted photons and reassigns them to their correct position. This revealed that TOPO II is enriched at the pericentromere but also localises to chromosome arms, albeit with fainter staining (Figure 4.1). In addition, TOPO II localisation does not appear to change between MI and MII.
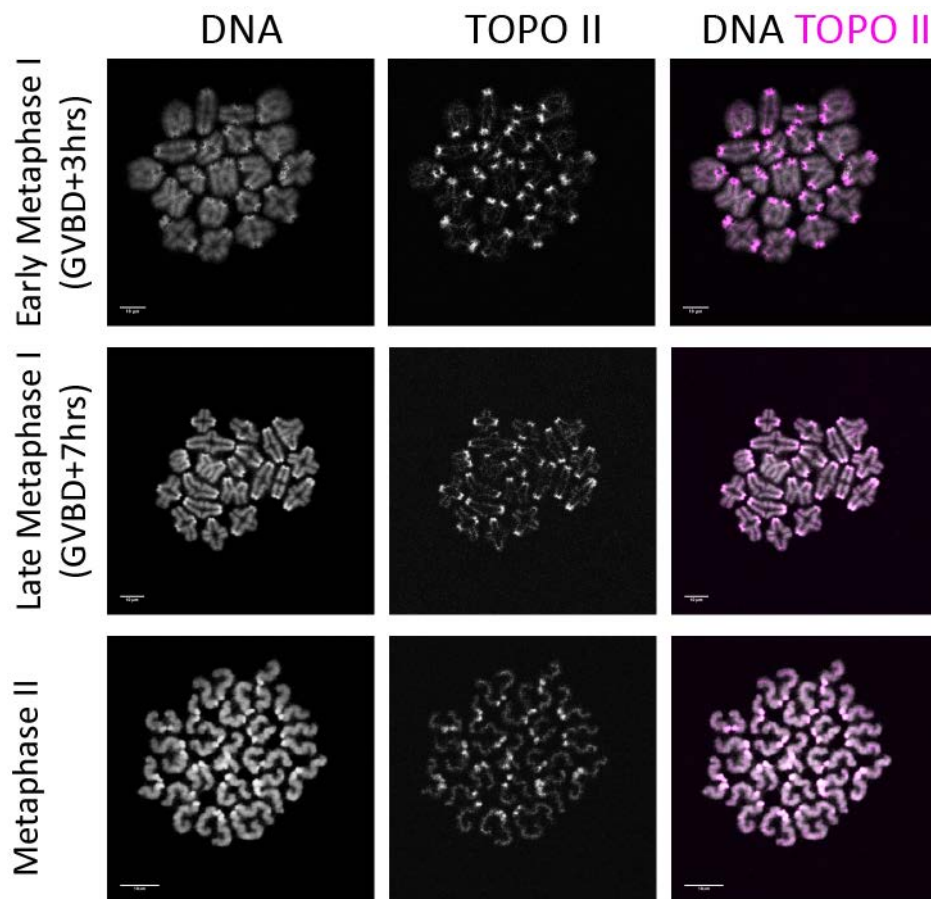
Figure 4.1 TOPO II localisation remains consistent throughout meiosis. *Images of 2 months old CD1 mouse early MI (GVBD+3hours), late MI (GVBD+7hours) and MII chromosome spreads immunolabelled for TOPO II. TOPO II remains enriched at the pericentromere with fainter staining along the chromosome arm. Scale bar 10µm.*

I next sought to investigate whether TOPO II can be used for segmentation of bivalent chromosomes allowing for recognition of distinct areas such as the pericentromere, axis or chromosome arm. To do this I prepared chromosome spreads of oocytes from C57BL/6 mice during M Phase of meiosis I (GVBD +5hrs) and immunolabelled them for SMC3 and TOPO II. Due to clear localisation patterns it is possible to distinguish different sections of the chromosome based on the intensity of staining (Figure 4.2a). This makes it suitable for segmentation to measure immunofluorescence (I.F) signals in different chromosomal regions (Figure 4.2b).
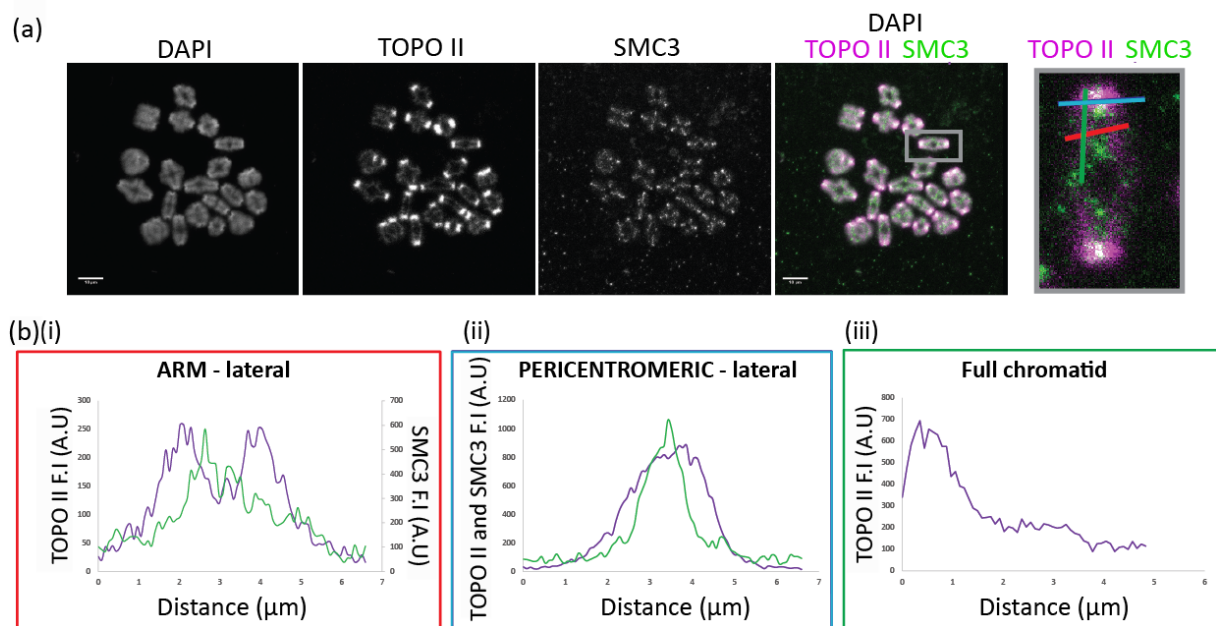
Figure 4.2 TOPO II can be used for segmenting different sections of bivalent chromosomes. *(a) Representative image of a MI chromosome spreads from a 2 month old C57BL/6 mouse. Scale bar 10µm. Inset (grey box) shows TOPO II and SMC3 staining for an individual bivalent chromosome rotated 90º. Red, blue and green lines correspond to graphs in same coloured boxes in (b). (b) Shows graphs produced from linescans over (i) bivalent arm-lateral (red) (ii) pericentromeric lateral (blue) and (iii) full chromatid (green).*

Finally, I wanted to determine whether TOPO II immunolabelling can help in detecting changes to bivalent architecture, such as the number of chiasma on a chromosome. This is important as it has been established from studies in cases of trisomy that the risk of meiotic segregation errors is correlated with the number and chromosomal localisation of the chiasma. Absence of chiasma, followed by sub-telomeric is the greatest risk of causing aneuploidy (Nagaoka et al., 2012). Observations in MI spreads of 2 month old C57BL/6 mice immunolabelled with TOPO II show that TOPO II immunolabelling helps to distinguish chiasma number as well as proximity to the telomere and pericentromere (Figure 4.3).
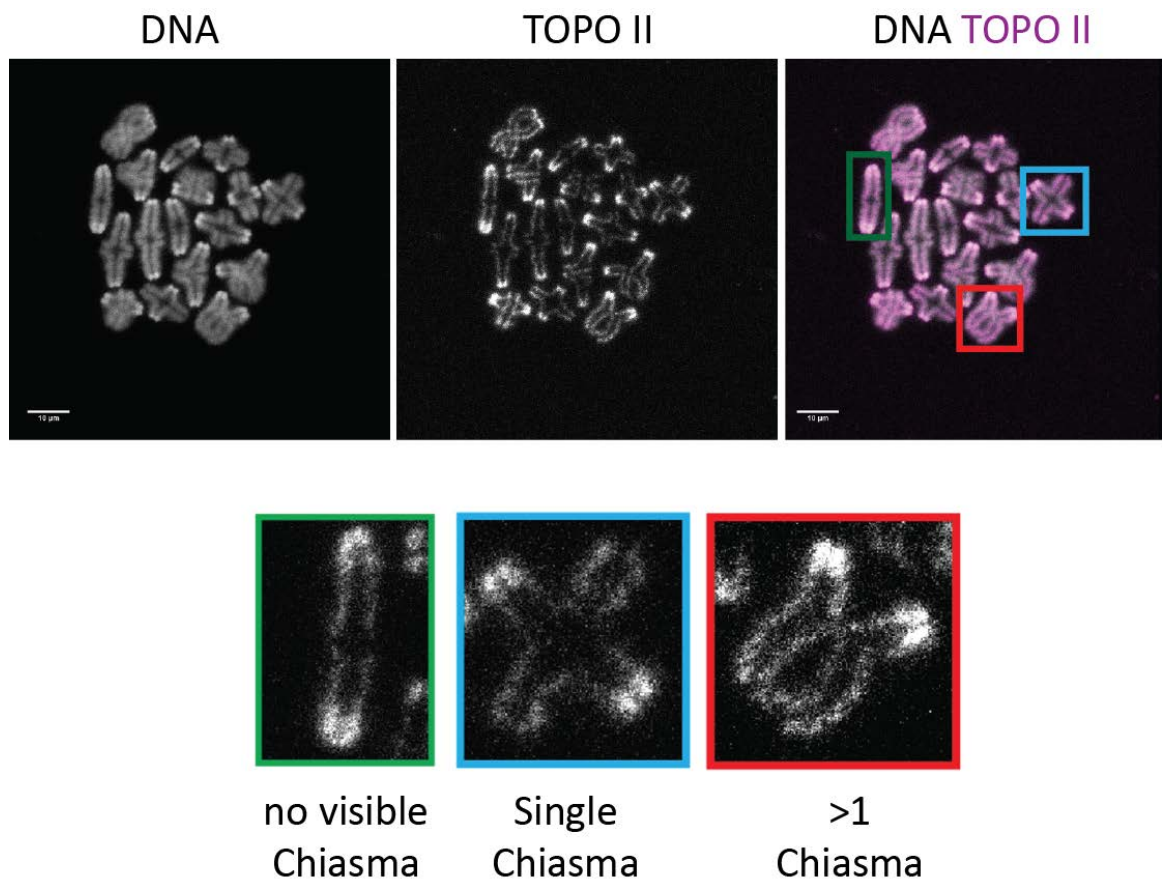
Figure 4.3. TOPO II is useful for determining bivalent chromosome architecture.
Representative image of MI oocyte chromosome spreads immunolabelled for TOPO II. Boxes show examples of no visible chiasma (green box), single chiasma (blue box) and >1 chiasma (red box). 10μm scale bar.

Attempts to establish if TOPO II could be used for measuring distances between centromeres suggests it cannot be used for this purpose. This was due to difficulties in consistently resolving the pericentromeric staining on individual sister pericentromeres. This is in part due to the TOPO II used in this work being conjugated with Alexa Fluor 647 which has a low resolution due to its high wavelength. It may be possible to improve this by using a shorter wavelength fluorescence tag however this would remove the possibility of imaging another protein of interest at a better resolution. In any case, it would in theory, be possible to use ACA to measure inter-kinetochore distance, as this does not depend heavily on the strength of the I.F signal.

Importantly for reproducibility, the TOPO II antibody used in this work is available commercially in a conjugated form. This means it can be used in conjunction with other antibodies regardless of what species they are raised in.

In summary, TOPO II satisfies the criteria of (i) consistent localisation, (ii) chromosome segmentation and (iii) resolution of chromosome architecture. (iv) This antibody is also commercially available in a conjugated form. Measuring the distance between sister centromeres is the only criteria that TOPO II does not satisfy. As there was no other clear candidate that would satisfy all these criteria, I proceeded to investigate whether TOPO II provides an effective standard for normalisation of proteins of interest in ageing experiments.

4.2 TOPO II is an effective marker for normalising chromosome-bound proteins in ageing studies

The most important aspect in determining whether TOPO II can be used for normalisation in aged mouse experiments is whether its expression changes with ageing. To address this I prepared M phase chromosome spreads at GVBD+5hrs using oocytes from 2 month (young) and 15-16 month (aged) old C57BL/6 mice. Oocyte chromosome spreads from young and aged mice were prepared on the same slide and immunolabelled with antibodies directed towards TOPO II and ACA. Chromosomal DNA was stained using DAPI. Chromosomes were imaged by confocal microscopy (Fig 4.4). Of the spreads prepared from oocytes from young (n = 24 oocytes from 3 mice) and aged mice (n =26 oocytes from 4 mice), it was evident by eye that ACA is noticeably reduced. This is consistent with previous findings (Lister et al., 2010, Yun et al., 2014). By contrast, TOPO II appears to show similar intensity at the pericentromeres between young and aged mice. However, TOPO II staining on chromosome arms appears much fainter in the aged mice, suggesting that this cannot be used for quantitative analysis.
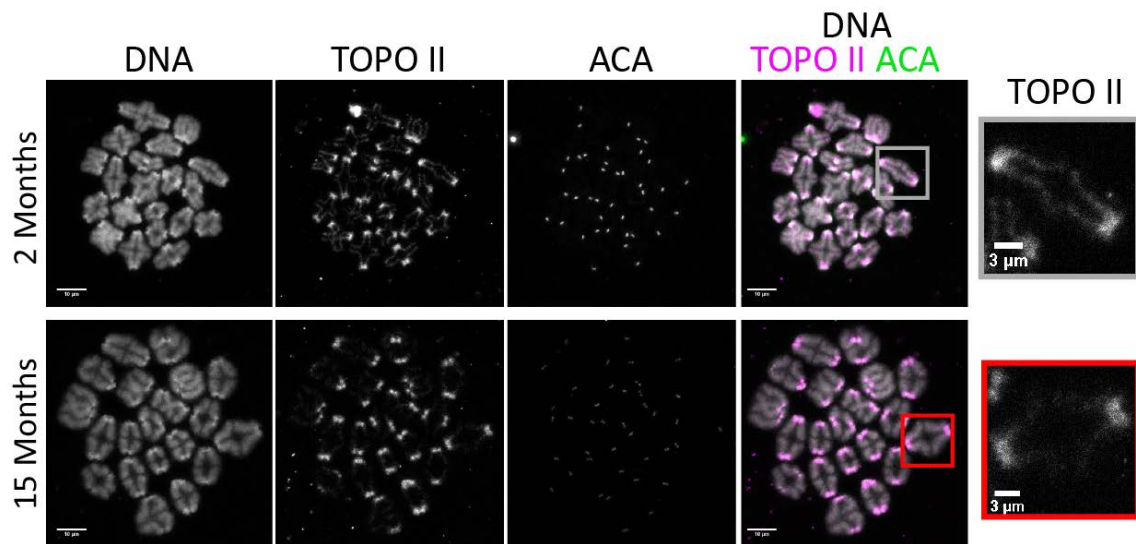
Figure 4.4 TOPO II appears not to be reduced at the pericentromere in aged mice MI air-dried chromosome spreads. *Representative images from air-dried MI chromosome spreads from 2 month and 15 month old C57BL/6 mice immunolabelled for TOPO II and ACA with the DNA stained using DAPI. Scale bar 10 µm. Inset shows individual TOPO II staining in MI bivalents. Individual chromosomes from young and aged mice in the grey and red box respectively. Scale bar 3 µm. (young n = 24 oocytes from 3 mice; aged mice n =26 oocytes from 4 mice).*

To address whether TOPO II immunofluorescence signal intensity changes with ageing, I established a data acquisition pipeline in Imaris using surface segmentation to segment pericentromeric TOPO II and ACA (Figure 4.5(a)). To create regions of interest (ROI) using surface segmentation, 3-dimensional z-stacks acquired by confocal microscopy were uploaded to the Imaris programme. To maintain a consistency between the number of z-stacks and to prevent measurement of out of focus signal, images were cropped so that only the 3 most in-focus z-steps would be measured. Immunofluorescence intensity and surface size thresholds were set and used to create the ROI for ACA and pericentromeric TOPO II (Figure 4.5(b) and 4.5(c)). This threshold was kept consistent for all chromosome spreads on the same slide. TOPO II signals from separate pericentromeres that were touching were separated using the surface cutter tool. Figure 4.5 shows representative examples of the data acquisition pipeline used.

63
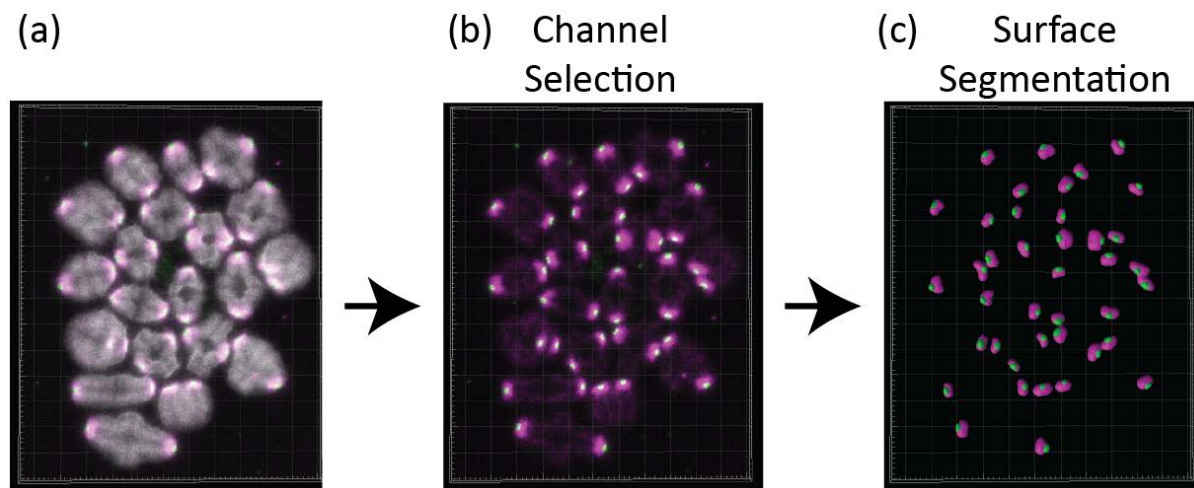
Figure 4.5 Imaris analysis of air-dried chromosome spreads (*a*) *confocal acquired images of air-dried chromosome spreads were loaded onto Imaris software and (b) the TOPO II and ACA channel were selected. (c) Segmentation was carried out using the surface detection tool to give regions of interest for the TOPO II and ACA.*

To compare TOPO II staining in oocytes from young and aged females I measured the peak fluorescence intensity (F.I) and the sum F.I for TOPO II. Peak fluorescence is the intensity of the brightest pixel in the ROI, whereas sum F.I is the summation of all the F.I values for each voxel in the region of interest. This information could be recalled from Imaris in an excel spread sheet showing this information for each channel per ROI (Figures 4.6 and 4.7). Comparisons of the spread in the data showed that within oocytes, as well as within ages, the sum F.I values had a greater variability than the peak F.I.

	2 MONTHS			15-16 MONTHS		
experiment	1	2	3	1	2	3
no. oocytes	7	10	7	7	9	10
no. mice	1	1	1	1	2	1
no. slides	2	3	2	2	3	2
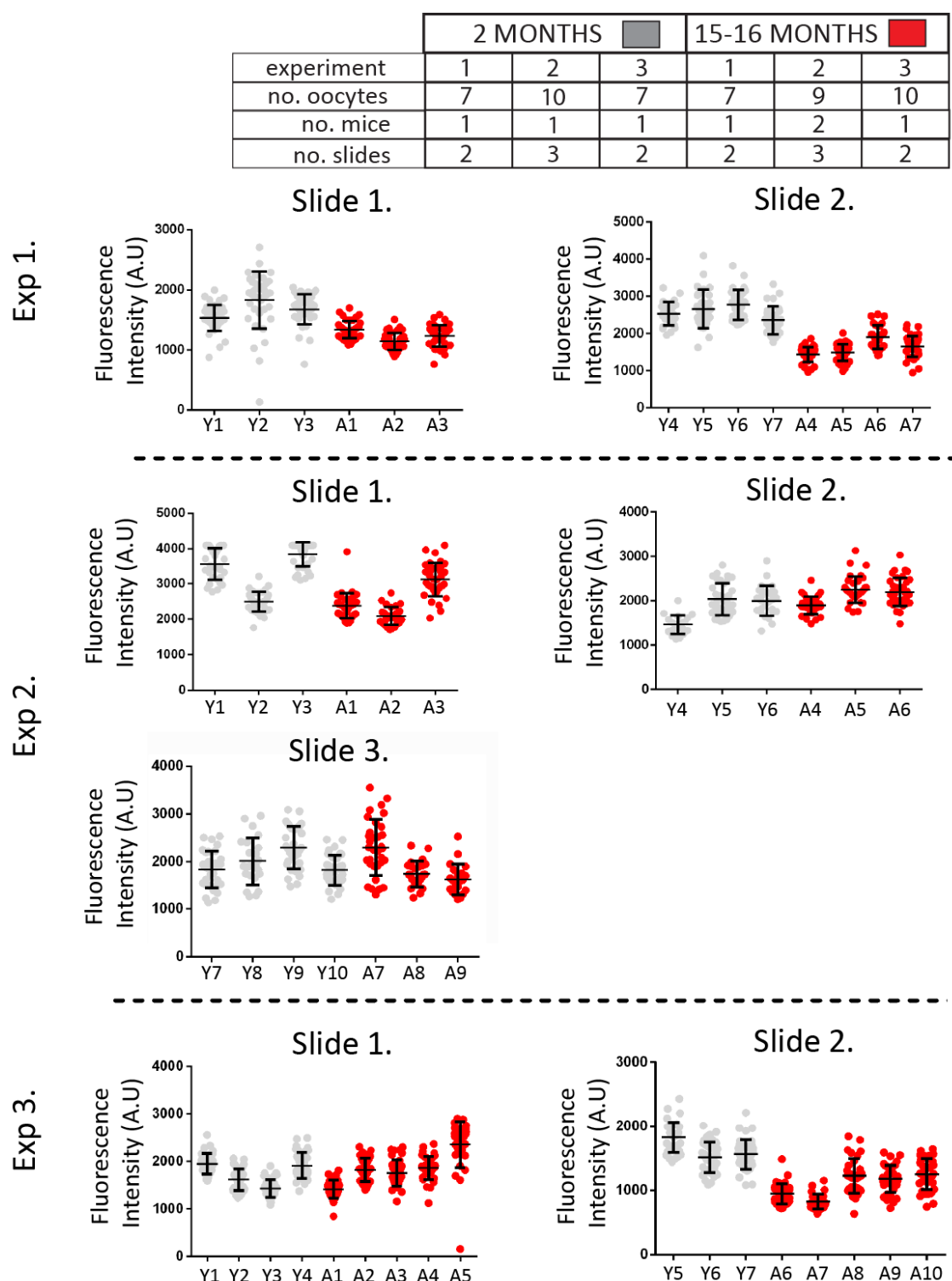
Figure 4.6 Peak TOPO II fluorescence intensity values for each oocyte from young and aged mice. *Graphs showing peak fluorescence intensity of TOPO II in young and aged C57BL/6 oocytes from air-dried MI chromosome spreads. Each graph represents a slide with experimental repeats separated by the dotted line. Each data point represents the peak F.I of TOPO II for each segmented pericentromere. Error bars represent the mean ± s.d for each oocyte. Table contains the number of oocytes, slides and mice used per experiment.*

65
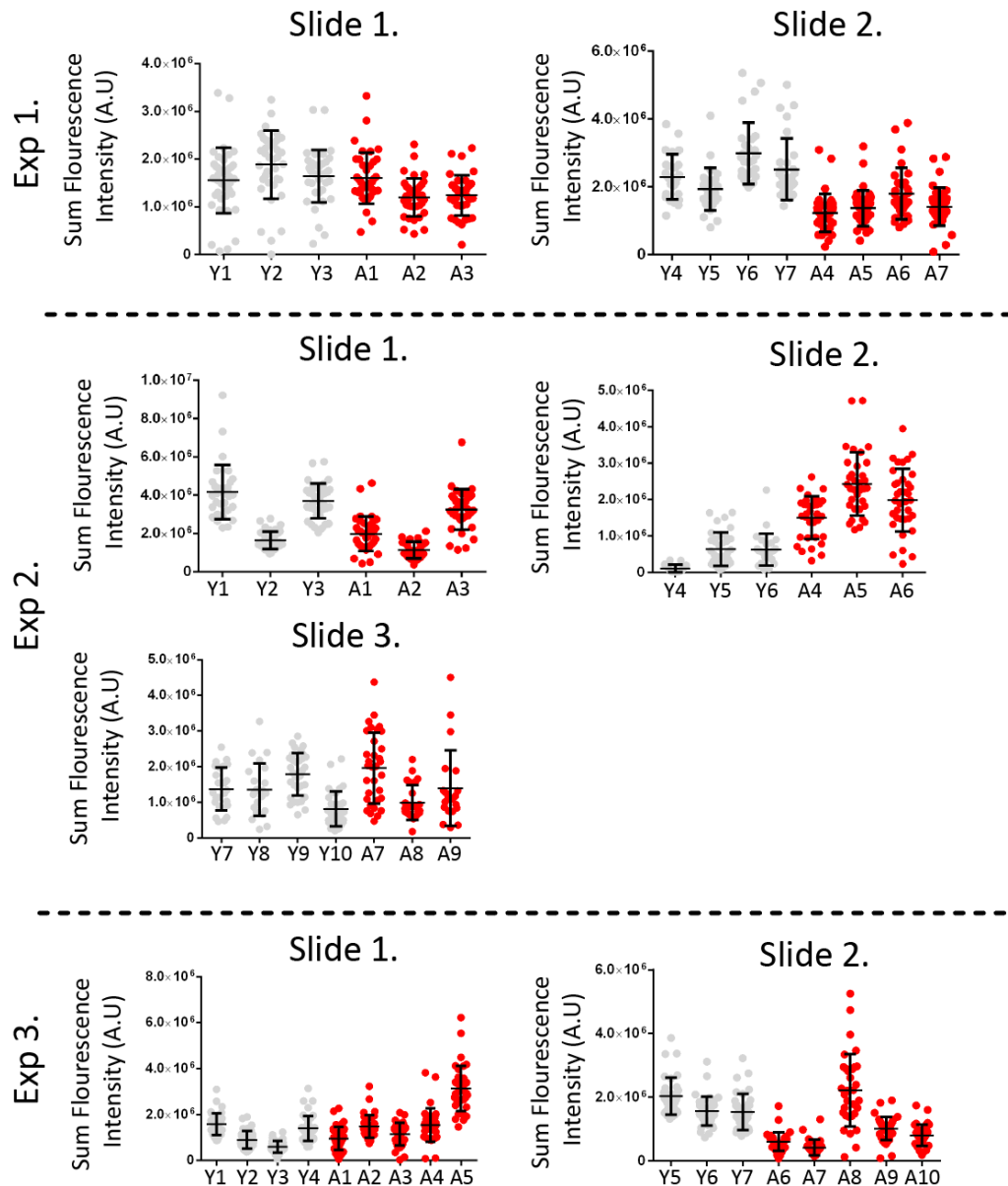
Figure 4.7 Sum TOPO II fluorescence intensity values for each oocyte from young and aged mice. *Graphs showing sum fluorescence intensity of TOPO II in young and aged mouse oocytes from air-dried chromosome spreads. Each graph represents a slide with experimental repeats separated by the dotted line. Each data point represents the sum F.I of TOPO II for each segmented pericentromere. Error bars represent the mean ± s.d for each oocyte. Table contains the number of oocytes, slides and mice used per experiment.*

66

To determine whether there is a significant difference between the peak F.I and sum F.I in the young and aged mice, the median value for each oocyte was taken and normalised to the average value of the 2 month old oocytes on the same slide (median pericentromere value per oocyte/ average of median for 2 month oocytes on slide*100) (young: 3 mice, 24 oocytes; aged: 4 mice, 26 oocytes) (Figure 4.8a and b). An unpaired t-test and a Mann-Whitney U test were used to compare the young and aged values for peak F.I and sum F.I respectively. This indicated that while there is a significant decrease (p=0.0062) in peak F.I there is no significant difference between young and aged for sum F.I (p=0.3279).

While these findings indicate that the peak F.I value for TOPO II declines with age but that the sum F.I does not, this is most likely a result of the variation seen with the sum F.I values for TOPO II. A point reflected in that the median value for the peak and sum F.I between ages is similar (peak F.I median value 2 month: 99.96%; 15-16 months: 77.04%; sum F.I median value 2 month: 98.47%; 15-16 months: 77.91%). As the sum F.I is dependent upon the area of the pericentromere in question, it is likely that differences in pericentromere size will generate a greater variation within and between oocytes.

I next determined whether TOPO II is a more appropriate tool for quantification than ACA based on comparisons of the peak and sum F.I for both (Figure 4.8). The results show that while TOPO II shows no significant difference for sum F.I, the Peak F.I for TOPO II and the sum and peak F.I for ACA are significantly reduced with age. (Peak F.I TOPO II p=0.0062; ACA p<0.0001 sum F.I: Mann-Whitney U test Topo II p=0.3279; unpaired t-test ACA p<0.0001). Importantly for normalisation, the median values for TOPO II is not as reduced (peak F.I: 2 month: 99.96%; 15-16 months: 77.04%; median value 2 month sum F.I: 98.47%; 15-16 months: 77.91%) as it is for ACA (median value 2 month sum F.I: 98.29% 15-16 months: 56.50%; peak F.I 2 month: 99.94%; 15-16 months: 65.70%). This suggests that TOPO II is a better tool for normalisation than ACA. The reduction in ACA with age also shows that the chromosome spreads being analysed are representative of what has previously been reported (Lister et al., 2010, Yun et al., 2014).
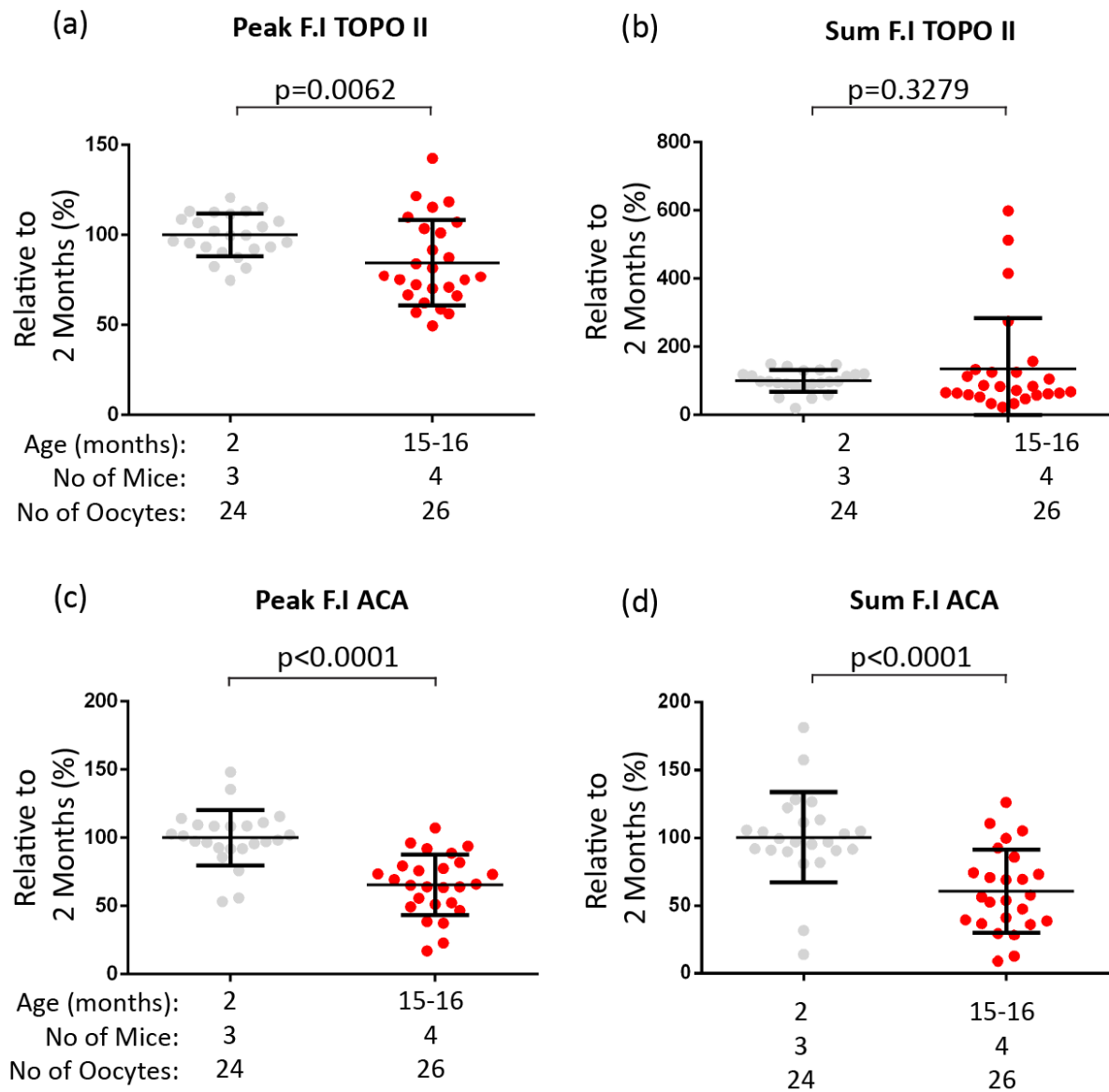
Figure 4.8 TOPO II is a more appropriate tool than ACA for quantification of chromosome-bound proteins in ageing studies. *Figure shows graphs of the median (a) peak fluorescence intensity and (b) sum fluorescence intensity of TOPO II and the median (c) peak fluorescence intensity and (d) sum fluorescence intensity of ACA in young and old mice per oocyte. Sum F.I for each oocyte median value was normalised to the average F.I of 2 month old mouse oocytes on the slide. Error bars represent the mean ± s.d for each age grouping. Mann-Whitney U tests revealed no significant difference between young and old (b) TOPO II for sum F.I (p=0.3574). Unpaired t-test showed a significant difference between young and old (a) peak F.I TOPO II (p=0.0062) and young and old (c) peak and (d) sum ACA (p<0.0001). (young n = 24 oocytes from 3 mice; aged mice n =26 oocytes from 4 mice).*

4.3 SMC3 appears to be reduced using Imaris surface segmentation, but less than would be expected on the basis of by eye observations

Next, I sought to determine whether Imaris surface segmentation using TOPO II as a normalisation tool can be used to determine depletion of cohesin subunits with age (Chiang et al., 2010, Lister et al., 2010). To do this I selected the universal cohesin subunit SMC3.

Representative examples of air-dried M phase (GVBD+5hrs) spreads showing immunolabelling for TOPO II and SMC3 with the DNA stained using DAPI indicate that, like REC8, SMC3 is also reduced with age (Figure 4.9) (young n = 24 oocytes from 3 mice; aged mice n =26 oocytes from 4 mice) (Chiang et al., 2010, Lister et al., 2010).
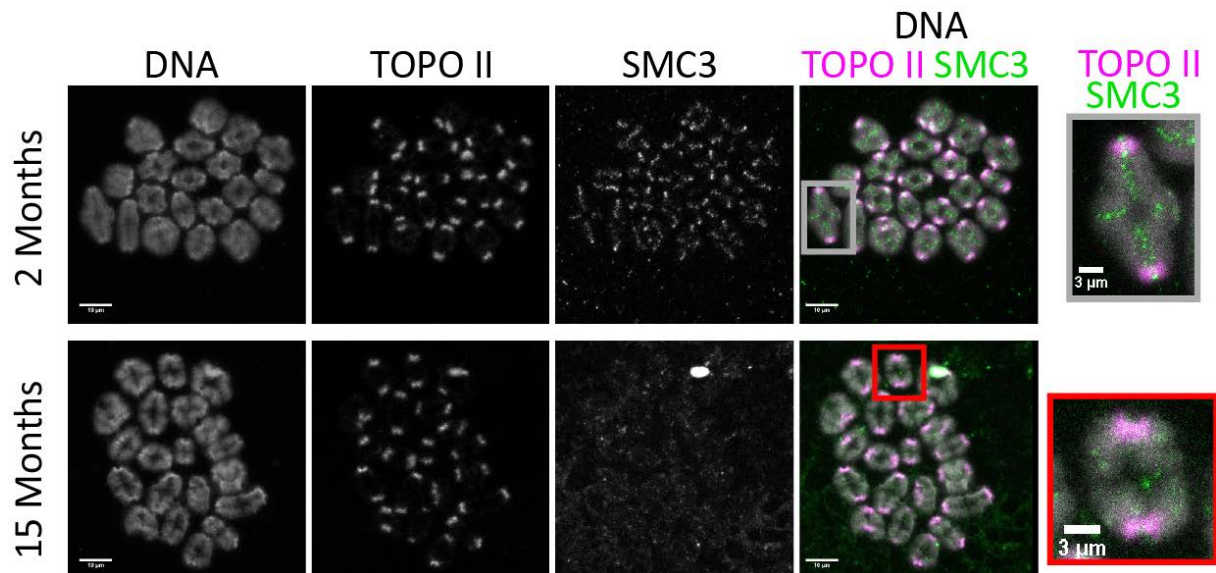
Figure 4.9 TOPO II appears unchanged while SMC3 appears to be completely absent by 15 months of age. *Representative images from air-dried MI chromosome spreads from 2 month and 15 month old C57BL/6 mice immunolabelled for TOPO II and SMC3 with the DNA stained using DAPI. Scale bar 10µm. Inset shows individual TOPO II and SMC3 staining in MI bivalents from young (grey box) and aged mice Scale bar 3µm (red box (young n = 24 oocytes from 3 mice; aged mice n =26 oocytes from 4 mice).*

To test whether TOPO II used with Imaris surface segmentation can be used to reliably measure levels of SMC3, I collected the sum and peak fluorescence intensity for SMC3 within the surface region segmented by the TOPO II pericentromere for

young and aged mouse oocytes (young: 3 mice, 24 oocytes; aged: 4 mice, 26 oocytes). The high level of variability in both TOPO II and SMC3 sum F.I (Figure 4.10) is noticeably reduced after ratioing the value (Figure 4.11). Peak F.I remains relatively more consistent in terms of both the individual values (Figure 4.12) and the ratioed values (Figure 4.13)
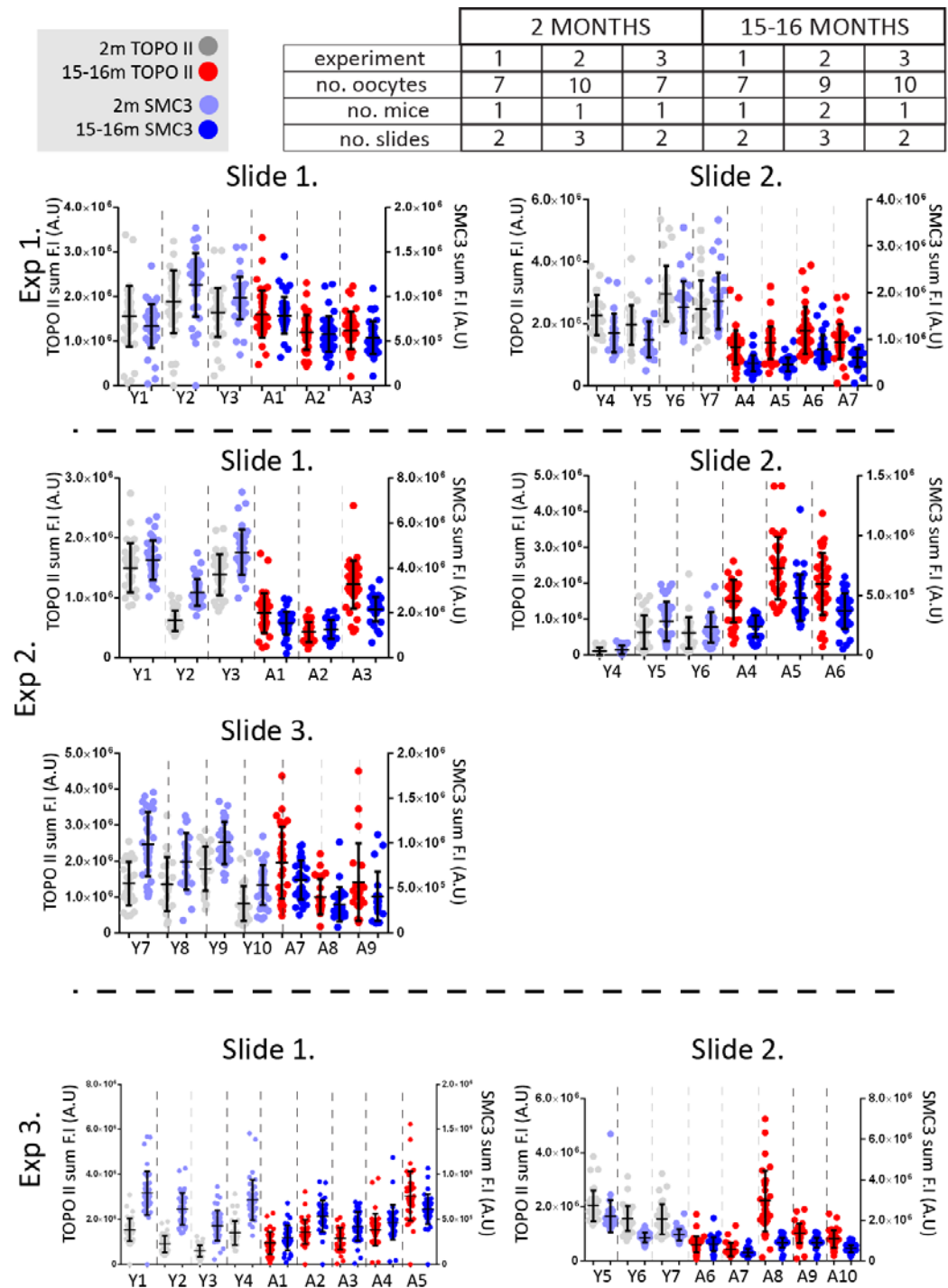
Figure 4.10 TOPO II and SMC3 Sum F.I values in young vs aged C57BL/6 females per oocyte. *Graphs showing sum F.I of TOPO II and SMC3 in young and aged mouse oocytes from air-dried chromosome spreads. Each graph represents a slide. Individual oocyte TOPO II and SMC3 values are separated by vertical dotted lines with experimental repeats separated by horizontal dotted lines. Each data point represents either the sum F.I of TOPO II for each segmented pericentromere or the sum F.I of SMC3 within that TOPO II region. Error bars represent the mean ± s.d for each oocyte. Table contains the number of oocytes, slides and mice used per experiment.*

		2 MONTHS			15-16 MONTHS		
experiment		1	2	3	1	2	3
no. oocytes		7	10	7	7	9	10
no. mice		1	1	1	1	2	1
no. slides		2	3	2	2	3	2

Figure 4.11 SMC3: TOPO II Sum F.I ratio in young vs aged C57BL/6 females per oocyte. *Dot plots showing the ratio of SMC3: TOPO II per segmented TOPO II pericentromere for young and aged mouse oocytes. Each graph represents a slide. Experimental repeats are separated by dotted lines. Each data point represents the ratio of sum F.I of SMC3 to TOPO II per pericentromere. Error bars represent the mean ± s.d for each oocyte. Table contains the number of oocytes, slides and mice used per experiment.*

72
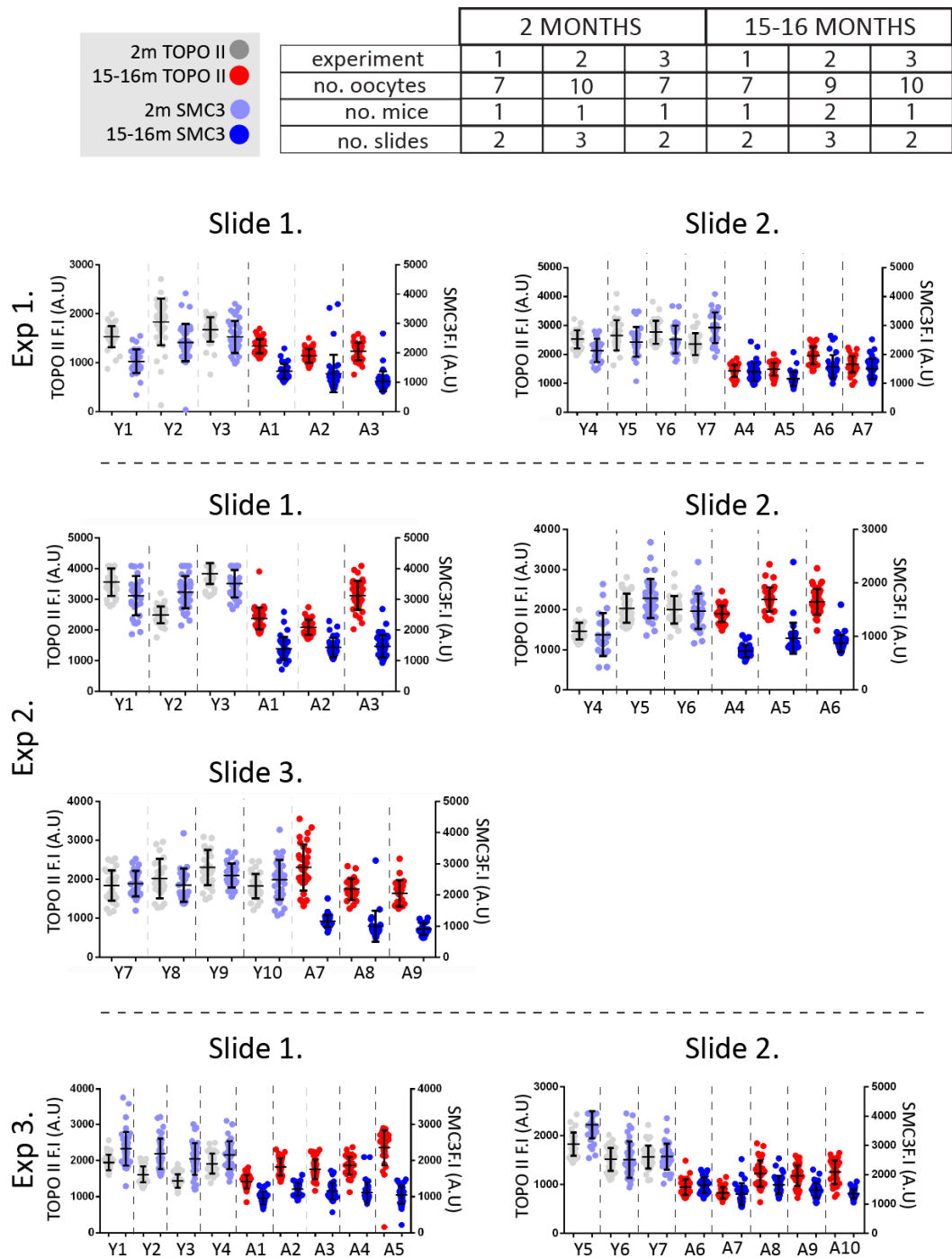
Figure 4.12 TOPO II and SMC3 Peak F.I values in young vs aged C57BL/6 females per oocyte. *Graphs showing peak F.I of TOPO II and SMC3 in young and aged mouse oocytes from air-dried chromosome spreads. Each graph represents a slide. Individual oocyte TOPO II and SMC3 values are separated by vertical dotted lines with experimental repeats separated by horizontal dotted lines. Each data point represents either the sum F.I of TOPO II for each segmented pericentromere or the sum F.I of SMC3 within that TOPO II region. Error bars represent the mean ± s.d for each oocyte. Table contains the number of oocytes, slides and mice used per experiment.*

	2 MONTHS			15-16 MONTHS		
experiment	1	2	3	1	2	3
no. oocytes	7	10	7	7	9	10
no. mice	1	1	1	1	2	1
no. slides	2	3	2	2	3	2

Figure 4.13 SMC3: TOPO II peak F.I ratio in young vs aged C57BL/6 females per oocyte. *Dot plots showing the ratio of SMC3: TOPO II per segmented TOPO II pericentromere for young and aged mouse oocytes. Each graph represents a slide. Experimental repeats are separated by dotted lines. Each data point represents the ratio of peak F.I of SMC3 to TOPO II per pericentromere. Error bars represent the mean ± s.d for each oocyte. Table contains the number of oocytes and mice used per experiment.*

74

As above (Figure 4.8), I combined the values for the ratios by taking the median value of per pericentromere ratios per egg and normalised it to the average of the median for the 2 month oocytes on the slide. The results indicates that SMC3 is significantly reduced in aged mouse oocytes compared to young when ratioed to TOPO II in both the peak and sum F.I (Figure 4.14)(peak F.I: unpaired t-test $p<0.0001$; sum F.I: Mann Whitney U-test $p<0.0001$).
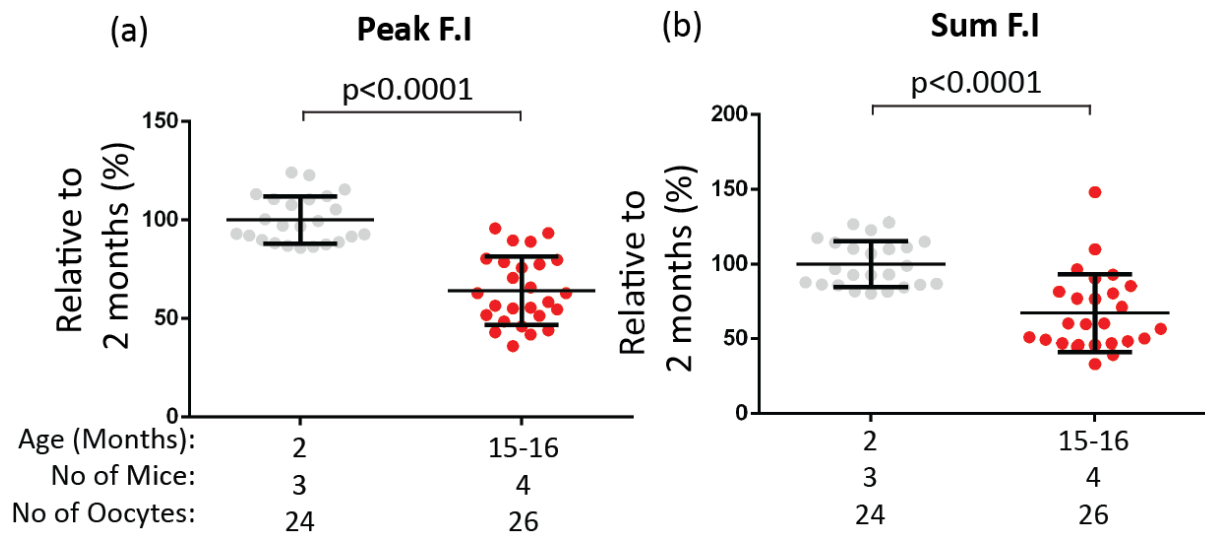
Figure 4.14 Using TOPO II for normalisation shows SMC3 is significantly reduced in aged mouse oocytes. *Figure shows graphs of the ratio of (a) peak F.I and (b) sum F.I of SMC3: TOPO II for young and aged mouse oocyte chromosome spreads. Each data point represents the median value of the SMC3: TOPO II ratio normalised to the mean of the median for the 2 month old mouse oocytes on that slide. Error bars represent the mean ± s.d for each age grouping. Mann-Whitney U tests and an unpaired t-test revealed a significant difference between young and aged mice for sum F.I and peak F.I respectively (p<0.0001) (young n = 24 oocytes from 3 mice; aged mice n =26 oocytes from 4 mice).*

4.4 Linescan analysis is a useful tool for quantification in chromosome spreads

While the data from the previous section (Figure 4.14) indicates that SMC3 is reduced with age, a comparison of the median values suggests a fold decline of 0.625 between young and aged mice. By eye observations of SMC3 would suggest a greater loss by 15 months. The high value for SMC3 at the pericentromere in aged mouse oocytes can be attributed to the Imaris surface segmentation tool. For the sum F.I Imaris compiles all the signal for SMC3 I.F. with no thresholding for background. This means that any background signal on that channel is also collected. As chromosome-bound SMC3 is only present in a small portion of the overall TOPO II signal, an ideal tool would allow for independent thresholding of both markers of interest. The presence of a signal on the chromosome arms for TOPO II in the younger oocytes causes difficulties in thresholding also. To ensure the arm staining is not included in the surface, a relatively high thresholds for TOPO II is required. This means excluding some pericentromeric TOPO II signal, in particular in the older oocytes.

The peak F.I is also problematic, as it does not distinguish between background and "true" SMC3 signal. This means that the value that is assigned as the peak F.I for SMC3 could in fact be from a background pixel.

To address these concerns I developed 'area-under the curve linescan analysis'. This involves using the line drawing tool on the free to download software ImageJ to produce a graph of immunofluorescence for each channel of interest that can be thresholded independently (Figure 4.15) (Macro developed by M. Lamb).
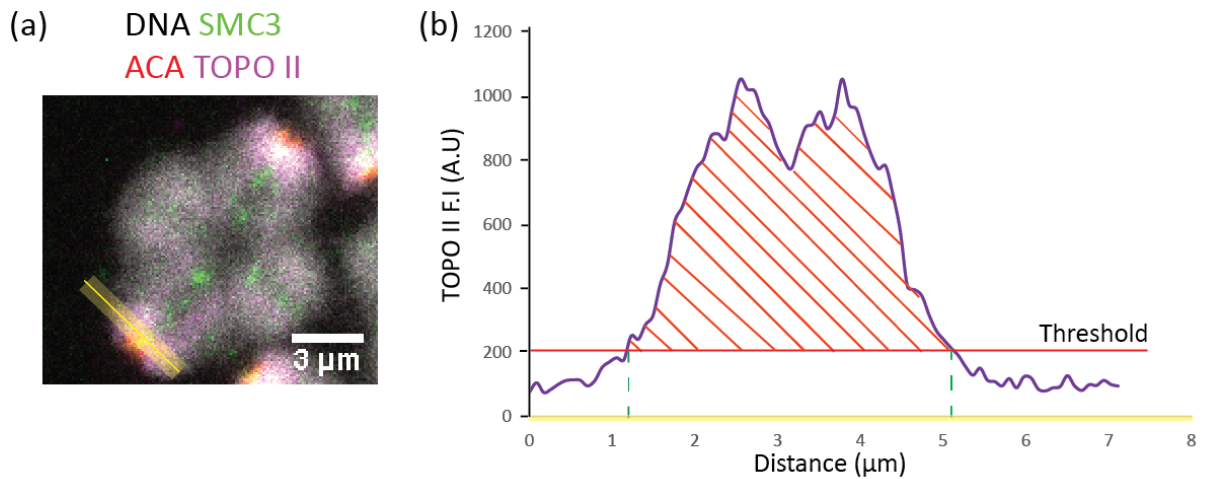
Figure 4.15 Linescan analysis of Topoisomerase II *(a) figure shows a representative example of a bivalent chromosome from a young C57BL/6 mouse. Yellow line shows the placing of a representative linescan that would be drawn across the pericentromere. (b) Shows the corresponding TOPO II graph that results from the line scan. After a threshold is set the area under the curve is calculated and this value is used for the pericentromere.*

After thresholding, the area under the curve is calculated for each line drawn on excel using the formula:

$$(A_1+A_2)/2*(D_1-D_2)$$

Were A is the fluorescence intensity value and D is the distance along the linescan value.

Having applied the line-scanning technique I next wished to test whether it is an effective tool for calculating changes in I.F and to compare it with the Imaris segmentation approach (Fig 4.14). To do this I performed linescans on the pericentromeres of bivalent chromosomes of the spreads analysed in section 4.2 and 4.3 (young: 3 mice, 24 oocytes; aged: 4 mice, 26 oocytes). Selecting a minimum of 10 pericentromeres, each one from an individual bivalent chromomosome, I carried out linescan analysis. Comparisons of the TOPO II and SMC3 values show a high level of variability within oocytes. However, the value for SMC3 appears more representative of what can be determined by eye (Figure 4.16). This remains the case when the value of SMC3 is ratioed to TOPO II (Figure 4.17).
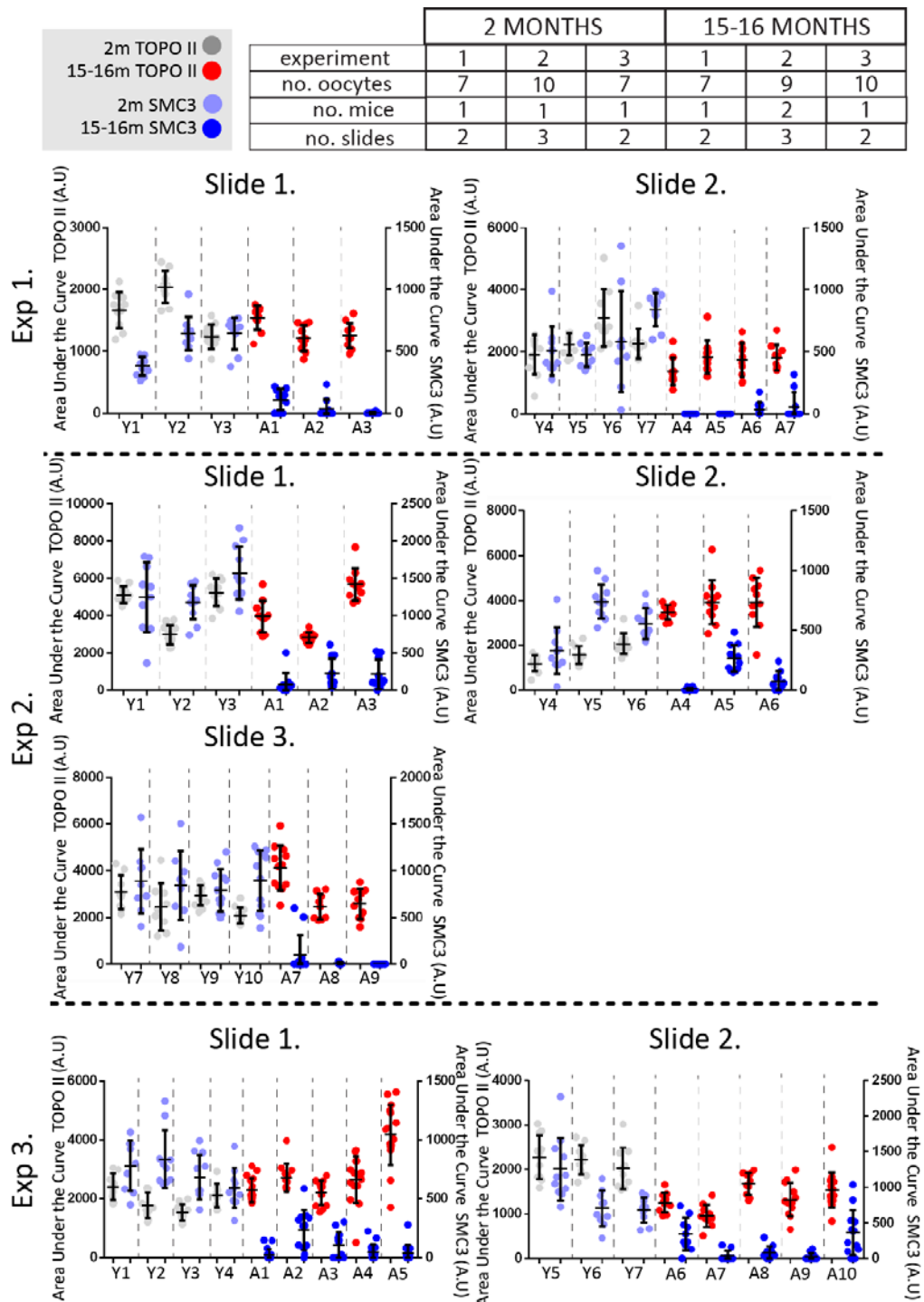
Figure 4.16 TOPO II and SMC3 area under the curve values in young vs old C57BL/6 females per oocyte. *Graphs showing area under the curve of TOPO II and SMC3 in young and aged mouse oocytes from air-dried chromosome spreads. Each graph represents a slide. Individual oocyte TOPO II and SMC3 are separated by vertical dotted lines with experimental repeats separated by horizontal dotted lines. Each data point represents area under the curve value of TOPO II or SMC3. Error bars represent the mean ± s.d for each oocyte. Table contains the number of oocytes, slides and mice used per experiment.*
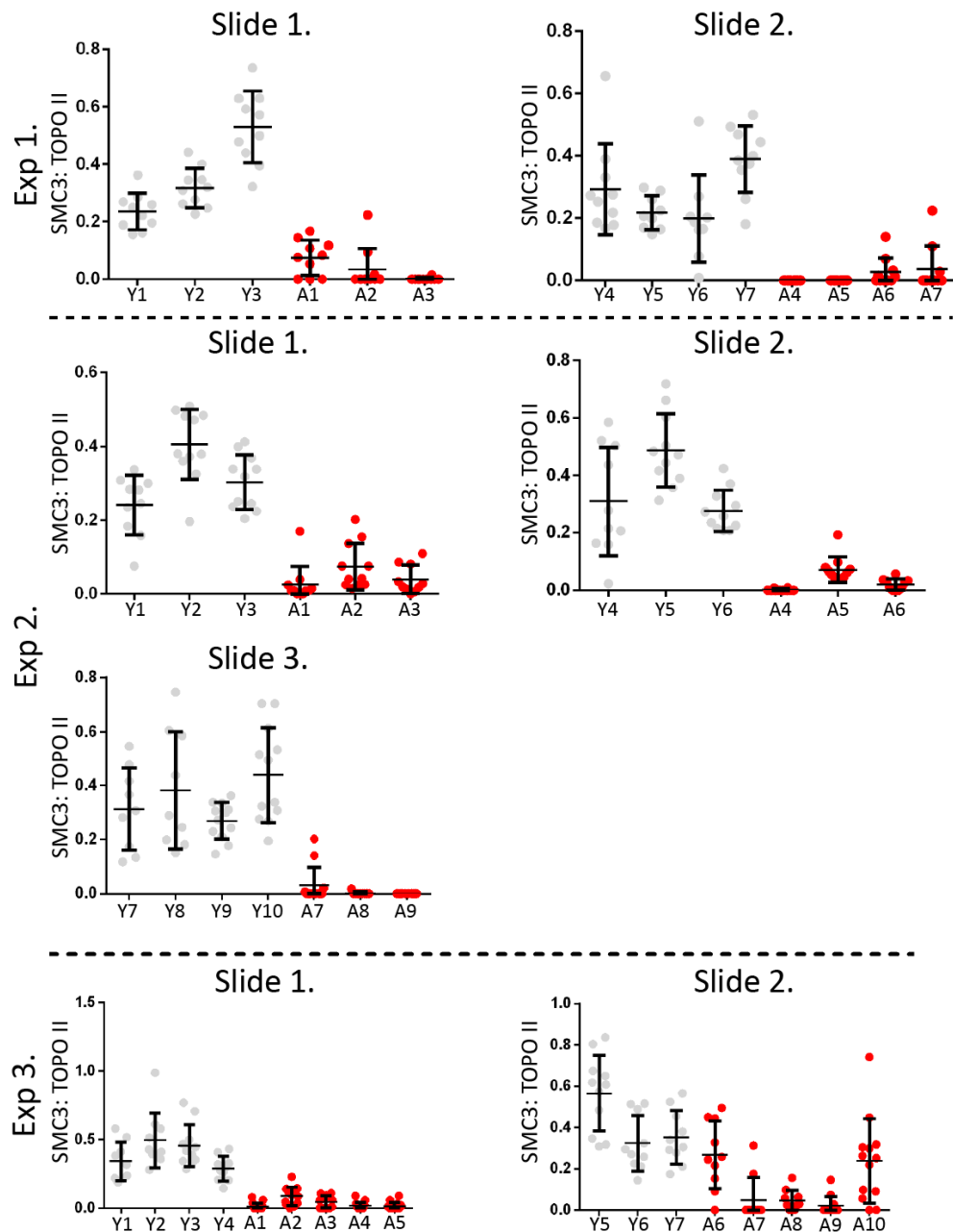
Figure 4.17 Ratio of SMC3 to TOPO II in young vs aged C57BL/6 air-dried MI chromosome spreads. *Dot plots showing the ratio of SMC3: TOPO II per pericentromere for young and aged mouse oocytes. Each graph represents a slide. Experimental repeats are separated by dotted lines. Each data point represents the ratio of area under the curve of SMC3 to TOPO II. Error bars represent the mean ±s.d for each oocyte. Table contains the number of oocytes, slides and mice used per experiment.*

79

Having carried out the linescan analysis I next wanted to determine whether the TOPO II values remained similar between young and aged mouse oocyte chromosome spreads. To address this I combined the values from the 3 experiments as in Figure 4.8. Similar to the sum values, there was no significant difference between the young and aged mice TOPO II values (Mann whitey U-test p=0.3279 and p=0.5414 respectively) (young: 3 mice, 24 oocytes; aged: 4 mice, 26 oocytes) (Figure 4.18). The linescan median value is also reduced less than that of the sum and peak F.I value (Imaris peak F.I 2 month: 99.96%; 15-16 months: 77.04%, sum F.I: 2 months = 97.56%; 15 – 16 months= 77.91%, linescan: 2 months = 102.1%; 15 – 16 months = 91.43%). These two factors would suggest that the linescan is a more effective tool for normalisation compared with the Imaris segmentation approach.
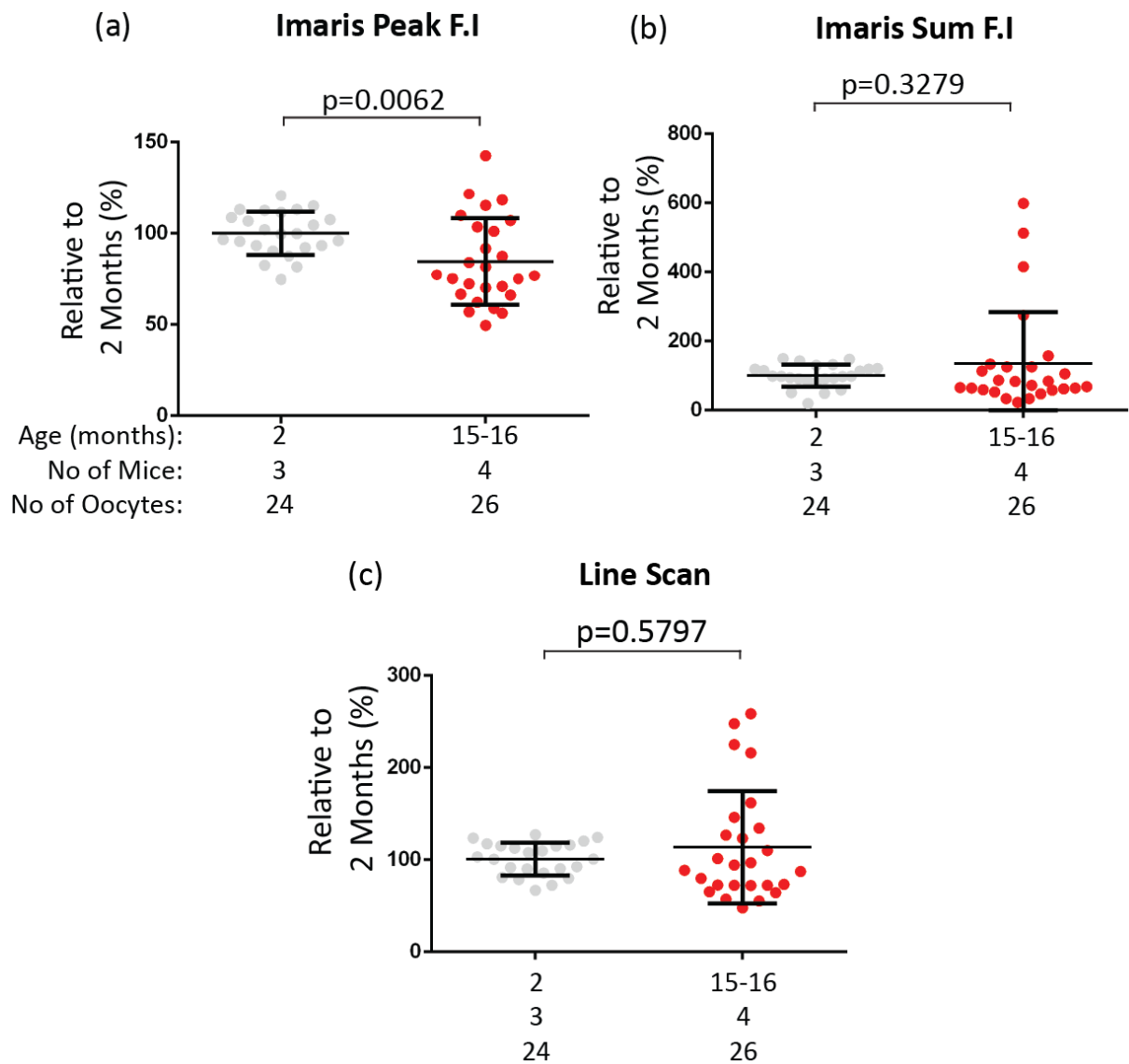
Figure 4.18 comparison of TOPO II Imaris Sum analysis vs linescan analysis.

Comparison between (a) Imaris peak F.I (b) Imaris sum F.I and (c) linescan analysis for TOPO II. An unpaired t-test showed a significant difference in (a) peak F.I (p=0.0062). Mann-Whitney U test show that there was no significant difference in either the (b) Imaris sum F.I (p=0.3279) or the (c) line scan area under the curve (p=0.5414). Error bars represent the mean ± s.d for each age grouping (young n = 24 oocytes from 3 mice; aged mice n =26 oocytes from 4 mice).

Having established the linescan as an effective tool for quantification between age groups I next compared the SMC3 values of the ratios for sum F.I to the line scan (Figure 4.19). Mann-Whitney U test showed both had a significant difference (p<0.0001) however the median values for the linescan anaylsis appear more representative of what could be seen by eye in the confocal acquired images (Figure

81

4.9) (peak F.I 2 month=96.98% 15–16 months=60.69%; sum F.I 2 months = 95.08% 15–16 months = 60.16%; linescan analysis 2 months =89.32% 15–16 months =0.00%). Overall this suggests that for carrying out quantification of chromosome associated proteins in ageing studies, use of TOPO II coupled with linescan analysis is a useful tool compared to Imaris segmentation.
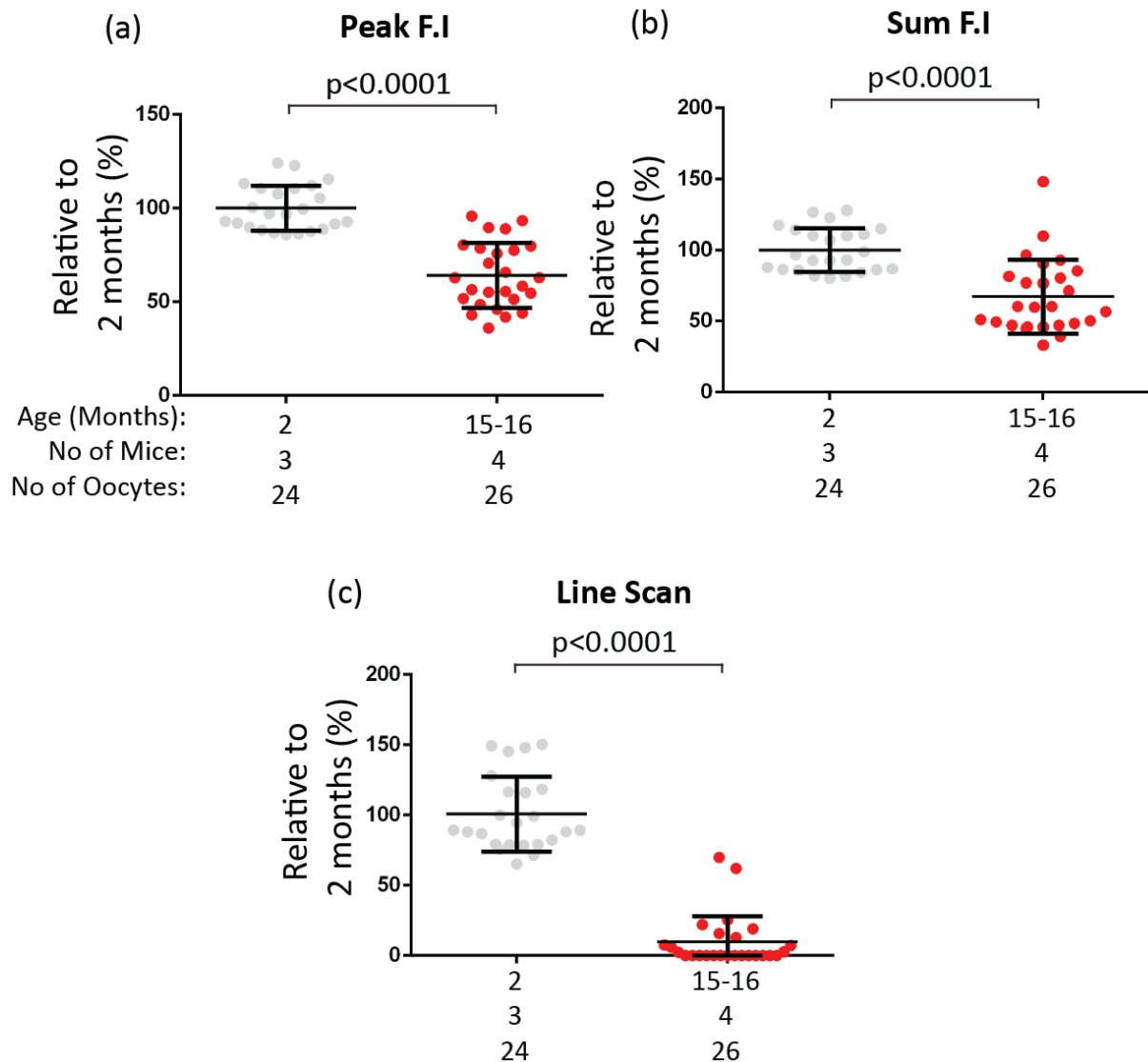
Figure 4.19 comparison of ratio of SMC3 to TOPO II in Imaris Sum analysis vs Linescan analysis. *Comparison of ratio of SMC3:TOPO II for (a) Imaris peak F.I (b) sum F.I and (c) linescan analysis. (a) Unpaired t-test of SMC3: TOPO II for peak F.I showed a significant reduction in SMC3 with age (p<0.0001). Mann-Whitney U test show a significant difference for Imaris sum F.I and linescan analysis (p<0.0001). Error bars represent the mean ± s.d for each age grouping (young: 3 mice, 24 oocytes; aged: 4 mice, 26 oocytes).*

4.5 Discussion

Despite there being clear differences by eye, accurate quantification of chromosome associated proteins in ageing studies has been hampered over the years due to a lack of appropriate tools for quantification. To address this I carried out an initial investigation of potential candidate markers that could be used. For the markers to be considered appropriate tools they had to be (i) static during meiosis (ii) useful for segmenting different areas of the chromosome (iii) informative of chromosome structure and (iv) commercially available and compatible with staining from widely used species. Having excluded various proteins as well as DNA stains based on this I selected the DNA catenation enzyme TOPO II. TOPO II is necessary for establishing transient double strand breaks in DNA and is expressed in both mitotic and meiotic cells (Nitiss, 2009). Importantly, the antibody used in this work is available in a conjugated form. Based on the staining protocol used by Shintomi *et al.* this meant I was able to stain using this antibody along with antibodies raised in the same species (Shintomi and Hirano, 2011).

Time series immunofluorescence analysis of topoisomerase II indicates that it maintains its localisation throughout MI and in to MII arrest. In oocytes, TOPO II has two distinct patterns of staining with a highly enriched area at the pericentromere and a fainter but still detectable level of staining on the chromosome arms. This allows for clear classification of where another protein of interest is localised on the chromosome. Its localisation along chromosome arms is also useful for not only determining the number of crossovers in a bivalent structure but also determining the proximity of them to the pericentromere. The number of crossovers and their localisation is key to determining the likelihood of a chromosomes to misegregate during MI (Hassold and Hunt, 2001). TOPO II may therefore be useful in addressing strain to strain variation in premature separation of sister centromeres in mouse oocytes (Danylevska et al., 2014). The one area in which the use of the TOPO II antibody was not beneficial was in establishing distance between separated centromeres. As the bulk of this work was done using an Alexa-flour 647 tagged antibody it may be as a result of using a higher wavelength antibody (resolution is calculated based on wavelength divided by numerical aperture).

To determine whether TOPO II is altered with age, I performed air-dried chromosome spreads of 2 month and 15–16 month old C57BL/6 mice. I immunolabelled them with

83

TOPO II as well as ACA and SMC3. The purpose of this was to compare the age-related decline in TOPO II with that of ACA. We also aimed to compare different methods of quantifying the extent of oocytes cohesin depletion during ageing. Previous attempts to do this using ACA or CREST were hampered by a marked decline in signal intensity during ageing. By eye observations of the TOPO II signal suggested that it was unchanged at the pericentromere during ageing, but that its intensity was reduced on the chromosome arms. For this reason I confined my measurements only at the pericentromere.

Using Imaris I analysed both the peak fluorescence intensity of the TOPO II signal and the sum fluorescence intensity. This analysis revealed that while there is a significant difference in peak fluorescence intensity there is no significant difference in sum fluorescence intensity. This most likely can be attributed to the high level of biological variation within the sum fluorescence intensity data. This is highlighted in the lack of a difference in the relative median value between the sum and peak F.I.

Comparisons between TOPO II and ACA indicated that the age-related reduction in ACA for both the sum and peak F.I was greater than the reduction seen in TOPO II. Suggesting that TOPO II is a more useful marker for normalisation.

Next I sought to investigate whether using the sum or peak fluorescence intensity of TOPOII would be an effective for measuring depleted proteins. Preliminary experiments had suggested that like REC8, SMC3 would be significantly reduced with ageing (Chiang et al., 2010, Lister et al., 2010). This would make it a useful control to determine whether Imaris measurements of TOPO II are useful for quantification. Comparisons of the ratio of SMC3: TOPO II indicated that Imaris analysis detects a significant difference. However, by eye observations of SMC3 would suggest that its fluorescence intensity should be considerably lower. This discrepancy is due to the surface segmentation analysis on Imaris. For the sum F.I it collects the signal within each voxel where the TOPO II surface is regardless of whether it is a true signal or not. This means that a significant portion of background fluorescence is picked up and contributes to the overall value when it is not actually "true signal" elevating the value. This is also true of the value assigned as the peak fluorescence intensity. While this reduces the efficacy of using Imaris surface segmentation analysis for measuring punctate signals, it would be a useful tool for analysing proteins of interest that are more uniformly distributed.

84

To address these concerns I developed the linescan method of analysis. This measures the area under the curve of a graph of fluorescence intensity generated from a linescan. This method allows for a more focused approach to the cohesin signal as it allows for setting of independent thresholds based on our current knowledge of cohesin localisation. Analysis using the linescan method, revealed no significant difference in TOPO II signal and a smaller reduction in the median value between the young and aged mice. This can be attributed in part to being able to set lower thresholds, as there is no interference from the arm staining as in the Imaris surface segmentation. Use of the linescan also provided what appeared to be a more representative interpretation of the reduction in SMC3.

There are some important caveats to note from this work before gaining reliable data using TOPO II for normalisation. Firstly, the values generated by the linescan analysis are still highly variable within and between oocytes. This is difficult to overcome as differences between pericentromere size and how chromosomes spread out on a slide will always affect this. Secondly, the consistency of TOPO II between ages is dependent upon the quality of the chromosome spreads in a way that it is not with ACA. If the chromosomal DNA is abnormal then the TOPO II staining will be affected. This meant that one slide of data could not be used due to difference between the chromosomal DNA morphology between the 2 months and 15–16 months. Finally, the lack of staining on the chromosome arms requires further investigation in aged oocytes. There are two potential reasons for this. The TOPO II antibody used in these experiments recognises TOPO IIα and TOPO IIβ. This discrepancy could be caused by one of these proteins being affected but not the other. Alternatively, the lack of bivalent chromosome structural integrity that occurs with age may be affecting the chromosome arms. If the signal was increased this may show arm staining over a wider area. This was not investigated as it would have resulted in bleaching of the pericentromeric signal.

With these caveats in mind, the experiments presented in this chapter indicate that TOPO II is an effective marker for quantification in ageing studies and that linescan analysis is an effective method for determining changes to cohesin sub-units. I have therefore applied this approach in further analysis (Chapter 6) of mouse and human oocytes.

85

Chapter 5. Results: Timing and mechanisms of cohesin depletion in oocytes

Studies in naturally aged mouse models indicate that fully grown meiosis I oocytes exhibit an age-related loss of cohesin (Chiang et al., 2010, Lister et al., 2010), which is accompanied by reduced recruitment of cohesin's protector SGOL2 (Lister et al., 2010). Together, these findings provide a plausible molecular basis for maternal age-related aneuploidy, in particular the prevalence of prematurely separated sister centromeres observed in mouse and human oocytes from older females (Herbert et al, 2015). While age-related cohesin deterioration has been established in mice for some time, important questions remain about the timing and underlying mechanisms. By understanding this in the mouse it is hoped that we may gain a better insight into cohesion dysfunction in human oocytes.

A key aspect to understanding the age-related loss of chromosome stability is that the majority of an oocytes existence is spent in primordial follicles, arrested at prophase. Based on our current understanding, the lifetime supply of oocytes are formed during foetal development (human), or shortly after birth (mouse) (Adhikari and Liu, 2009). They are maintained as arrested in prophase of meiosis I within primordial follciles, from which they are recruited for growth throughout life (McGee and Hsueh, 2000). Cohesin is established on the chromosomes of oocytes during S-phase before bivalents are formed during meiotic recombination (Brooker and Berkowitz, 2014). Based on findings in mice (Tachibana-Konwalski et al., 2010, Burkhardt et al., 2016), there is no subsequent reloading of cohesive cohesin complexes. Thus, cohesin established in oocytes during embryo development must be maintained for decades in the case of humans and months in the case of mice.

Using the mouse as a model, Dr. R. Ballesteros-Mejia in our lab found that chromosome-bound REC8 is very much reduced in primordial-stage oocytes between the ages of 2 and 12 months. However, whether removal of cohesin occurs progressively during female ageing, or whether it occurs acutely at advanced age is currently unknown. Furthermore, the only study to have looked at other cohesin subunits in mouse oocytes did not remove soluble cohesin. Based on R. Ballesteros-Meija work soluble cohesin does not appear to be affected by age (Tsutsumi et al.,

2014). It is therefore unclear what the effect of age on other chromosome-bound cohesin subunits is.

Potential candidates for investigating the loss of cohesin have naturally focused on the proteins and pathways involved in cohesin protection and removal during meiosis. If separase is not adequately inhibited, it is possible that "leaky inhibition" of separase could progressively cleave cohesin during the prolonged period of prophase arrest. Yeast models show that early release of separase from securin in prophase, through deletion of the APC^{AMA1} inhibitor Mnd2, have premature separation of chromosomes (Oelschlaegel et al., 2005, Penkner et al., 2005). While CDK1 inhibits separase by phosphorylation, CDK1 is not active in primordial-stage oocytes, and so would not play a role in suppression of separase at this stage (Adhikari et al., 2016). Work carried out by R. Ballesteros-Meija suggests that separase is not responsible for cohesin depletion, however, this was not investigated in primordial-stage oocytes, where age-related cohesin loss occurs.

During MI, both SGO1 and SGOL2 localise to the centromeres of bivalent chromosomes (Lee et al., 2008). However, knockdown of SGO1 or SGOL2 in fully grown oocytes indicated that SGOL2 is the key protector during meiosis I, with knockdown of SGO1 showing only mild defects (Lee et al., 2008). This role for SGOL2 was confirmed through knockout mice which are infertile and showed high levels of premature separation of sister chromatids (Lee et al., 2008, Llano et al., 2008).

Evidence from yeast indicates that recruitment of PP2A by Sgo counteracts phosphorylation of REC8 and hence prevents its cleavage by separase. This has also recently been shown in *C. elegans* with LAB-1 and PP1 preventing cohesin cleavage (Ishiguro et al., 2010, Katis et al., 2010, Ferrandiz et al., 2018). This is likely to be conserved in mammalian oocytes but has not yet been tested directly. The function of SGO1 during meiosis is less clear as the only information we have to date is based on siRNA (Lee et al., 2008). No oocyte specific deletion of SGO1 has so far been studied. Furthermore, we do not know whether SGO1 and/or SGOL2 function to protect cohesin during the prolonged prophase arrest. This is particularly interesting in the case of SGO1 whose canonical purpose in mitotic cells is to protect centromeric cohesin from removal by the separase-independent prophase pathway (Haarhuis et al., 2014).

87

In this Chapter I aimed to address the temporal and mechanistic basis of cohesin loss in ageing. In relation to timing, I determine whether cohesin depletion during the prolonged prophase arrest at the primordial stage occurs gradually during female ageing. To investigate the mechanistic basis, I ask whether separase is expressed during prolonged prophase arrest and whether leaky inhibition of separase contributes to removal of cohesin in primordial-stage oocytes. In addition, I ask whether SGO proteins, which protect cohesin, are present at the primordial stage and whether this is affected by female ageing.

5.1 Identification of primordial-stage oocytes in ovarian tissue

The vast majority of an oocyte's lifespan is spent arrested at the prophase of MI, encapsulated in a primordial follicle (Herbert et al., 2015). To understand how ageing impacts on oocytes it is necessary to study the oocyte at this stage. The optimum method for doing this would be to extract live primordial-stage oocytes from the ovaries of young and aged mice for western blotting and immunofluorescence staining. Studies in mice have suggested that primordial-stage oocytes can be extracted from adult ovaries using FACS. Each extraction requires ovaries from between 6 to 10 mice aged 7–8 weeks old, and antibody labelling of the oocytes (Zhang et al., 2015). Due to the continuous decline in the number of primordial-stage oocytes during female ageing, FACS does not provide a feasible option for studying oocytes from older females (Broekmans et al., 2007). While it would still be useful to extract primordial-stage oocytes from younger mice, repeated attempts to do this based on methodology used to extract germ cells from embryonic ovaries proved unsuccessful (Wojtasz et al., 2009). As a result, it was necessary to use histological techniques on ovaries to determine and quantify protein expression in primordial-stage oocytes.

To do this I utilised both paraffin wax and OCT embedded ovarian sections. The advantage of paraffin sections is that due to the antigen retrieval step (where the sample is boiled in a pressure cooker with citrate buffer pH 6.0 for several minutes, breaking up methylene bridges caused during fixation) proteins of interest are more likely to be bound successfully by antibodies. However, while paraffin wax embedded sections are more suitable for informing whether a protein is expressed and where it

localises in the cell, they are less useful in terms of protein quantification and higher resolution imaging. For this reason we used OCT embedded ovarian sections for quantification of proteins in the primordial stage oocyte. OCT sections also have the added advantage of being easier to cut at thicker sections of 30μm which is harder to do in wax sections. This allows for greater opportunity to locate whole primordial oocyte nuclei.

To help identify primordial-stage oocytes using just DAPI staining and without the need for specific markers, it was necessary to train my eye in distinguishing them from other cells in the ovary. I did this by using antibodies targeted to DDX4 and REC8-MYC for paraffin and OCT embedded ovarian sections respectively. DDX4 (also known as VASA) is a member of the DEAD-Box family of genes and is expressed in germ-cells (Tanaka et al., 2000). REC8 is a meiosis-specific a-kleisin subunit of the cohesin complex (Nasmyth and Haering, 2009)(Figure 5.1). To make REC8 detection and measurements easier we acquired the REC8-MYC mouse strain. This is a transgenic mouse with a B6CBAF2 background. REC8 is expressed from a bacterial artificial chromosome which has nine tandem copies of human c-myc epitope at its C terminus (Kudo et al., 2009). Work done by R. Ballesteros-Meija in our group reported that, consistent with other strains, oocytes from the REC8-MYC exhibit age-related depletion of cohesin loss and chromosome segregation errors.

The images in Figure 5.1 show that in both non-growing primordial and primary follicles, DDX4 is localised to the cytoplasm, while REC8 is localised to the nucleus. Although these two proteins are both expressed after oocyte growth, the number and morphology of the surrounding granulosa cells makes it possible to distinguish between different stages. While the granulosa cells are cuboidal and form a complete ring around primary oocytes, in non-growing primordial follicles the oocytes is surrounded by flattened granulosa cells (Adhikari and Liu, 2009). This allows for clear distinction between non-growing primordial-stage oocytes and oocytes at later stages. It also became clear in searching for primordial-stage oocytes that they tend to reside in the ovarian cortex. This allowed me to acquire images quicker by only scanning the outer region of the ovarian sections.
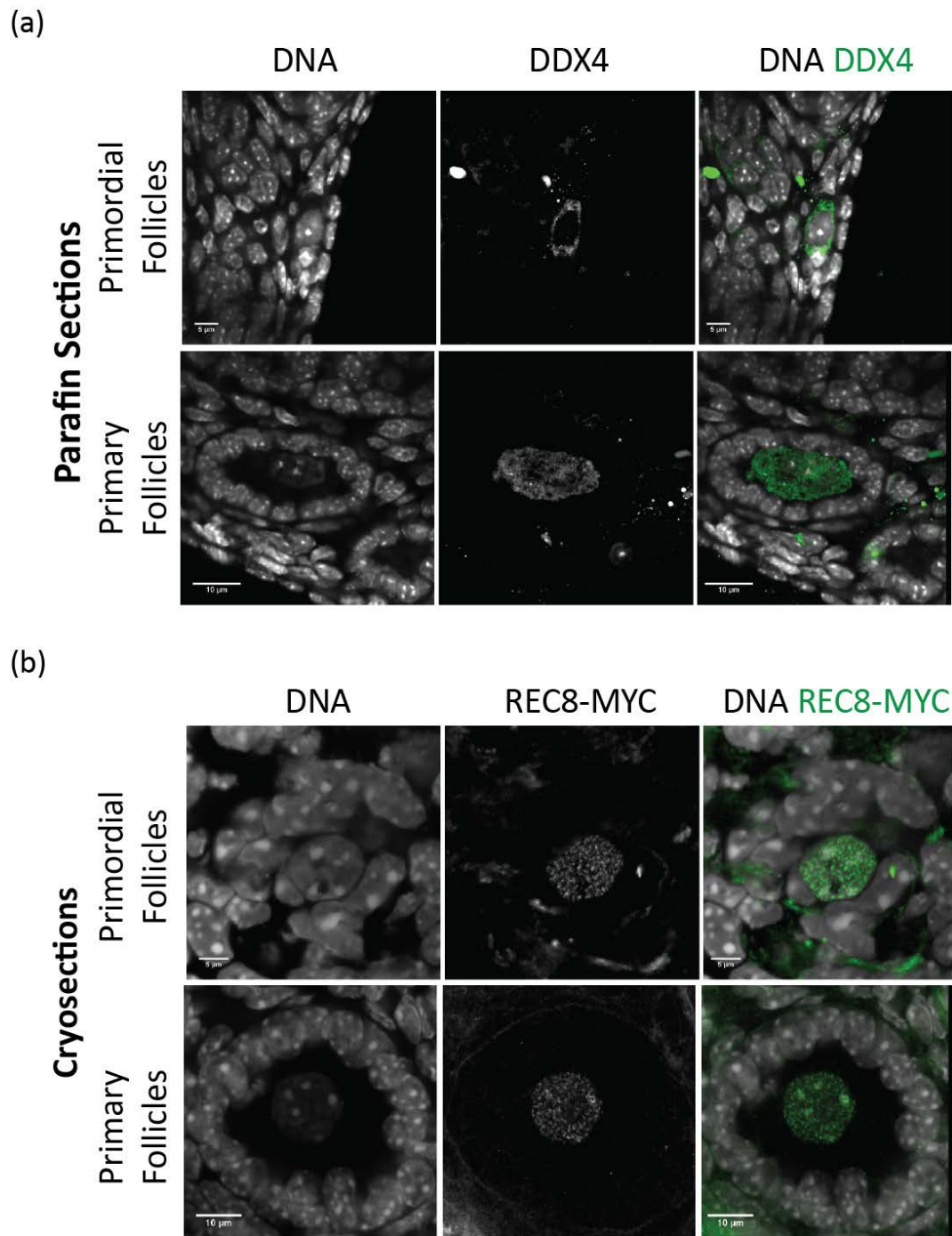
Figure 5.1 Primordial-stage oocyte recognition in ovarian sections.

Representative images of (a) paraffin wax and (b) OCT- embedded primordial and primary follicles from ovarian sections. (a) Paraffin wax sections were immunolabelled with DDX4 and (b) OCT- embedded section with MYC antibody targeted to REC8-MYC. DDX4 localises to the oocyte cytoplasm while REC8-MYC is localised to the nucleus. Primordial and primary follicles can be distinguished by the surrounding granulosa cells. Scale bar 5μm and 10 μm for primordial and primary follicles respectively.

DNA staining in ovarian sections revealed discrete areas of intense staining in the nucleus. Based on our knowledge of chromosome structure after GVBD, the pericentromeres of chromosomes are enriched with heterochromatin (Allshire and Karpen, 2008). They are also a key area for localisation of proteins essential for accurate chromosome segregation. To determine whether the DNA rich areas in the primordial-stage oocytes corresponded to the same area in condensed chromosomes, I immunolabelled ovarian cryosections with antibodies targeted to trimethylation of H3-lysine 9 (H3K9me3) (a marker of heterochromatin) and CREST (Becker et al., 2016). DNA was labelled with the monomeric cyanine stain TO-PRO-3, which stoichiometrically labels DNA (Bink et al., 2001) (Figure 5.2). As can be seen in the primordial oocyte, areas enriched by H3K9me3 co-localise with CREST. This is the same as observed in condensed chromosomes, which I confirmed by immunolabelling metaphase I chromosome spreads with H3K9me3 and CREST (Figure 5.2). This suggests that these are the same area of the bivalent chromosome in primordial stage oocytes and fully grown oocytes.
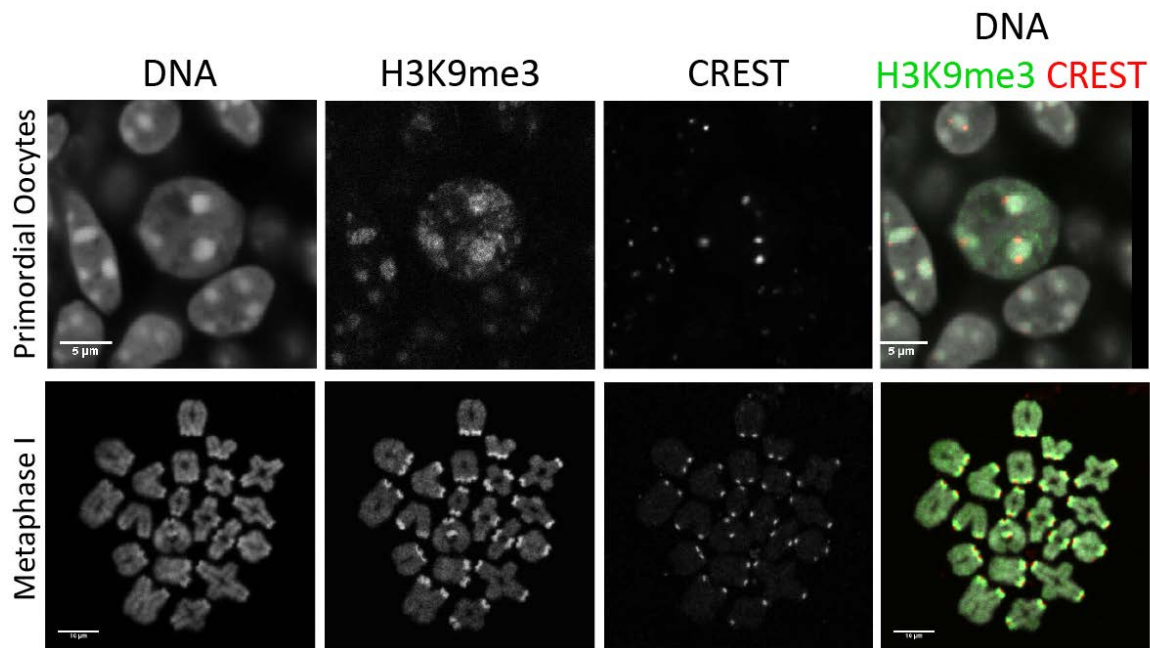
Figure 5.2 H3K9me3 and CREST co-localise throughout meiosis on oocyte chromosomes. *Representative confocal images of a primordial oocyte and a metaphase I chromosome spread, immunolabelled with H3K9me3 and CREST. DNA is labelled with TO-PRO-3 in primordial stage oocytes and DAPI in the metaphase I spread. Scale bar 5µm and 10 µm for primordial follicles and primary follicles respectively.*

91

5.2 Cell death recognition in primordial stage oocytes

Due to the relatively high levels of cell death by atresia in ovarian primordial follicles, it was necessary to distinguish atretic primordial-stage oocytes from healthy ones. To do this, I stained ovarian sections using TUNEL (TdT-mediated dUTP-biotin nick end labelling) (Figure 5.3) (Gavrieli et al., 1992). This adds labelled nucleoutides to fragmented DNA (de Torres et al., 1997). TUNEL-positive cells, which I found to be rare, were excluded from analysis.
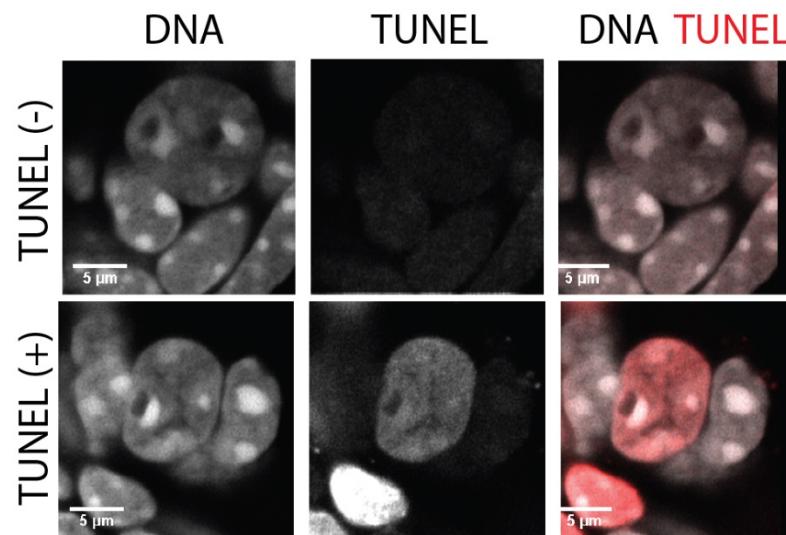
Figure 5.3 Cell death recognition in primordial stage oocytes. *Representative images of primordial-stage oocytes stained for TUNEL in ovarian sections. Top and bottom set of images shows primordial oocyte negative and positive for TUNEL respectively.Scale bar 5µm.*

5.3 Cohesin is lost progressively from DNA in primordial-stage oocytes

While recent work in our lab indicated that depletion of REC8 occurs predominantly at the primordial-stage of oogenesis in aged mice (R. Ballesteros-Meija), it is not clear whether cohesin depletion occurs progressively during ageing, or whether it occurs acutely at older ages. To address this, I immunolabelled ovarian sections from C57BL/6 mice aged 2, 6 and 12 months old with anti-REC8 antibody and labelled the DNA using TO-PRO-3. Sections were also stained using DAPI to locate the primordial-stage oocytes. While females are still fertile at 6 months, I anticipated that it would allow for sufficient time for cohesin depletion to be detected if it occurs progressively. Work carried out by R. Ballesteros-Meija showed that primordial-stage

oocytes contain a large quantity of soluble cohesin even at 12 months of age. Therefore, to study chromosome-bound cohesin it is necessary to remove soluble cohesin. To do this, ovarian cryosections were treated with a detergent wash of 1% Triton-PBS before fixation and a 1% lipsol-PBS wash after primary antibody incubation. This permeabilises the cells in the section and removes the cytoplasm. Images were acquired by confocal mode and airyscan mode microscopy on a Zeiss lsm880. Comparison of REC8 fluorescence intensity in primordial-stage oocytes by eye suggested that REC8 was reduced in sections from 6 months compared with 2 months old females. However, this reduction was not as pronounced as the reduction seen at 12 months of age (2 months n= 25 oocytes from 3 mice; 6 months n= 23 oocytes from 3 mice; 12 months n= 22 oocytes from 3 mice) (Figure 5.4).
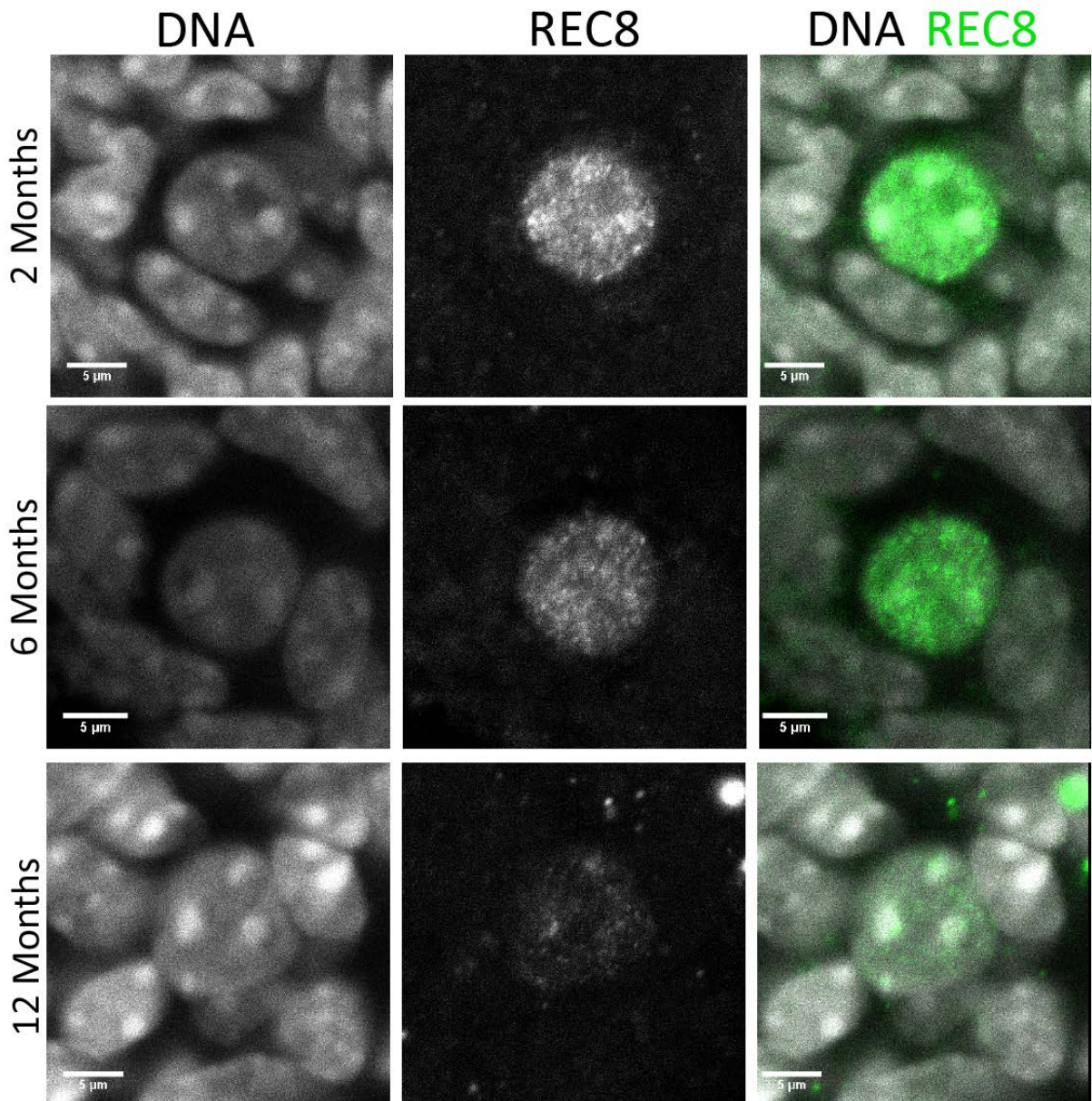
Figure 5.4 REC8 appears reduced in 6 month old mouse primordial-stage oocytes. R*epresentative images of primordial-stage oocytes from 2, 6 and 12 months old C57BL/6 background mice, immunolabelled with an antibody targeted to REC8 and withTO-PRO-3 staining the DNA. Scale bar 5µm (2 months n= 25 oocytes from 3 mice; 6 months n= 23 oocytes from 3 mice; 12 months n= 22 oocytes from 3 mice).*

To calculate the chromosome associated REC8 in the primordial-stage oocytes I used Volocity software. This allows for calculation of fluorescence intensity within a hand-drawn region of interest (ROI). The ROI was drawn around the primordial oocyte and cropped so as to be as tight to the oocyte nucleus as possible. I then used the 'detect objects' function and set a fluorescence intensity threshold that was

kept consistent per slide for each marker being measured. The 'sum fluorescence intensity' (sum F.I) for REC8 and TO-PRO-3 for each oocyte was calculated (Figure 5.5). Sections were cut at 30μm in thickness to increase the likelihood of finding primordial-stage oocytes in which the whole nucleus could be imaged. To control for experimental variations sections from the 2, 6 and 12 months old mice were mounted on the same slide, and labelled and imaged on the same day.
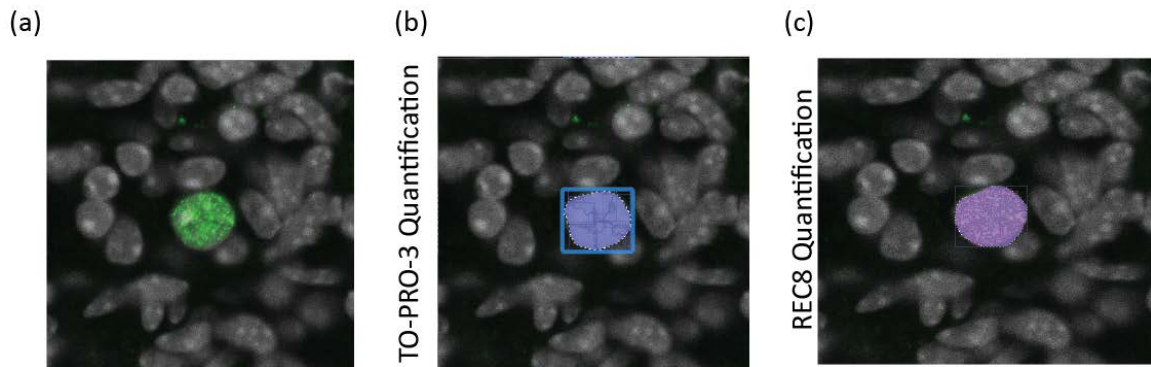
Figure 5.5 REC8 quantification in primordial-stage oocytes *(a) Representative image of a primordial oocyte immunolabelled with REC8 and TO-PRO-3. (b) TO-PRO-3 and (c) REC8 are selected through hand-drawing regions of interest around the primordial oocyte. The 'sum fluorescence intensity' of REC8 and TO-PRO-3 was then calculated and values were compared for oocytes from 2, 6 and 12m old females.*

Because TO-PRO-3 binds stoichiometrically to DNA, I aimed to normalise the sum F.I of REC8-Myc to the sum F.I of TO-PRO-3 for each primordial in order to detect age-related changes in REC8 levels. However, I found that TO-PRO-3 F.I varied considerably between different experimental groups and this did not appear to be age-dependent (Figure 5.6 (a) By contrast, REC8 F.I declined with age, except for one experiment in which REC8 levels were comparable between 2 and 6 month old ovaries (Figure 5(b)). Interestingly, TO-PRO-3 staining was also elevated in the 6 month ovaries from that experiment. The unexpected variation in To-PRO-3 F.I casts doubts on the validity of using the sum F.I values for normalisation of REC8 levels. Unfortunately, Topo II, which I used successfully for normalisation of the cohesin sub-unit SMC3 in chromosome spreads from fully grown oocytes (Chapt 4.4), was not detectable in primordial stage oocytes. Calculation of the ratio of REC8 F.I to TO-PRO-3 F.I for each suggests that by 6 months, a significant portion of chromosome-bound cohesin in primordial-stage oocytes has already been lost. (Figure 5.6 (c).

However, as TO-PRO-3 varied significantly throughout the different age groups, it appears to be a poor tool for normalising the fluorescence signal of REC8.

	2 MONTHS			6 MONTHS			12 MONTHS		
experiment	1	2	3	1	2	3	1	2	3
no. primodials	10	10	5	6	10	7	5	11	6
no. mice	1	1	1	1	1	1	1	1	1
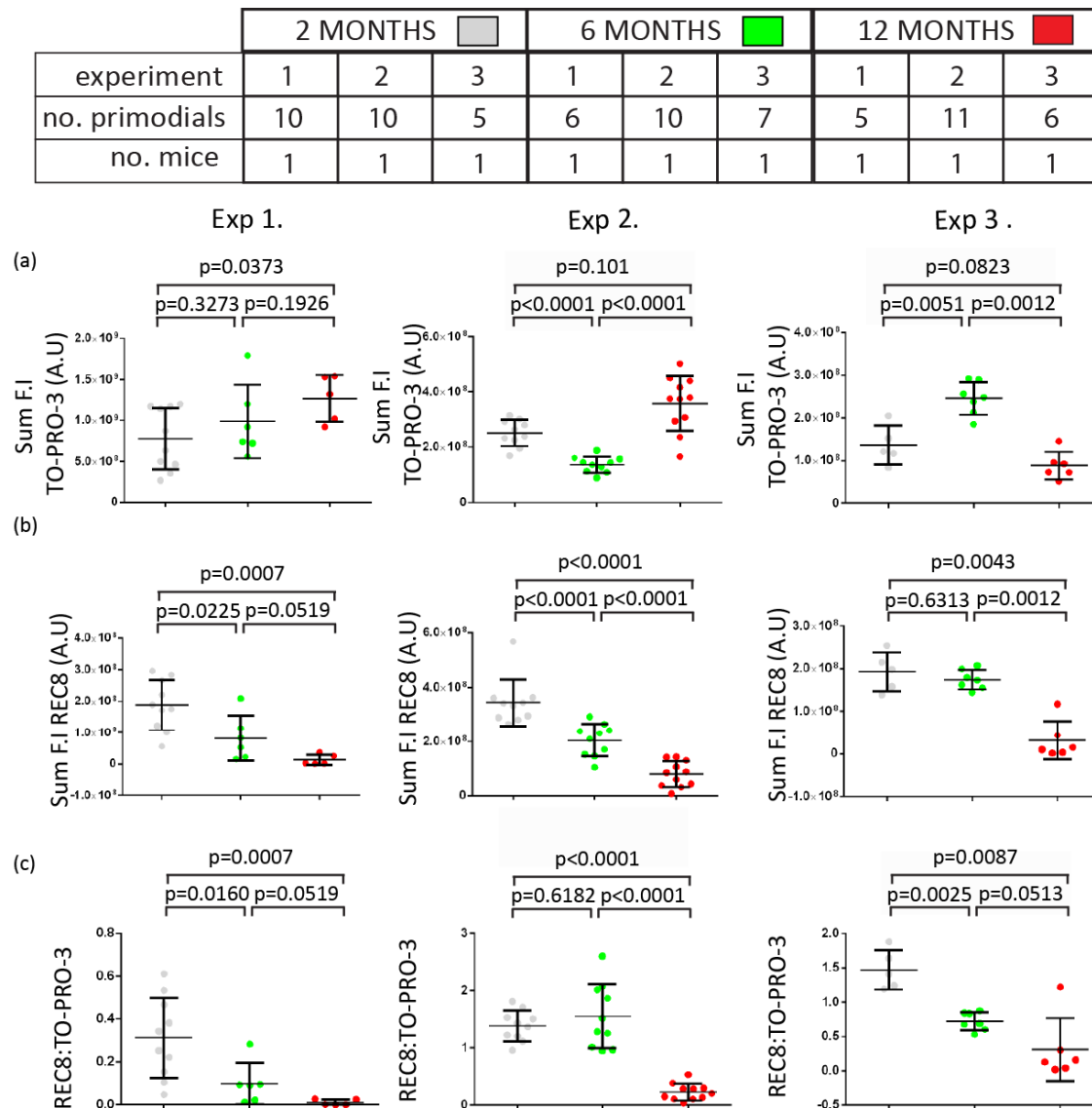
Figure 5.6 Comparison of DNA bound REC8 in 2, 6 and 12 months old primordial-stage oocytes. *Graphs show (a) sum TO-PRO-3 fluorescence intensity (b) Sum REC8 fluorescence intensity and (c) ratio of REC8: TO-PRO-3 for primordial-stage oocytes in 2, 6 and 12 months old primordial-stage oocytes. A Mann-Whitney U-test test was used to establish p-values with a p-value of less than 0.05 classed as significant. The number of oocytes and mice used from each age group and each experiment is shown in the table above.*

While there is a decline in the REC8 sum fluorescence intensity in each experiment, the variation in TO-PRO-3 within experiments skews the ratio. Because the variation in TO-PRO-3 appears to be independent of age I normalised the values relative to the median 2 months value for each experiment and combined them over all. This revealed much variation between oocytes within each experiment, however it showed no significant difference in TO-PRO-3 F.I between 2 months and 6 months, and the 6 months and 12 months (Figure 5.7(a) Mann Whitney U-test p=0.9877 and p=0.406 respectively). By contrast, normalisation of REC8 F.I to the median value for the 2 month old mouse revealed a significant difference in the levels of REC8 detected in primordial-stage oocytes from 2, 6 and 12 month old ovaries (Figure 5.7 (b) Mann Whitney U-test 2 months vs 6months p<0.0001, 6 months vs 12 months p<0.0001; and (Figure 5.7 (c) REC8:TO-PRO-3 ratio (Mann Whitney U-test 2 months vs 6 months p=0.0133, 6 months vs12 months p<0.0001)). These findings indicate significant depletion of chromosome-bound cohesin by 6 months with a further depletion by 12 months.
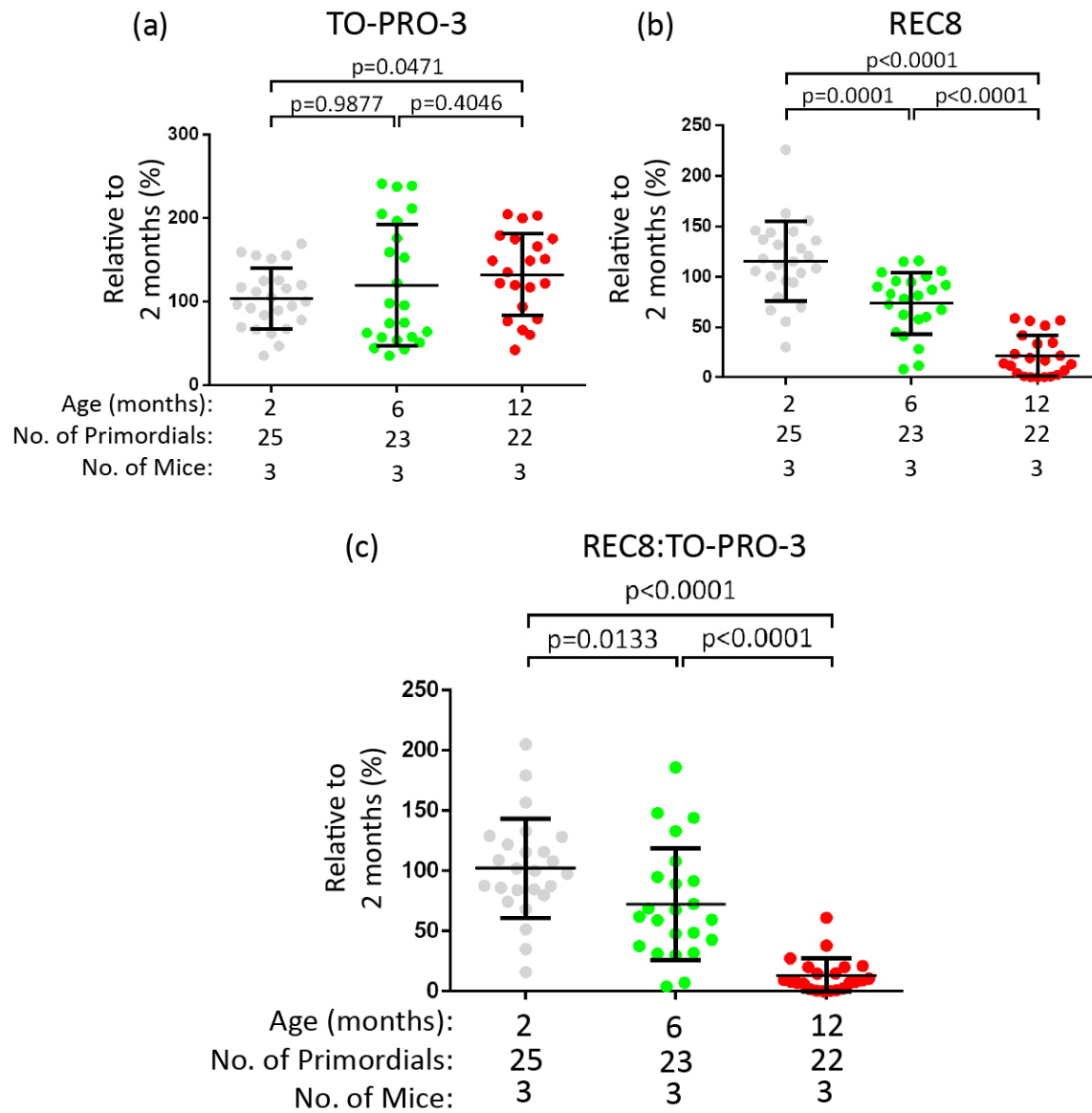
Figure 5.7 REC8 is significantly reduced in primordial stage oocyte at 6 months of age. *Graphs show sum fluorescence intensity for (a) TO-PRO-3 (b) REC8 and (c) REC8:TO-PRO-3 relative to 2 months for the 3 experimental repeats used. A Mann-Whitney U-test test was used to establish p-values with a p-value of less than 0.05 classed as significant. Error bars represent the mean ± s.d. for each age group. Error bars represent the mean ± s.d. for each mouse. (a) 2 months vs 6 months p=0.9877 and 6 months vs 12 months p=0.406 (b) 2 months vs 6 months p<0.0001 and 6 months vs 12 months p<0.0001 (c) 2 months vs 6 months p=0.0133, 6 months vs 12 months p<0.0001. (2 months n= 25 oocytes from 3 mice; 6 months n= 23 oocytes from 3 mice; 12 months n= 22 oocytes from 3 mice)*

To assess whether the loss of cohesin is progressive or occurs at an increased rate with age, I plotted the median values of 2, 6 and 12 months REC8:TO-PRO-3 on a line graph (Figure 5.8). This graph shows that the loss of REC8 appears to be linear with the reduction occurring at a consistent rate.
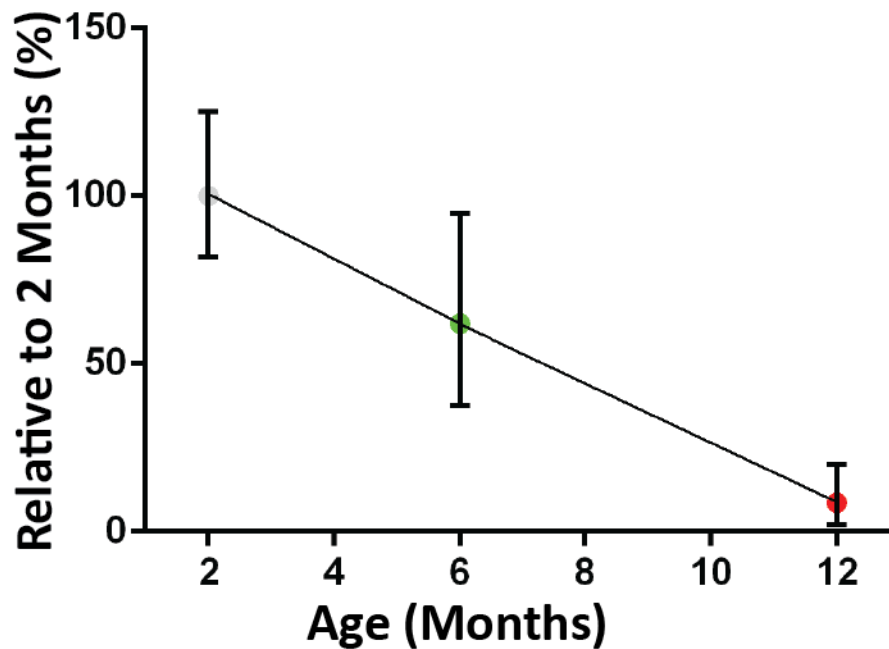
Figure 5.8 Age-related progressive loss of cohesin occurs in a linear fashion. *Line graph showing the median values of normalised 2, 6 and 12 months old primordial-stage oocytes from ovarian sections. Error bars represent inter-quartile values for each set. (2 months n= 25 oocytes from 3 mice; 6 months n= 23 oocytes from 3 mice; 12 months n= 22 oocytes from 3 mice)*

5.4 The cohesin subunit SMC3 is depleted with age in mouse primordial-stage oocytes

While it appears that the age-related loss of REC8 in primordial-stage oocytes occurs in a progressive manner, I was interested to determine whether other cohesin subunits show a similar decline. SMC3 is of particular interest as it is required for chromosomal cohesion in somatic cells and during meiosis (Nasmyth and Haering, 2009). Thus, should RAD21-containing complexes be present on the chromosomes of primordial stage oocytes, analysis of SMC3 levels will provide a comprehensive picture of cohesin loss during female ageing.

First I sought to determine the localisation of SMC3 in primordial-stage oocytes relative to REC8. To address this I co-stained SMC3 and REC8 in ovarian cryosections from 2 and 12 months old REC8-MYC mice.

As discussed above, I permeabilised the ovarian sections using a 1% Triton-PBS and 1% lipsol-PBS solution to minimise soluble cohesin. The DNA was labelled using TO-PRO-3 (Figure 5.9). Analysis from the linescans indicate that like REC8-MYC, SMC3 is enriched at the sites of heterochromatin in primordial-stage oocytes (2 months n= 30 eggs from 3 mice). Interestingly, enrichment of SMC3 at heterochromatin is not evident in the surrounding somatic cells in which cohesin complexes consist only of RAD21.
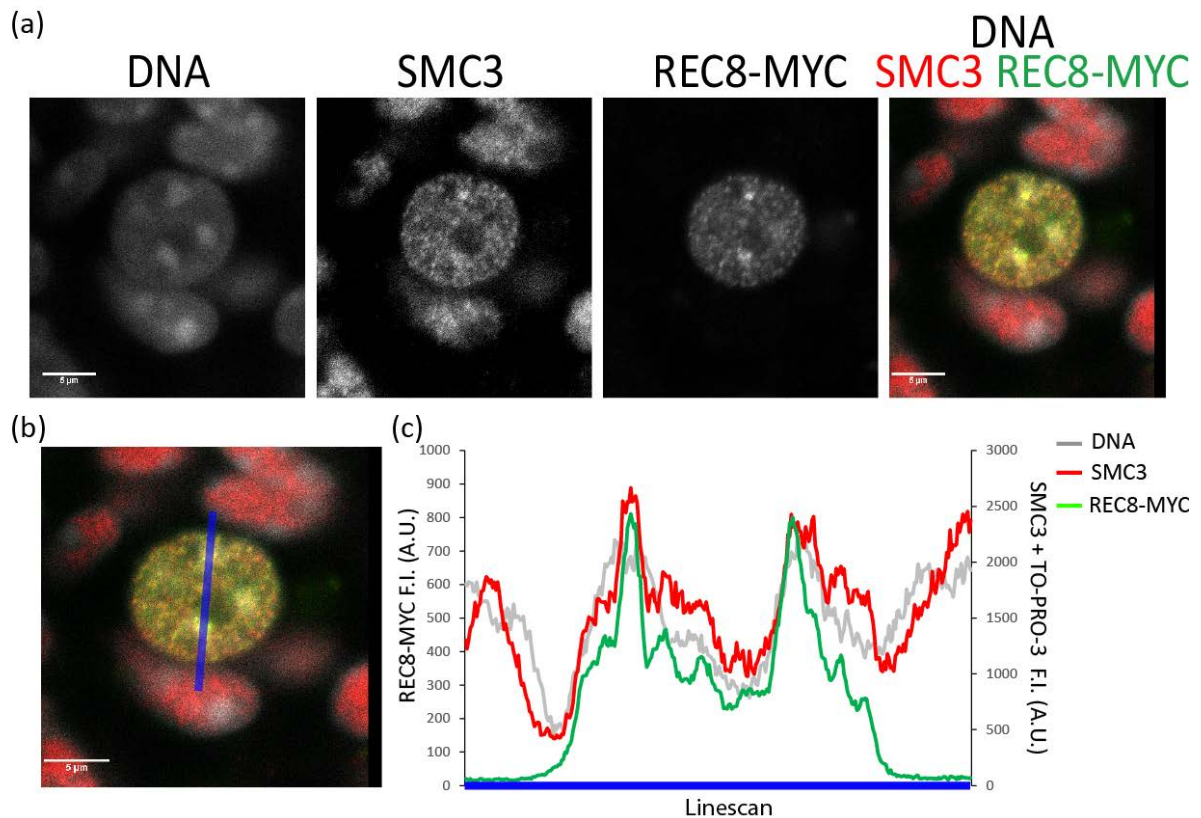
Figure 5.9 SMC3 is enriched at primordial oocyte heterochromatin. *(a)*
Representative images of a primordial stage oocyte from a REC8-MYC mouse
immunolabelled for REC8-MYC and SMC3; DNA was stained using TO-PRO-3. (b)
Linescan analysis covering heterochromatic and euchromatic. Scale bar 5µm. (c)
Areas of the primordial showed that SMC3 localisation tracks the localisation of
REC8-MYC with increased SMC3 and REC8-MYC at the areas of heterochromatin (2
months n= 30 eggs from 3 mice).

To determine whether SMC3 is reduced in primordial-stage oocytes, I
immunolabelled OCT embedded ovarian sections from 2 and 12 months old REC8-
MYC mice. This was done using antibodies targeted to SMC3 and REC8-MYC with
the DNA stained using TO-PRO-3. Sections were also stained using DAPI to locate
the primordial-stage oocytes (Figure 5.10). Images were acquired by airyscan and
confocal mode microscopy on a Zeiss lsm880 microscope. Consistent with its
expression in somatic cells, SMC3 was detected in the cells surrounding the oocytes
(Fig 5.10). Comparison of the I.F signal by eye suggested that like REC8-MYC,
SMC3 is also reduced during ageing in primordial stage oocytes, but does not appear
to be as reduced in the surrounding somatic cells (Fig 5.10).
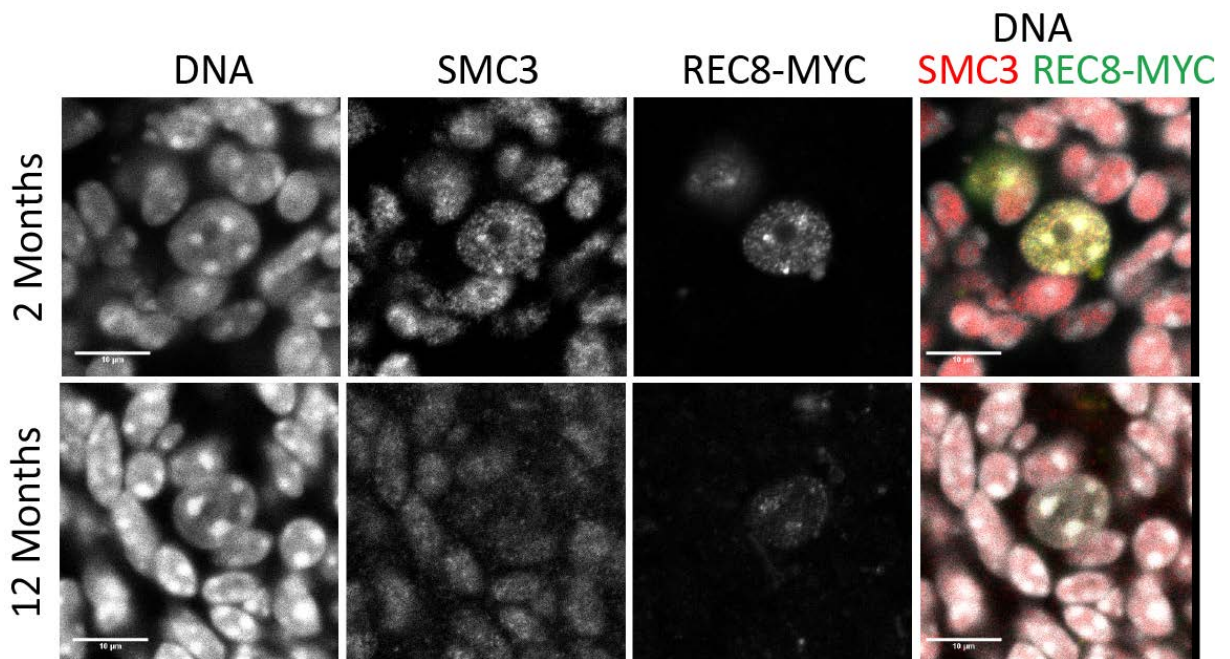
Figure 5.10 Chromatin bound SMC3 levels in primordial-stage oocytes are reduced as a function of age. *Figure shows single plain images of a primordial oocyte in ovarian sections from 2 and 12 months old females. Ovarian sections were immunolablled for SMC3 and REC8-MYC, with DNA stained with DAPI. Both SMC3 and REC8-MYC show a marked reduction in fluorescence intensity in the 12 months old mouse compared to the 2 months scale bar 10µm (2 months n= 30 eggs from 3 mice; 12 months n= 18 eggs from 3 mice).*

As above (Figure 5.5), I used Volocity software to quantify the levels of REC8 and SMC3 in primordial stage oocytes at different ages (Figure 5.11). The results indicate that like REC8-MYC, SMC3 also declines significantly with age (3 experiments $p < 0.05$).

	2 MONTHS			12 MONTHS		
experiment	1	2	3	1	2	3
no. primordials	9	11	10	7	5	6
no. mice	1	1	1	1	1	1
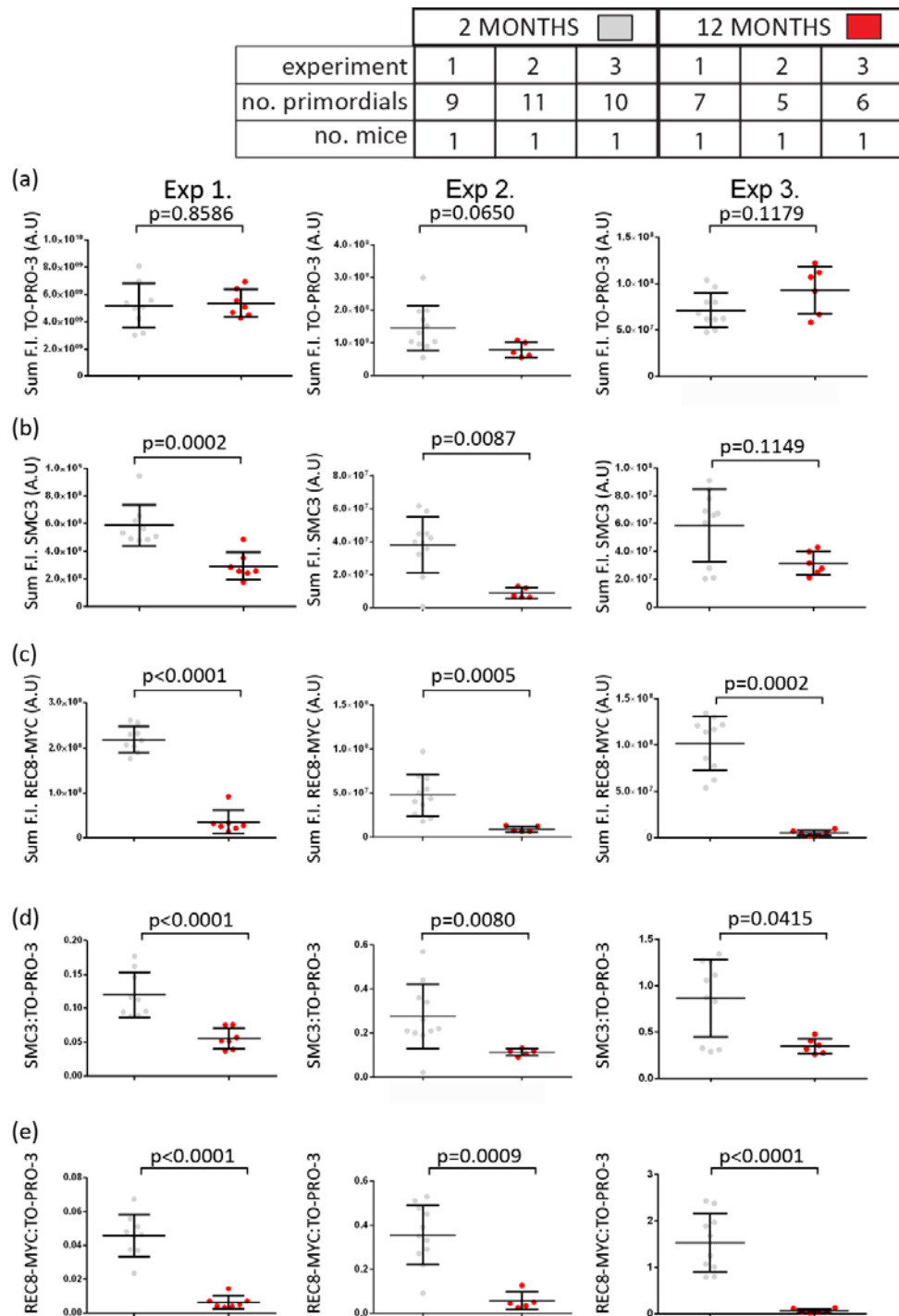
Figure 5.11 SMC3 is reduced significantly in primordial stage oocyte during female ageing. *Graphs show dot plots of (a) sum TO-PRO-3 fluorescence intensity (b) sum REC8-MYC fluorescence intensity (c) sum SMC3 fluorescence intensity (d) ratio of REC8-MYC:TO-PRO-3 (e) ratio of SMC3:TO-PRO-3, for primordial-stage oocytes in 2 and 12 months old REC8-MYC mice. Each dot represents an individual primordial oocyte. A Mann-Whitney U-test was used to establish p-values with a p-value of less than 0.05 classed as significant. The number of oocytes and mice used from each age group and each experiment is shown in the table above.*

103

While these findings indicate a significant decline in REC8 and SMC3 levels in primordial stage oocytes between the ages of 2 and 12 months, the effect size appears greater for REC8 compared with SMC3. To investigate this further, I normalised the results across the 3 experiments, with the 2 month old median value as 100% (Figure 5.12). While the difference in SMC3 and REC8-MYC between young and old remains significant, the fold reduction of 2.2 for SMC3 is not as high as the 11.9 times reduction in REC8-MYC.
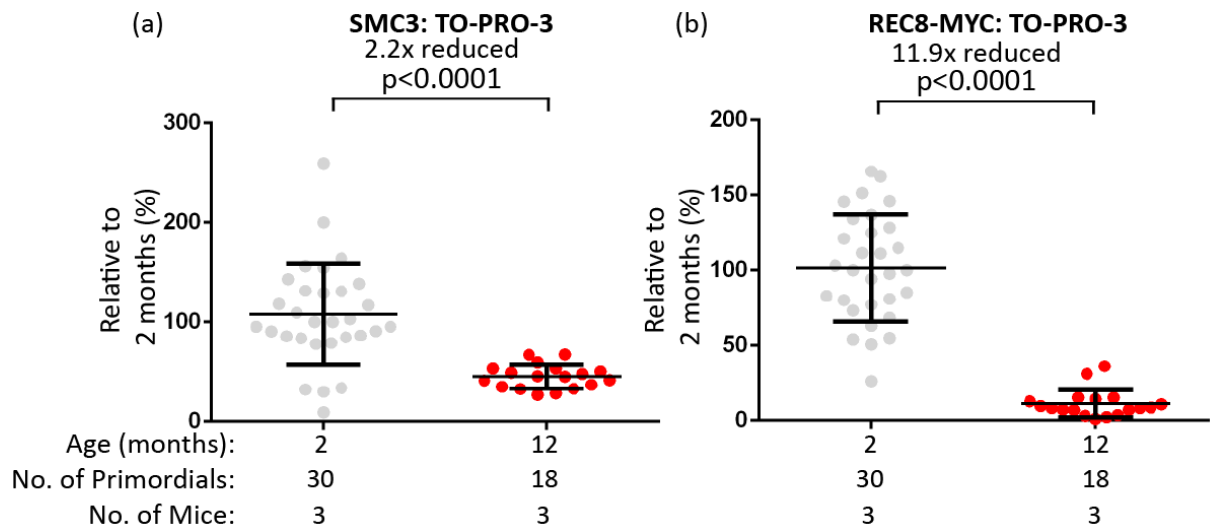
Figure 5.12 SMC3 is reduced significantly in primordial stage oocyte during female ageing, but not as significantly as REC8-MYC. *Graphs show ratio of (a) SMC3: TO-PRO-3 and (b) REC8-MYC:TO-PRO-3. Each dot represents an individual primordial oocyte relative to 2 month median value for the 3 experimental repeats in 2 vs 12 months old REC8-MYC mouse ovarian sections. A Mann-Whitney U-test was used to establish p-values with a p-value of less than 0.05 classed as significant. Mean fold reduction of SMC3 and REC8-MYC was calculated (2 months n= 30 eggs from 3 mice; 12 months n= 18 eggs from 3 mice).*

One possible implication of the increased age-related depletion of REC8 compared with SMC3, is that primordial stage oocytes also contain RAD21-containing complexes. To address this, I determined whether RAD21 can be detected in the nuclei of primordial stage oocytes. While I could not find a RAD21 antibody which worked in cryosections, staining of RAD21 in wax embedded ovarian sections from young CD1 mice suggests the presence of RAD21 in the primordial-stage oocytes (Figure 5.13). Thus, it is possible that a fraction of SMC3 is in complex with RAD21. Previous work from the Nasmyth lab indicates that cohesion in mouse oocytes is orchestrated solely by REC8-containing complexes (Tachibana-Konwalski et al.,

104

2010). While the functional significance for cohesion is unclear, it is possible that RAD21-containing complexes are replenished. For example, they may be involved in DNA damage repair (Nasmyth, 2011). This would explain the lesser extent of oocyte SMC3 depletion during female ageing compared with REC8. Further work is required to determine whether Rad21 levels decline or increase with age.
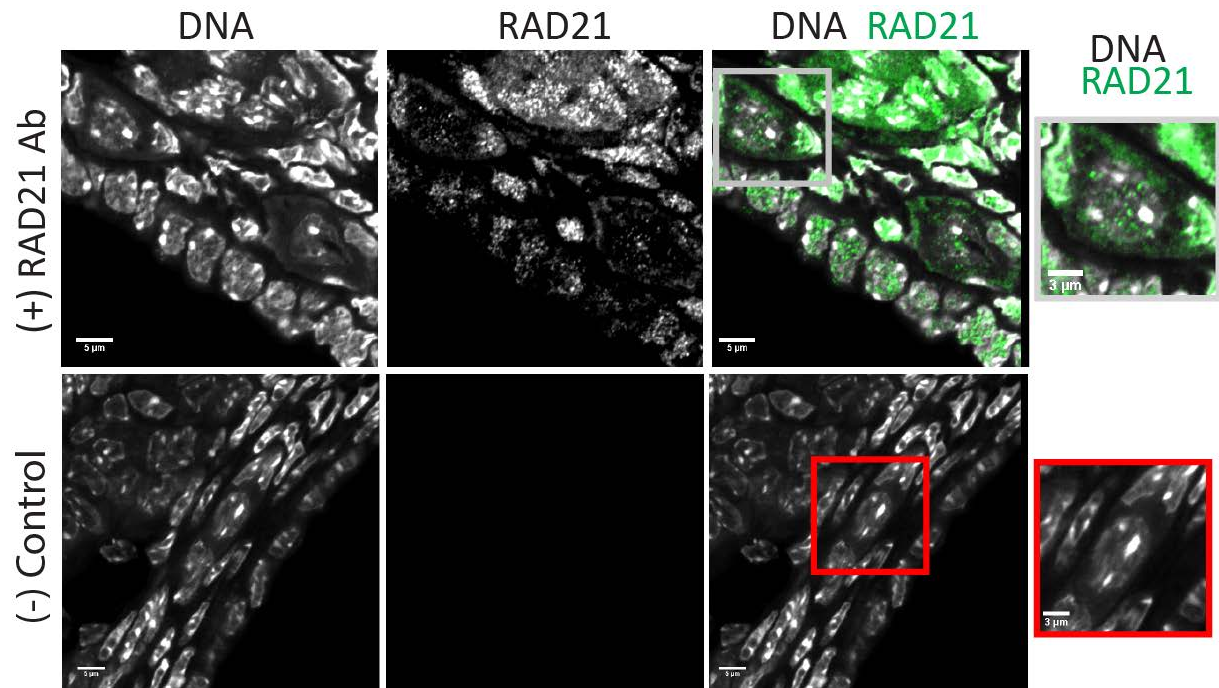
Figure 5.13 RAD21 is expressed in a relatively low level in early oogenesis oocytes. *Wax ovarian sections showing primordial-stage oocytes immunolabelled for RAD21 with DNA stained using DAPI. Secondary only controls were used to judge staining. Grey and red box show individual primordial-stage oocytes for stained and secondary only control respectively Scale bar 5µm. inset scale bar 3µm.*

5.5 Separase is expressed in primordial stage oocytes

Having determined that chromosome-bound cohesin is lost progressively in the nucleus of primordial stage oocytes, I next sought to determine what mechanisms could be responsible. One potential mechanisms for the age-related loss of cohesin in oocytes would be through leaky inhibition of the cysteine protease separase. Separase is responsible for the removal of cohesin from chromosome arms by cleaving REC8 during anaphase I. Separase is also necessary for cleaving centromeric REC8 during anaphase II and centromeric RAD21 in mitotic cells (Kudo

et al., 2006). It is possible that if separase becomes dissociated from its inhibitor securin, it may be cleaving cohesin progressively over time.

In budding yeast, separase is expressed in prophase of MI, and cleaves cohesin in *mnd2Δ* mutants, which prematurely degrade securin (Penkner et al., 2005, Oelschlaegel et al., 2005). If separase is also expressed in prophase arrested oocytes, it is conceivable that leaky inhibition during this time would cause progressive loss of cohesin. To determine whether separase is expressed in primordial stage oocytes I carried out immunolabelling of paraffin wax ovarian sections with antibodies targeted to separase. The antibody was validated to work in mouse tissue through western blotting of primary culture mouse fibroblasts (Figure 5.14a). Control experiments were performed using a blocking peptide to exclude the possibility that the signal was due to non-specific binding of the separase antibody. To ensure that any separase detected could be attributed to the primordial oocyte rather than the surrounding cells, I co-stained with DDX4 to mark the primordial cytoplasm. The DNA was stained using DAPI (Figure 5.14b). Results of the line-scan indicate that separase localises to the cytoplasm in primordial stage oocytes (n= 2 CD1 mice: 12 oocytes with no blocking peptide; 9 oocytes with blocking peptide). While separase was not detected in the nucleus, I cannot exclude the possibility that it localises transiently to the nucleus, or is present at very low levels. Unfortunately I was unable to establish whether securin is also expressed in primordial-stage oocytes due to the lack of an appropriate antibody for immunolabelling. Analysis of Single-Cell RNA-seq data in human foetal germ cells suggests securin is expressed in oocytes during oogenesis (Li et al., 2017). The presence of securin in primordial-stage oocytes should be determined as it is necessary for separase stability and control.
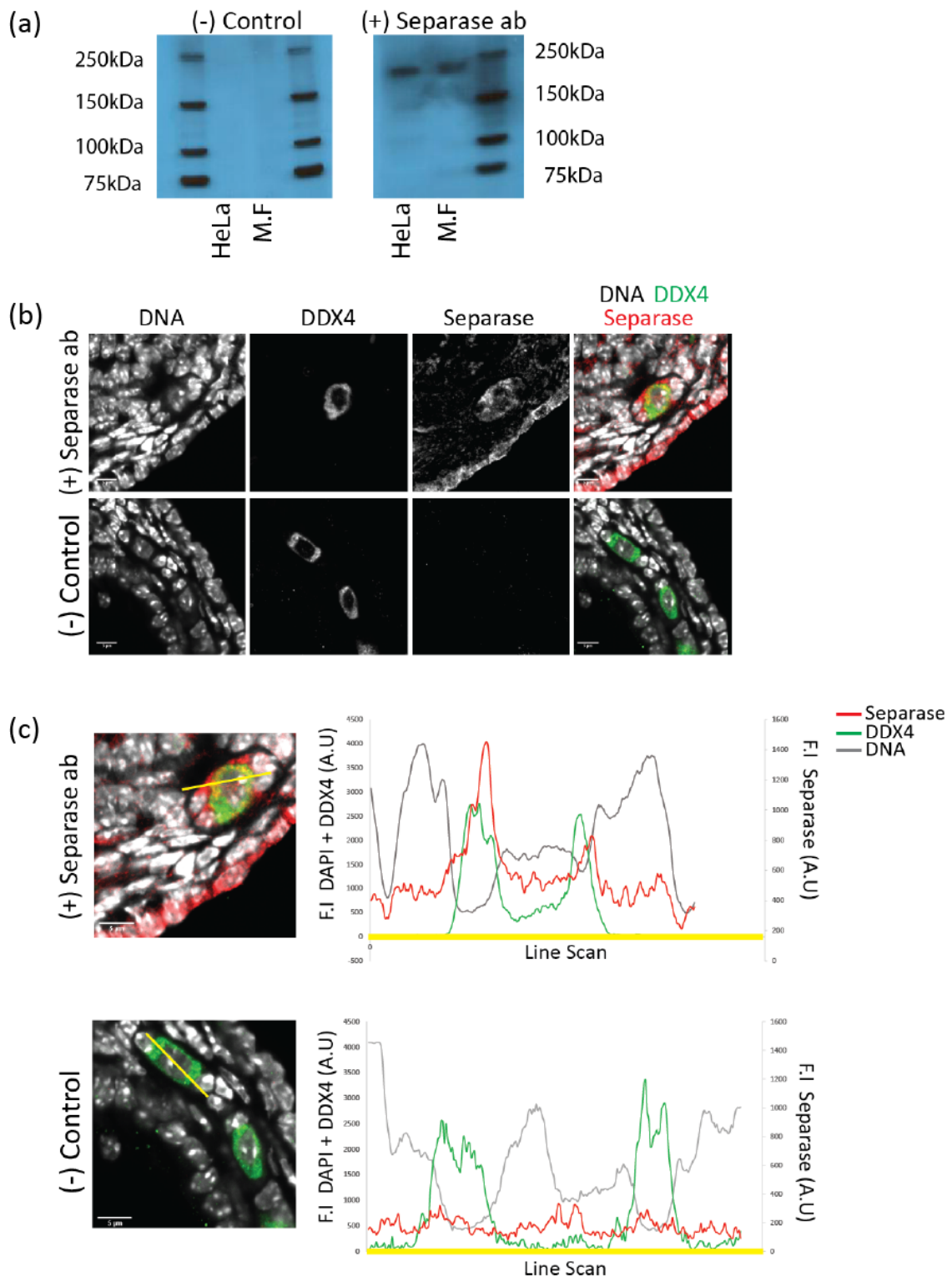
Figure 5.14. Separase localises to the cytoplasm in primordial stage oocytes.

(a) Antibody recognition of mouse separase was validated through western blotting of mouse fibroblasts, using blocking peptide as a negative control and HeLa cells as a positive control. (233 kDa) (b) Representative images of primordial stage oocytes from paraffin wax embedded ovarian sections, immunolabelled with antibodies targeted to separase (with or without blocking peptide). Ovarian sections were also

107

immunolabelled with antibodies targeted to DDX4. Scale bar 5µm (c) Representative line-scan separase peaks with DDX4 while it remains unchanged in those with blocking peptide Scale bar 5µm (n= 2 CD1 mice: 12 oocytes with no blocking peptide; 9 oocytes with blocking peptide).

5.6 Separase does not appear to be responsible for cohesin loss in primordial stage oocytes

While recent work in our lab indicated that cohesin loss in fully grown MI oocytes (GVBD+5hrs) cannot be explained by leaky inhibition of separase, the effect of an oocyte specific deletion of separase on cohesin at the primordial stage has not been tested. As the data above suggests that separase is expressed in the primordial oocyte, I next sought to determine whether the reduction in REC8 in primordial-stage oocytes could be attributed to mis-regulation of separase. To do this I used the separase knockout mouse line developed by Wirth et al. (Wirth et al., 2006). This mouse has the wild-type *separase* gene replaced with a version that has the 8 COOH-terminal exons (exon 24 to exon 31) flanked by *loxP* sights. These exons contain part of the conserved protease domain that is necessary for REC8 cleavage and is removed when *iCre* is expressed (Figure 5.15).
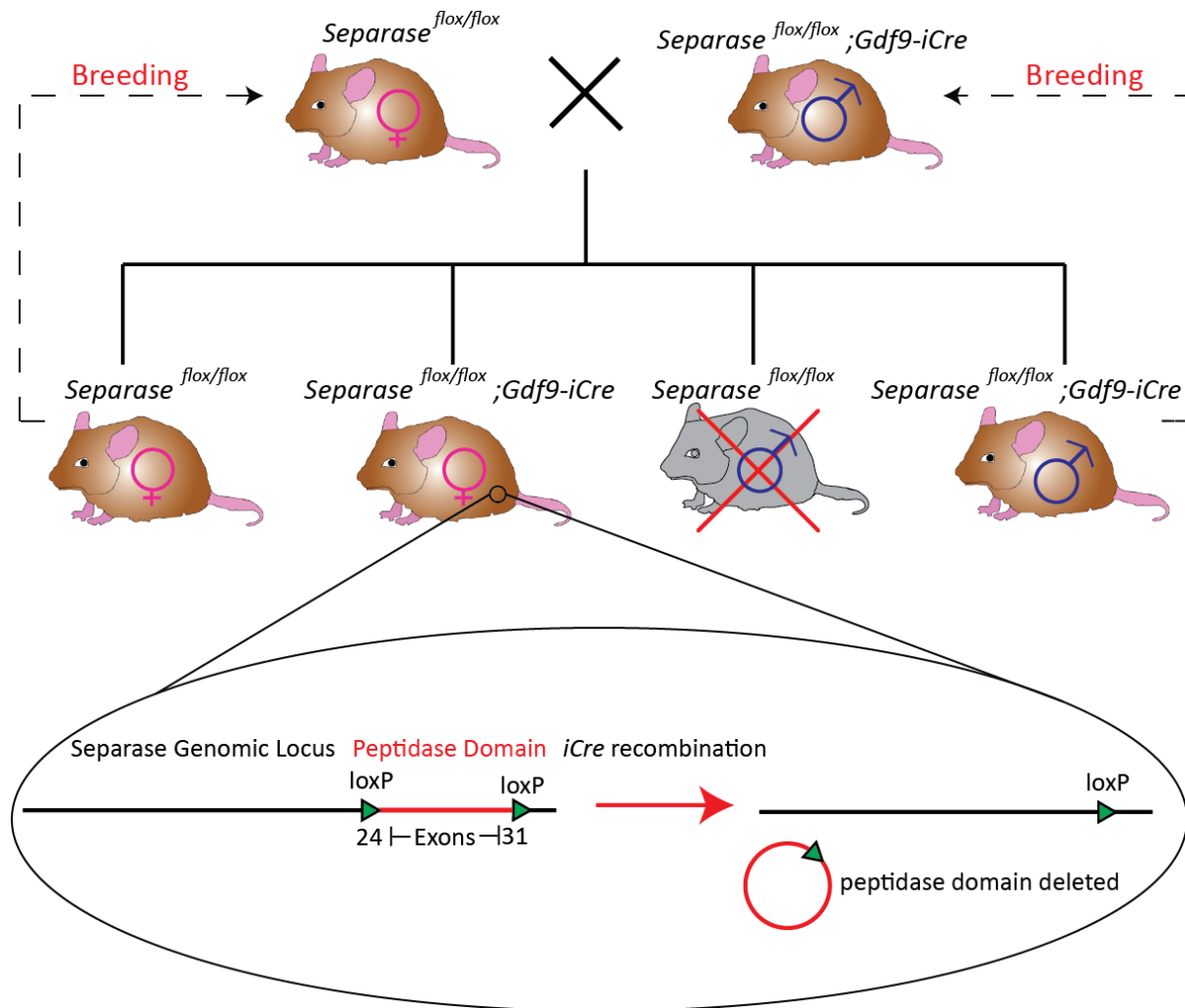
Figure 5.15 Generating oocyte-specific separase knockout mouse. *Schematic diagram showing strategy for breeding. Sep^{f/f};Gdf9-iCre males were breed with Sep^{f/f} females to produce either Sep^{f/f};Gdf9-iCre or Sep^{f/f} offspring. Sep^{f/f} males were culled and Sep^{f/f};Gdf9-iCre males were used for breeding. Sep^{f/f} females were used either as experimental controls or for breeding while Sep^{f/f};Gdf9-iCre females were used for experiments. Expanded circle shows how the separase gene has loxP sites situated at exon 24 and 31. Expression of iCre results in this section being deleted.*

To achieve separase knockout specifically in primordial-stage oocytes, floxed regions of the separase gene were targeted for deletion by *iCre* expression driven from the *Gdf9* promoter (McGrath et al., 1995). *Gdf9* is a member of the transforming growth factor-β superfamily and is expressed in primordial-stage oocytes (Dong et al., 1996). It has been used extensively as a promoter in knockout mice where removal of the investigated gene – in this case separase - is required in the resting primordial oocyte pool (this does not affect the endogenous *Gdf9* gene) (Lan et al., 2004,

Burkhardt et al., 2016). Figure 5.15 shows the breeding strategy to generate $Sep^{f/f}$;Gdf9-iCre. As *iCre* is driven from the Gdf9 promoter, male carriers of *iCre* are fertile with functioning separase. These were used for breeding while $Sep^{f/f}$ males were culled. $Sep^{f/f}$;Gdf9-iCre females were used for experiments with the $Sep^{f/f}$ used as experimental controls, or for breeding. Validation of the knockout was carried out by R. Ballesteros-Meija. He showed that the $Sep^{f/f}$;Gdf9-iCre females are able to resume meiosis but are incapable of undergoing anaphase.

To investigate if separase is responsible for cohesin loss in primordial-stage oocytes I cryo-embedded ovaries from 2 months and 12 months old $Sep^{f/f}$;Gdf9-iCre and $Sep^{f/f}$ mice. These were then sectioned and immunolabelled with antibodies targeted to REC8. DNA was labelled with TO-PRO-3 as a quantification control, and DAPI for locating primordials in the section (Figure 5.16). Confocal images of primordials from $Sep^{f/f}$ and $Sep^{f/f}$;Gdf9-iCre suggest that the loss of REC8 in primordials occurs even in the absence of separase (2 months $Sep^{f/f}$ n=28 from 3 mice, 12 months $Sep^{f/f}$ n=15 from 3 mice 2 months $Sep^{f/f}$;Gdf9-iCre n=18 from 2 mice, 12 months $Sep^{f/f}$;Gdf9-iCre n=5 oocytes from 2 mice).
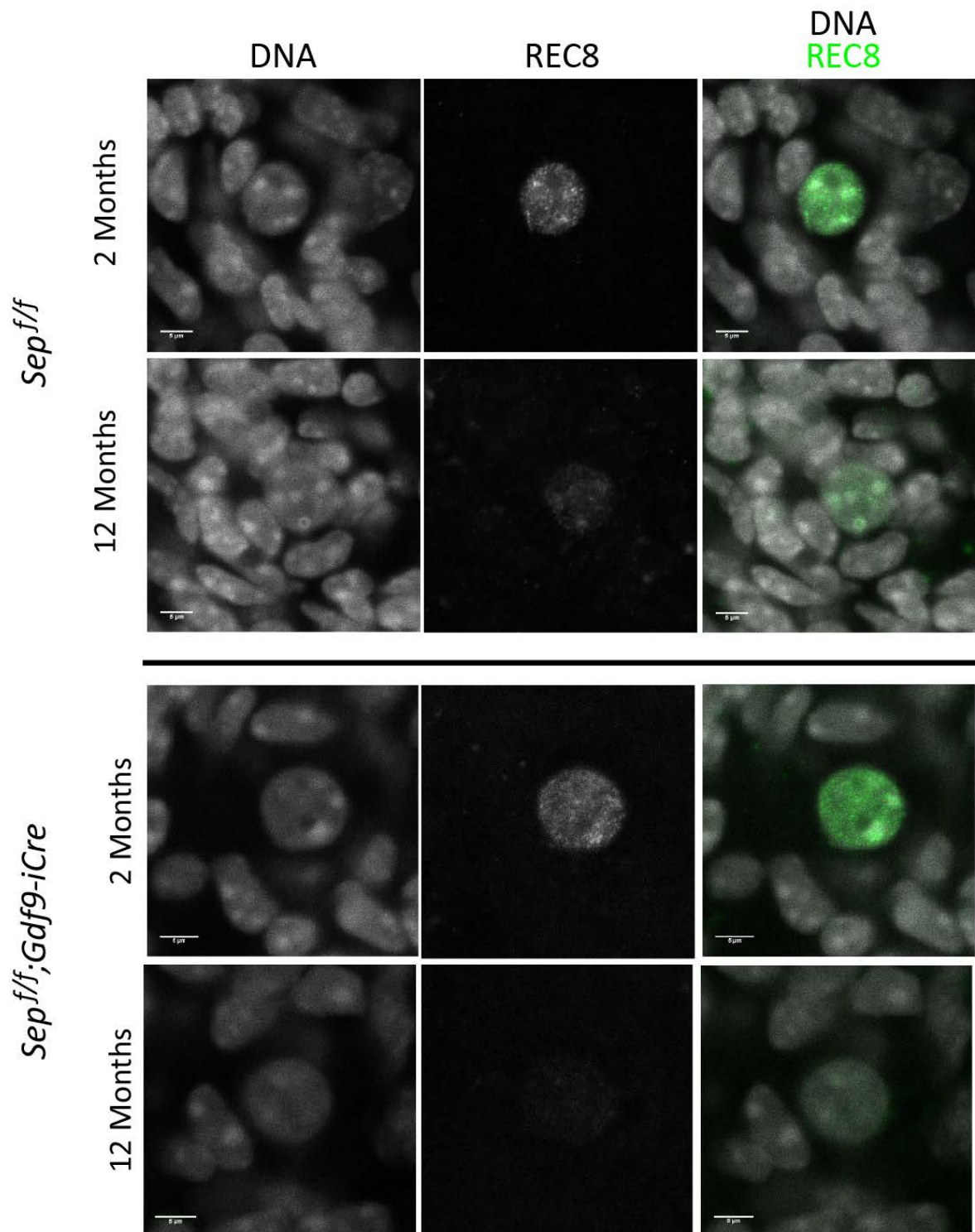
Figure 5.16. REC8 appears reduced in *Separase null* mice with age.

Representative images of REC8 immunolabelling in 2 and 12 months Sep^{f/f} and Sep^{f/f};Gdf9-iCre primordial-stage oocytes. DNA was stained using TO-PRO-3. In both genotypes REC8 appears significantly reduced as a function of age. Scale bar 5μm (2 months Sep^{f/f} n= 28 from 3 mice, 12 months Sep^{f/f} n= 15 from 3 mice 2 months Sep^{f/f};Gdf9-iCre n= 18 from 2 mice, 12 months Sep^{f/f};Gdf9-iCre n=5 oocytes from 2 mice)

111

A consistant problem in attempting to quantify REC8 in *Sep^{f/f};Gdf9-iCre* mice was the difficulty in finding primordials at 12 months of age. For both *Sep^{f/f}* and REC8-Myc mice, 3 sections at 30μm thickness was usually sufficient for finding several primordials in 12 months old mice. This was not the case for *Sep^{f/f};Gdf9-iCre,* which would require 5 sections per-slide to find any primordial.

To quantify chromosome-bound REC8 within primordial stage oocytes, I used Volocity software to segment primordial-stage oocytes as in Figure 5.5. I then calculated the ratio of REC8 to TO-PRO-3 for both *Sep^{f/f}* and *Sep^{f/f};Gdf9-iCre* (Figure 5.17 and Figure 5.18) and looked at the results when all values are combined across the experimental repeats (Figure 5.19) (2 months *Sep^{f/f}* n=28 from 3 mice, 12 months *Sep^{f/f}* n=15 from 3 mice 2 months *Sep^{f/f};Gdf9-iCre* n=18 from 2 mice, 12 months *Sep^{f/f};Gdf9-iCre* n=5 oocytes from 2 mice).

	2 MONTHS			12 MONTHS		
experiment	1	2	3	1	2	3
no. primoridals	11	10	7	7	3	5
no. mice	1	1	1	1	1	1
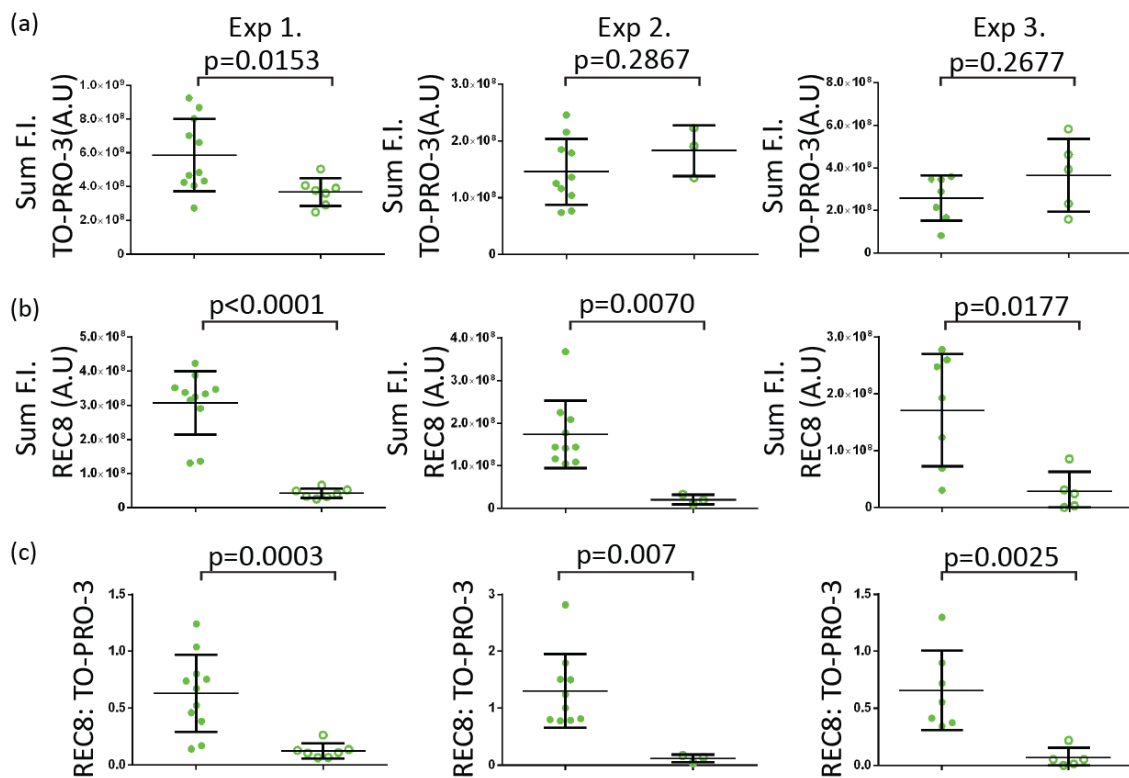
Figure 5.17 Comparison of TO-PRO-3, REC8 and REC8:TO-PRO-3 in *Sep^{f/f}*

primordials. *Dot plots of comparisons between 2 and 12 months for Sep^{f/f}, each experiment showing (a) total TO-PRO-3 fluorescence intensity (b) total REC8 fluorescence intensity and (c) ratio of REC8: TO-PRO-3 for each primordial oocyte. A Mann-Whitney U-test was used to establish p-values, with a p-value of less than 0.05 classed as significant. Error bars represent the mean ± s.d. for each mouse. The number of oocytes and mice used from each age group and each experiment is shown in the table above.*

	2 MONTHS ■		12 MONTHS □	
experiment	1	2	1	2
no. primordials	9	9	3	2
no. mice	1	1	1	1

(a)

(b)

(c)
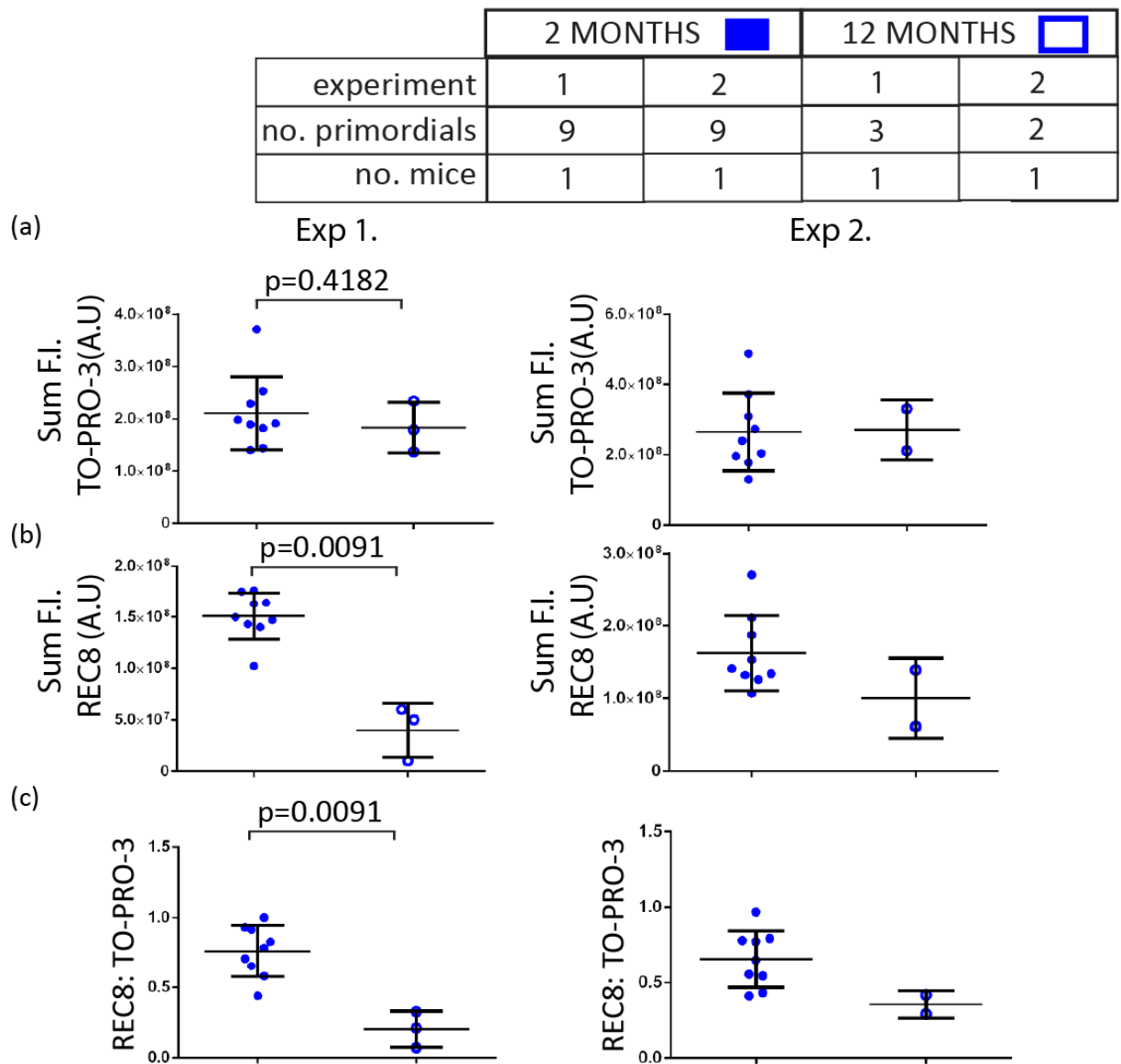
Figure 5.18 Comparison of TO-PRO-3, REC8 and REC8: TO-PRO-3 in Sep$^{f/f}$;Gdf9-iCre primordials. *Dot plots of comparisons between 2 and 12 months for Sep$^{f/f}$;Gdf9-iCre, each experiment showing (a) total TO-PRO-3 fluorescence intensity (b) total REC8 fluorescence intensity and (c) ratio of REC8:TO-PRO-3 for each primordial oocyte. A Mann-Whitney U-test was used to establish p-values, with a p-value of less than 0.05 classed as significant. Error bars represent the mean ± s.d. for each mouse. The number of oocytes and mice used from each age group and each experiment is shown in the table above.*
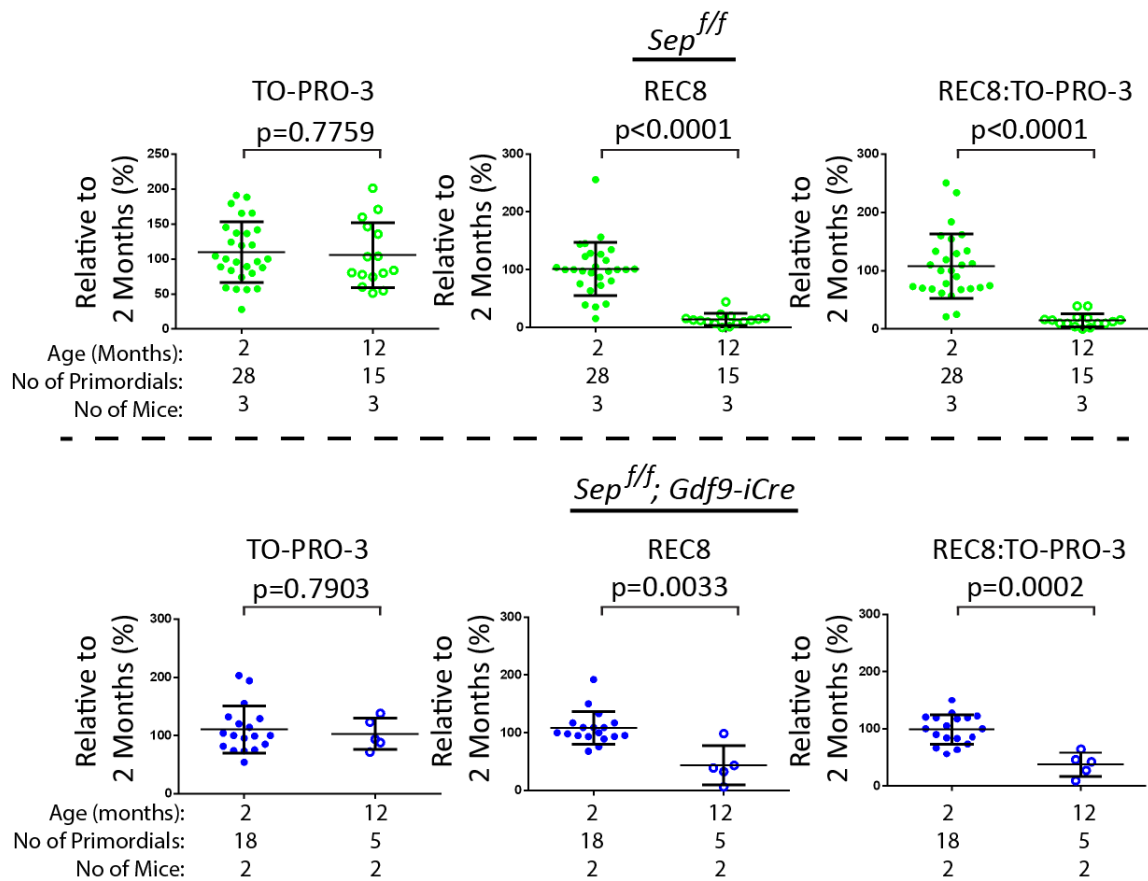
Figure 5.19 REC8 is significantly reduced regardless of the presence of separase. *Combined values relative to 2 months old for TO-PRO-3, REC8 and REC8:TO-PRO-3 for Sep^{f/f};Gdf9-iCre and Sep^{f/f}. An unpaired t-test was used to establish p-values for TO-PRO-3 and REC8:TO-PRO-3. A Mann-Whitney U-test was used for REC8. A p-value of less than 0.05 classed as significant. Error bars represent the mean ± s.d. (2 months Sep^{f/f} n= 28 from 3 mice, 12 months Sep^{f/f} n= 15 from 3 mice 2 months Sep^{f/f};Gdf9-iCre n= 18 from 2 mice, 12 months Sep^{f/f};Gdf9-iCre n=5 oocytes from 2 mice).*

The results herein suggest that the decline in REC8 occurs in primordial-stage oocytes in both *Sep^{f/f}* (p<0.0001) and *Sep^{f/f};Gdf9-iCre* mice (p=0.0002). This suggests that regardless of the presence of functioning separase, REC8 is lost with ageing. These results are in agreement with the work carried out by R. Ballesteros-Meija in aged *Sep^{f/f};Gdf9-iCre* and *Sep^{f/f}* fully grown mouse oocytes at metaphase I (GVBD+5hours). These results indicated a reduction in REC8 in *Sep^{f/f};Gdf9-iCre* at 12 months, similar to that in the control *Sep^{f/f}*. This combined work suggests that separase is most likely not responsible for the progressive loss of cohesin in primordial stage oocyte development.

115

5.7 Are the protectors of cohesin compromised in primordial-stage oocytes from older females?

The findings from R Ballesteros-Meija work and mine suggest that age-related cohesin loss occurs by a separase independent mechanism. I next asked whether the age related loss of cohesin happens as result of the cohesin protectors being compromised during prophase arrest. SGO1 and SGOL2 are both expressed in fully grown mouse oocytes, with SGOL2 playing the key role in recruitment of PP2A and cohesin protection in mammalian meiosis (Lee et al., 2008, Rattani et al., 2013). While SGO1 knockdown caused a significant difference in misalignment 14 hours after GVBD, its knockdown at the GV stage was reported not to result in segregation errors (Lee et al., 2008). As we have seen from R. Ballesteros-Meija and my own work, the loss of cohesin occurs well before this stage and so any loss of protection should be looked for in primordial-stage oocytes.

Analysis of transcriptomic data from single cell RNAseq of human germline cells shows expression of SGO1 and SGOL2 in germline cells, suggesting that both are expressed in early development (Figure 5.20) (Li et al., 2017).
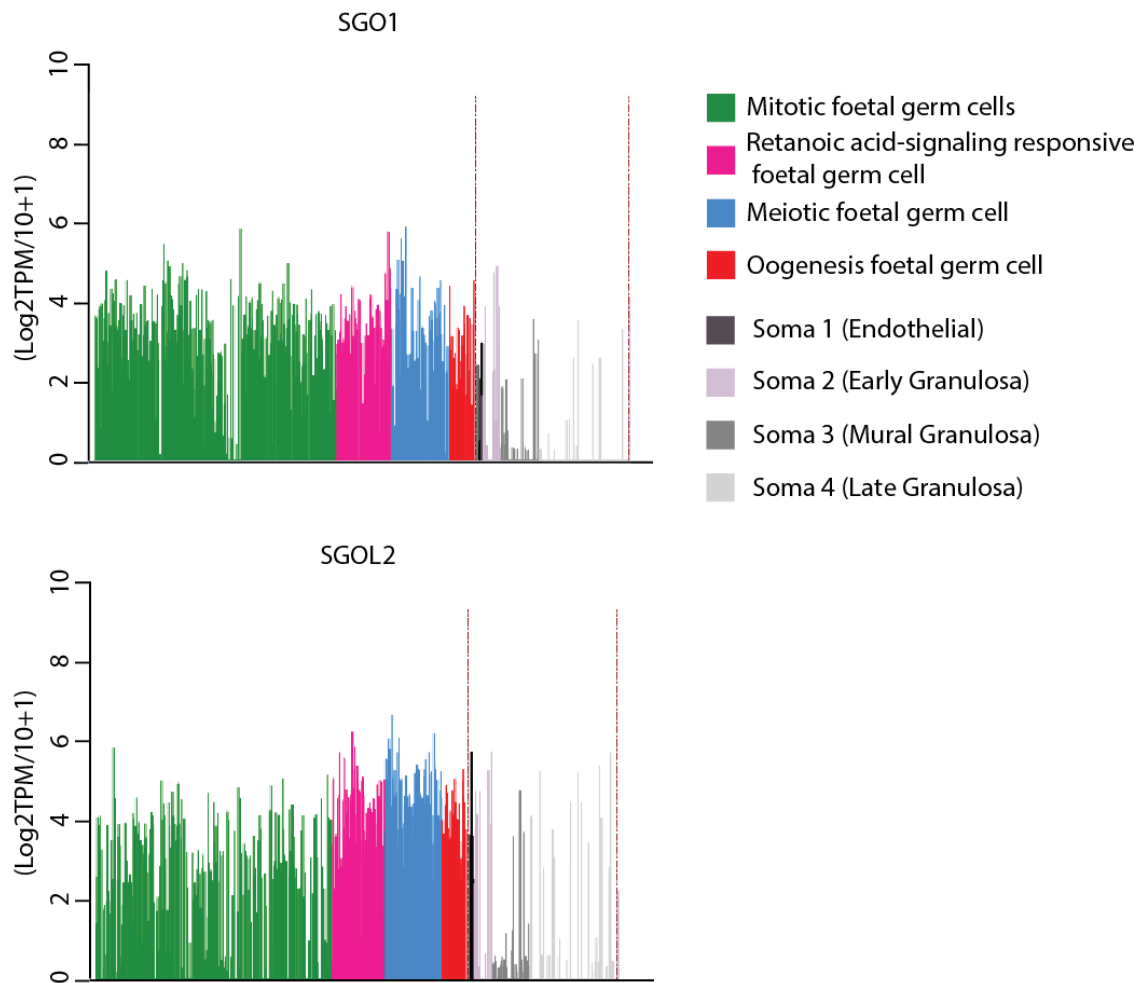
Figure 5.20 SGO1 and SGOL2 appear to be expressed during oogenesis in humans. *Graphs showing transcriptomic analysis of SGO1 and SGOL2 during oogenesis as well as in somatic cells. Both transcriptomes appear to be expressed throughout oogenesis with SGOL2 expressed most at the later stages of oocyte development (Li et al., 2017).*

Repeated attempts to immunolabel SGOL2 in primordial-stage oocytes in paraffin wax and OCT embedded sections did not indicate any clear staining. While it is possible that this could be as a result of experiment specific antibody failure, results from *Lister et al. 2010* show that SGOL2 is localised in the nucleolus of GV stage oocytes. This is then recruited to the centromeres during early metaphase I (Lister et al., 2010). Thus, while SGOL2 appears to be sequestered in the nucleoli in fully grown oocytes, we cannot rule out the possibility that it is present on chromosomes in primordial stage oocytes.

117

To investigate SGO1 localisation I immunolabelled ovarian sections with antibodies targeted to SGO1 (2 months n=29 eggs from 3 mice). SGO1 is clearly enriched on regions of heterochromatin in primordial-stage oocytes. This enrichment appears to be maintained through GV stage and resumption of meiosis (Figure 5.21).
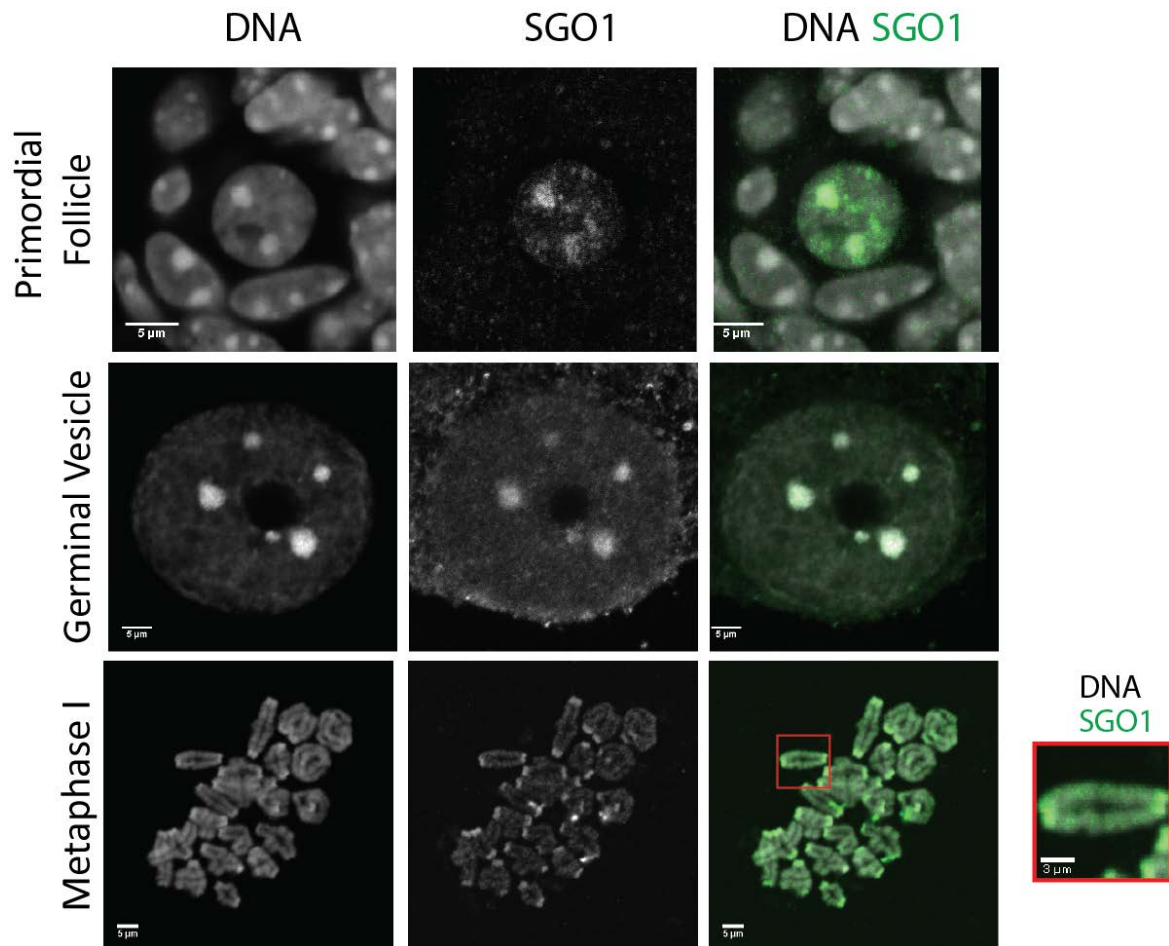
Figure 5.21 SGO1 is enriched at oocyte chromocentres and pericentromeres throughout oogenesis. *Confocal images of representative Primordial Follicle, Germinal Vesicle and metaphase I oocytes. Scale bar 5µm. Inset of metaphase I shows an individual bivalent chromosome with SGO1 localising to the pericentromeres. Scale bar 3µm*

To investigate whether ageing has any impact on SGO1 in primordial-stage oocytes, I carried out immunolabelling with antibodies targeted to SGO1 on ovarian sections from 2 months and 12 months old C57BL/6 mice (2 months n=29 eggs from 3 mice; 12 months n=18 eggs from 3 mice). Representative images of primordial stage oocytes from young and aged mice suggest that by 12 months the localisation of SGO1 to heterochromatin is lost, with SGO1 more prevalent on areas of euchromatin (Figure 5.22).
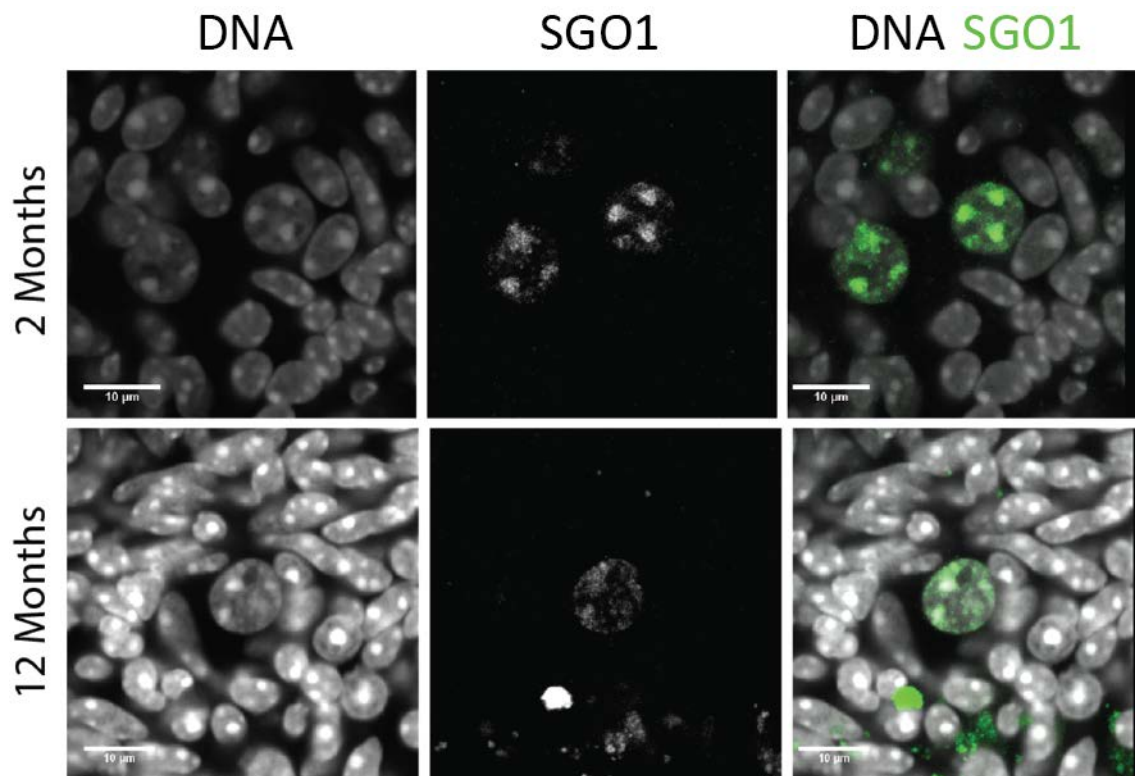
Figure 5.22 SGO1 appears to have reduced localisation to the heterochromatin with age. *Representative images of primordial-stage oocytes from 2 and 12 months old C57BL/6 mice, immunolabelled for SGO1 and the DNA stained using TO-PRO-3.SGO1 localisation to heterochromatin appears reduced with age mice. Scale bar 10µm (2 months n= 29 eggs from 3 mice; 12 months n= 18 eggs from 3 mice).*

To determine the significance of this reduced localisation I used the Volocity software co-localisation function, to determine the co-localisation between SGO1 and heterochromatin regions marked by TO-PRO-3. ROIs were drawn round primordial-stage oocytes and the Pearsons co-efficient value calculated. This suggest that SGO1 becomes mislocalised as a result of ageing in primordial-stage oocytes (mean Pearsons co-efficient: 2 months - 0.58; 12 months - 0.35) (2 months n= 29 eggs from 3 mice; 12 months n= 18 eggs from 3 mice) (Figure 5.23).

119
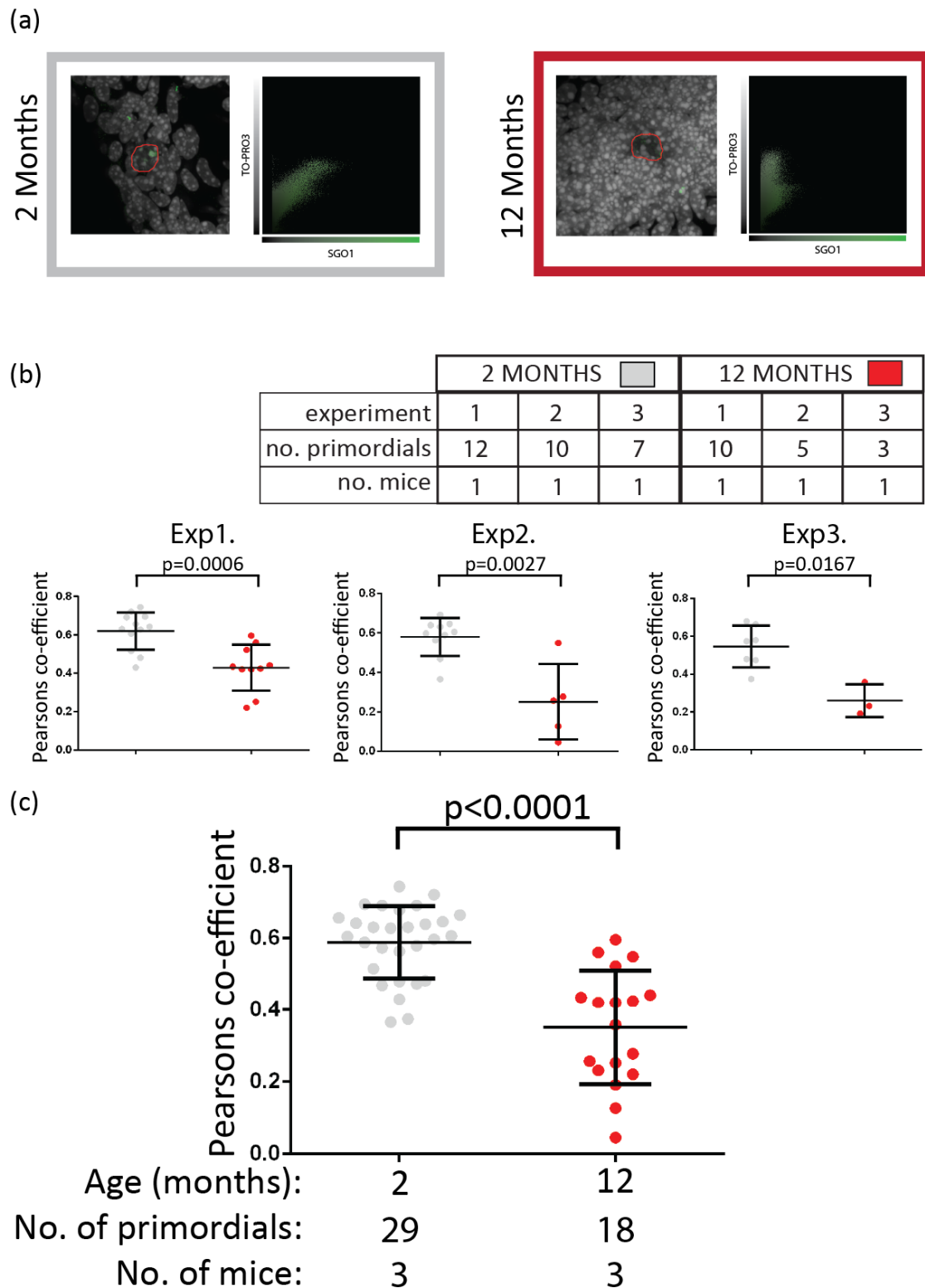
Figure 5.23 SGO1 becomes mislocalised with age in primordial-stage oocytes.

(a) Co-localisation analysis was carried out with regions of interest (Red circles) drawn around primordial-stage oocytes in z-stacks. The fluorescence intensity for SGO1 and TO-PRO-3 in each pixel was plotted against each other in a scatter plot and the Pearsons co-efficient calculated. (b) Dot-plots showing the Pearsons co-efficient for each primordial oocyte (SGO1vsTO-PRO-3) in the 3 experimental

repeats. A Mann-Whitney U test was used to test significance (p<0.05) between the 2 and 12 months. Error bars represent mean and ± s.d. (c) shows a combined dot-plot of the Pearsons co-efficient from all 3 experiments. Unpaired t-test show that there is a significant reduction in correlation between SGO1 and TO-PRO-3 between 2 and 12 months (p<0.0001). (2 months n= 29 eggs from 3 mice; 12 months n= 18 eggs from 3 mice)

I next sought to determine whether this mislocalisation from heterochomatin is accompanied by a global loss of SGO1 in primordial-stage oocytes. To do this I used Volocity software as in Figure 5.5 to calculate the sum fluorescence intensity of Sgo1 and TO-PRO-3 in each primordial oocyte. The data shown in Figure 5.24 indicates that SGO1 was significantly reduced in only 1 of the 3 pairs of mice included in this experiment. This suggests that the mislocalisation seen in Figure 5.23 does not always result in an overall loss of SGO1 in the primordial oocyte.

		2 MONTHS			12 MONTHS		
experiment		1	2	3	1	2	3
no. primordials		12	10	7	10	5	3
no. mice		1	1	1	1	1	1
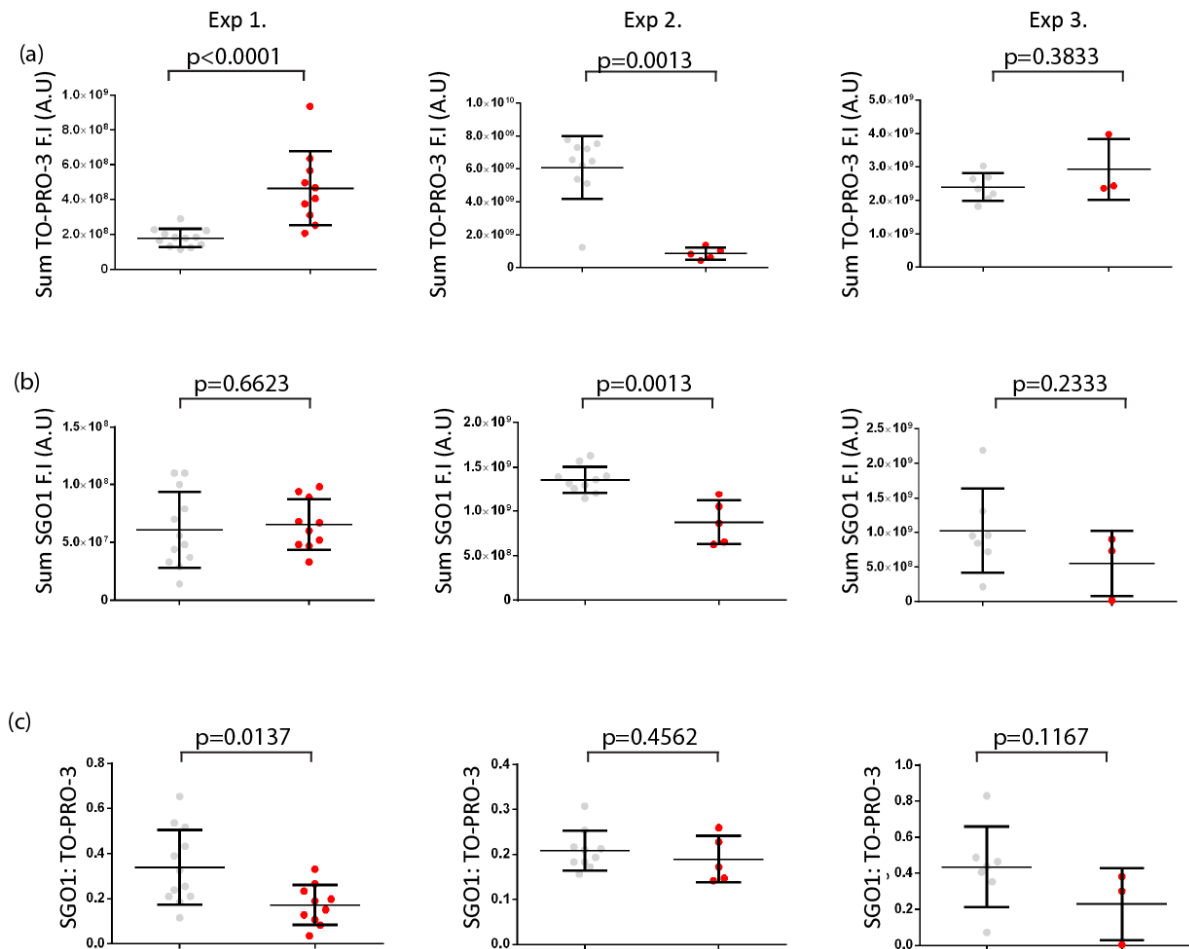
Figure 5.24 SGO1 does not appear to be reduced overall in primordial-stage oocytes. *Dot plots from each experiment showing (a) sum TO-PRO-3 fluorescence intensity (b) sum SGO1 fluorescence intensity and (c) ratio of SGO1 to TO-PRO-3. Each primordial oocyte is represented by an individual dot. Error bars represent mean and ± s.d. A Mann-Whitney U-test was used to establish p-values with a p-value of less than 0.05 classed as significant. The ratio of SGO1:TO-PRO-3 showed no significant difference in 2 of the 3 experiments.*

The results in this section suggest SGO1 localisation is affected by ageing but that it does not cause a total loss of the protein. While I was unable to establish if PP2A is expressed in primordial-stage oocytes, this work suggests that if SGO1 does provide protection against the prophase pathway in meiosis then this protection could be compromised with age.

5.8 Discussion

The age-related loss of cohesin in oocytes presents a viable model for the increase in premature separation of sister centromeres in meiosis (Chiang et al., 2010, Lister et al., 2010). While this has been understood in mouse oocytes for some time, the mechanisms involved in cohesin loss have remained elusive.

Oocytes differ from sperm in that they are produced well before puberty and undergo a prolonged prophase arrest which can last several decades in humans and several months in mice (Herbert et al., 2015). It was until recently unclear whether cohesin depletion occurs during the prolonged prophase arrest experienced by oocytes from older females, or whether cohesin is lost as a consequence of the intense metabolic activity associated with oocyte growth. It is conceivable that this may result in increased reactive oxygen species (ROS) generation in oocytes of older women, leading to damage to cohesin. Work done by R. Ballesteros-Meija in our group however, suggests that the loss of cohesin occurs before the growth phase, at the primordial follicle stage. While this was an important finding it does not tell us whether this loss occurs progressively over time, or if non-REC8 containing forms of cohesin are in the nucleus. To gain a greater understanding of what mechanisms could be involved it was first necessary to define the time frame in which cohesin is lost.

Studies on primordial-stage oocytes have been hampered due to the difficulty in distinguishing them from other cells in the ovary. This is made even more difficult in ageing studies as the number of primordial-stage oocytes decreases as a result of ovarian exhaustion (Adhikari and Liu, 2009). To address this it was necessary to first train my eye in the recognition of primordial stage oocytes in both cryo- and paraffin wax embedded sections. This was done through the immunolabelling of proteins present only in meiotic cells. I then validated whether I had selected one correctly based on whether it showed any staining. As has been described in previous publications, primordial-stage oocytes can be distinguished from more developed follicles due to the presence of a single layer of flattened granulosa cells and the absence of a ring of cuboidal cells (Adhikari and Liu, 2009). This allowed me to spot them by eye without the need for continued use of these markers.

Imaging of DNA in cryosections of primordial-stage oocytes, revealed discrete areas of DNA enrichment. I sought to define how the DNA in the primordial oocyte is compacted compared to in fully grown oocytes after GVBD. Antibody staining using the heterochromatin marker H3K9me3 and the marker of centromeric proteins CREST, showed that they co-localised in primordial-stage oocytes. This revealed that the future pericentromeres of primordial-stage oocytes form clusters during prophase before DNA condensation. As so many proteins which are necessary for accurate chromosome segregation localise to the pericentromere during meiosis, it is important to distinguish this region from the rest of the DNA, as its integrity is essential for the two sequential divisions (Herbert et al., 2015).

Another issue in terms of studying primordial-stage oocytes is the high level of cell death that is known to occur. To ensure that the primordial-stage oocytes being measured are not in fact atretic, I used the cell death marker TUNEL to label any potentially dead primordial-stage oocytes in the ovary. During the course of this work, however, I only encountered a few TUNEL-positive primordial-stage oocytes. This contrasts with previous findings in the lab and the basis for this is currently unclear. In humans, primordial oocyte atresia was modelled at around 1000 a month after puberty. This number increased around 37 years of age until menopause (Faddy and Gosden, 1996, Faddy, 2000). It is possible that in this work, the ages being used avoided periods of higher cell death.

Having established how to locate primordial stage oocytes as well as distinguish their DNA morphology, I sought to compare chromosome-bound REC8 through immunolabelling in cryosections from 2, 6 and 12 months old mice. The results indicated, that when all experiments are combined, that REC8 is lost by a significant amount by 6 months of age, with further reductions by 12 months. After plotting the median value of each REC8: TO-PRO-3 for each age group, it appeared that the loss of REC8 occurs in a linear fashion rather than an accelerated one with ageing. While this progressive loss with age is in agreement with the results in *Chiang et al. 2010*, they saw an accelerated loss happening with age in fully grown MI oocytes (Chiang et al., 2010). While it is possible this is occurring, previous difficulties in accurately quantifying proteins on chromosome whole-oocyte fixations and spreads, due to changes in chromosome morphology, mean there may be some discrepancies. This
124

is borne out by the fact that in their results, they see an increase in REC8 between 12 and 15 months.

This result provides information in regards to what mechanisms could be involved in cohesin loss. It suggests that the mechanism leading to loss of cohesin is acting throughout the mouse's life. It would be interesting to see if loss of cohesin in human primordial-stage oocytes occurs in a similar fashion. It is clear from observations of trisomy rates that there is a breaking point around 35 years of age when aneuploidy becomes significantly more likely (Hassold and Hunt, 2001). The only study to look at this in human ovarian sections did not remove soluble cohesin, obscuring any age-related affected on chromosome-bound cohesin (Tsutsumi et al., 2014).

The results in these experiments cast some doubt on the effectiveness of TO-PRO-3 as a tool for normalising proteins of interest to. It is unclear why this is the case as DNA labelling should remain consistent with age. This does not negate the work previously carried out in our lab which suggested it to be an effective tool. Indeed, the subsequent experiments in this Chapter, it often remains consistent within an experiment. It is also not appropriate to remove normalisation from the analysis as regions of interest can vary based on how easy the primordial is to segment from the surrounding somatic cells. As the variation in TO-PRO-3 appears to be agnostic to age, and is often lost when the data from individual experiments are combined its use is still required for analysis of primordial oocytes.

I next investigated whether SMC3 is also lost in primordial stage oocytes similarly to REC8. SMC3 is the only conserved component between both mitotic and meiotic cohesin and its acetylation by ESCO1 and ESCO2 is key for establishing cohesive cohesin (Minamino et al., 2015). While REC8 is undoubtedly the key α-kleisin subunit in meiosis, it is not clear if other cohesin complexes may be present in the primordial oocyte during this time. Work carried out in SMC1β knockout mice indicated that even in its absence, single chromatids do not start to appear until 4 months of age (Hodges et al., 2005). To investigate if SMC3 is also depleted in a similar manner to REC8, I co-stained SMC3 with REC8 in REC8-MYC mice. SMC3 and REC8 co-localise together in primordial-stage oocytes, with both showing discrete staining at areas of enriched heterochromatin. This is absent from the surrounding somatic cells

which show an absence of SMC3 in areas of heterochromatin compared to the euchromatin.

Quantification of SMC3 indicated that by 12 months it was significantly reduced in primordial-stage oocytes, similar to REC8. However, comparisons of the magnitude of the decline suggest that REC8 is lost to a greater extent. While it is worth noting that there are technical reasons for this difference in decline (such as encroachment from the surrounding somatic cells or variations in background), it cannot be excluded that there may be other cohesin complexes in the oocyte.

To address whether there may be other cohesin complexes present I carried out immunolabelling for RAD21 in paraffin wax sections. This showed a small but detectable amount of RAD21 in primordial-stage oocytes. The significance or purpose of this RAD21 is unclear. Experiments in which all REC8 was artificially cleaved during metaphase I in mouse oocytes indicated that acute and complete loss of REC8 results in resolution of bivalents to their four constituent chromatids. When this was replicated for RAD21 there was no separation showing it does not provide significant cohesion (Tachibana-Konwalski et al., 2010). It would be interesting to determine how RAD21 levels are affected by ageing in primordial-stage oocytes.

Observations of the SMC3 in the surrounding granuolsa cells also suggests that they do not suffer the same loss of cohesin as the oocyte does. It remains unclear whether the granulosa cells which surround the oocyte must be maintained along with the oocyte until they are recruited to undergo growth. As they are so crucial for signalling and ovulation it would be interesting to investigate whether they are turned over at all during development and, if not, what affect ageing has on them?

Previous work in our group looking at an age-related reduction of cohesin in fully grown oocytes from *separase null* mice showed that separase is not responsible for cohesin loss. However, this was not investigated in primordial-stage oocytes were the age-related loss of cohesin occurs. Several factors led us to select leaky inhibition of separase as a likely culprit for cohesin loss. Separase is undoubtedly the key orchestrator of cohesin cleavage in meiosis (Kudo et al., 2006). Our understanding from Mnd2 mutants in yeast, which have destruction of securin during prophase arrest, also suggests that separase can act during prophase (Penkner et

126

al., 2005, Oelschlaegel et al., 2005). Using immunofluorescence staining, I was able to detect separase in the cytoplasm of primordial-stage oocytes in paraffin wax embedded sections. This indicates that separase is present in primordial stage oocytes.

Staining of ovarian sections for REC8 in *Sep^{f/f};Gdf9-iCre* and *Sep^{f/f}* mice showed that REC8 was reduced with ageing regardless of whether separase is expressed or not. Interestingly, however, attempts to find primordial-stage oocytes in *Sep^{f/f};Gdf9-iCre* mice was on the whole harder than in *Sep^{f/f}*. This requires more investigation including counts of primordial-stage oocytes in sections, however it is an intriguing prospect. It is understood that cohesin is necessary for DNA repair (Nasmyth, 2011) . If this cohesin was perhaps removed by separase after DNA repair (which would not be present in the knockout) its absence could lead to increased cell death over time due to DNA damage not being fixed.

With separase not appearing responsible for cohesin loss during prophase arrest, it is possible that cohesin is being removed through a separase independent mechanism. It would also be possible that cohesin is being damaged by reactive oxygen species, and due to the lack of turnover in cohesin it is not replaced. These are potential mechanisms which should be further investigated.

As the age-related loss of cohesin appeared to be separase-independent, it was therefore pertinent to ask whether cohesin is provided with any protection during prophase arrest. Cohesin protection is entrusted to SGOL2 after GVBD (Rattani et al., 2013, Llano et al., 2008, Lee et al., 2008). While it would appear that both SGOL2 and Sgo1 are expressed in oocytes during oogenisis, the results in this section suggest that it is only SGO1 that localises to the heterochromatic regions of primordial-stage oocytes. A co-localisation that appears to be maintained in fully grown prophase arrested oocytes as well as during M phase of meiosis I. Co-localisation analysis of SGO1 at the pericentromeres however, showed that this becomes compromised with ageing in primordial-stage oocytes. While the overall level of SGO1 appears unaffected by age, the fraction co-localising with heterochromatin is markedly reduced and this is accompanied by increased staining on euchromatin. Localisation of SGO1 is dependent upon phosphorylation of H2A-T210, which allows docking of SGO1 at the pericentromeres (Tang et al., 2004,

127

Kitajima et al., 2005, Kawashima et al., 2010). It would therefore be interesting to see if changes in chromatin or BUB1 or both are responsible for mislocalisation of SGO1 during female ageing. Also, to determine whether PP2A is present as it is required for SGO1 to protect cohesin (Kitajima et al., 2006, Riedel et al., 2006).

The results in this section suggest that cohesin is lost progressively in primordial-stage oocytes via a separase independent mechanism. Also, that other non-REC8 containing cohesin complex are present in the primordial-stage oocyte.

Chapter 6. Results: Effects of ageing on chromosome-bound cohesin in human oocytes

The age-related depletion of chromosome-bound cohesin in mouse oocytes, provides a plausible molecular basis for the increase in chromosomal segregation errors seen in human oocytes (Lister et al., 2010, Chiang et al., 2010). While the clinical significance of cohesin depletion has not been directly tested, several observations in human oocytes are consistent with findings in the mouse. Firstly, the age-related segregation errors in human oocytes appear to be as a result of a lack of chromosomal cohesion (Angell, 1991, Sakakibara et al., 2015). This is reflected in the tendency towards premature separation of sister centromeres leading to single chromatid rather than whole chromosome errors in oocytes from older women (Pellestor et al., 2003). Secondly, a number of studies on human oocytes have reported that the distance between sister centromeres increases as a function of age. This is often used as a proxy measurement for depletion of centromeric cohesin (Zielinska et al., 2015, Sakakibara et al., 2015, Lister et al., 2010, Lagirand-Cantaloube et al., 2017, Duncan et al., 2012, Chiang et al., 2010, Patel et al., 2015).

To date, there is only one report (Tsutsumi et al., 2014), of direct measurements of cohesin in human oocytes. This was performed on ovarian sections and reported only a modest decline, which was not detected until an advance age (49 years old) (Tsutsumi et al., 2014). However, soluble cohesin was not removed in this study and recent findings in our lab indicate that the quantity of soluble cohesin remains unchanged with age (R. Ballesteros-Meija). Another study looking at air-dried chromosome spreads claimed to see no significant difference in REC8 between younger and older women in immunofluorescence analysis. However this study did not involve a systematic comparison of cohesin levels in oocytes obtained from younger and older women; the oldest woman in the study was 34 years old (Garcia-Cruz et al., 2010).

One reason for the continued difficulty in determining whether cohesin is affected by age is a lack of appropriate sample material. The predominant source of oocytes used for research into female human meiosis are those that fail to mature following ovarian stimulation and can therefore not be used for ICSI (Webster and Schuh, 2017). In all, 15-20% of oocytes obtained following ovarian

stimulation are either still arrested in prophase of meiosis I (GV stage) or in M phase (MI). While these "ICSI-reject" oocytes have been intensively investigated, it is not known whether this population of oocytes reflects the "wildtype". For example, whatever caused delayed progression through the meiotic divisions, might also affect chromosome segregation. More generally, our knowledge of oocyte aneuploidy, particularly at advanced female age, is derived from high-risk cases undergoing IVF treatment. We therefore aimed to obtain a supply of oocytes from volunteer donors ranging in age from 18 to 45 years old with no previous history of infertility. In this Chapter, I present an analysis of reproductive ageing in our population of volunteer donors. The work also represents the first systematic investigation of age-related changes to chromosomal cohesin in fully grown human oocytes.

6.1 ICSI-reject vs oocytes retrieved from non-patient donors: retrieval strategy

To circumvent using ICSI-reject oocytes for future research, we established an oocyte donation programme involving volunteer, non-patient donors at Newcastle Fertility Centre. We sought to retrieve oocytes before they had completed the first meiotic division, and ideally at the GV stage, before entering M phase of meiosis I. During IVF treatment, the transition from prophase to M phase of meiosis is triggered by administration of human chorionic gonadotrophan (hCG). Oocytes are normally harvested 36-38 hours after hCG injection, when the majority(~80%) have completed the first meiotic division, which is ascertained by the presence of the first polar body. Our strategy to obtain oocytes before completion of meiosis I was to reduce the interval from hCG injection to oocyte harvest. Because the time course of meiotic progression in human oocytes in vivo is unknown, the initial stages of the project involved some trial and error to identify the optimal time to obtain immature oocytes, ranging from 12-37 hours post-hCG injection. Figure 6.1 shows the oocyte retrieval schemes used for ICSI-reject oocytes and non-patient donor oocytes.
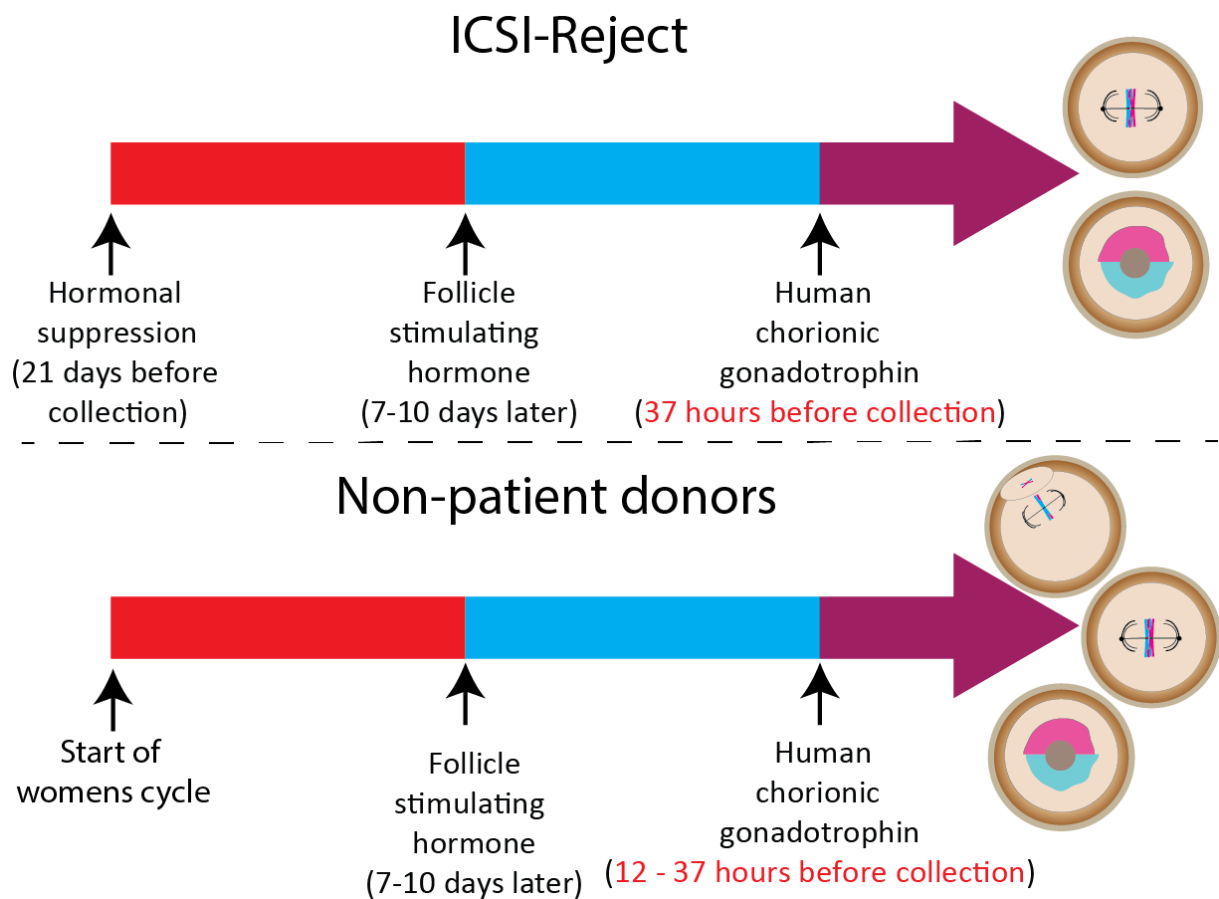
Figure 6.1 Stimulation regimes used for obtaining oocytes from human donors.
Figure shows schematic of the two stimulation regimes used for obtaining oocytes. ICSI-reject oocytes consist of the small population of immature oocytes collected at 37 hours post hCG administration. These are not suitable for ICSI due to the lack of a polar body. Non-patient donor eggs were collected 12- 37 hours post hCG with the oocyte collection regime timed to the woman's natural cycle rather than with hormonal suppression.

According to our current understanding, the decline in fertility during female ageing is a consequence of the combined effects of (i) depletion of the ovarian reserve of primordial follicles (also known as ovarian ageing (Broekmans et al., 2007) and (ii) the increased incidence of aneuploidy (Herbert et al., 2015). To investigate the decline in ovarian reserve in our population of donors, I analysed a number of measures of ovarian function (Figure 6.2). This included levels of anti-Müllerian hormone (AMH), which is produced by growing follicles and is taken as a measure of ovarian reserve. AMH levels become progressively lower as women approach the menopause (Visser et al., 2006). I also analysed the effect

131

of female age on the number of antral follicles detected by ultrasound scan before the hCG injection. As would be expected, follicle number and AMH declined as a function of female age. The strongest relationship is a negative correlation between AMH and the age of the woman (r= -0.6218). Consistent with this, there is also a negative correlation between follicle number and age (r= -0.5118) and a positive correlation between follicle number and AMH (r= 0.5067 respectively) (Figure 6.2). I excluded the number of oocytes retrieved in this comparison, as this varied, depending on the time interval from hCG injection to oocyte harvest.
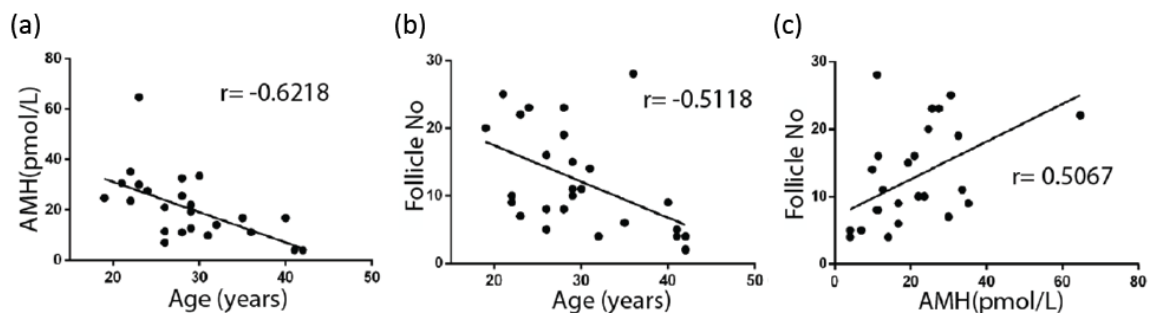
Figure 6.2 Age, follicle number and AMH levels are correlated in non-patient donor population. *Figure shows dot plots of (a) AMH vs age, (b) follicle number vs age, (c) follicle number vs AMH. Pearson's co-efficient for each graph shows a strong correlation with (a) and (b) having a negative correlation (r= -0.6218 and r= -0.5118respectively) and (c) showing a positive correlation between AMH and follicle number (r= 0.5067). (25 donors)*

6.2 The number of oocytes retrieved and the stage of meiosis they have reached is dependent on age and post-hCG retrieval time

Prior to this study, our understanding of obtaining immature oocytes from women has relied on what we can infer from oocytes retrieved for IVF treatment. A primary measure of success of the donation scheme is the number of oocytes retrieved. Consistent with the findings above, the number of oocytes retrieved declines with age (p=0.0282) (Figure 6.3).
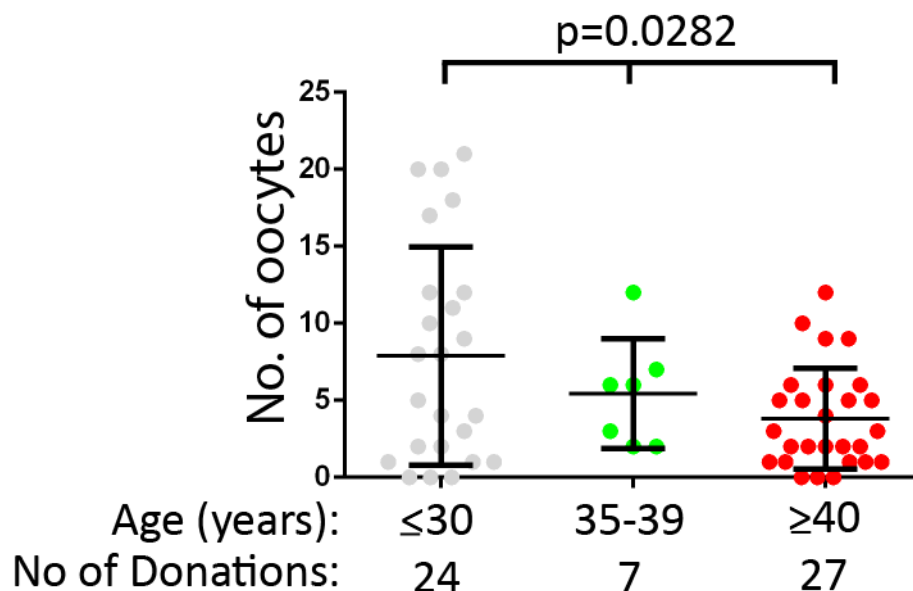
Figure 6.3 More oocytes are retrieved from younger women in non-patient donor scheme but numbers vary significantly within age groups. *Figure shows the comparison of oocytes retrieved from non-patient donors. Each dot represents the number of follicles collected in a retrieval for each of the 3 age categories (≤30: 24 donations, 35-39: 7 donations and ≥40: 27 donations). Error bars represent the mean ± s.d for each age group. A one-way ANOVA was used to establish significance with a p-value of less than 0.05 classed as significant (p=0.0282).*

However, the data indicate a pronounced spread within each age group (Figure 6.3). I therefore determined the effect of the interval from hCG injection to oocyte harvest for the youngest (≤30 years) and oldest (≥40 years) donors. My findings indicate a non-significant trend towards an increased oocyte yield as the interval from hCG injection to oocyte harvest is increased (Figure 6.4). This is consistent with the oocyte becoming more easily detachable from the granulosa cell layers as the differentiation programme within the Graafian follicle proceeds in preparation for release of the egg at the time of ovulation.

133
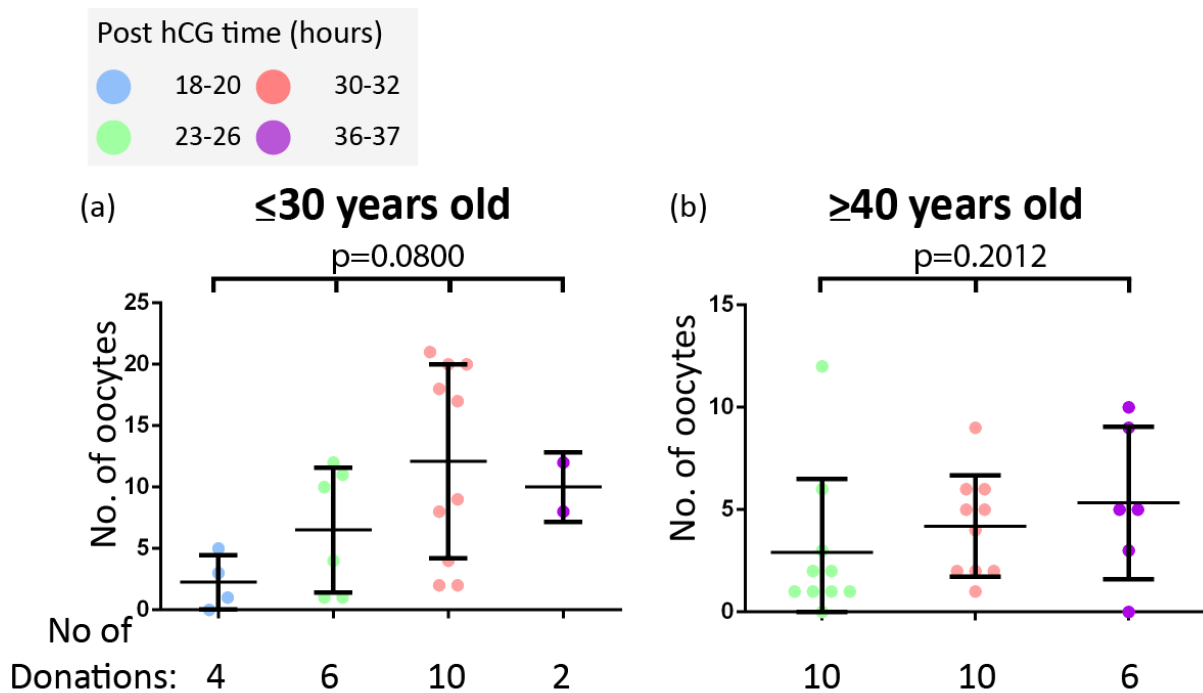
Figure 6.4 A trend towards a positive correlation between the number of oocytes harvested and the hours post hCG injection. *Comparisons of the number of non-patient donor follicles retrieved from (a) women ≤30 (b) ≥ 40. Error Bars represent the mean ± s.d for each age group. A one-way ANOVA and a Kruskal-Wallis test was used to establish p-value for ≤30 and ≥40 age categories respectively. A p-value of less than 0.05 was classed as significant. (a) ≤ 30 years old post hCG retrieval times of 18-20 hours n=4 donations; 23-26 hours=6 donations; 30-32 hours=10 donations and 36-37 hours=2 donations (b) ≥40 years old post hCG retrieval times of 23-26 hours=10 donations; 30-32 hours=10 donations and 36-37 hours=6 donations*

I next determined the relationship between maturation status of the oocyte and the time interval from hCG injection to oocyte harvest (Figure 6.5). The stage of meiosis was determined by the presence of a GV or a polar body when the oocytes were released to the research team immediately after the oocyte retrieval procedure.

In reflection of the challenging nature of harvesting oocytes at earlier times post-hCG, there was a clear operator effect. In this regard, our lead research clinician Dr Meena Choudhary had considerably more success than her clinician colleagues. As a result, analysis of maturation stage was only carried out on oocyte retrieval perfomed by Dr Choudhary.

Interestingly, we found that the majority (53.47%) of oocytes from women aged ≤30 years had completed the first meiotic division by 30-32 hours post hCG injection and a small fraction (3.92%) had done so at 23-26 hours after hCG (Figure 6.5 (a)). A proportion of oocytes (30.77%) from the older age group (≥40 years) had also completed meiosis I by 30-32 hours post hCG (Figure 6.5 (b)). This effect was not as marked as in the younger women and may be explained by technical reasons related to the timing at which the maturation status was assessed.

+hCG time (hour)	≤30 Years old				≥ 40 Years old		
	18 - 20	23 - 26	30 - 32	36 - 37	23 - 26	30 - 32	36 - 37
no. oocytes	8	54	104	19	28	39	32
no. donations	3	6	8	2	9	9	5
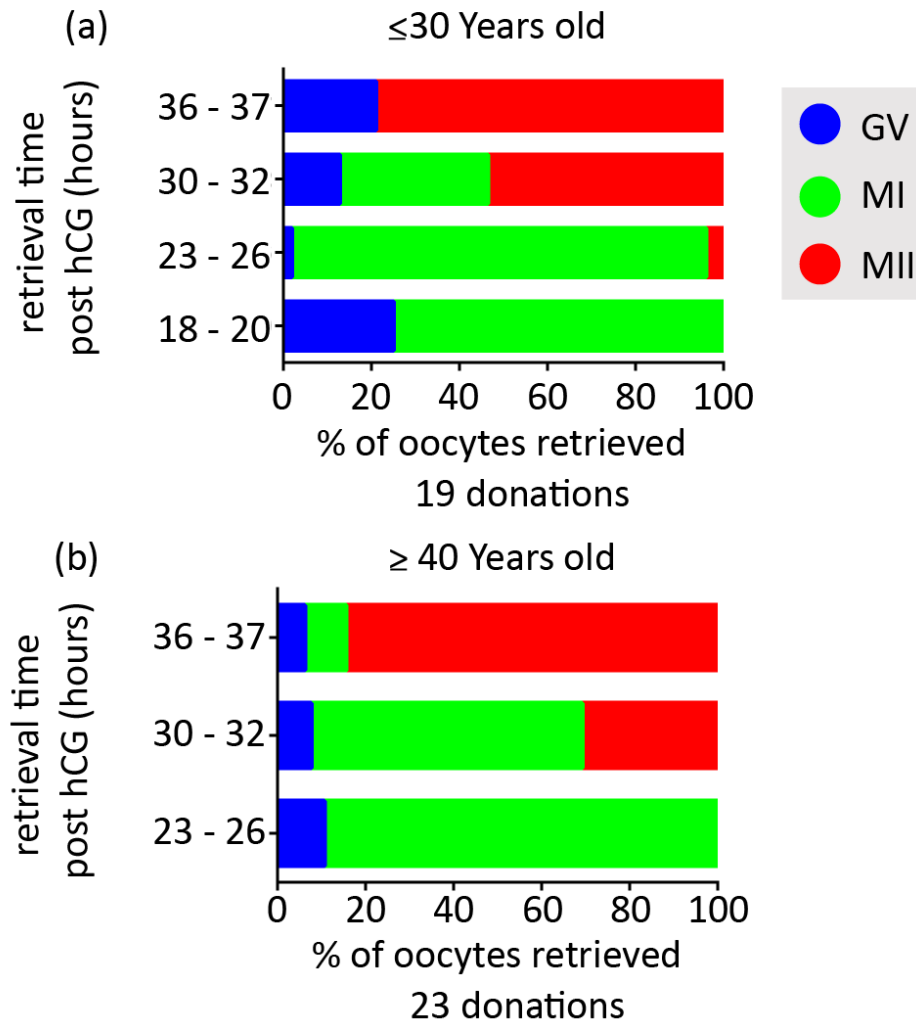
Figure 6.5 Reducing post-hCG retrieval time results in a greater number of MI oocytes. *Stack charts of the stage of maturation of oocytes retrieved at post hCG retrieval times for women aged (i) ≤30 and (ii) ≥40 years old. (i) ≤30 years old post hCG retrieval times of 18-20 hours (3 donations, 8 oocytes) 23-26 hours (6 donations, 54 oocytes) 30-32 hours (8 donations, 104 oocytes) and 36-37 hours (2 donations, 19 oocytes). The number of MII oocytes retrieved increases with longer +hCG retrieval time. (ii) ≥40 years old post hCG retrieval time 23-26 hours (9 donations, 28 oocytes) 30-32 hours (9 donations, 39 oocyte) 36-37 hours (5 donations, 32 oocytes). The number of MII oocytes retrieved increases with longer +hCG retrieval time.*

The finding that a considerable proportion of oocytes have already transitioned to meiosis II at 30-32 hours post-hCG is surprising. The normal practice in IVF clinics is to harvest oocytes 36-38 hr after hCG injection and to inseminate, either by conventional IVF or ICSI, some hours later. Thus, human oocytes undergoing IVF/ICSI treatment may remain arrested at meiosis II for >10 hours before sperm entry. It would be interesting to determine whether this contributes to oocyte aneuploidy.

Analysis of maturation status of oocytes at various times post-hCG also revealed a surprising low proportion of GV stage oocytes at the earlier time points (Figure 6.5). This likely reflects a difficulty in detaching those oocytes that had not yet resumed meiosis from the follicle's mural granulosa cells during aspiration of the follicular fluid. It is possible that this problem could be overcome by using an oocyte retrieval needle designed to scrape the wall of the follicle.   Interestingly, the proportion of GV stage oocytes was comparatively large when oocytes were retrieved at 37 hours post hCG. This may be indicative of follicle atresia, which involves granulosa cell apoptosis (Hsueh et al., 1994). Under these conditions, the oocytes may become more easily detachable from the surrounding layers of granulosa cells.

The results of this section highlight the challenges associated with obtaining healthy immature human oocytes. The findings indicate that progression through meiosis in vivo occurs in an asynchronous manner and that a considerable proportion of oocytes transition from meiosis I to meiosis II within 30 hours of hCG injection. Moreover, the findings indicate that efficient retrieval of GV stage oocytes will require modification of conventional oocyte retrieval practices. Using the current techniques, there is a trade-off between maturation status and the number of oocytes harvested.

6.3 Pilot Study: Cohesin is mislocalised but not reduced overall in MI oocytes of ICSI-reject oocytes

Before carrying out any experimentation on the non-patient donor oocytes, we carried out a pilot study using ICSI-reject oocytes. The rationale for this is based on cost: ICSI-reject oocytes come at no cost to the research budget whereas each non-patient donor cycle costs ~£1500. Thus, ICSI-rejects provide a useful resource for resolving technical problems, antibody optimisation, and for gaining

137

some indication as to whether chromosome-bound cohesin is affected by ageing. Carrying out quantitative work in human oocytes comes with unique challenges relative to mouse work. This centres mostly on when and how many oocytes are available at a given time. This means it is difficult to conduct parallel experiments with young and old donors on the same slide.

My starting point was to determine whether ageing is accompanied by a loss of bivalent chromosome structural integrity in the ICSI-reject oocytes. Observations in mouse oocytes indicated an increase in distally associated chromosomes in which homologues were tenuously attached at the telomeres. In addition, the distance between oocyte sister centromeres also increased during female ageing at 14 months of age (Chiang et al., 2010, Lister et al., 2010). Consistent with this, previous reports from studies on oocytes indicate a significant increase in distance between sister centromeres with advancing female age, suggesting a loss of cohesin (Duncan et al., 2012, Lagirand-Cantaloube et al., 2017, Sakakibara et al., 2015, Zielinska et al., 2015).

In collaboration with my colleague Dr Lisa Lister, we performed chromosome spreads of ICSI-reject oocytes and immunolabelled them for REC8 and CREST, staining the DNA with DAPI. We classified women ≤30 years as our younger group and women ≥35 years as our older age group. We chose 35 years old as the age boundary for the older group because several lines of evidence indicate that the incidence of oocyte chromosome segregation errors increase from the mid-thirties onwards (Nagaoka et al., 2012). Confocal images of chromosome spreads suggested that bivalent chromosomes of meiosis I oocytes are not held together as tightly in the oocytes from older women compared to younger women. There was evidence of premature resolution of bivalents to dyad chromosomes and to single chromatids (Figure 6.6)
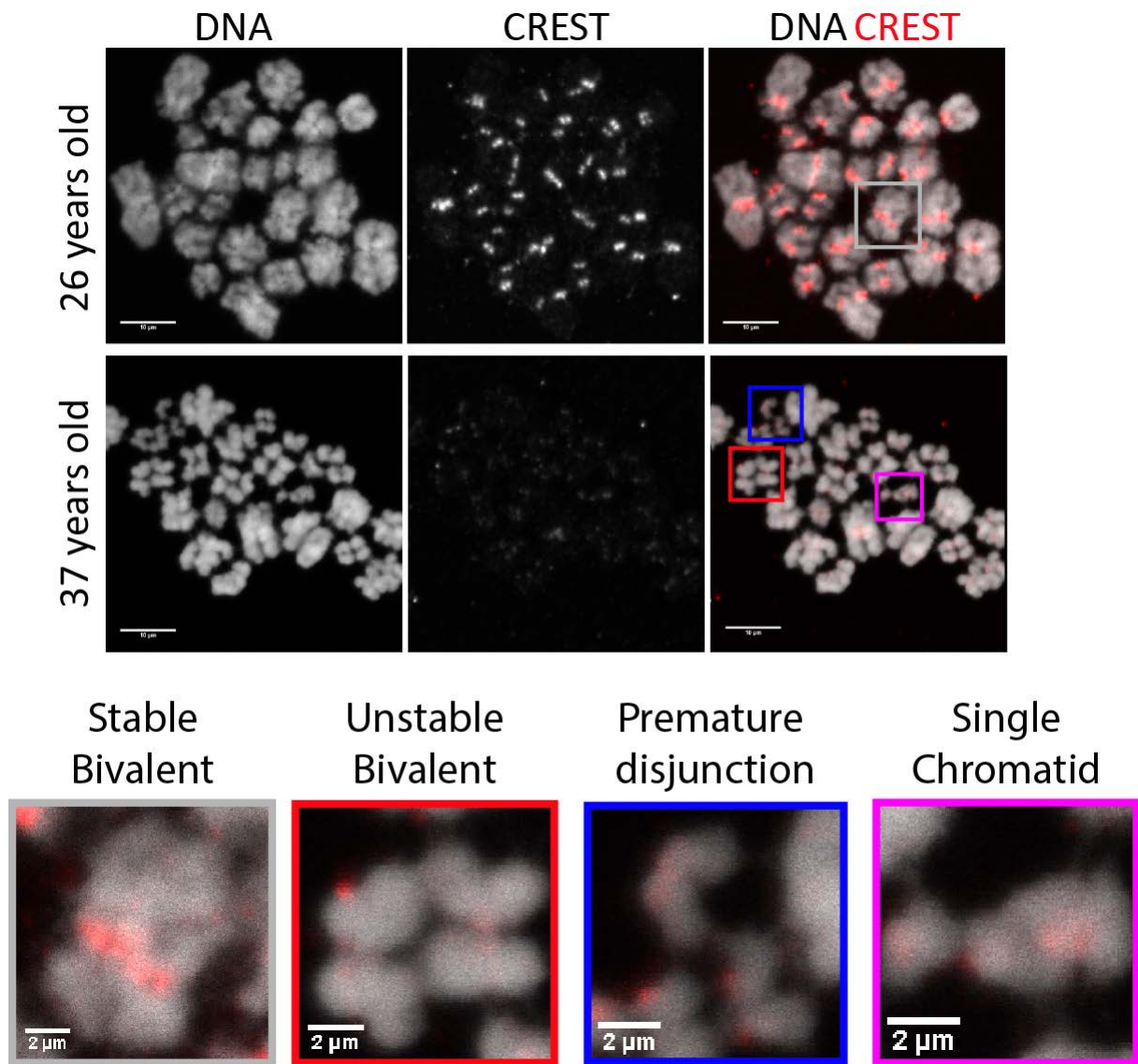
Figure 6.6 Categories of bivalent chromosome structures and defects. *Figure shows images of bivalent chromosomes in MI oocyte chromosome spreads for a woman aged 26 and 37 years old. Scale bar 10μm. Boxes show zoomed in examples of 4 different structural forms of bivalent chromosomes found in MI oocytes. These are: stable bivalents (grey box), unstable bivalents (red box), premature disjunction (blue box) and single chromatids (purple box) (≤30 n=14 oocytes from 11 donations, mean age of donor per oocytes donated: 26.00 s.d: ±1.83; ≥35 n=10 oocytes from 9 donors mean age of donor per oocytes donated: 37.50 s.d: ±1.76)*

To quantify this, I confined the analysis to oocytes in which bivalent chromosomes could be clearly distinguished from one another. I classified the bivalents into four different structural forms based on their morphology (Figure

139

6.6). These were stable bivalents (where the chromatids in the chromosome are all tightly held together), unstable bivalents (where all 4 chromatids are in close proximity to one another but their attachment to one another appears loose), premature disjunction to dyad chromosomes and single chromatids. Analysis of the prevalence of these four different configurations indicates a pronounced age-related increase in unstable bivalents (5.6% vs 37.8% for women aged ≤30 and ≥35 years respectively) and a reduction in stable bivalents (90.7% vs 48.5% for women aged ≤30 years and ≥35 years respectively) (Figure 6.7). Premature resolution of bivalents into dyads and single chromatids was also more prevalent in the older age group (Figure 6.7) (premature disjunction: 3.8% vs 10.3% for women aged ≤30 years and ≥35 years respectively; premature separation: 0% vs 3.1% for women aged ≤30 years and ≥35 years respectively)
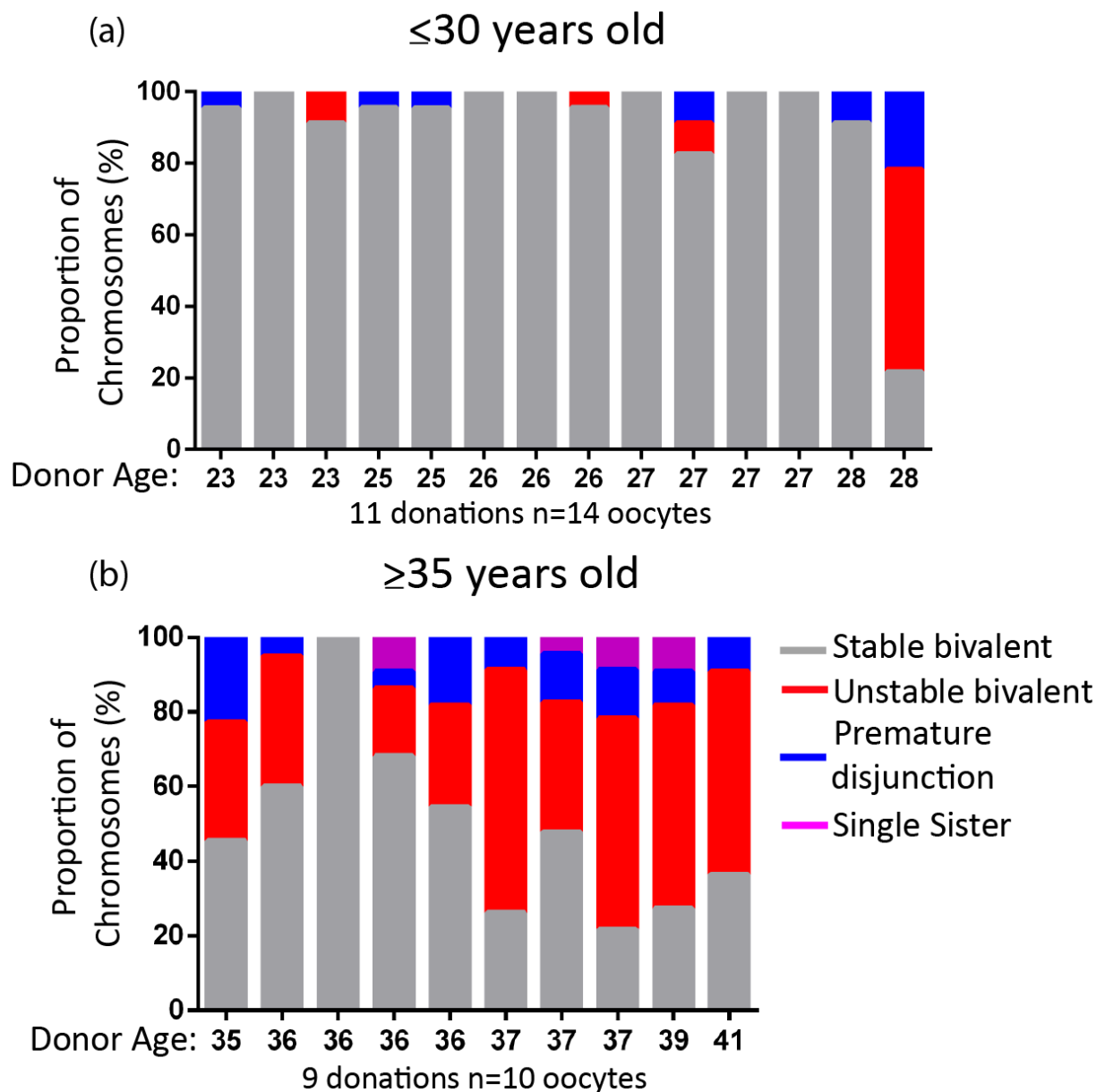
Figure 6.7 Ageing is accompanied by a loss of bivalent chromosome structural integrity in ICSI-reject oocytes. *Stack graphs showing the proportion of bivalent chormosomes structures per oocyte for women (a) ≤30 and (b) ≥35 years old. Bivalent chromosomes were classified as either stable, unstable, prematurely disjoined or separated into single chromatids. (≤30 n=14 oocytes from 11 donations mean age of donor per oocytes donated: 26.00 s.d: ±1.83; ≥35 n=10 oocytes from 9 donors mean age of donor per oocytes donated: 37.50 s.d: ±1.76)*

We next sought to analyse if the distance between sister centromere in the chromosome spreads of our ICSI-reject population increased with age. The cohesin located at the centromeres of chromosomes is essential for maintaining

141

dyads during anaphase I and for biorientation during metaphase II (Hauf and Watanabe, 2004, Herbert et al., 2015). Any loss of centromeric cohesin could be particularly consequential in raising the likelihood of segregation errors. To quantify the inter-centromere distance, linescans were drawn between sister centromeres and the distance between the points of peak fluorescence for CREST was calculated (Figure 6.8). This indicated that, as women get older, the inter-centromere distance increases (0.7µm vs 1.1µm for ≤30 and ≥35 years respectively; p=0.0007) Together these findings from ICSI-reject oocytes indicate that human oocytes, like mouse oocytes exhibit deterioration of bivalent stability during female ageing (Chiang et al., 2010, Lister et al., 2010).
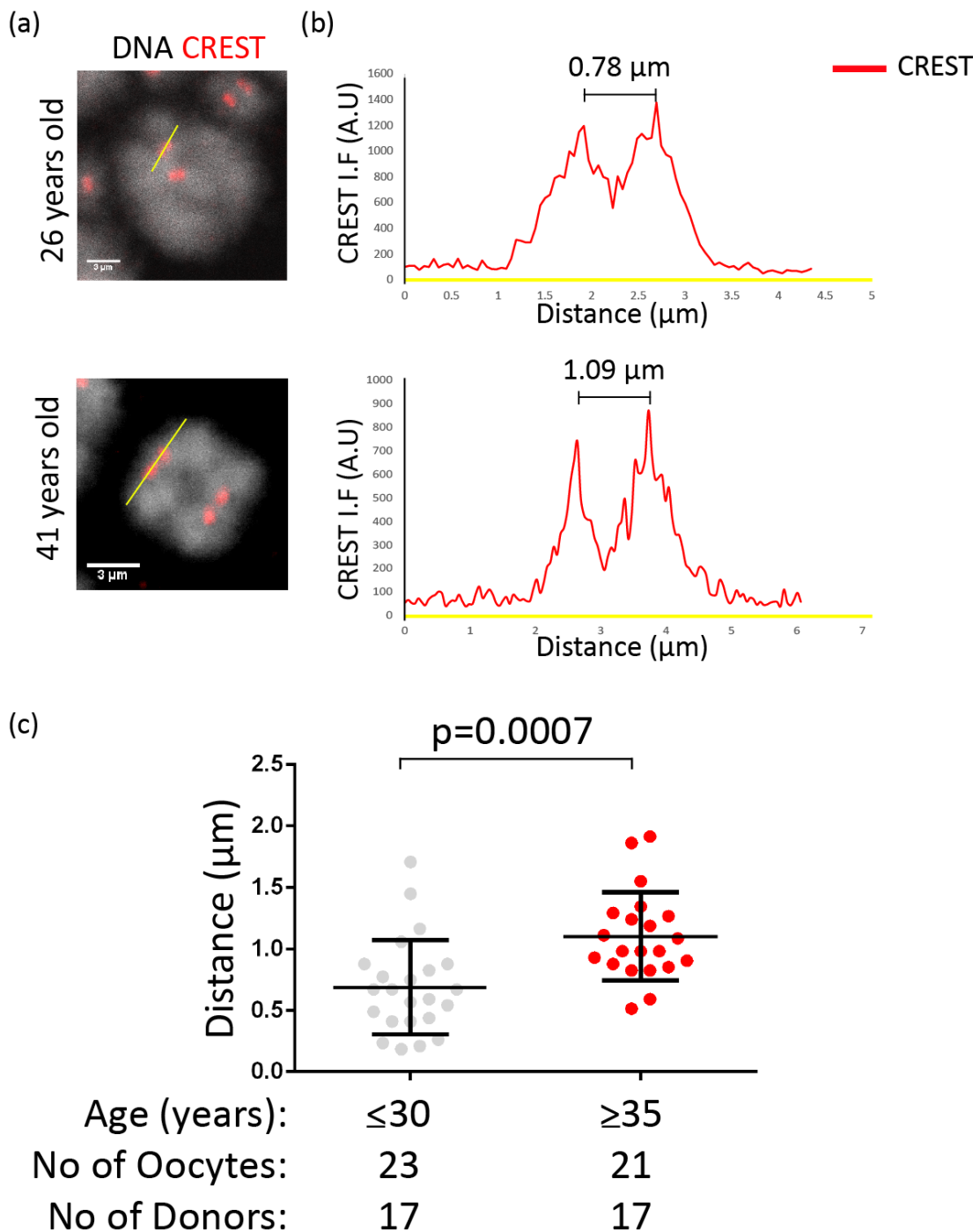
Figure 6.8 Inter-centromere distance increases with age in MI human oocytes from ICSI-reject oocyte population *(a) Representative image of a bivalent chromosome from a 26 year old and a 41 year old woman showing an example linescan across the centromeres. Scale bar 3µm. (b) Corresponding linescan shows two peaks for the CREST signal representing both centromeres. ExtremaPlus software was used to calculate the distance between the two peaks. (c) Comparison of median inter-centromere distance per oocyte for women aged ≤30 and ≥35. An unpaired t-test was used to establish significance with a p-value of less than 0.05 classed as significant. This showed a significant increase in*

143

The observations of the loss of bivalent stability and increased inter-centromeric distance with age is consistent with depletion of chromosome associated cohesin during female ageing. To test this, we prepared chromosome spreads from ICSI-reject oocytes and stained for the meiotic cohesin subunit REC8. However, because of large variation in the intensity of the REC8 signal within age groups, quantification was difficult to achieve. It was therefore necessary to minimise variation due to differences in experimental conditions. For this, we created a stockpile of vitrified ICSI-reject oocytes. This ultra-rapid method of cryopreservation is used to maintain viability of oocytes in clinical IVF practice (Gook and Edgar, 2007).

Vitrified oocytes were warmed in batches consisting of oocytes donated by younger and older ICSI patients. This enabled us to spread them on the same slide. Spreads were immunolabelled with antibodies targeted to REC8 and CREST; DNA was stained using DAPI (Figure 6.9). Consistent with our observations using unmatched spreads, there was large variation in the intensity of the REC8 signal between oocytes from the same age group (Figure 6.9). While oocytes from older women frequently displayed bright staining for REC8 on the chromosomes, enrichment between sister centromeres and arms was much reduced (Figure 6.9). While these differences were clearly evident by eye, quantification of the difference between young and old was challenging.
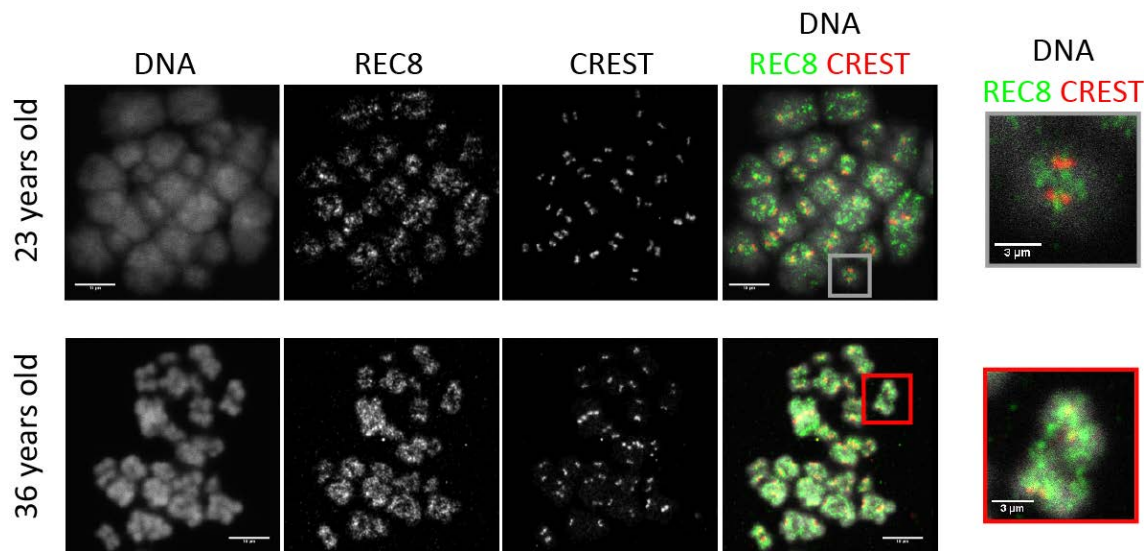
Figure 6.9 REC8 appears mislocalised in MI oocytes with age. *Images of MI oocyte air-dried chromosome spreads from younger and older female's immunolabelled with REC8 and CREST. DNA was labelled using DAPI. Images show that in older women REC8 is no longer localised to the chromosome axis. Scale bar 10µm. Inset shows individual bivalent chromosomes immunolabelled for CREST and REC8. Scale bar 3µm. Chromosome spreads carried out by L. M. Lister (<30 n=9 oocytes from 8 donations mean age of donor per oocytes donated: 25.67 S.d: ±2.24; >35 n=9 oocytes from 8 donations mean age of donor per oocytes donated: 37.67 S.d: ±2.07).*

To quantify this mislocalisation, I analysed the immunofluorescence intensity of REC8 between centromeres in relation to the REC8 overlapping the CREST signal (Figure 6.10). This analysis included spreads from the batch staining and others that had been spread and imaged on different days. I excluded oocytes from donors that showed highly de-condensed chromatin or the oocytes from the ≤30 age category that showed high levels of bivalent instability and non-disjunction as they were not reflective of the majority of the younger population. linescans of REC8 and CREST indicated that in oocytes from younger women the REC8 signal peaks between the CREST foci (Figure 6.10). By contrast, in oocytes from the older age group, the REC8 peak was generally absent from between the CREST foci. Instead REC8 overlapped the CREST foci, frequently extending beyond them showing a diffused distribution (Figure 6.10). This differs from mouse oocytes, were ageing was associated with a more global depletion of Rec8 (Chiang et al., 2010, Lister et al., 2010).

145
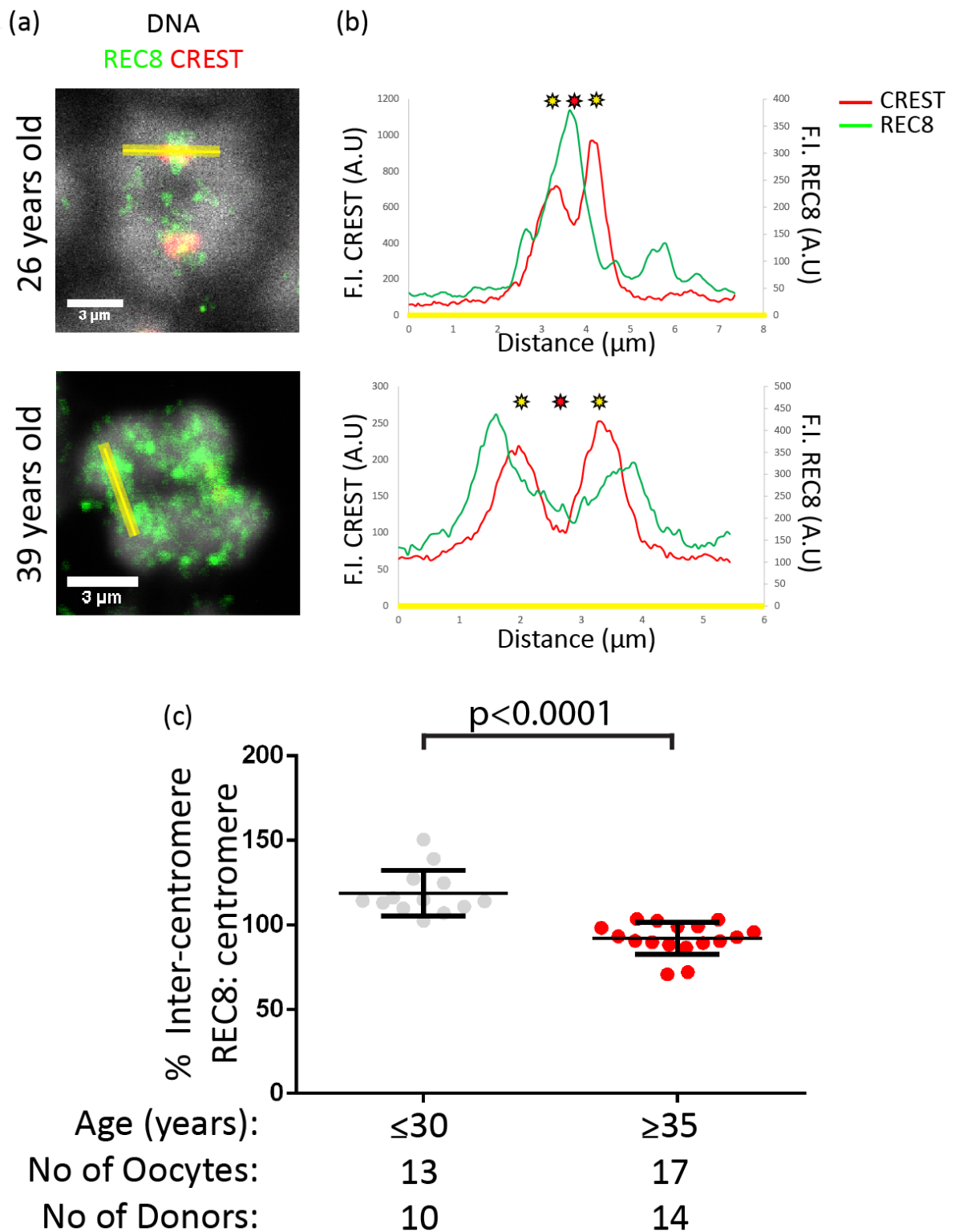
Figure 6.10 REC8 is mislocalised in oocytes from older women. *(a)*
Representative bivalent chromosome from women aged 26 years old and 39
years old with linescans. Linescans were drawn across MI chromosome sister
centromere pairs and graphs produced of the fluorescence intensity across the
line. Scale bar 3 µm. (b) The central REC8 F.I value between the CREST peaks
(red star) was collected and a percentage of its value against the F.I of the REC8

signal on the two peaks of CREST (yellow stars) was generated. (c) Graph shows the median % value of the inter-centromere REC8 vs CREST co-localised REC8. Mann-Whitney U-test shows a significant decrease in inter-centromere REC8 relative to REC8 on the centromere with age (p<0.0001). Error bars show mean ± s.d. (≤30 n=13 oocytes from 10 donors, mean age of donor per oocytes donated: 25.44 s.d: ±2.07; ≥35 n= 17 oocytes from 14 donors mean age of oocytes donated: 37.56 s.d: ±2.07).

Next, I sought to determine whether there is an overall loss of REC8 at the centromeres. To do this I carried out linescan analysis on the MI chromosome spreads from the batch staining. These oocytes had been spread and imaged on the same day with the same microscope settings used. Figure 6.11 shows the analysis used to quantify the CREST and REC8 signal. Ideally, it would be possible to set independent threshold for each marker using the linescan analysis, but the morphology of human bivalent chromosomes means that the REC8 value at the centromere can be infringed by REC8 signal from other parts of the chromosome. Also the variation in CREST signal between younger and older women made it difficult to set an independent threshold for the CREST signal. As a result, the REC8 values used are from the initial point from where the CREST increases to when it decreases after the second peak.
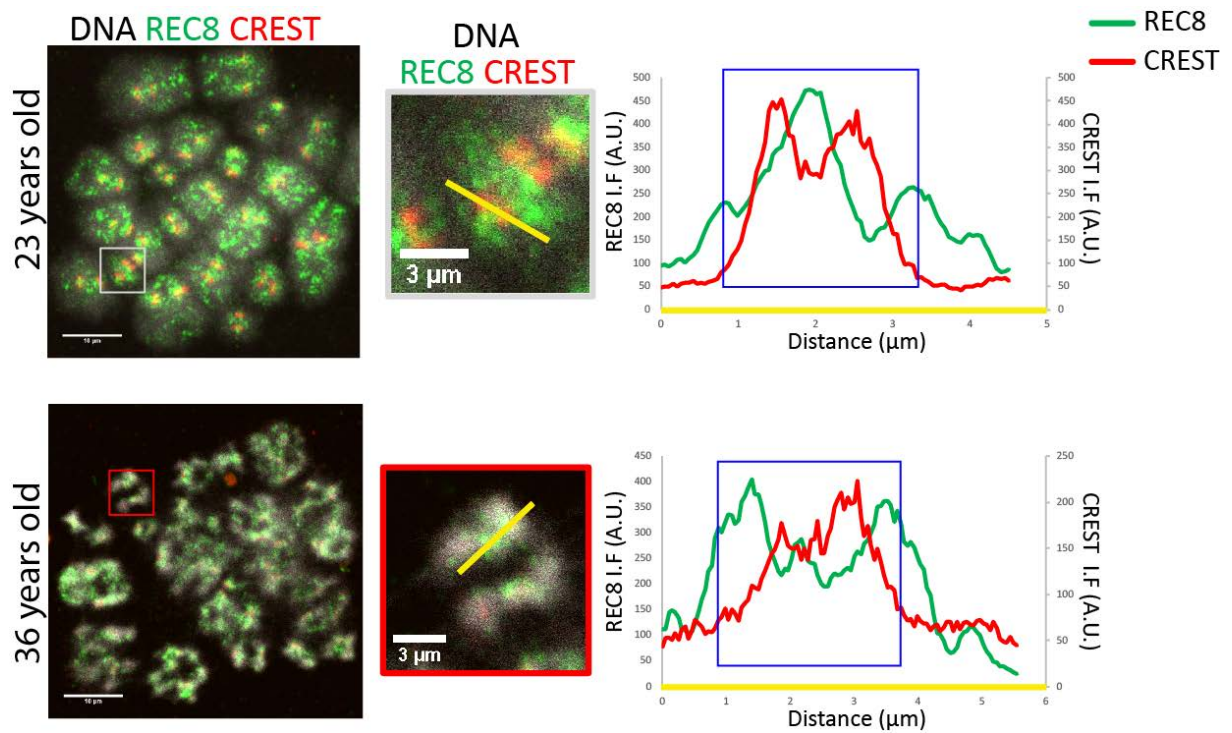
Figure 6.11 Area under the curve analysis used for REC8 and CREST quantification. *Figure shows representative analysis of REC8 and CREST at centromeres of chromosome spreads from a 23 and a 36 year old woman. Scale bar 10µm, inset scale bar 3 µm. Blue box indicates the area under the curve that was collected for CREST and REC8 at the point where the initial CREST signal could be detected. Spreads and imaging carried out by L.M. Lister (< 30 n=9 oocytes from 8 donations mean age of donor per oocytes donated: 25.67 s.d: ±2.24; >35 n=9 oocytes from 8 donations mean age of donor per oocytes donated: 37.67 s.d: ±2.07).*

Comparisons of the area under the curve values for REC8 and CREST on a slide by slide basis as well as the ratio of REC8 to CREST showed a high level of variation within the younger and older age groups (Figure 6.12 and Figure 6.13 respectively).
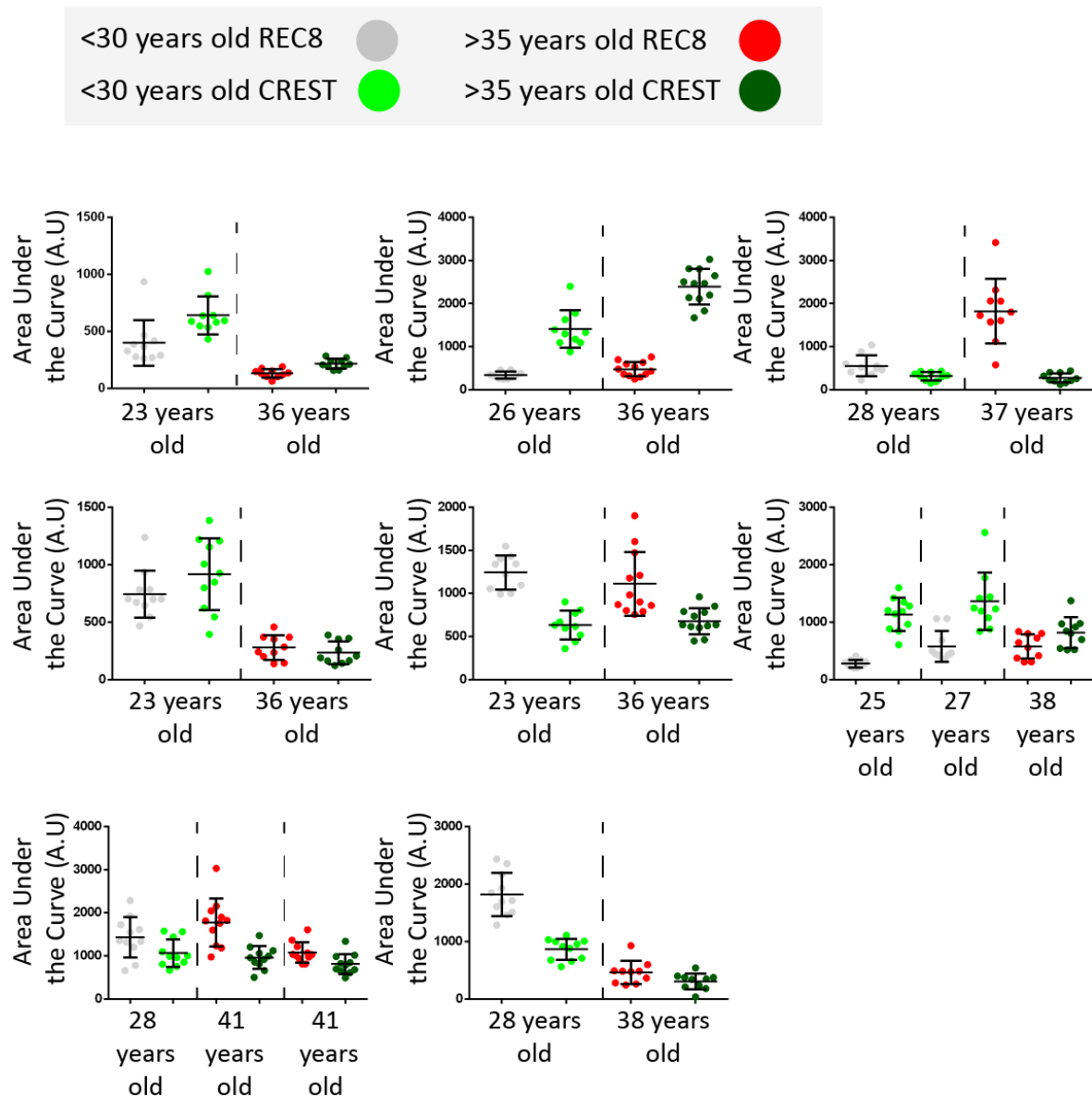
Figure 6.12 REC8 and CREST area under the curve values per oocyte from younger and older ICSI-reject donors. *Dot plots of REC8 and CREST for each oocyte on each slide used in the warmed from vitrification oocyte set. Each dot represents the area under the curve value for the REC8 or CREST signal per individual centromere. The age of the donor of each oocyte analysed is written under the values. Error bars show mean ± s.d. (< 30 n=9 oocytes from 8 donations, mean age of donor per oocytes donated: 25.67 s.d: ±2.24; > 35 n=9 oocytes from 8 donations, mean age of donor per oocytes donated: 37.67 s.d: ±2.07).*

149
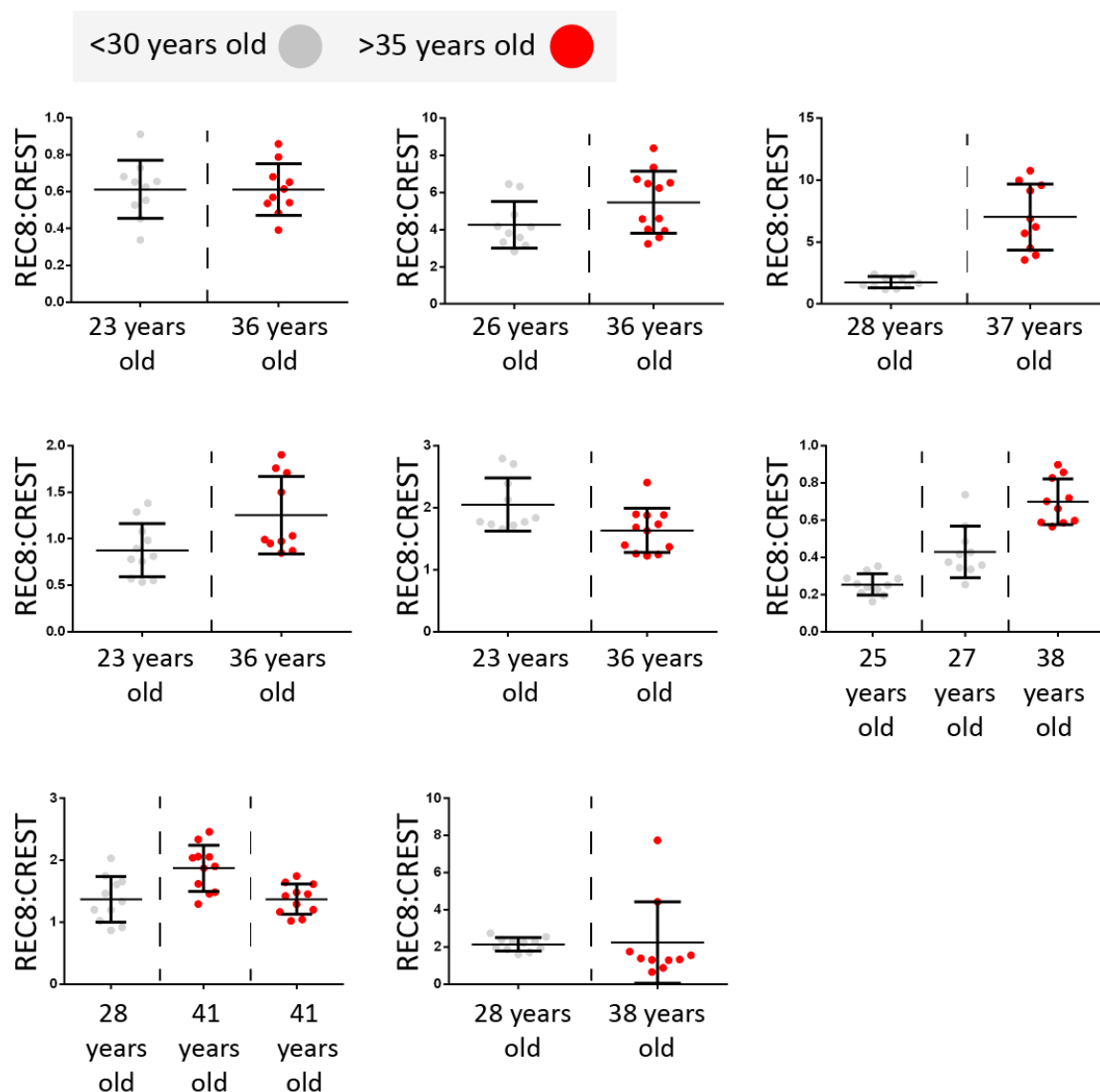
Figure 6.13 REC8: CREST ratio per oocyte from younger and older ICSI-reject donors *Dot plots of the ratio of REC8: CREST ratio for each oocyte on each slide used in the warmed from vitrification oocyte set. Each dot represents the area under the curve ratio of REC8: CREST per individual centromere. The age of the donor of each oocyte analysed is written under the values. Error bars show mean ± s.d. (under 30 n=9 oocytes from 8 donation, mean age of donor per oocytes donated: 25.67 s.d: ±2.24; over 35 n=9 oocytes from 8 donations, mean age of donor per oocytes donated: 37.67 s.d: ±2.07).*

To determine whether there is a significant change in cohesin levels during ageing, the median value for REC8 and CREST of centromeres per oocyte was calculated and normalised to the younger donor (Figure 6.14). The results indicate that there is no significant difference for REC8 and CREST with ageing (Mann-Whitney U test: p=0.4122 and 0.1051 respectively). When a ratio of REC8 to CREST is used, there appears to be a non-significant increase in REC8 in the oocytes from older women compared to the younger ones (p=0.4612). The results for CREST are at odds with by eye observations between good quality chromosome spreads of young and old oocytes. In good quality spreads, older donors CREST is quite clearly reduced in a similar way to in mouse oocytes (Yun et al., 2014). This is indicative of the problem of relying on ICSI-reject oocytes for quantification analysis.
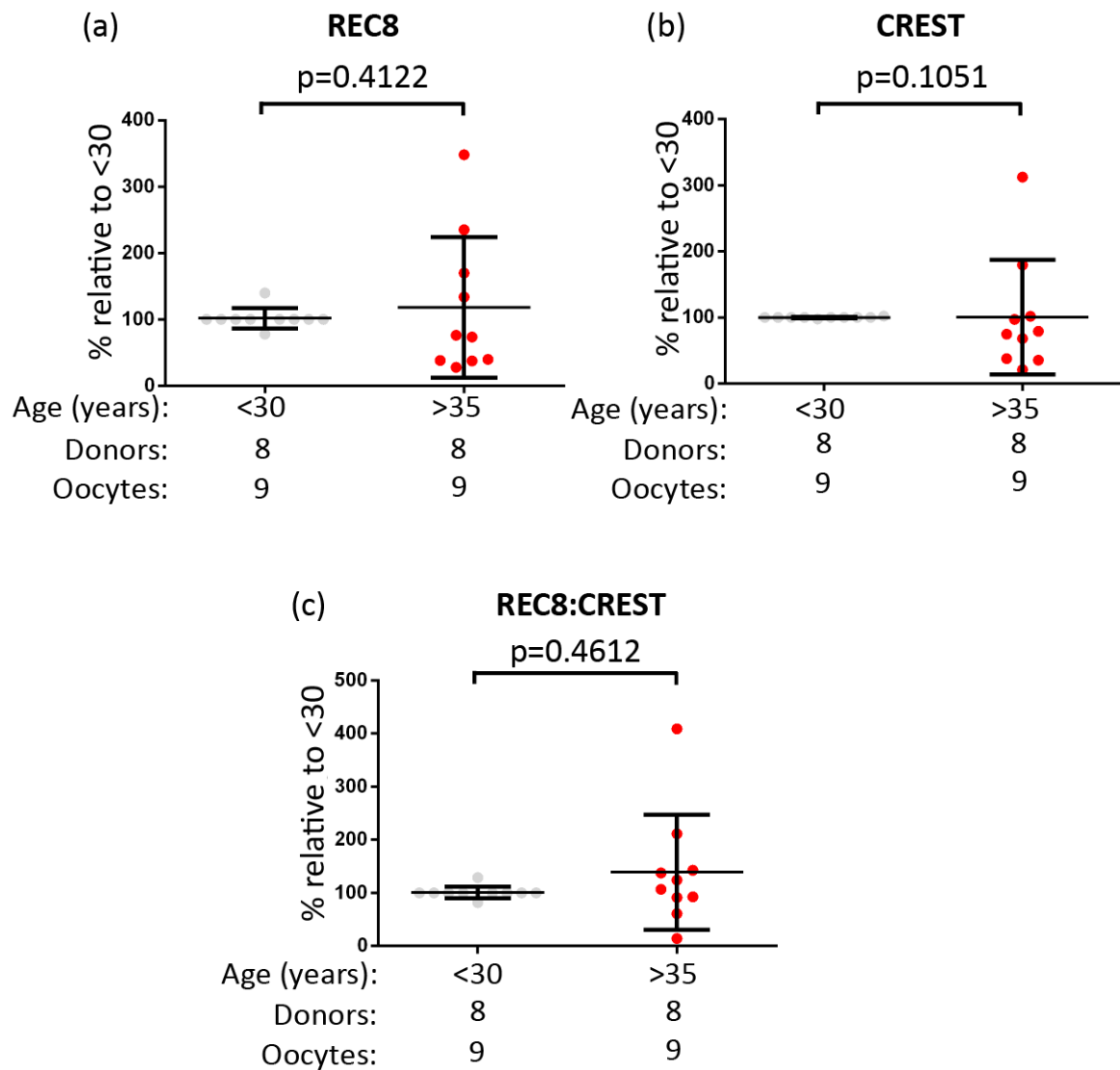
Figure 6.14 Normalising of Flourescence intensity to under 30 year olds chromosome spreads on same slide does reveals no significant difference between age groups for REC8 or CREST. *Dot plot showing median value for each oocyte chromosome spread for (a) REC8 (b) CREST and (c) REC8: CREST ratio. Median values for over 35 were normalised to those from women under 30 on the same slide. Error bars show ± s.d. Mann-Whitney U test revealed no significant difference in area under the curve analysis for (a) REC8 (p=0.4122) (b) CREST (p=0.1051) and (c) REC8:CREST (p=0.4612). (under 30 n=9 oocytes from 8 donations, mean age of donor per oocytes donated: 25.67 s.d: ±2.24; over 35 n=9 oocytes from 8 donations, mean age of donor per oocytes donated: 37.67 s.d: ±2.07).*

The results from this pilot study inform us of several key aspects in attempting to understand the relationship between ageing and REC8 in human oocytes and the use of ICSI-reject oocytes. Firstly, the high levels of REC8 associated with chromatin in aged oocytes makes quantification difficult as it is not possible to distinguish cohesive cohesin between sister centromeres from "spurious" cohesin diffusely scattered on the chromatin. It is not clear whether the latter is actually bound to chromatin or whether it is due to reduced dissipation of cytoplasm during the spreading procedure in oocytes from the older women.   Secondly, there is a high level of variation in REC8 and CREST F.I within age groups. This complication is not mitigated by the spreads from young and old ICSI-reject oocytes being spread on the same slide. While the data from Figure 6.14 suggests CREST is not significantly reduced with age, this data is skewed by chromosome spreads from young oocytes that appear to be of a poor quality. Finally, quantifying REC8 at centromeres in MI oocytes is difficult due to cohesin from other parts of the chromosome. To avoid these issues we required new methods of acquisition and analysis.

6.4 Strategy for carrying out investigation into cohesin in human oocytes

The chromosome spreads used in the batch staining of the pilot study were conducted using vitrified oocytes. While vitrification is an essential tool for storing oocytes and embryos for IVF, the technique is particularly expensive and requires a high level of technical ability to carry it out without losing oocytes in the vitrification or warming processes. The main benefit of vitrification for this work is that it allows for eggs from women of different ages to be obtained on different days, spread on the same slide and imaged together. However, the precious nature of these human oocytes means that no more than three oocytes will be spread at any one time on one slide to avoid any being lost. This makes it difficult to use the methods for compiling results used in Chapter 4. For these reasons I sought a more cost effective solution which would reduce the chances of oocyte loss and allow for storage over a prolonged periods of time with minimum damage to the proteins and DNA in the chromosome spread. Our idea to address this was through freezing of chromosome spreads rather than short term storage in PBS at 4°C. This required modification of our current methods used for

153

chromosome spreads. Based on chromosome spreads used for yeast, I sought to test out if using sucrose as a cryo-protectant would help in the longer term storage (Grubb et al., 2015). Air-dried chromosome spreads from metaphase II-arrested mouse oocytes were frozen overnight before being warmed in PBS at room temperature the next day. The spreads were then immunolabelled with antibodies targeted to ACA and TOPO II and the DNA was stained using DAPI (Figure 6.15.)

A	No Sucrose
B	3.4% sucrose/1% PFA
C	3.4% sucrose/1% PFA - 1.5hour wait - reapply 3.4% sucrose/1% PFA
D	3.4% sucrose/1% PFA - left for 15 minutes - 1% lypsol - 3.4% sucrose/1% PFA re-applied
E	3.4% sucrose/1% PFA - left for 30 minutes - 1% lypsol - 3.4% sucrose/1% PFA re-applied
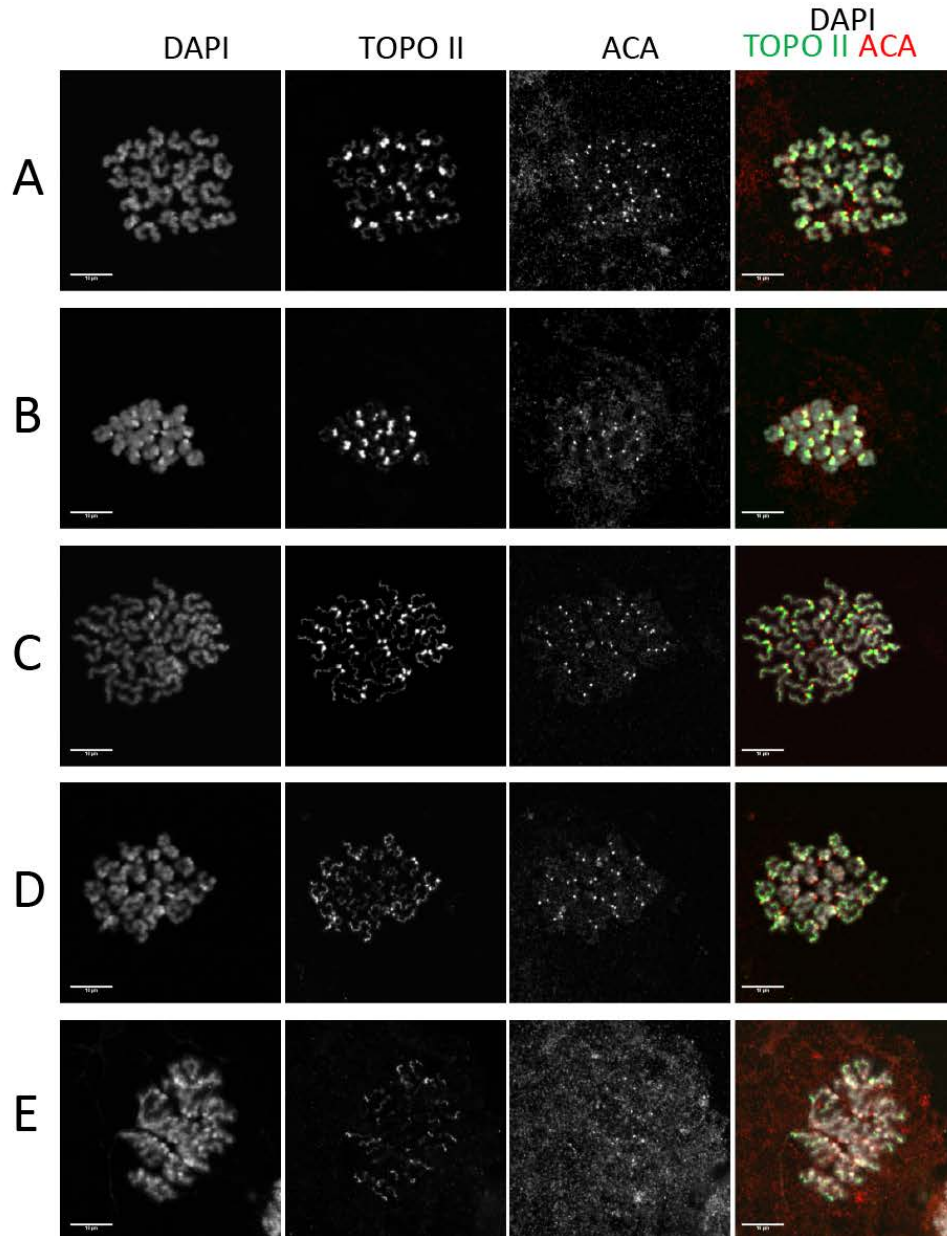
Figure 6.15 Sucrose in PFA with re-application 1.5 hours later appears best for freezing air-dried oocyte chromosome spreads. *Figure shows example images of chromosome spreads prepared from mouse oocytes immunolabelled with TOPOII and ACA with DNA stained using DAPI. Letters beside image correspond to experimental procedure used before freezing. Scale bar 10µm.*

The findings from this experiment indicated that the best spreads were those that had no sucrose (Figure 6.15A) and those that had sucrose re-applied after an hour and a half (Figure 6.15C). As a consistent problem with human oocyte spreads is high levels of cytoplasm, I also carried out a lipsol (a detergent) wash between PFA steps to see if this could help reduce background (Figure 6.15 D and E). However, the lipsol appeared to damage the areas of heterochromatin in the spreads. It also resulted in reduced number of oocytes located on each slide. This was most likely due to the oocytes not being adequately adhered to the slides and so they were being washed off by the lipsol. I concluded that the optimal technique was the re-application of sucrose/PFA.

I next determined whether this method of freezing with sucrose would be appropriate for more prolonged periods of time. This was confirmed on a group of ICSI-reject chromosome spreads that had been frozen for several months. The slides were washed in PBS and immunolabelled with antibodies targeted to REC8, ACA and TOPO II. DNA was stained using DAPI. Of the 9 oocytes spread, 7 out of 9 were present on the slide showing good retention after sucrose/PFA solution re-application (Figure 6.16).
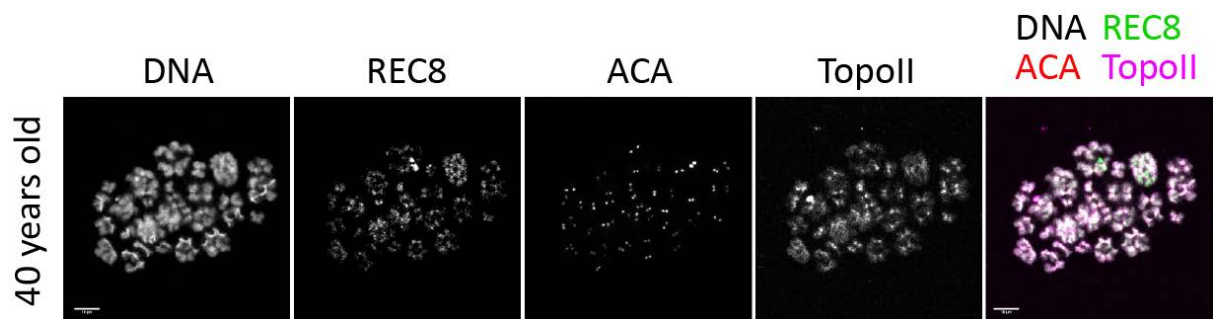
Figure 6.16 ICSI-reject frozen chromosome spread shows clear staining after a prolonged period at -20⁰C. *Representative Airyscan processed image of an oocyte chromosome spread fixed using 3.4% sucrose/1% PFA with re-application 1.5 hours later and frozen at -20°C. Staining and spread is consistent with those spread in just 1% PFA solution and stored at 4°C. Scale bar 10µm (imaging by L.M Lister).*

Having accumulated a significant number of chromosome spreads from non-patient donors, we began batch staining for REC8, ACA and TOPO II. These were imaged using a Zeiss lms880 with airyscan post-processing.

156

To determine whether slides stained and imaged on different days could be combined as one data set, I carried out the linescan analysis and compared the area under the curve between batches of the <30 category of MII spreads (Figure 6.17). These were imaged on a Zeiss lsm880 microscope rather than the Nikon A1R confocal which should have a more consistent laser power output. While there was no difference in the area under the curve values for TOPO II intensity between experiments (p=0.6227), REC8 and the ratio of REC8: TOPO II showed a significant decrease (p=0.0027 and p=0.0153 respectively). While biological variation cannot be ruled out, this suggests that using the lsm880 can still result in significant variation in laser power output between days and so combining all values would not be suitable.
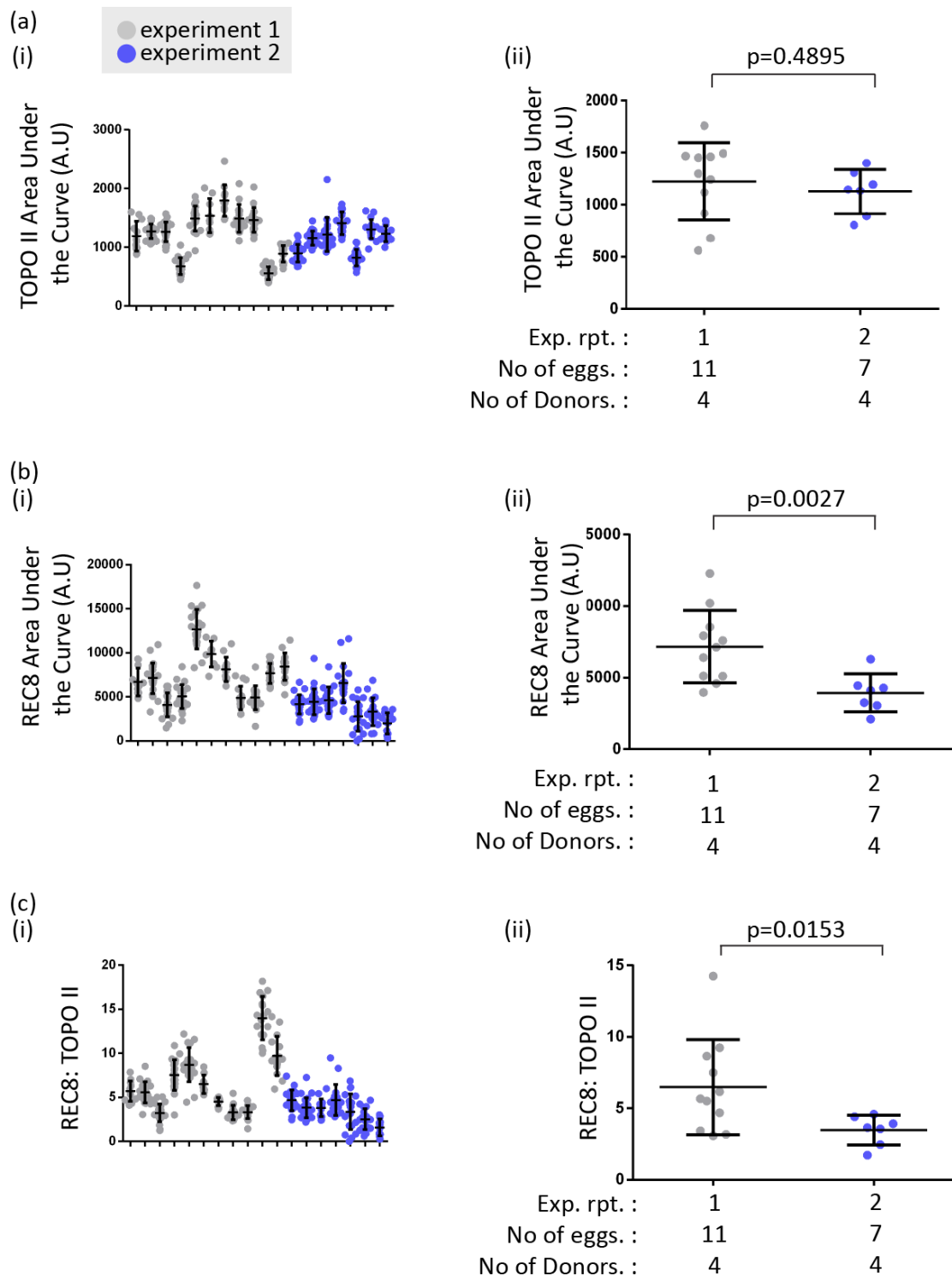
Figure 6.17 Significant difference in REC8 fluorescence intensity between air-dried MII oocyte chromosome spreads from younger women imaged on different days. *Dot plots showing the area under the curve values for (a) TOPO II and (b) REC8 and the (c) REC8:TOPO II ratio. (i) Shows the area under the curve values and the REC8:TOPO II ratio for each pericentromere per oocyte. (ii) Shows comparisons of the median values of each oocyte compared between the two experiments imaged on different days. A Mann-Whitney U test revealed a*

significant difference between REC8 area under the curve and the ratio of REC8: TOPOII for experiments imaged on different days (p=0.0027 and p=0.0153 respectively). TOPO II area under the curve showed no significant difference. Error bars show mean ± s.d. (Exp 1. n=11 oocytes from 4 donors; exp2. n=7 oocytes from 4 donors)

The next test of our methodology was to investigate if protein detection through I.F was significantly affected by long term freezer storage of the spreads. Observations of the TOPO II and REC8 between the under 30 chromosome spreads suggest no obvious impact based on when the chromosomes were spread (Figure 6.18). This shows that long term freezing and then imaging in batches is an appropriate methodology for approaching long term studies using chromosome spreads.

Donor no.	Exp1. Days in freezer	Exp2. Days in freezer
Germ016	427 days	N/A
Germ020	420 days	434 days
Germ023	399 days	413 days
Germ027	N/A	360 days
Germ028	346 days	N/A
Germ036	N/A	279 days

(a)

Experiment 1.

Experiment 2.

(b)

Experiment 1.

Experiment 2.
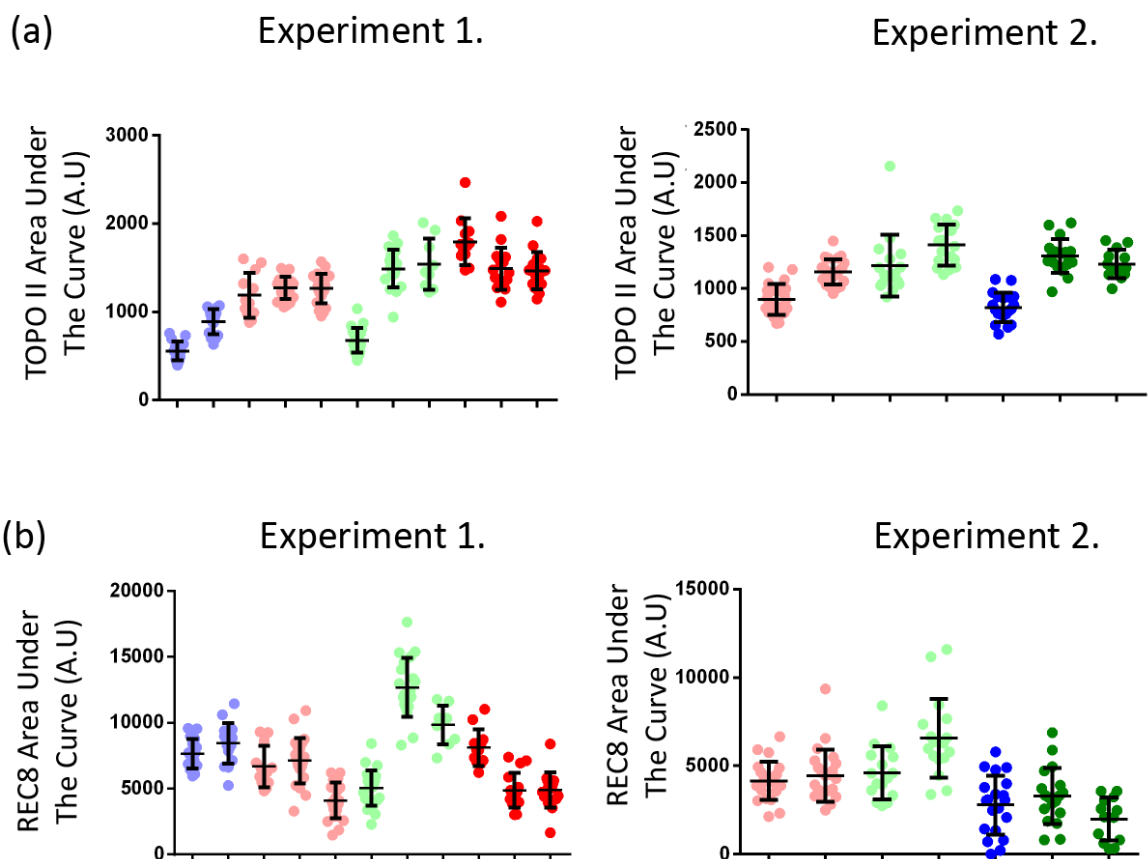
Figure 6.18 Antibody detection of proteins of interest is not affected by long term freezing *Dot plots showing the area under the curve values for (a) TOPO II and (b) REC8 per MII oocyte air-dried chromosome spread. Each dot represents the area under the curve value per pericentromere. Table shows corresponding colour code and date the chromosome spread was carried out per donation. Error bars show mean ± s.d. (Exp 1. n=11 oocytes from 4 donors; exp2. n=7 oocytes from 4 donors)*

160

6.5 REC8 is mislocalised from the chromosome axis, but not reduced with age in human oocytes at MII

The results from the pilot study in MI oocytes indicated that overall, cohesin does not appear to be reduced during female ageing. However, its localisation changes so that it is not enriched between centromeres. Because ICSI-reject oocytes may not provide a good representation of human oocytes progressing through meiosis in a normal time frame, I investigated whether an age-related loss of cohesin occurs in oocytes from our non-patient donor population. To make quantification easier I looked at MII stage oocytes. These are easier to measure due to the localisation of REC8 in the centromeric region, reducing the chance of interference from non-centromeric REC8.

Air-dried MII chromosome spreads were removed from the freezer and washed in PBS to remove residual fixative. They were then immunolabelled with antibodies targeted to TOPO II, ACA and REC8. The DNA was labelled using DAPI and slides were imaged using the Zeiss lsm880 with Airyscan. For metaphase II arrested eggs, dyads with intact centromeres can be identified by the location of TOPO II and ACA as well as the DNA structure (Fig 6.19).
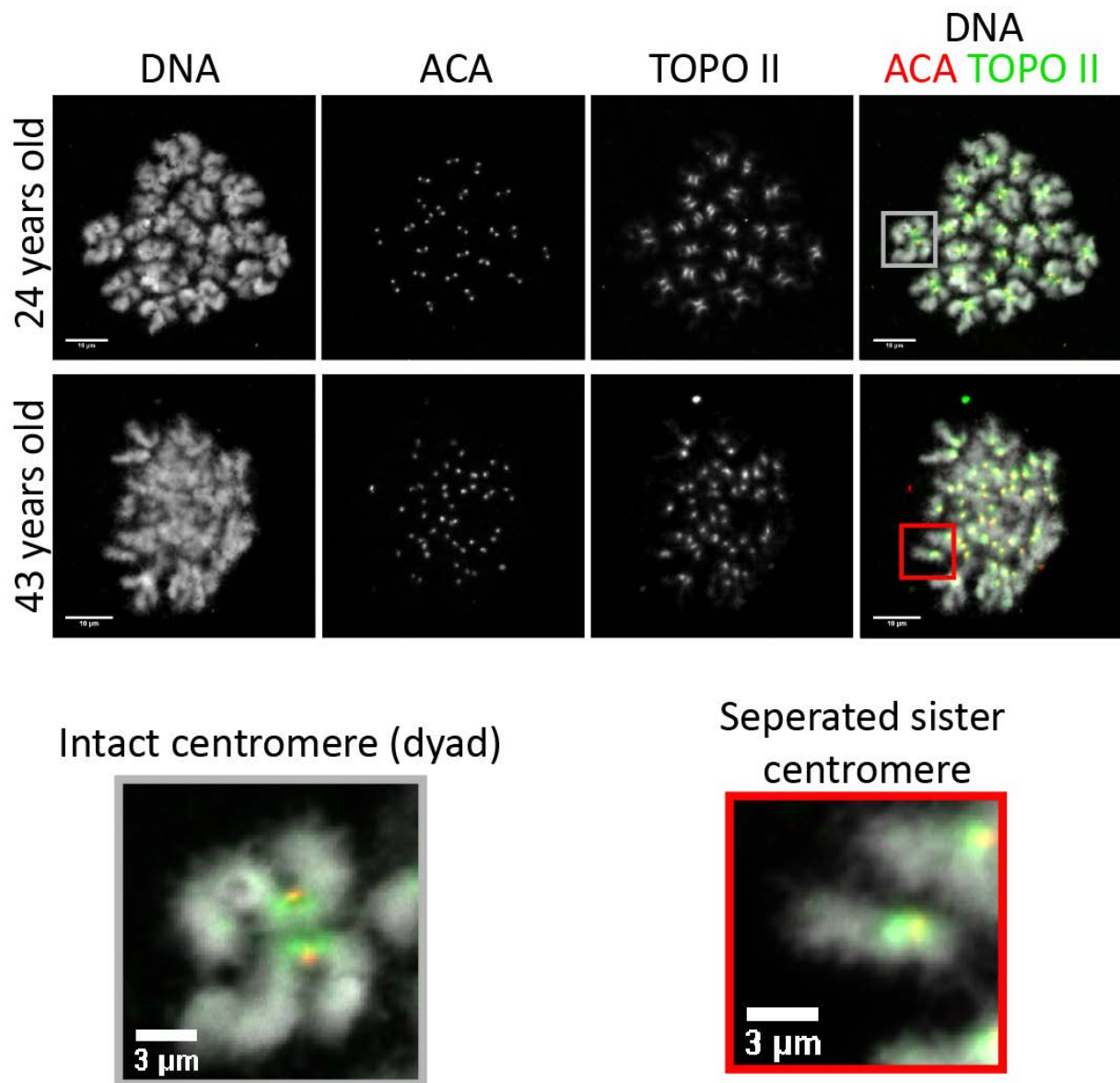
Figure 6.19 structure and defects in dyads from MII oocytes. *Figure shows representative sum-stack z-projection images of MII air-dried oocyte chromosome spreads from a 24 year old and a 43 year old woman. Scale bar 10µm. Images show immuno-labeling for TOPO II and ACA with the DNA stained using DAPI. Inset show zoomed in examples of an intact centromere (Dyad – grey box) and a separated sister centromere (red box). Scale bar 3µm (<30 n=23 eggs from 6 donors, mean age of oocytes donated: 26.57 s.d: ±1.95; >35 n=8 eggs from 6 donors, mean age of oocytes donated: 41.00 s.d: ±2.07).*

162

Oocytes from the younger (<30 years) women showed a low incidence of abnormalities, only 3/23 oocytes showed separation of centromeres affecting a single chromosome (Figure 6.20) (<30 years old n= 23 oocytes from 6 donors; >35 years old n=8 oocytes from 6 donors). By contrast, analysis of MII oocytes (n=8) from the older non-patient donors revealed that 7/8 contained prematurely separated centromeres and multiple chromosomes were affected in 4/8 oocytes (Figure 6.20).

Interestingly, the oocytes from the 43 year old donor showing a high level of separation belonged to a cohort of 12 oocytes retrieved from this woman. This is an extraordinarily high number of oocytes for a woman of this age and the finding of extensive abnormalities indicates that ovarian ageing and cohesin depletion occur by parallel but independent pathways. Should this finding prove to be consistent, it raises a question over the use of commercially available kits sold to women to assess their ovarian age. Such a measure could lull women into a false sense of complacency about when to start a family.
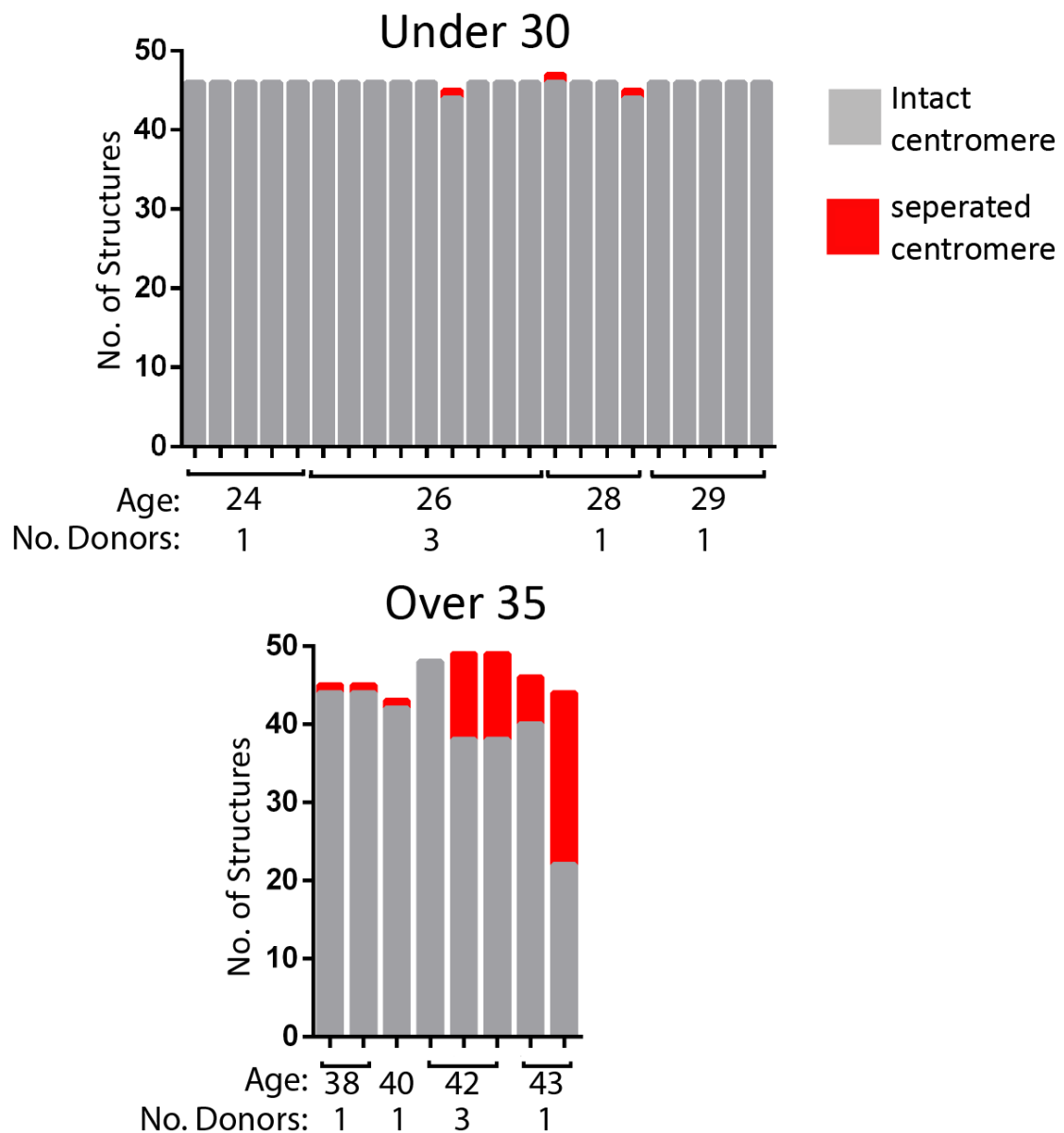
Figure 6.20 Separation of sister centromeres increases with age in MII oocytes from non-patient donor population. *Stacked bar graphs showing number of intact (grey) and separated centromeres (red) per oocyte. Healthy oocytes should contain 46 intact centromeres per oocyte. Age of the donor of the oocyte and the number of donors is written below the graphs (<30 n=23 eggs from 6 donors, mean age of oocytes donated: 26.57 s.d: ±1.95; >35 n=8 eggs from 6 donors, mean age of oocytes donated: 41.00 s.d: ±2.07).*

Consistent with findings in mouse (Chiang et al., 2010, Lister et al., 2010) and in ICSI reject oocytes, analysis of the distance between centromeres increases with advancing female age in the non-patient donor population (Figure 6.21). The

mean distance for oocytes from young women was 1.78µm compared with 2.31µm for those aged >35 years (Figure 6.21).
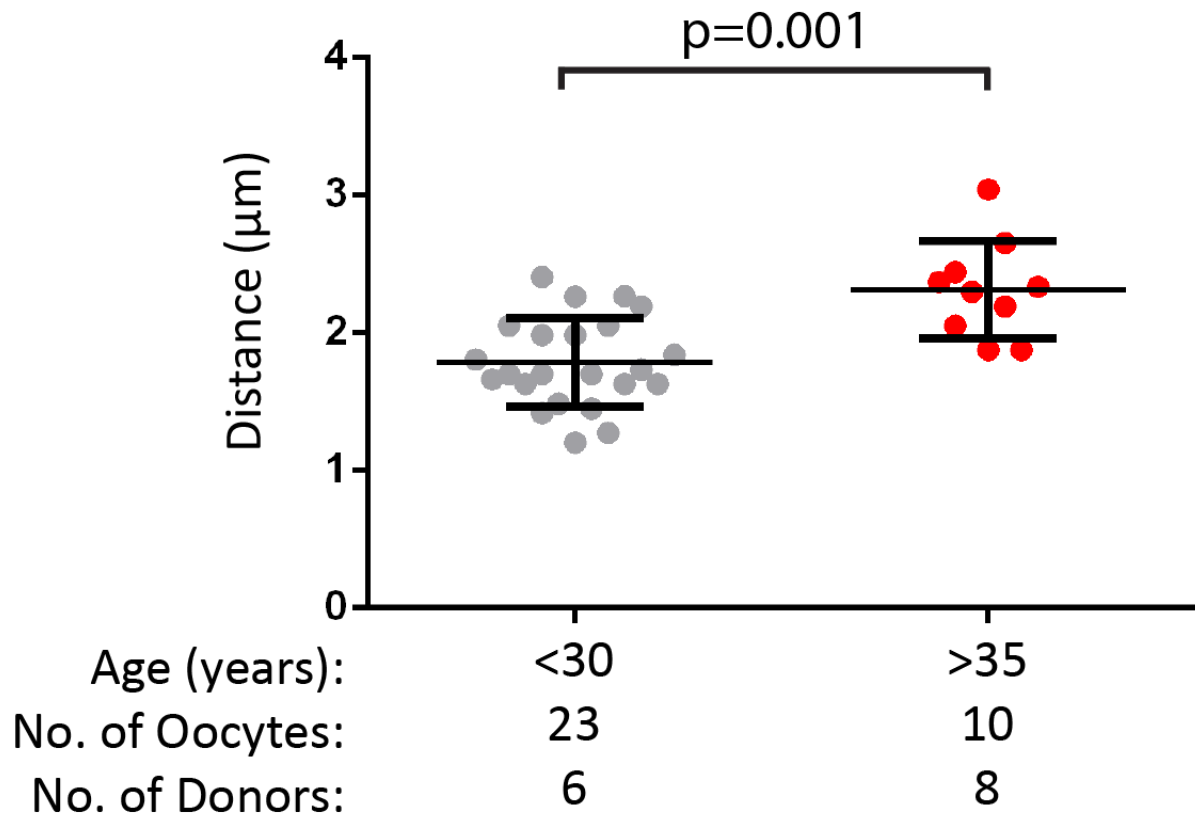
Figure 6.21 Inter-centromere distance increases with age in MII chromosome spreads from non-patient donors. *Dot plot showing a comparison of the median distance values between CREST signals of MII dyads. Unpaired t-test shows a significant increase in distance in the women over 35 indicating a reduction in chromosomal cohesion (p=0.001). (<30 n=23 oocytes from 6 donors, mean age of oocytes donated: 26.57 s.d: ±1.95 Avg distance: 1.78µm s.d: ± 0.322; >35 n=10 oocytes from 8 donors, mean age of oocytes donated: 41.30 s.d: ±2.07 Avg distance: 2.31µm S.d: ± 0.35).*

Comparisons of airyscan-processed images indicated that once again, REC8 was still present on the chromosomes of older women but that, in contrast to the oocytes from the younger women, it is not enriched between sister centromeres (Figure 6.22). Importantly, it was evident from these MII oocytes that the diffused distribution of cohesin on the chromosome arms of the meiosis I ICSI-reject oocytes was not present. This raises the possibility that the diffusely distributed

165

cohesin is cleaved during anaphase I. However, it will be important to determine whether the "scattered" arm cohesin is also a feature of meiosis I oocytes from the non-patient donors.
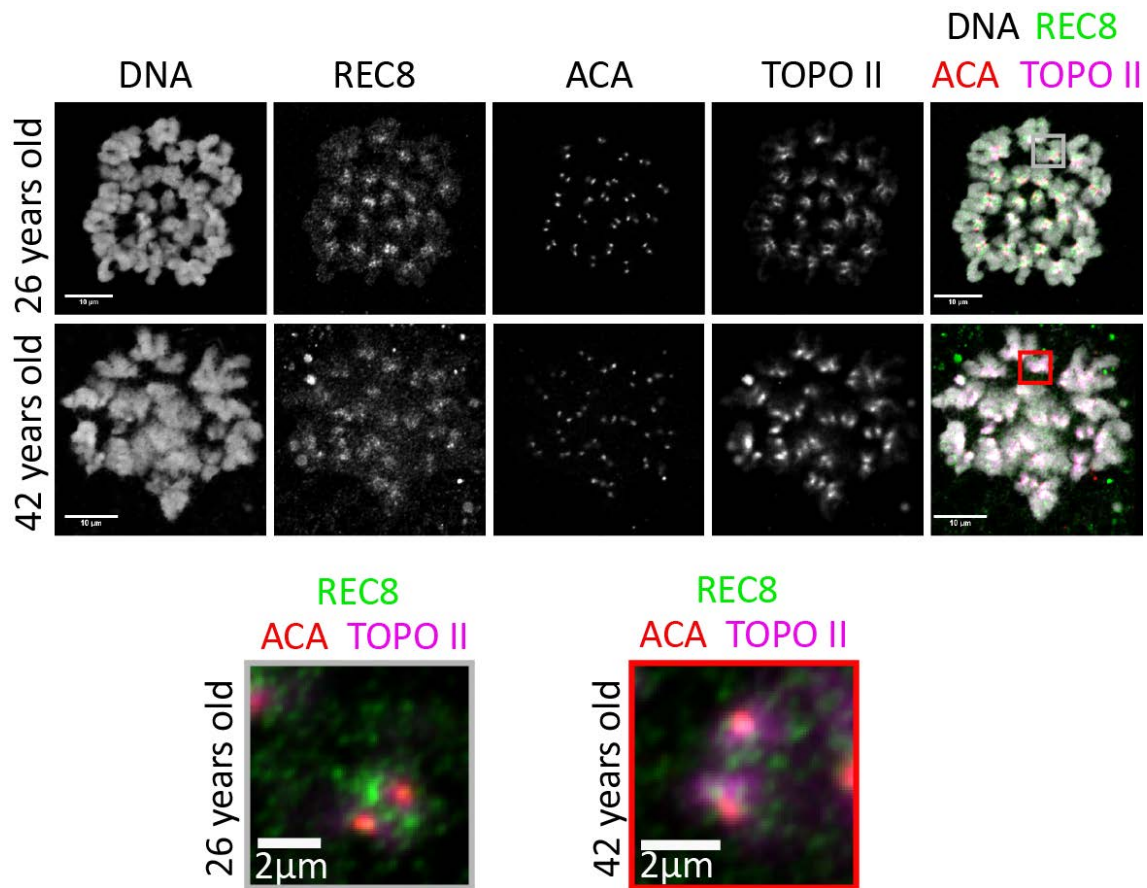
Figure 6.22 REC8 appears to mislocalise to chromosome kinetochore in chromosome spreads from women over 35. *Representative Airyscan processed images of MII chromosome spreads from a 26 years old and 42 year old woman. Spreads were immunolabelled with antibodies to REC8, ACA and TOPO II. DNA was labelled using DAPI. Scale bar 10µm. Inset boxes show enhanced images of dyads from the younger (grey box) and older woman (red box). Scale bar 2µm (under 30 n=23 oocytes from 6 donors, mean age of oocytes donated: 26.57 s.d: ±1.947; over 35 n=10 oocyte from 8 donors mean age of oocytes donated: 41.30 s.d: ±2.070).*

As in the meiosis I chromosome spreads from the pilot study (Figure 6.10), it appears that REC8 in oocytes form older donors is not enriched between sister centromeres, but is instead present in the general region of the centromeres, overlapping and extending beyond the ACA foci (p<0.0001) (Figure 6.23).

167
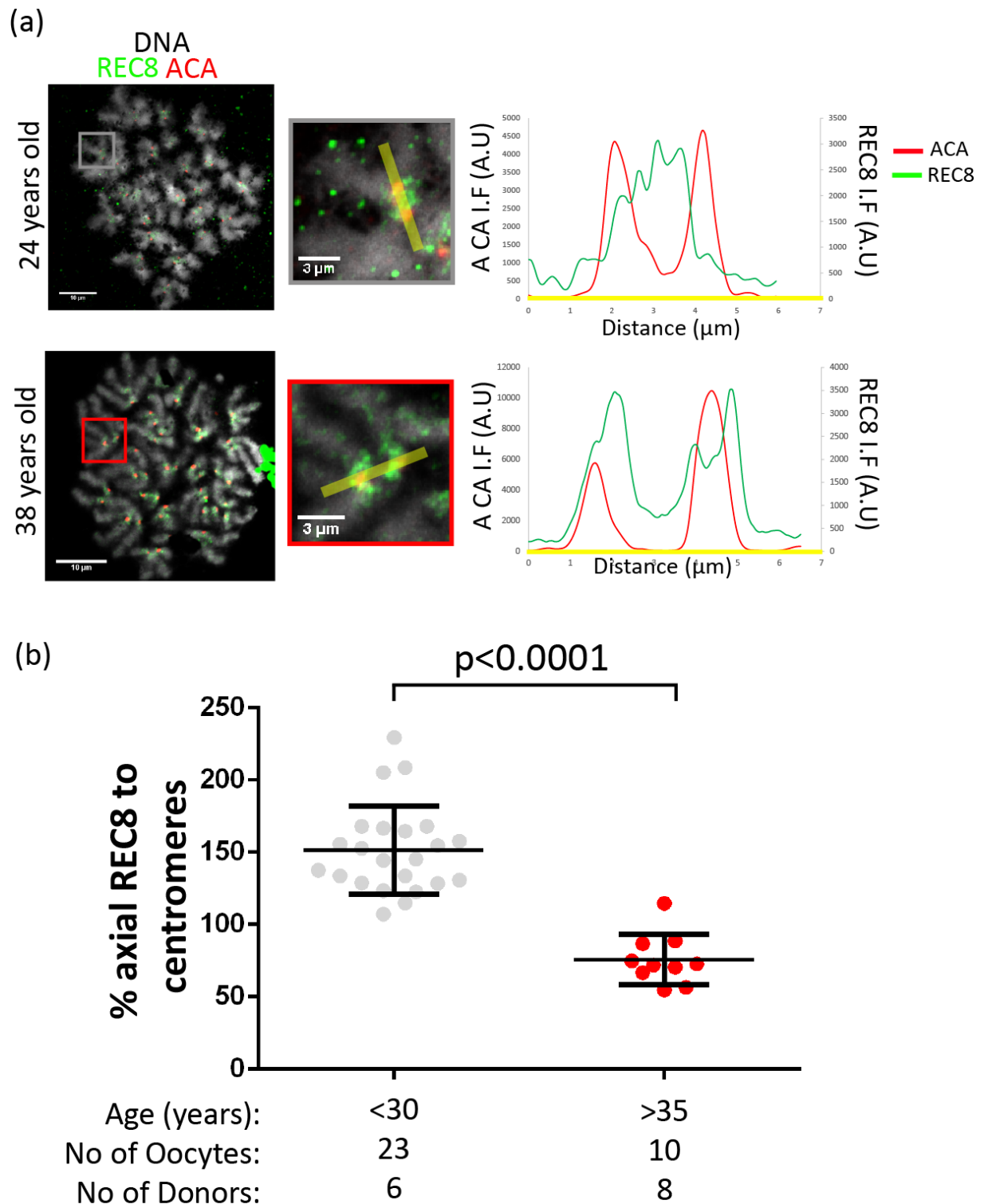
Figure 6.23 Cohesin is mislocalised from the inter-chromatid domain as a result of ageing in MII oocytes. *(a) Example images of MII chromosome spreads from a 24 year old and a 38 year old woman. Linescans show ACA and REC8 immunoflourescence relative to position on the corresponding linescan. Scale bar 10µm, inset Scale bar 3µm (b) Dot plot of the % of axial REC8 to REC8 located on the centromeres. Unpaired t-test showed a significant difference (p<0.0001) showing*

168

reduction in inter-chromatid REC8 to the REC8 on the chromosome DNA. (under 30 n=23 oocytes from 6 donors, mean age of oocytes donated*: 26.57 s.d: ±1.947; over 35 n= 10 oocyte* mean age of oocytes donated*: 41.30 s.d: ±2.070)*

To determine whether the reduction in REC8 between sister centromeres in MII oocytes is associated with an overall decline in the level of REC8, I drew linescans across the centromeres of each and set independent thresholds based on an overall observation of both young and old sets within a batch (Figure 6.24).
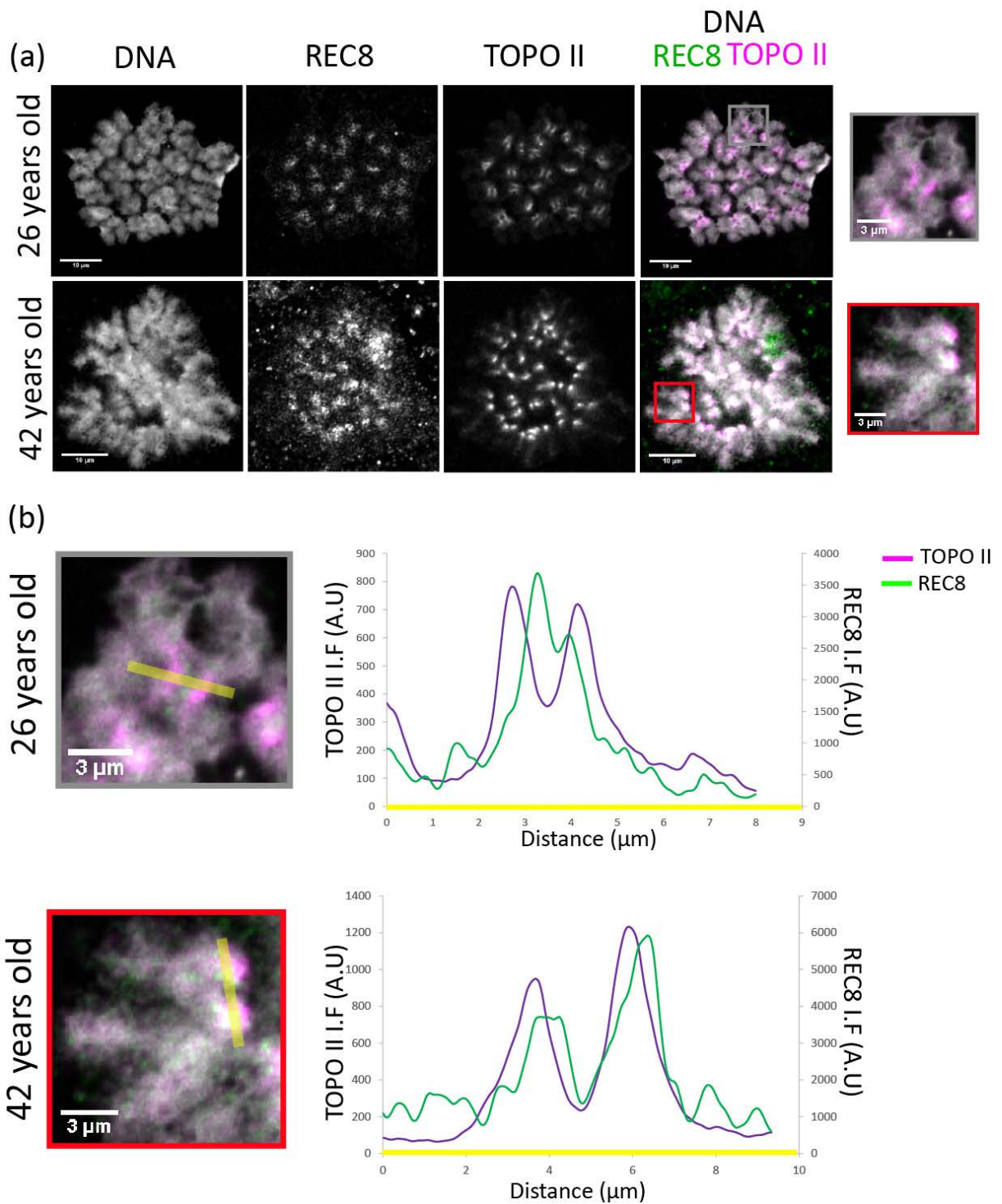
Figure 6.24 Linescan analysis of non-patient donor oocytes. *(a) Representative example of MII chromosome spreads from a 26 year old and 42 year old donor immunolabelled for REC8 and TOPO II. DNA was stained using DAPI. Scale bar 10μm. Inset shows example dyads. Scale bar 3μm (b) Linescans were drawn across pericentromeres and used to establish the area under the curve for each dyad. (under 30 n=21 oocytes from 6 donors, oocyte mean age: 26.43 S.d: ±1.86; over 35 n=8 oocytes from 6 donors, oocyte mean age: 41.00 S.d: ±1.95).*

Area under the curve values for REC8 and TOPO II per centromere per oocyte were calculated (Figure 6.25) and the ratio of REC8: TOPO II was established (Figure 6.26). This showed that REC8 and TOPO II in the oocytes from the women over 35 appeared more abundant that in the oocytes from the younger women.

Figure 6.25 REC8 and TOPO II area under the curve values for younger and older women from non-patient donor population *Dot plots show the area under the curve values for REC8 and TOPO II in younger and older female oocytes from air-dried chromosome spreads. Each graph represents a batch of staining. Individual oocyte REC8 and TOPO II are separated by vertical dotted lines with each batch separated by horizontal dotted lines. Each dot represents an area under the curve value for REC8 or TOPO II. Errors bars represent the mean ± s.d for each oocyte. Table contains the number of oocytes and number of donations per batch.*

	<30 years old			>35 years old		
batch	1	2	3	1	2	3
no. oocytes	11	7	3	6	1	1
no. donors	4	4	2	5	1	1
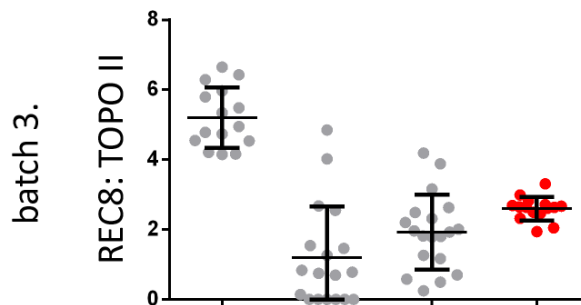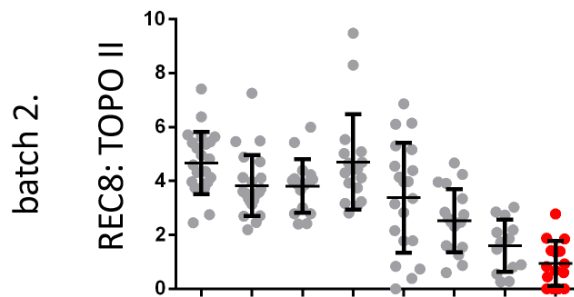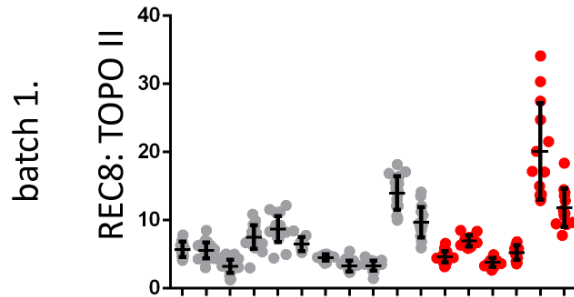
Figure 6.26 REC8: TOPO II ratio for younger and older women from non-patient donor population. *Dot plots showing the ratio of REC8: TOPO II per pericentromere for younger and older women. Each graph represents a batch of staining. Experimental repeats are separated by dotted lines. Each data point represents the ratio of the area under the curve of REC8 to TOPO II. Error bars represent the mean ±s.d for each oocyte. Table contains the number of oocytes and number of donations per batch.*

To combine the experiments across the 3 batches, I normalised the median values per oocyte to the average of the medians for the under 30 age group. This indicated that REC8 in the older donors is increased in the region of the pericentromeres. However, when REC8 is normalised to TOPO II, there is no significant difference in REC8 between the under 30 age group and the over 35 (p=0.7014) (Figure 6.27). This suggests that REC8 around the centromeres is not reduced with age in human oocytes. However, the enrichment of Rec8 between centromeres appears to be diminished in MII oocytes from the older women. This is consistent with the finding that premature separation of sister centromeres is strongly correlated with age in human oocytes (Pellestor et al., 2003).
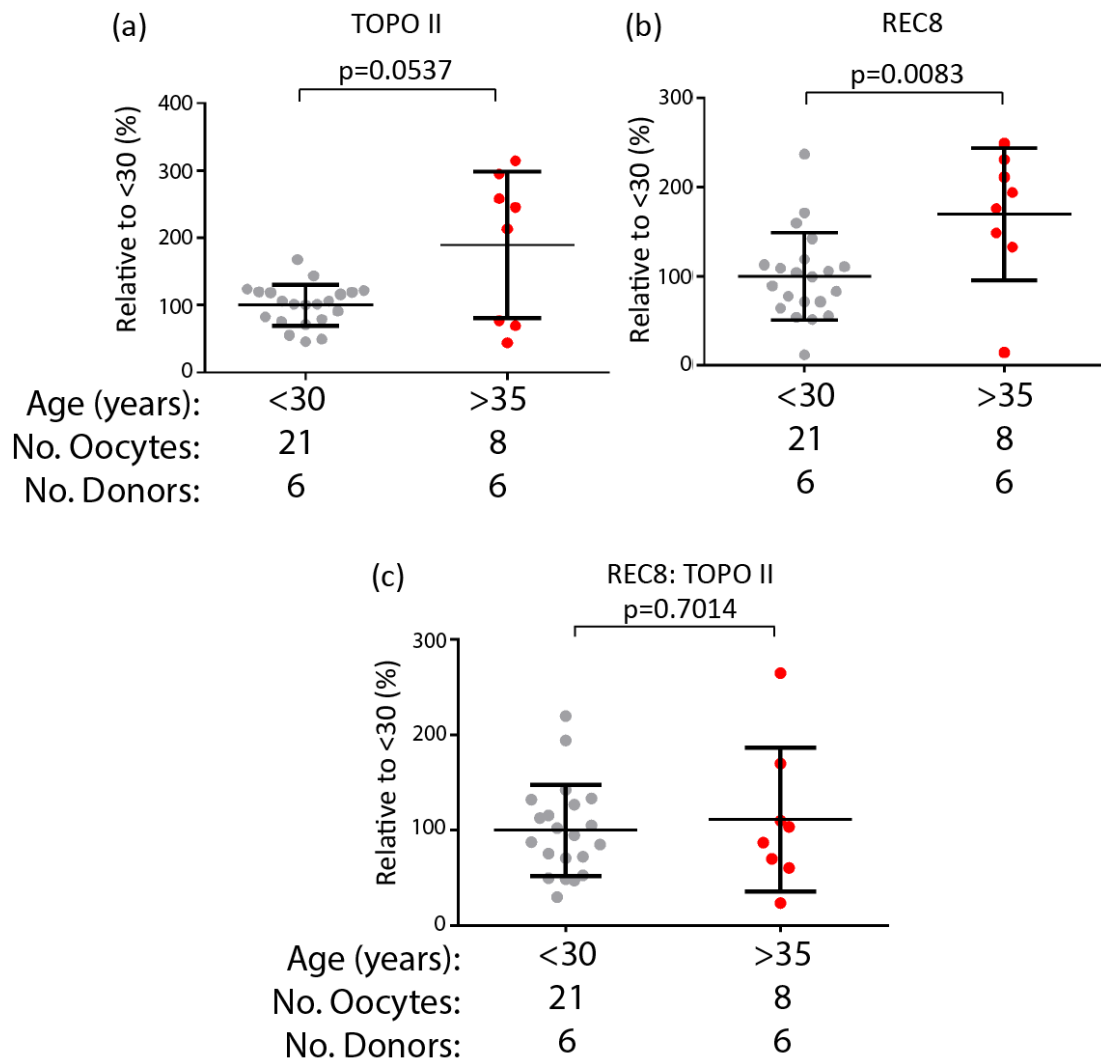
Figure 6.27 REC8:TOPO II ratio does not show a significant difference between younger and older women in MII air-dried chromosome spreads. *Comparisons between young and old donors of the median area under the curve values per oocyte for (a) TOPO II (b) REC8 normalised to the average of the median per oocyte for the under 30 years old donors. An unpaired t-test and a Mann Whitney U test were used to determine the significance of the difference between TOPO II and REC8 respectively. TOPO II exhibited no difference (p=0.0537) while the values for REC8 area under the curve suggested that there is more REC8 on the pericentromeres of older women compared to younger women. (c) When REC8 is normalised to TOPO II this significant difference is lost with an unpaired t-test showing no significant difference between younger and older donors (p=0.7014). (under 30 n=21 oocytes from 6 donors, oocyte mean age: 26.43 S.d: ±1.859; over 35 n=8 oocytes from 6 donors, oocyte mean age: 41.00 S.d: ±1.947)*

175

6.6 Discussion

A woman's age at the time of pregnancy is the greatest determinant of whether she will have a healthy child or a pregnancy ending in miscarriage (Hassold and Hunt, 2001). This is due to an age-related reduction in chromosomal cohesion leading to premature separation of sister centromeres (Angell, 1991, Angell, 1997, Pellestor et al., 2003, Sakakibara et al., 2015). Work using naturally aged mice indicated an age-related depletion of the cohesin complex (Lister et al., 2010, Chiang et al., 2010). However, whether human oocytes exhibit a similar age-related effect had, until now, not been directly tested.

One of the difficulties in determining loss of cohesin in human oocytes is the lack of a reliable source of healthy oocytes. Studies in mice extract oocytes through maceration of the ovary to release GV oocytes which can then be synchronised to resume meiosis using a phosphodiesterase inhibitor, such as IBMX, to inhibit entry into M Phase (Bornslaeger et al., 1986). Human studies on the other hand have relied on the small population of oocytes considered unsuitable for ICSI (Webster and Schuh, 2017). These account for around 15-20% of oocytes retrieved during egg collection and are rejected based on the absence of a polar body (Reichman et al., 2010). These oocytes are at GV and MI stage and it is unclear why they have not proceeded through meiosis like the majority of other oocytes. This means that the majority of work carried out in human oocytes has depended upon potentially abnormal biological material.

To address this we established an oocyte donation scheme were women would donate their oocytes exclusively for use by our research team. This would include MII oocytes as well as any MI or GV stage oocytes. The women donating in this project showed a consistent trend of having lower follicle counts and AMH levels with age. These factors show that the women who donated in this study are representative of the wider population of women.

Initial comparisons of the number of follicles provided to research irrespective of hCG retrieval time showed an expected decrease in the number of follicles retrieved with age. There was, however, quite a noticeable spread in the numbers of follicles retrieved in all age categories. When the number of follicles retrieved was broken down in to retrieval time post hCG there was a non-significant trend towards greater

176

oocyte retrieval at later hCG times. This means that future work in this field will require development of new techniques for collecting these smaller follicles. In part, the lack of a significant difference in oocyte retrieval numbers is down to advances being made in the collection of small follicles within our study.

As we sought oocytes at GV and MI stage, we reduced the hCG retrieval time. Interestingly our results in the 30 and under age category indicates that while a greater proportion of MI oocytes are found when the interval from hCG to oocytes harvest is reduced, there was a non-significant trend towards a higher proportion of GV-stage oocytes at later time points. The most likely explanation is that GV stage oocytes collected at the later times post-hCG are coming from follicles that are undergoing atresia, making the oocyte easier to aspirate with the follicular fluid. By contrast, healthy GV stage oocytes are expected to be tightly attached to the follicles mural granulosa cells.

To investigate whether cohesin is reduced with age in human oocytes, we launched a pilot study using data from previously acquired MI human oocyte chromosome spreads and those from a stockpile of vitrified oocytes, from which air-dried chromosome spreads were prepared. Initial analysis showed that in our population of ICSI-reject oocytes, bivalent stability decreases with age, with bivalents showing premature resolution to dyad chromosomes and sometimes to single chromatids. Measurements of the distance between sister centromeres also increases with age. This was indicative of a reduction in cohesin seen in previous studies. Compromise of bivalent chromosome structure has been highlighted in both mice and humans as being significant in causing chromosome segregation errors (Lister et al., 2010, Sakakibara et al., 2015, Zielinska et al., 2015). Observations in whole fixed human oocytes reported that an increase in age resulted in an increase in split bivalent kinetochores. These split kinetochores are more susceptible to merotelic attachment and subsequent segregation errors (Zielinska et al., 2015).

 After attempts to quantify REC8 using spreads that were imaged separately, we tried to control for experimental variation by preparing a batch of chromosome spreads from our stockpile of vitrified oocytes which were stained and imaged at the same time. I.F staining indicated that there was still clear staining for REC8 in the older women. This differs from mouse oocytes which display a total loss of REC8 with age (Lister et al., 2010, Chiang et al., 2010). Closer observations of
177

the images however suggested that the REC8 is mis-localised in oocytes from older women. Instead of being enriched in the inter-chromatid domain, REC8 showed a diffused distribution on the chromosomes without any enrichment in any location. To validate this observations I calculated the average REC8 fluorescence intensity on the CREST signal compared to directly between the CREST signal. Comparisons between young and old showed that a significant difference existed between over 35s were REC8 was located more on the actual chromosomes than between them.

The results of the pilot study informed us of several key features. Firstly, that measuring REC8 is complicated by the presence of non-axial REC8 on the chromosome arms. This produces a high value for REC8 in quantitative analysis but does not appear to provide any actual cohesion. Secondly, avoiding CREST as a tool for normalisation would be optimal. Third, attempting to spread oocytes from younger and older women on the same slide is ineffective as the numbers will always be too small. Finally the variation seen in the raw value numbers may be as a result of using ICSI-reject oocytes.

Analysis of the MII oocytes from the non-patient donors showed that they had an expected phenotype of an increase in segregation errors as well as an increase in inter-centromeric distances. What is more, the non-axial REC8 localisation continues to exist on the chromosomes, but only at the centromeres. This would suggest that the cohesin that mislocalises to the DNA is removed during anaphase in a similar manner to arm cohesin removed during anaphase I. It also suggests that this mislocalisation cannot be attributed to cytoplasmic cohesin sticking to the DNA during spreading. Comparisons of total fluorescent intensity however, showed that there was no overall reduction in REC8 at the MII stage of meiosis.

The results of this Chapter suggest some discrepancies between how ageing effects mouse and human oocytes. While in mice there is a loss of chromosome-bound cohesin during prophase arrest, in human oocytes it appears to be mislocalied. While this seems contradictory between the two organisms there are potential mechanisms that could explain both and warrant investigating. It is possible that the cohesin ring could be opening or becoming damaged but not actually removed from the DNA in human oocytes where as in the mouse it would be.

178

It should be noted however that the work in this Chapter has only looked at REC8. Future work should also analyse AcSMC3, as this is indicative of cohesive cohesin. If this showed a similar patterns of localisation to the REC8 then it would be informative of whether this mislocalised cohesin is providing any actual cohesion.

The results in this Chapter show for the first time that that while cohesin is affected by ageing in human oocytes, it differs from the effect that occurs in mice. This suggests some discrepancies between the human and the mouse models that will require further investigation.

Chapter 7. Discussion and Conclusion

7.1 Discussion

Despite the continued increase in human life expectancy and health over the past few centuries, the decline in female fertility by the fourth decade of life followed by the menopause in the fifth has remained stubbornly persistent (Lambalk et al., 2009). The reason for this loss of fertility, is due to a continuous depletion of available oocytes, with the remaining few having a reduced ability to accurately segregate their chromosomes (Herbert et al., 2015). If one of these poorer quality oocytes is fertilised, the likelihood of the pregnancy ending in miscarriage or the child being born with birth defects is severe (Hassold and Hunt, 2001). Investigations into mouse and human oocytes have revealed that ageing results in a loss of bivalent chromosome stability due to a loss of chromosomal cohesion (Chiang et al., 2010, Lister et al., 2010, Duncan et al., 2012, Patel et al., 2015, Sakakibara et al., 2015, Zielinska et al., 2015, Lagirand-Cantaloube et al., 2017). This is thought to increase the chances of aneuploidy, with premature separation of sister chromatids being the leading cause (Angell, 1997, Sakakibara et al., 2015). In mouse oocytes, this has been strongly linked to a loss of chromosome-bound cohesin during the prolonged prophase arrest (Chiang et al., 2010, Lister et al., 2010). The question remains, however, around what mechanisms are responsible for this loss of cohesin in mouse oocytes. It is also not known whether a loss of cohesin with ageing is responsible for the increase in segregation errors in human oocytes.

Part of the difficulty in establishing which proteins are affected by ageing relates to a lack of appropriate tools for quantification. One of the most effective methods for assessing changes to chromosome-bound proteins is the use of air-dried chromosome spreads. Yet, due to the large number of proteins affected by ageing, normalisation of the protein of interest to a standard marker has proved difficult. To address this I sought out a marker that would be effective for this purpose. This led me to the DNA catenation enzyme TOPO II. This appeared to be an appropriate tool as it showed consistent localisation through meiosis, could be used for segmentation of sections of chromosomes, and was informative of chromosome architecture. Importantly for reproducibility, the antibody targeted to TOPO II is commercially available and conjugated, so can be used by other researchers with any combination of other antibodies.

Comparisons of TOPO II, ACA and SMC3 using the software programme Imaris shows that while both decline with age, TOPO II is less affected. Use of both the peak F.I and Sum F.I in Imaris analysis was useful for determining loss of the universal cohesin subunit SMC3. However, the reduction did not appear representative of what could be seen by eye. To address this, I established a new form of analysis. This measures the area under the curve across a linescan for TOPO II and the protein of interest. This allowed for independent thresholds to be set and for a more representative interpretation of the data. The combination of TOPO II and linescan analysis should provide an easy-to-use methodology for further research in this field.

The finding by our group and others indicating that a loss of chromosome-bound REC8 in mouse oocytes occurs during the prolonged prophase arrest of oogenesis, is crucial to understanding which mechanisms could be responsible for cohesin loss (Tsutsumi et al., 2014). It is also important as it informs of the viability of potential interventions to maintain female fertility. However, it was not clear whether this loss occurs progressively with age, or whether other forms of cohesin are present in the primordial oocyte. Using protein quantification on cryosections for REC8 and SMC3 I showed that the loss of cohesin is progressive, and that there is a universal loss of chromosome-bound cohesin in primordial-stage oocyte with age. However, the fold decline in SMC3 was noticeably less than that of REC8. Staining for RAD21 in primordial-stage oocytes suggests that it is expressed in the primordial oocyte nucleus. It therefore cannot be ruled out that the difference in the fold decline in REC8 and SMC3 may be down to RAD21 containing cohesin in primordial-stage oocytes. It will be necessary to carry out ageing studies to find if this RAD21 is reduced or loaded with ageing. The prospect of non-REC8 containing cohesin complex in the primordial-stage oocytes is particularly interesting considering SMC3 appeared to be undetectable with age in metaphase I oocytes in Chapter 4. It may be possible that any non-REC8 containing cohesin complexes are removed before resumption of meiosis. Two recent findings from our group suggest this may be possible. The first is that PLK1 is expressed in fully grown oocytes but not primordial stage oocytes, and that when PLK1 is inhibited using BI2536 in GV stage oocytes, more cohesin is seen on the chromosomes than compared to controls (work carried out by R. Ballesteros-Meija and C. Lodge). This may represent a function for the prophase pathway before resumption of meiosis.

Having determined that cohesin is progressively lost with ageing, I next sought to establish what mechanisms could be involved in this loss. For this, I investigated whether leaky inhibition of separase could be actively cleaving cohesin over time. This was investigated previously in our group in fully grown oocytes but not in primordial-stage oocytes, where cohesin loss occurs. Several reasons pointed to separase as a potential cause of cohesin loss. Firstly, separase is responsible for REC8 cleavage during both stages of meiosis (Kudo et al., 2006, Kudo et al., 2009). Secondly, experiments in yeast where separase is released from securin during prophase show it is capable of cleaving cohesin (Oelschlaegel et al., 2005, Penkner et al., 2005). Thirdly, during prophase in oocytes, CDK1-mediated phosphorylation of separase would be inhibited as CDK1 is suppressed (Adhikari et al., 2016). Through use of an oocyte-specific *separase* null mouse on the *Gdf9* promoter, I showed that leaky inhibition of separase is not the cause of cohesin loss in primordial-stage oocytes. This would suggest that cohesin is lost via another mechanism in oocytes. However, the lower prevalence of primordial-stage oocytes in *separase null* mice compared to separase-wild type mice suggests a possible role for separase during prophase arrest. As cohesin is necessary for DNA damage repair, if separase is required for removal of that cohesin, a lack of separase may trigger atresia reducing the number of primordial stage oocytes (Wu and Yu, 2012).

The need for cohesin protection after resumption of meiosis has been well investigated in mice (Lee et al., 2008, Llano et al., 2008, Rattani et al., 2013). However, little work has been done on whether cohesin is protected during the prolonged prophase arrest, where cohesin is lost. My work suggests that if there is any protection of meiotic cohesin, it is quite likely compromised with ageing. SGOL2 does not appear on the chromosomes until after GVBD and while SGO1 is expressed, I have discovered that it becomes mislocalised with ageing, suggesting it could lose its function. Several criteria should be further tested to determine whether SGO1 provides protection. This should be done first through determining whether the holoenzyme PP2A is localised to SGO1 in primordial-stage oocytes, and if so, chromosome bound cohesin should then be quantified in an oocyte-specific SGO1-knockout mouse.

However, on its own these finds hint to other dysfunctions within the oocyte. BUB1 is necessary for SGO1 localisation and has been indicated as being partially involved in SGOL2 localisation, which could indicate a loss of BUB1 with age (El Yakoubi et al.,

182

2017). Alternatively, this mislocalisation could indicate changes in chromatin structure, a well-characterised aspect of aged and cancerous cell lines in somatic cells (Lopez-Otin et al., 2013, Abe et al., 2016, Higgins and Prendergast, 2016). Other work has suggested that Sgo1 is necessary for biorentation in *S. cerevisiae* (Peplowska et al., 2014). If a similar function occurs in MII, this could mean the loss of SGO1 is required for accurate segregation in the second meiotic division.

Having investigated the timing and mechanisms around loss of cohesin I next sought to determine whether the mouse model of cohesin loss is representative of the age-related increase in human oocyte segregation errors. Hitherto, studies on human oocytes have relied on the small percentage that are rejected from IVF. It is unclear why, even after a full stimulation regime, they do not proceed to MII by 37 hours post administration of hCG. To avoid this issue we established a non-patient oocyte donation scheme were the woman's oocytes would be collected at shorter post hCG times. This was intended to provide more oocytes at GV and MI stage. We discovered that, while reducing the timeframe provided more oocytes at MI stage, it did not yield a greater number of GV stage oocytes. Also, reducing the time between hCG and oocyte collection appeared to reduce the number of oocytes that could be aspirated. These findings suggests that new techniques for oocyte collection must be developed to capture all immature oocytes. To determine how best to study chromosome-associated proteins in human oocytes, and to give an indication of how REC8 is affected by ageing, we set up a pilot study using air-dried chromosome spreads at MI from ICSI-rejected oocytes. The findings from the pilot study support previous reports in humans and in mouse oocytes, showing that ageing is accompanied by a loss of bivalent structural integrity and an increase in distance between sister centromeres (Lister et al., 2010, Duncan et al., 2012, Patel et al., 2015, Sakakibara et al., 2015, Zielinska et al., 2015, Lagirand-Cantaloube et al., 2017). However, it did not show a quantifiable loss of REC8 with age similar to the mouse. Instead REC8 appears to be mislocalised onto the chromosome arms, away from the axis. While it was possible that this may have been a result of cytoplasmic REC8 sticking to the chromosomes, the non-patient donor oocytes showed the same localisation. Importantly however, this localisation was only at the centromeres of the MII oocytes, suggesting this may in fact represent a biological mechanism of ageing.

The question, therefore, is whether the mouse should now be considered an invalid model for investigating segregation errors in humans. In my opinion, this is premature and it is still likely that variations on a common dysfunction could explain the loss of chromosomal cohesion.

The results from Chapter 5 suggest that separase is not predominantly responsible for cohesin loss. This leaves the door open for other mechanisms such as protein damage from ROS to the cohesin ring. It is possible that damaged REC8 containing cohesin in mouse oocytes are removed, while in the humans it remains on the DNA not providing any cohesion. This could first be tested by staining for AcSMC3 which is required for cohesive cohesin (Zhang et al., 2008).

7.2 Conclusion and future work

The work in my thesis presents advances in our current knowledge of the mechanisms behind age-related aneuploidy in human and mouse oocytes. This suggests that an age related dysfunction in REC8-containing cohesin leads to a loss of bivalent chromosome stability. In mice this appears to occur progressively during oogenesis. While in the mouse this dysfunction manifests as loss of cohesin, in humans it results in mislocalisation. In terms of further understanding the mechanism by which this occurs, the role of age-related protein damage to REC8-containing cohesin during prophase-arrest should be investigated in mice and humans.

My work also suggests the presence of non-REC8 containing cohesin complexes in primordial stage mouse oocytes. What role they play during oogenesis, and whether they are removed before resumption of meiosis remains unclear. This should be investigated by studying the proteins involved in the prophase-pathway during oogenesis.

Clinically, my work supports the theory of a deterioration of oocyte quality during prophase arrest. If this deterioration occurs as a result of protein damage over time it is unlikely that there is any reversible mechanism that could be employed to help older women. As a result, currently, cryo-preservation of a woman's oocytes in her late 20's remains the most viable option for prolonging fertility into later life.

Bibliography

ABE, Y., SAKO, K., TAKAGAKI, K., HIRAYAMA, Y., UCHIDA, K. S., HERMAN, J. A., DELUCA, J. G. & HIROTA, T. 2016. HP1-Assisted Aurora B Kinase Activity Prevents Chromosome Segregation Errors. *Dev Cell,* 36**,** 487-97.

ADHIKARI, D., BUSAYAVALASA, K., ZHANG, J., HU, M., RISAL, S., BAYAZIT, M. B., SINGH, M., DIRIL, M. K., KALDIS, P. & LIU, K. 2016. Inhibitory phosphorylation of Cdk1 mediates prolonged prophase I arrest in female germ cells and is essential for female reproductive lifespan. *Cell Res,* 26**,** 1212-1225.

ADHIKARI, D. & LIU, K. 2009. Molecular mechanisms underlying the activation of mammalian primordial follicles. *Endocr Rev,* 30**,** 438-64.

ALBERTINI, D. F., COMBELLES, C. M., BENECCHI, E. & CARABATSOS, M. J. 2001. Cellular basis for paracrine regulation of ovarian follicle development. *Reproduction,* 121**,** 647-53.

ALLSHIRE, R. C. & KARPEN, G. H. 2008. Epigenetic regulation of centromeric chromatin: old dogs, new tricks? *Nat Rev Genet,* 9**,** 923-37.

ANGELL, R. 1997. First-meiotic-division nondisjunction in human oocytes. *Am J Hum Genet,* 61**,** 23-32.

ANGELL, R. R. 1991. Predivision in human oocytes at meiosis I: a mechanism for trisomy formation in man. *Hum Genet,* 86**,** 383-7.

ARGUELLO-MIRANDA, O., ZAGORIY, I., MENGOLI, V., ROJAS, J., JONAK, K., OZ, T., GRAF, P. & ZACHARIAE, W. 2017. Casein Kinase 1 Coordinates Cohesin Cleavage, Gametogenesis, and Exit from M Phase in Meiosis II. *Dev Cell,* 40**,** 37-52.

BAKER, D. J., JEGANATHAN, K. B., CAMERON, J. D., THOMPSON, M., JUNEJA, S., KOPECKA, A., KUMAR, R., JENKINS, R. B., DE GROEN, P. C., ROCHE, P. & VAN DEURSEN, J. M. 2004. BubR1 insufficiency causes early onset of aging-associated phenotypes and infertility in mice. *Nat Genet,* 36**,** 744-9.

BAUDAT, F., IMAI, Y. & DE MASSY, B. 2013. Meiotic recombination in mammals: localization and regulation. *Nat Rev Genet,* 14**,** 794-806.

BECKER, J. S., NICETTO, D. & ZARET, K. S. 2016. H3K9me3-Dependent Heterochromatin: Barrier to Cell Fate Changes. *Trends Genet,* 32**,** 29-41.

BINK, K., WALCH, A., FEUCHTINGER, A., EISENMANN, H., HUTZLER, P., HOFLER, H. & WERNER, M. 2001. TO-PRO-3 is an optimal fluorescent dye for nuclear counterstaining in dual-colour FISH on paraffin sections. *Histochem Cell Biol,* 115**,** 293-9.

BOLAND, A., MARTIN, T. G., ZHANG, Z., YANG, J., BAI, X. C., CHANG, L., SCHERES, S. H. & BARFORD, D. 2017. Cryo-EM structure of a metazoan separase-securin complex at near-atomic resolution. *Nat Struct Mol Biol,* 24**,** 414-418.

BORNSLAEGER, E. A., MATTEI, P. & SCHULTZ, R. M. 1986. Involvement of cAMP-dependent protein kinase and protein phosphorylation in regulation of mouse oocyte maturation. *Dev Biol,* 114**,** 453-62.

BROEKMANS, F. J., KNAUFF, E. A., TE VELDE, E. R., MACKLON, N. S. & FAUSER, B. C. 2007. Female reproductive ageing: current knowledge and future trends. *Trends Endocrinol Metab,* 18**,** 58-65.

BROOKER, A. S. & BERKOWITZ, K. M. 2014. The roles of cohesins in mitosis, meiosis, and human health and disease. *Methods Mol Biol,* 1170**,** 229-66.

BUHEITEL, J. & STEMMANN, O. 2013. Prophase pathway-dependent removal of cohesin from human chromosomes requires opening of the Smc3-Scc1 gate. *EMBO J,* 32**,** 666-76.

BURKHARDT, S., BORSOS, M., SZYDLOWSKA, A., GODWIN, J., WILLIAMS, S. A., COHEN, P. E., HIROTA, T., SAITOU, M. & TACHIBANA-KONWALSKI, K. 2016. Chromosome Cohesion Established by Rec8-Cohesin in Fetal Oocytes Is Maintained without Detectable Turnover in Oocytes Arrested for Months in Mice. *Curr Biol,* 26**,** 678-85.

CAMPBELL, L., TRENDELL, J. & SPEARS, N. 2013. Identification of cells migrating from the thecal layer of ovarian follicles. *Cell Tissue Res,* 353**,** 189-94.

CASTRILLON, D. H., MIAO, L., KOLLIPARA, R., HORNER, J. W. & DEPINHO, R. A. 2003. Suppression of ovarian follicle activation in mice by the transcription factor Foxo3a. *Science,* 301**,** 215-8.

CHAMBON, J. P., TOUATI, S. A., BERNEAU, S., CLADIERE, D., HEBRAS, C., GROEME, R., MCDOUGALL, A. & WASSMANN, K. 2013. The PP2A inhibitor I2PP2A is essential for sister chromatid segregation in oocyte meiosis II. *Curr Biol,* 23**,** 485-90.

CHAN, K. L., ROIG, M. B., HU, B., BECKOUET, F., METSON, J. & NASMYTH, K. 2012. Cohesin's DNA exit gate is distinct from its entrance gate and is regulated by acetylation. *Cell,* 150**,** 961-74.

CHIANG, T., DUNCAN, F. E., SCHINDLER, K., SCHULTZ, R. M. & LAMPSON, M. A. 2010. Evidence that weakened centromere cohesion is a leading cause of age-related aneuploidy in oocytes. *Curr Biol,* 20**,** 1522-8.

CHIANG, T., SCHULTZ, R. M. & LAMPSON, M. A. 2011. Age-dependent susceptibility of chromosome cohesion to premature separase activation in mouse oocytes. *Biol Reprod,* 85**,** 1279-83.

CIOSK, R., SHIRAYAMA, M., SHEVCHENKO, A., TANAKA, T., TOTH, A., SHEVCHENKO, A. & NASMYTH, K. 2000. Cohesin's binding to chromosomes depends on a separate complex consisting of Scc2 and Scc4 proteins. *Mol Cell,* 5**,** 243-54.

CIOSK, R., ZACHARIAE, W., MICHAELIS, C., SHEVCHENKO, A., MANN, M. & NASMYTH, K. 1998. An ESP1/PDS1 complex regulates loss of sister chromatid cohesion at the metaphase to anaphase transition in yeast. *Cell,* 93**,** 1067-76.

CLARKSON, Y. L., MCLAUGHLIN, M., WATERFALL, M., DUNLOP, C. E., SKEHEL, P. A., ANDERSON, R. A. & TELFER, E. E. 2018. Initial characterisation of adult human ovarian cell populations isolated by DDX4 expression and aldehyde dehydrogenase activity. *Sci Rep,* 8**,** 6953.

CRAWLEY, O., BARROSO, C., TESTORI, S., FERRANDIZ, N., SILVA, N., CASTELLANO-POZO, M., JASO-TAMAME, A. L. & MARTINEZ-PEREZ, E. 2016. Cohesin-interacting protein WAPL-1 regulates meiotic chromosome structure and cohesion by antagonizing specific cohesin complexes. *Elife,* 5**,** e10851.

CUI, L. B., HUANG, X. Y. & SUN, F. Z. 2005. Transfer of germinal vesicle to ooplasm of young mice could not rescue ageing-associated chromosome misalignment in meiosis of oocytes from aged mice. *Hum Reprod,* 20**,** 1624-31.

DA SILVA-BUTTKUS, P., JAYASOORIYA, G. S., MORA, J. M., MOBBERLEY, M., RYDER, T. A., BAITHUN, M., STARK, J., FRANKS, S. & HARDY, K. 2008. Effect of cell shape and packing density on granulosa cell proliferation and formation of multiple layers during early follicle development in the ovary. *J Cell Sci,* 121**,** 3890-900.

DANYLEVSKA, A., KOVACOVICOVA, K., AWADOVA, T. & ANGER, M. 2014. The frequency of precocious segregation of sister chromatids in mouse female meiosis I is affected by genetic background. *Chromosome Res,* 22**,** 365-73.

DE TORRES, C., MUNELL, F., FERRER, I., REVENTOS, J. & MACAYA, A. 1997. Identification of necrotic cell death by the TUNEL assay in the hypoxic-ischemic neonatal rat brain. *Neurosci Lett,* 230**,** 1-4.

DONG, J., ALBERTINI, D. F., NISHIMORI, K., KUMAR, T. R., LU, N. & MATZUK, M. M. 1996. Growth differentiation factor-9 is required during early ovarian folliculogenesis. *Nature,* 383**,** 531-5.

DUNCAN, F. E., CHIANG, T., SCHULTZ, R. M. & LAMPSON, M. A. 2009. Evidence that a defective spindle assembly checkpoint is not the primary cause of maternal age-associated aneuploidy in mouse eggs. *Biol Reprod,* 81**,** 768-76.

DUNCAN, F. E., HORNICK, J. E., LAMPSON, M. A., SCHULTZ, R. M., SHEA, L. D. & WOODRUFF, T. K. 2012. Chromosome cohesion decreases in human eggs with advanced maternal age. *Aging Cell,* 11**,** 1121-4.

EARNSHAW, W. C. & COOKE, C. A. 1989. Proteins of the inner and outer centromere of mitotic chromosomes. *Genome,* 31**,** 541-52.

EDSON, M. A., NAGARAJA, A. K. & MATZUK, M. M. 2009. The mammalian ovary from genesis to revelation. *Endocr Rev,* 30**,** 624-712.

EL YAKOUBI, W., BUFFIN, E., CLADIERE, D., GRYAZNOVA, Y., BERENGUER, I., TOUATI, S. A., GOMEZ, R., SUJA, J. A., VAN DEURSEN, J. M. & WASSMANN, K. 2017. Mps1 kinase-dependent Sgo2 centromere localisation mediates cohesin protection in mouse oocyte meiosis I. *Nat Commun,* 8**,** 694.

EUROSTAT 2015. People in the EU: who are we and how do we live? 2015 ed.

FADDY, M. J. 2000. Follicle dynamics during ovarian ageing. *Mol Cell Endocrinol,* 163**,** 43-8.

FADDY, M. J. & GOSDEN, R. G. 1996. A model conforming the decline in follicle numbers to the age of menopause in women. *Hum Reprod,* 11**,** 1484-6.

FERRANDIZ, N., BARROSO, C., TELECAN, O., SHAO, N., KIM, H. M., TESTORI, S., FAULL, P., CUTILLAS, P., SNIJDERS, A. P., COLAIACOVO, M. P. & MARTINEZ-PEREZ, E. 2018. Spatiotemporal regulation of Aurora B recruitment ensures release of cohesion during C. elegans oocyte meiosis. *Nat Commun,* 9**,** 834.

FLOROS, V. I., PYLE, A., DIETMANN, S., WEI, W., TANG, W. C. W., IRIE, N., PAYNE, B., CAPALBO, A., NOLI, L., COXHEAD, J., HUDSON, G., CROSIER, M., STRAHL, H., KHALAF, Y., SAITOU, M., ILIC, D., SURANI, M. A. & CHINNERY, P. F. 2018. Segregation of mitochondrial DNA heteroplasmy through a developmental genetic bottleneck in human embryos. *Nat Cell Biol,* 20**,** 144-151.

FRAGOULI, E., ALFARAWATI, S., GOODALL, N. N., SANCHEZ-GARCIA, J. F., COLLS, P. & WELLS, D. 2011. The cytogenetics of polar bodies: insights into female meiosis and the diagnosis of aneuploidy. *Mol Hum Reprod,* 17**,** 286-95.

FRAGOULI, E., ALFARAWATI, S., SPATH, K., JAROUDI, S., SARASA, J., ENCISO, M. & WELLS, D. 2013. The origin and impact of embryonic aneuploidy. *Hum Genet,* 132**,** 1001-13.

FRANASIAK, J. M., FORMAN, E. J., HONG, K. H., WERNER, M. D., UPHAM, K. M., TREFF, N. R. & SCOTT, R. T., JR. 2014. The nature of aneuploidy with increasing age of the female partner: a review of 15,169 consecutive trophectoderm biopsies evaluated with comprehensive chromosomal screening. *Fertil Steril,* 101**,** 656-663 e1.

GANDHI, R., GILLESPIE, P. J. & HIRANO, T. 2006. Human Wapl is a cohesin-binding protein that promotes sister-chromatid resolution in mitotic prophase. *Curr Biol,* 16**,** 2406-17.

GARCIA-CRUZ, R., BRIENO, M. A., ROIG, I., GROSSMANN, M., VELILLA, E., PUJOL, A., CABERO, L., PESSARRODONA, A., BARBERO, J. L. & GARCIA CALDES, M. 2010. Dynamics of cohesin proteins REC8, STAG3, SMC1 beta and SMC3 are consistent with a role in sister chromatid cohesion during meiosis in human oocytes. *Hum Reprod,* 25**,** 2316-27.

GASSLER, J., BRANDAO, H. B., IMAKAEV, M., FLYAMER, I. M., LADSTATTER, S., BICKMORE, W. A., PETERS, J. M., MIRNY, L. A. & TACHIBANA, K. 2017. A mechanism of cohesin-dependent loop extrusion organizes zygotic genome architecture. *EMBO J,* 36**,** 3600-3618.

GAVRIELI, Y., SHERMAN, Y. & BEN-SASSON, S. A. 1992. Identification of programmed cell death in situ via specific labeling of nuclear DNA fragmentation. *J Cell Biol,* 119**,** 493-501.

GERAEDTS, J., MONTAG, M., MAGLI, M. C., REPPING, S., HANDYSIDE, A., STAESSEN, C., HARPER, J., SCHMUTZLER, A., COLLINS, J., GOOSSENS, V., VAN DER VEN, H., VESELA, K. & GIANAROLI, L. 2011. Polar body array CGH for prediction of the status of the corresponding oocyte. Part I: clinical results. *Hum Reprod,* 26**,** 3173-80.

GERLICH, D., KOCH, B., DUPEUX, F., PETERS, J. M. & ELLENBERG, J. 2006. Live-cell imaging reveals a stable cohesin-chromatin interaction after but not before DNA replication. *Curr Biol,* 16**,** 1571-8.

GOMEZ, R., VALDEOLMILLOS, A., PARRA, M. T., VIERA, A., CARREIRO, C., RONCAL, F., RUFAS, J. S., BARBERO, J. L. & SUJA, J. A. 2007. Mammalian SGO2 appears at the inner centromere domain and redistributes depending on tension across centromeres during meiosis II and mitosis. *EMBO Rep,* 8**,** 173-80.

GOOK, D. A. & EDGAR, D. H. 2007. Human oocyte cryopreservation. *Hum Reprod Update,* 13**,** 591-605.

GOOK, D. A., EDGAR, D. H., BORG, J., ARCHER, J., LUTJEN, P. J. & MCBAIN, J. C. 2003. Oocyte maturation, follicle rupture and luteinization in human cryopreserved ovarian tissue following xenografting. *Hum Reprod,* 18**,** 1772-81.

GRIFFIN, J., EMERY, B. R., HUANG, I., PETERSON, C. M. & CARRELL, D. T. 2006. Comparative analysis of follicle morphology and oocyte diameter in four mammalian species (mouse, hamster, pig, and human). *J Exp Clin Assist Reprod,* 3**,** 2.

GRUBB, J., BROWN, M. S. & BISHOP, D. K. 2015. Surface Spreading and Immunostaining of Yeast Chromosomes. *J Vis Exp***,** e53081.

GRUBER, S., ARUMUGAM, P., KATOU, Y., KUGLITSCH, D., HELMHART, W., SHIRAHIGE, K. & NASMYTH, K. 2006. Evidence that loading of cohesin onto chromosomes involves opening of its SMC hinge. *Cell,* 127**,** 523-37.

HAARHUIS, J. H., ELBATSH, A. M. & ROWLAND, B. D. 2014. Cohesin and its regulation: on the logic of X-shaped chromosomes. *Dev Cell,* 31**,** 7-18.

HAARHUIS, J. H. I., VAN DER WEIDE, R. H., BLOMEN, V. A., YANEZ-CUNA, J. O., AMENDOLA, M., VAN RUITEN, M. S., KRIJGER, P. H. L., TEUNISSEN, H., MEDEMA, R. H., VAN STEENSEL, B., BRUMMELKAMP, T. R., DE WIT, E. & ROWLAND, B. D. 2017. The Cohesin Release Factor WAPL Restricts Chromatin Loop Extension. *Cell,* 169**,** 693-707 e14.

HAERING, C. H., LOWE, J., HOCHWAGEN, A. & NASMYTH, K. 2002. Molecular architecture of SMC proteins and the yeast cohesin complex. *Mol Cell,* 9**,** 773-88.

HANDYSIDE, A. H. 2013. 24-chromosome copy number analysis: a comparison of available technologies. *Fertil Steril,* 100**,** 595-602.

HANDYSIDE, A. H., MONTAG, M., MAGLI, M. C., REPPING, S., HARPER, J., SCHMUTZLER, A., VESELA, K., GIANAROLI, L. & GERAEDTS, J. 2012. Multiple meiotic errors caused by predivision of chromatids in women of advanced maternal age undergoing in vitro fertilisation. *Eur J Hum Genet,* 20**,** 742-7.

HASSOLD, T. & HUNT, P. 2001. To err (meiotically) is human: the genesis of human aneuploidy. *Nat Rev Genet,* 2**,** 280-91.

HASSOLD, T. J. & JACOBS, P. A. 1984. Trisomy in man. *Annu Rev Genet,* 18**,** 69-97.

HAUF, S., ROITINGER, E., KOCH, B., DITTRICH, C. M., MECHTLER, K. & PETERS, J. M. 2005. Dissociation of cohesin from chromosome arms and loss of arm cohesion during early mitosis depends on phosphorylation of SA2. *PLoS Biol,* 3**,** e69.

HAUF, S., WAIZENEGGER, I. C. & PETERS, J. M. 2001. Cohesin cleavage by separase required for anaphase and cytokinesis in human cells. *Science,* 293**,** 1320-3.

HAUF, S. & WATANABE, Y. 2004. Kinetochore orientation in mitosis and meiosis. *Cell,* 119**,** 317-27.

HENDERSON, S. A. & EDWARDS, R. G. 1968. Chiasma frequency and maternal age in mammals. *Nature,* 218**,** 22-8.

HERBERT, M., KALLEAS, D., COONEY, D., LAMB, M. & LISTER, L. 2015. Meiosis and maternal aging: insights from aneuploid oocytes and trisomy births. *Cold Spring Harb Perspect Biol,* 7**,** a017970.

HERBERT, M., LEVASSEUR, M., HOMER, H., YALLOP, K., MURDOCH, A. & MCDOUGALL, A. 2003. Homologue disjunction in mouse oocytes requires proteolysis of securin and cyclin B1. *Nat Cell Biol,* 5**,** 1023-5.

HEYTING, C. 1996. Synaptonemal complexes: structure and function. *Curr Opin Cell Biol,* 8**,** 389-96.

HFEA 2018. Fertility Treatment 2014 - 2016 - Trends and Figures.

HIGGINS, J. M. & PRENDERGAST, L. 2016. Mitotic Mysteries: The Case of HP1. *Dev Cell,* 36**,** 477-8.

HIRANO, M. & HIRANO, T. 2002. Hinge-mediated dimerization of SMC protein is essential for its dynamic interaction with DNA. *EMBO J,* 21**,** 5733-44.

HODGES, C. A., REVENKOVA, E., JESSBERGER, R., HASSOLD, T. J. & HUNT, P. A. 2005. SMC1beta-deficient female mice provide evidence that cohesins are a missing link in age-related nondisjunction. *Nat Genet,* 37**,** 1351-5.

HOMER, H. A., MCDOUGALL, A., LEVASSEUR, M., YALLOP, K., MURDOCH, A. P. & HERBERT, M. 2005. Mad2 prevents aneuploidy and premature proteolysis of cyclin B and securin during meiosis I in mouse oocytes. *Genes Dev,* 19**,** 202-7.

HSUEH, A. J., BILLIG, H. & TSAFRIRI, A. 1994. Ovarian follicle atresia: a hormonally controlled apoptotic process. *Endocr Rev,* 15**,** 707-24.

HSUEH, A. J., KAWAMURA, K., CHENG, Y. & FAUSER, B. C. 2015. Intraovarian control of early folliculogenesis. *Endocr Rev,* 36**,** 1-24.

ISHIGURO, T., TANAKA, K., SAKUNO, T. & WATANABE, Y. 2010. Shugoshin-PP2A counteracts casein-kinase-1-dependent cleavage of Rec8 by separase. *Nat Cell Biol,* 12**,** 500-6.

JALLEPALLI, P. V., WAIZENEGGER, I. C., BUNZ, F., LANGER, S., SPEICHER, M. R., PETERS, J. M., KINZLER, K. W., VOGELSTEIN, B. & LENGAUER, C. 2001. Securin is required for chromosomal stability in human cells. *Cell,* 105**,** 445-57.

JOHN, G. B., GALLARDO, T. D., SHIRLEY, L. J. & CASTRILLON, D. H. 2008. Foxo3 is a PI3K-dependent molecular switch controlling the initiation of oocyte growth. *Dev Biol,* 321**,** 197-204.

JOHNSON, J., CANNING, J., KANEKO, T., PRU, J. K. & TILLY, J. L. 2004. Germline stem cells and follicular renewal in the postnatal mammalian ovary. *Nature,* 428**,** 145-50.

KATIS, V. L., LIPP, J. J., IMRE, R., BOGDANOVA, A., OKAZ, E., HABERMANN, B., MECHTLER, K., NASMYTH, K. & ZACHARIAE, W. 2010. Rec8 phosphorylation by casein kinase 1 and

Cdc7-Dbf4 kinase regulates cohesin cleavage by separase during meiosis. *Dev Cell,* 18**,** 397-409.

KAWASHIMA, S. A., YAMAGISHI, Y., HONDA, T., ISHIGURO, K. & WATANABE, Y. 2010. Phosphorylation of H2A by Bub1 prevents chromosomal instability through localizing shugoshin. *Science,* 327**,** 172-7.

KERR, J. B., BROGAN, L., MYERS, M., HUTT, K. J., MLADENOVSKA, T., RICARDO, S., HAMZA, K., SCOTT, C. L., STRASSER, A. & FINDLAY, J. K. 2012. The primordial follicle reserve is not renewed after chemical or gamma-irradiation mediated depletion. *Reproduction,* 143**,** 469-76.

KIM, J., ISHIGURO, K., NAMBU, A., AKIYOSHI, B., YOKOBAYASHI, S., KAGAMI, A., ISHIGURO, T., PENDAS, A. M., TAKEDA, N., SAKAKIBARA, Y., KITAJIMA, T. S., TANNO, Y., SAKUNO, T. & WATANABE, Y. 2015. Meikin is a conserved regulator of meiosis-I-specific kinetochore function. *Nature,* 517**,** 466-71.

KITAJIMA, T. S., HAUF, S., OHSUGI, M., YAMAMOTO, T. & WATANABE, Y. 2005. Human Bub1 defines the persistent cohesion site along the mitotic chromosome by affecting Shugoshin localization. *Curr Biol,* 15**,** 353-9.

KITAJIMA, T. S., OHSUGI, M. & ELLENBERG, J. 2011. Complete kinetochore tracking reveals error-prone homologous chromosome biorientation in mammalian oocytes. *Cell,* 146**,** 568-81.

KITAJIMA, T. S., SAKUNO, T., ISHIGURO, K., IEMURA, S., NATSUME, T., KAWASHIMA, S. A. & WATANABE, Y. 2006. Shugoshin collaborates with protein phosphatase 2A to protect cohesin. *Nature,* 441**,** 46-52.

KLECKNER, N. 2006. Chiasma formation: chromatin/axis interplay and the role(s) of the synaptonemal complex. *Chromosoma,* 115**,** 175-94.

KOUZNETSOVA, A., LISTER, L., NORDENSKJOLD, M., HERBERT, M. & HOOG, C. 2007. Bi-orientation of achiasmatic chromosomes in meiosis I oocytes contributes to aneuploidy in mice. *Nat Genet,* 39**,** 966-8.

KUDO, N. R., ANGER, M., PETERS, A. H., STEMMANN, O., THEUSSL, H. C., HELMHART, W., KUDO, H., HEYTING, C. & NASMYTH, K. 2009. Role of cleavage by separase of the Rec8 kleisin subunit of cohesin during mammalian meiosis I. *J Cell Sci,* 122**,** 2686-98.

KUDO, N. R., WASSMANN, K., ANGER, M., SCHUH, M., WIRTH, K. G., XU, H., HELMHART, W., KUDO, H., MCKAY, M., MARO, B., ELLENBERG, J., DE BOER, P. & NASMYTH, K. 2006. Resolution of chiasmata in oocytes requires separase-mediated proteolysis. *Cell,* 126**,** 135-46.

KUENG, S., HEGEMANN, B., PETERS, B. H., LIPP, J. J., SCHLEIFFER, A., MECHTLER, K. & PETERS, J. M. 2006. Wapl controls the dynamic association of cohesin with chromatin. *Cell,* 127**,** 955-67.

KULIEV, A., ZLATOPOLSKY, Z., KIRILLOVA, I., SPIVAKOVA, J. & CIESLAK JANZEN, J. 2011. Meiosis errors in over 20,000 oocytes studied in the practice of preimplantation aneuploidy testing. *Reprod Biomed Online,* 22**,** 2-8.

LAGIRAND-CANTALOUBE, J., CIABRINI, C., CHARRASSE, S., FERRIERES, A., CASTRO, A., ANAHORY, T. & LORCA, T. 2017. Loss of Centromere Cohesion in Aneuploid Human Oocytes Correlates with Decreased Kinetochore Localization of the Sac Proteins Bub1 and Bubr1. *Sci Rep,* 7**,** 44001.

LAM, I. & KEENEY, S. 2014. Mechanism and regulation of meiotic recombination initiation. *Cold Spring Harb Perspect Biol,* 7**,** a016634.

LAMB, N. E., YU, K., SHAFFER, J., FEINGOLD, E. & SHERMAN, S. L. 2005. Association between maternal age and meiotic recombination for trisomy 21. *Am J Hum Genet,* 76**,** 91-9.

LAMBALK, C. B., VAN DISSELDORP, J., DE KONING, C. H. & BROEKMANS, F. J. 2009. Testing ovarian reserve to predict age at menopause. *Maturitas,* 63**,** 280-91.

LAN, Z. J., XU, X. & COONEY, A. J. 2004. Differential oocyte-specific expression of Cre recombinase activity in GDF-9-iCre, Zp3cre, and Msx2Cre transgenic mice. *Biol Reprod,* 71**,** 1469-74.

LARA-GONZALEZ, P., WESTHORPE, F. G. & TAYLOR, S. S. 2012. The spindle assembly checkpoint. *Curr Biol,* 22**,** R966-80.

LEE, J. & HIRANO, T. 2011. RAD21L, a novel cohesin subunit implicated in linking homologous chromosomes in mammalian meiosis. *J Cell Biol,* 192**,** 263-76.

LEE, J., KITAJIMA, T. S., TANNO, Y., YOSHIDA, K., MORITA, T., MIYANO, T., MIYAKE, M. & WATANABE, Y. 2008. Unified mode of centromeric protection by shugoshin in mammalian oocytes and somatic cells. *Nat Cell Biol,* 10**,** 42-52.

LEE, J., OGUSHI, S., SAITOU, M. & HIRANO, T. 2011. Condensins I and II are essential for construction of bivalent chromosomes in mouse oocytes. *Mol Biol Cell,* 22**,** 3465-77.

LEE, J., OKADA, K., OGUSHI, S., MIYANO, T., MIYAKE, M. & YAMASHITA, M. 2006. Loss of Rec8 from chromosome arm and centromere region is required for homologous chromosome separation and sister chromatid separation, respectively, in mammalian meiosis. *Cell Cycle,* 5**,** 1448-55.

LEMAIRE-ADKINS, R. & HUNT, P. A. 2000. Nonrandom segregation of the mouse univalent X chromosome: evidence of spindle-mediated meiotic drive. *Genetics,* 156**,** 775-83.

LI, L., DONG, J., YAN, L., YONG, J., LIU, X., HU, Y., FAN, X., WU, X., GUO, H., WANG, X., ZHU, X., LI, R., YAN, J., WEI, Y., ZHAO, Y., WANG, W., REN, Y., YUAN, P., YAN, Z., HU, B., GUO, F., WEN, L., TANG, F. & QIAO, J. 2017. Single-Cell RNA-Seq Analysis Maps Development of Human Germline Cells and Gonadal Niche Interactions. *Cell Stem Cell,* 20**,** 891-892.

LI, X. M., YU, C., WANG, Z. W., ZHANG, Y. L., LIU, X. M., ZHOU, D., SUN, Q. Y. & FAN, H. Y. 2013. DNA topoisomerase II is dispensable for oocyte meiotic resumption but is essential for meiotic chromosome condensation and separation in mice. *Biol Reprod,* 89**,** 118.

LISTER, L. M., KOUZNETSOVA, A., HYSLOP, L. A., KALLEAS, D., PACE, S. L., BAREL, J. C., NATHAN, A., FLOROS, V., ADELFALK, C., WATANABE, Y., JESSBERGER, R., KIRKWOOD, T. B., HOOG, C. & HERBERT, M. 2010. Age-related meiotic segregation errors in mammalian oocytes are preceded by depletion of cohesin and Sgo2. *Curr Biol,* 20**,** 1511-21.

LIU, L. & KEEFE, D. L. 2004. Nuclear origin of aging-associated meiotic defects in senescence-accelerated mice. *Biol Reprod,* 71**,** 1724-9.

LLANO, E., GOMEZ, R., GUTIERREZ-CABALLERO, C., HERRAN, Y., SANCHEZ-MARTIN, M., VAZQUEZ-QUINONES, L., HERNANDEZ, T., DE ALAVA, E., CUADRADO, A., BARBERO, J. L., SUJA, J. A. & PENDAS, A. M. 2008. Shugoshin-2 is essential for the completion of meiosis but not for mitotic cell division in mice. *Genes Dev,* 22**,** 2400-13.

LOPEZ-OTIN, C., BLASCO, M. A., PARTRIDGE, L., SERRANO, M. & KROEMER, G. 2013. The hallmarks of aging. *Cell,* 153**,** 1194-217.

MACLENNAN, M., CRICHTON, J. H., PLAYFOOT, C. J. & ADAMS, I. R. 2015. Oocyte development, meiosis and aneuploidy. *Semin Cell Dev Biol,* 45**,** 68-76.

MADGWICK, S., HANSEN, D. V., LEVASSEUR, M., JACKSON, P. K. & JONES, K. T. 2006. Mouse Emi2 is required to enter meiosis II by reestablishing cyclin B1 during interkinesis. *J Cell Biol,* 174**,** 791-801.

MAHESHWARI, A. & FOWLER, P. A. 2008. Primordial follicular assembly in humans--revisited. *Zygote,* 16**,** 285-96.

MAKKER, A., GOEL, M. M. & MAHDI, A. A. 2014. PI3K/PTEN/Akt and TSC/mTOR signaling pathways, ovarian dysfunction, and infertility: an update. *J Mol Endocrinol,* 53**,** R103-18.

MCGEE, E. A. & HSUEH, A. J. 2000. Initial and cyclic recruitment of ovarian follicles. *Endocr Rev,* 21**,** 200-14.

MCGRATH, S. A., ESQUELA, A. F. & LEE, S. J. 1995. Oocyte-specific expression of growth/differentiation factor-9. *Mol Endocrinol,* 9**,** 131-6.

MCGUINNESS, B. E., ANGER, M., KOUZNETSOVA, A., GIL-BERNABE, A. M., HELMHART, W., KUDO, N. R., WUENSCHE, A., TAYLOR, S., HOOG, C., NOVAK, B. & NASMYTH, K. 2009. Regulation of APC/C activity in oocytes by a Bub1-dependent spindle assembly checkpoint. *Curr Biol,* 19**,** 369-80.

MCGUINNESS, B. E., HIROTA, T., KUDO, N. R., PETERS, J. M. & NASMYTH, K. 2005. Shugoshin prevents dissociation of cohesin from centromeres during mitosis in vertebrate cells. *PLoS Biol,* 3**,** e86.

MINAMINO, M., ISHIBASHI, M., NAKATO, R., AKIYAMA, K., TANAKA, H., KATO, Y., NEGISHI, L., HIROTA, T., SUTANI, T., BANDO, M. & SHIRAHIGE, K. 2015. Esco1 Acetylates Cohesin via a Mechanism Different from That of Esco2. *Curr Biol,* 25**,** 1694-706.

MOROI, Y., PEEBLES, C., FRITZLER, M. J., STEIGERWALD, J. & TAN, E. M. 1980. Autoantibody to centromere (kinetochore) in scleroderma sera. *Proc Natl Acad Sci U S A,* 77**,** 1627-31.

MORRIS, J. K. & ALBERMAN, E. 2009. Trends in Down's syndrome live births and antenatal diagnoses in England and Wales from 1989 to 2008: analysis of data from the National Down Syndrome Cytogenetic Register. *BMJ,* 339**,** b3794.

MUSACCHIO, A. & SALMON, E. D. 2007. The spindle-assembly checkpoint in space and time. *Nat Rev Mol Cell Biol,* 8**,** 379-93.

NABTI, I., REIS, A., LEVASSEUR, M., STEMMANN, O. & JONES, K. T. 2008. Securin and not CDK1/cyclin B1 regulates sister chromatid disjunction during meiosis II in mouse eggs. *Dev Biol,* 321**,** 379-86.

NAGAO, K. & YANAGIDA, M. 2006. Securin can have a separase cleavage site by substitution mutations in the domain required for stabilization and inhibition of separase. *Genes Cells,* 11**,** 247-60.

NAGAOKA, S. I., HASSOLD, T. J. & HUNT, P. A. 2012. Human aneuploidy: mechanisms and new insights into an age-old problem. *Nat Rev Genet,* 13**,** 493-504.

NAKAJIMA, M., KUMADA, K., HATAKEYAMA, K., NODA, T., PETERS, J. M. & HIROTA, T. 2007. The complete removal of cohesin from chromosome arms depends on separase. *J Cell Sci,* 120**,** 4188-96.

NASMYTH, K. 2011. Cohesin: a catenase with separate entry and exit gates? *Nat Cell Biol,* 13**,** 1170-7.

NASMYTH, K. & HAERING, C. H. 2009. Cohesin: its roles and mechanisms. *Annu Rev Genet,* 43**,** 525-58.

NIKOLIC, A., VOLAREVIC, V., ARMSTRONG, L., LAKO, M. & STOJKOVIC, M. 2016. Primordial Germ Cells: Current Knowledge and Perspectives. *Stem Cells Int,* 2016**,** 1741072.

NISHIYAMA, T., LADURNER, R., SCHMITZ, J., KREIDL, E., SCHLEIFFER, A., BHASKARA, V., BANDO, M., SHIRAHIGE, K., HYMAN, A. A., MECHTLER, K. & PETERS, J. M. 2010. Sororin mediates sister chromatid cohesion by antagonizing Wapl. *Cell,* 143**,** 737-49.

NISHIYAMA, T., SYKORA, M. M., HUIS IN 'T VELD, P. J., MECHTLER, K. & PETERS, J. M. 2013. Aurora B and Cdk1 mediate Wapl activation and release of acetylated cohesin from chromosomes by phosphorylating Sororin. *Proc Natl Acad Sci U S A,* 110**,** 13404-9.

NITISS, J. L. 2009. DNA topoisomerase II and its growing repertoire of biological functions. *Nat Rev Cancer,* 9**,** 327-37.

NORRIS, R. P., RATZAN, W. J., FREUDZON, M., MEHLMANN, L. M., KRALL, J., MOVSESIAN, M. A., WANG, H., KE, H., NIKOLAEV, V. O. & JAFFE, L. A. 2009. Cyclic GMP from the surrounding somatic cells regulates cyclic AMP and meiosis in the mouse oocyte. *Development,* 136**,** 1869-78.

OELSCHLAEGEL, T., SCHWICKART, M., MATOS, J., BOGDANOVA, A., CAMASSES, A., HAVLIS, J., SHEVCHENKO, A. & ZACHARIAE, W. 2005. The yeast APC/C subunit Mnd2 prevents premature sister chromatid separation triggered by the meiosis-specific APC/C-Ama1. *Cell,* 120**,** 773-88.

OLIVER, T. R., FEINGOLD, E., YU, K., CHEUNG, V., TINKER, S., YADAV-SHAH, M., MASSE, N. & SHERMAN, S. L. 2008. New insights into human nondisjunction of chromosome 21 in oocytes. *PLoS Genet,* 4**,** e1000033.

ORISAKA, M., TAJIMA, K., TSANG, B. K. & KOTSUJI, F. 2009. Oocyte-granulosa-theca cell interactions during preantral follicular development. *J Ovarian Res,* 2**,** 9.

PAGE, S. L. & HAWLEY, R. S. 2004. The genetics and molecular biology of the synaptonemal complex. *Annu Rev Cell Dev Biol,* 20**,** 525-58.

PARELHO, V., HADJUR, S., SPIVAKOV, M., LELEU, M., SAUER, S., GREGSON, H. C., JARMUZ, A., CANZONETTA, C., WEBSTER, Z., NESTEROVA, T., COBB, B. S., YOKOMORI, K., DILLON, N., ARAGON, L., FISHER, A. G. & MERKENSCHLAGER, M. 2008. Cohesins functionally associate with CTCF on mammalian chromosome arms. *Cell,* 132**,** 422-33.

PATEL, J., TAN, S. L., HARTSHORNE, G. M. & MCAINSH, A. D. 2015. Unique geometry of sister kinetochores in human oocytes during meiosis I may explain maternal age-associated increases in chromosomal abnormalities. *Biol Open,* 5**,** 178-84.

196

PELLESTOR, F., ANDREO, B., ARNAL, F., HUMEAU, C. & DEMAILLE, J. 2003. Maternal aging and chromosomal abnormalities: new data drawn from in vitro unfertilized human oocytes. *Hum Genet,* 112**,** 195-203.

PENKNER, A. M., PRINZ, S., FERSCHA, S. & KLEIN, F. 2005. Mnd2, an essential antagonist of the anaphase-promoting complex during meiotic prophase. *Cell,* 120**,** 789-801.

PENROSE, L. S. 1933. The relative effects of paternal and maternal age in mongolism. *Journal of Genetics,* 27**,** 219-24.

PEPLING, M. E. & SPRADLING, A. C. 1998. Female mouse germ cells form synchronously dividing cysts. *Development,* 125**,** 3323-8.

PEPLING, M. E. & SPRADLING, A. C. 2001. Mouse ovarian germ cell cysts undergo programmed breakdown to form primordial follicles. *Dev Biol,* 234**,** 339-51.

PEPLOWSKA, K., WALLEK, A. U. & STORCHOVA, Z. 2014. Sgo1 regulates both condensin and Ipl1/Aurora B to promote chromosome biorientation. *PLoS Genet,* 10**,** e1004411.

PETER, M., CASTRO, A., LORCA, T., LE PEUCH, C., MAGNAGHI-JAULIN, L., DOREE, M. & LABBE, J. C. 2001. The APC is dispensable for first meiotic anaphase in Xenopus oocytes. *Nat Cell Biol,* 3**,** 83-7.

PETERS, J. M. & NISHIYAMA, T. 2012. Sister chromatid cohesion. *Cold Spring Harb Perspect Biol,* 4.

PETRONCZKI, M., SIOMOS, M. F. & NASMYTH, K. 2003. Un menage a quatre: the molecular biology of chromosome segregation in meiosis. *Cell,* 112**,** 423-40.

RATTANI, A., WOLNA, M., PLOQUIN, M., HELMHART, W., MORRONE, S., MAYER, B., GODWIN, J., XU, W., STEMMANN, O., PENDAS, A. & NASMYTH, K. 2013. Sgol2 provides a regulatory platform that coordinates essential cell cycle processes during meiosis I in oocytes. *Elife,* 2**,** e01133.

REDDY, P., LIU, L., ADHIKARI, D., JAGARLAMUDI, K., RAJAREDDY, S., SHEN, Y., DU, C., TANG, W., HAMALAINEN, T., PENG, S. L., LAN, Z. J., COONEY, A. J., HUHTANIEMI, I. & LIU, K. 2008. Oocyte-specific deletion of Pten causes premature activation of the primordial follicle pool. *Science,* 319**,** 611-3.

REED, B. G. & CARR, B. R. 2000. The Normal Menstrual Cycle and the Control of Ovulation. *In:* DE GROOT, L. J., CHROUSOS, G., DUNGAN, K., FEINGOLD, K. R., GROSSMAN, A., HERSHMAN, J. M., KOCH, C., KORBONITS, M., MCLACHLAN, R., NEW, M., PURNELL, J., REBAR, R., SINGER, F. & VINIK, A. (eds.) *Endotext.* South Dartmouth (MA).

REICHMAN, D. E., POLITCH, J., GINSBURG, E. S. & RACOWSKY, C. 2010. Extended in vitro maturation of immature oocytes from stimulated cycles: an analysis of fertilization

potential, embryo development, and reproductive outcomes. *J Assist Reprod Genet,* 27**,** 347-56.

REVENKOVA, E., EIJPE, M., HEYTING, C., HODGES, C. A., HUNT, P. A., LIEBE, B., SCHERTHAN, H. & JESSBERGER, R. 2004. Cohesin SMC1 beta is required for meiotic chromosome dynamics, sister chromatid cohesion and DNA recombination. *Nat Cell Biol,* 6**,** 555-62.

RICHARDSON, B. E. & LEHMANN, R. 2010. Mechanisms guiding primordial germ cell migration: strategies from different organisms. *Nat Rev Mol Cell Biol,* 11**,** 37-49.

RIEDEL, C. G., KATIS, V. L., KATOU, Y., MORI, S., ITOH, T., HELMHART, W., GALOVA, M., PETRONCZKI, M., GREGAN, J., CETIN, B., MUDRAK, I., OGRIS, E., MECHTLER, K., PELLETIER, L., BUCHHOLZ, F., SHIRAHIGE, K. & NASMYTH, K. 2006. Protein phosphatase 2A protects centromeric sister chromatid cohesion during meiosis I. *Nature,* 441**,** 53-61.

RISCH, N., STEIN, Z., KLINE, J. & WARBURTON, D. 1986. The relationship between maternal age and chromosome size in autosomal trisomy. *Am J Hum Genet,* 39**,** 68-78.

ROMANIENKO, P. J. & CAMERINI-OTERO, R. D. 2000. The mouse Spo11 gene is required for meiotic chromosome synapsis. *Mol Cell,* 6**,** 975-87.

SAKAKIBARA, Y., HASHIMOTO, S., NAKAOKA, Y., KOUZNETSOVA, A., HOOG, C. & KITAJIMA, T. S. 2015. Bivalent separation into univalents precedes age-related meiosis I errors in oocytes. *Nat Commun,* 6**,** 7550.

SALIC, A., WATERS, J. C. & MITCHISON, T. J. 2004. Vertebrate shugoshin links sister centromere cohesion and kinetochore microtubule stability in mitosis. *Cell,* 118**,** 567-78.

SAUER, M. V. 1998. The impact of age on reproductive potential: lessons learned from oocyte donation. *Maturitas,* 30**,** 221-5.

SCHMIDT, A., DUNCAN, P. I., RAUH, N. R., SAUER, G., FRY, A. M., NIGG, E. A. & MAYER, T. U. 2005. Xenopus polo-like kinase Plx1 regulates XErp1, a novel inhibitor of APC/C activity. *Genes Dev,* 19**,** 502-13.

SCHMIDT, A., RAUH, N. R., NIGG, E. A. & MAYER, T. U. 2006. Cytostatic factor: an activity that puts the cell cycle on hold. *J Cell Sci,* 119**,** 1213-8.

SCHMIDT, L., SOBOTKA, T., BENTZEN, J. G., NYBOE ANDERSEN, A., REPRODUCTION, E. & SOCIETY TASK, F. 2012. Demographic and medical consequences of the postponement of parenthood. *Hum Reprod Update,* 18**,** 29-43.

SCHON, E. A., DIMAURO, S. & HIRANO, M. 2012. Human mitochondrial DNA: roles of inherited and somatic mutations. *Nat Rev Genet,* 13**,** 878-90.

198

SEBESTOVA, J., DANYLEVSKA, A., NOVAKOVA, L., KUBELKA, M. & ANGER, M. 2012. Lack of response to unaligned chromosomes in mammalian female gametes. *Cell Cycle,* 11**,** 3011-8.

SHINTOMI, K. & HIRANO, T. 2011. The relative ratio of condensin I to II determines chromosome shapes. *Genes Dev,* 25**,** 1464-9.

SRINIVASAN, M., SCHEINOST, J. C., PETELA, N. J., GLIGORIS, T. G., WISSLER, M., OGUSHI, S., COLLIER, J. E., VOULGARIS, M., KURZE, A., CHAN, K. L., HU, B., COSTANZO, V. & NASMYTH, K. A. 2018. The Cohesin Ring Uses Its Hinge to Organize DNA Using Non-topological as well as Topological Mechanisms. *Cell,* 173**,** 1508-1519 e18.

STEMMANN, O., ZOU, H., GERBER, S. A., GYGI, S. P. & KIRSCHNER, M. W. 2001. Dual inhibition of sister chromatid separation at metaphase. *Cell,* 107**,** 715-26.

TACHIBANA-KONWALSKI, K., GODWIN, J., VAN DER WEYDEN, L., CHAMPION, L., KUDO, N. R., ADAMS, D. J. & NASMYTH, K. 2010. Rec8-containing cohesin maintains bivalents without turnover during the growing phase of mouse oocytes. *Genes Dev,* 24**,** 2505-16.

TAIEB, F. E., GROSS, S. D., LEWELLYN, A. L. & MALLER, J. L. 2001. Activation of the anaphase-promoting complex and degradation of cyclin B is not required for progression from Meiosis I to II in Xenopus oocytes. *Curr Biol,* 11**,** 508-13.

TANAKA, S. S., TOYOOKA, Y., AKASU, R., KATOH-FUKUI, Y., NAKAHARA, Y., SUZUKI, R., YOKOYAMA, M. & NOCE, T. 2000. The mouse homolog of Drosophila Vasa is required for the development of male germ cells. *Genes Dev,* 14**,** 841-53.

TANG, Z., SUN, Y., HARLEY, S. E., ZOU, H. & YU, H. 2004. Human Bub1 protects centromeric sister-chromatid cohesion through Shugoshin during mitosis. *Proc Natl Acad Sci U S A,* 101**,** 18012-7.

TE VELDE, E. R., DORLAND, M. & BROEKMANS, F. J. 1998. Age at menopause as a marker of reproductive ageing. *Maturitas,* 30**,** 119-25.

TOTH, A., RABITSCH, K. P., GALOVA, M., SCHLEIFFER, A., BUONOMO, S. B. & NASMYTH, K. 2000. Functional genomics identifies monopolin: a kinetochore protein required for segregation of homologs during meiosis i. *Cell,* 103**,** 1155-68.

TOUATI, S. A., CLADIERE, D., LISTER, L. M., LEONTIOU, I., CHAMBON, J. P., RATTANI, A., BOTTGER, F., STEMMANN, O., NASMYTH, K., HERBERT, M. & WASSMANN, K. 2012. Cyclin A2 is required for sister chromatid segregation, but not separase control, in mouse oocyte meiosis. *Cell Rep,* 2**,** 1077-87.

TSUTSUMI, M., FUJIWARA, R., NISHIZAWA, H., ITO, M., KOGO, H., INAGAKI, H., OHYE, T., KATO, T., FUJII, T. & KURAHASHI, H. 2014. Age-related decrease of meiotic cohesins in human oocytes. *PLoS One,* 9**,** e96710.

UHLMANN, F., LOTTSPEICH, F. & NASMYTH, K. 1999. Sister-chromatid separation at anaphase onset is promoted by cleavage of the cohesin subunit Scc1. *Nature,* 400**,** 37-42.

UHLMANN, F., WERNIC, D., POUPART, M. A., KOONIN, E. V. & NASMYTH, K. 2000. Cleavage of cohesin by the CD clan protease separin triggers anaphase in yeast. *Cell,* 103**,** 375-86.

VISSER, J. A., DE JONG, F. H., LAVEN, J. S. & THEMMEN, A. P. 2006. Anti-Mullerian hormone: a new marker for ovarian function. *Reproduction,* 131**,** 1-9.

VON STETINA, J. R. & ORR-WEAVER, T. L. 2011. Developmental control of oocyte maturation and egg activation in metazoan models. *Cold Spring Harb Perspect Biol,* 3**,** a005553.

WAIZENEGGER, I. C., HAUF, S., MEINKE, A. & PETERS, J. M. 2000. Two distinct pathways remove mammalian cohesin from chromosome arms in prophase and from centromeres in anaphase. *Cell,* 103**,** 399-410.

WASSMANN, K., NIAULT, T. & MARO, B. 2003. Metaphase I arrest upon activation of the Mad2-dependent spindle checkpoint in mouse oocytes. *Curr Biol,* 13**,** 1596-608.

WATANABE, Y. 2012. Geometry and force behind kinetochore orientation: lessons from meiosis. *Nat Rev Mol Cell Biol,* 13**,** 370-82.

WEBSTER, A. & SCHUH, M. 2017. Mechanisms of Aneuploidy in Human Eggs. *Trends Cell Biol,* 27**,** 55-68.

WENDT, K. S., YOSHIDA, K., ITOH, T., BANDO, M., KOCH, B., SCHIRGHUBER, E., TSUTSUMI, S., NAGAE, G., ISHIHARA, K., MISHIRO, T., YAHATA, K., IMAMOTO, F., ABURATANI, H., NAKAO, M., IMAMOTO, N., MAESHIMA, K., SHIRAHIGE, K. & PETERS, J. M. 2008. Cohesin mediates transcriptional insulation by CCCTC-binding factor. *Nature,* 451**,** 796-801.

WIRTH, K. G., WUTZ, G., KUDO, N. R., DESDOUETS, C., ZETTERBERG, A., TAGHYBEEGLU, S., SEZNEC, J., DUCOS, G. M., RICCI, R., FIRNBERG, N., PETERS, J. M. & NASMYTH, K. 2006. Separase: a universal trigger for sister chromatid disjunction but not chromosome cycle progression. *J Cell Biol,* 172**,** 847-60.

WOJTASZ, L., DANIEL, K. & TOTH, A. 2009. Fluorescence activated cell sorting of live female germ cells and somatic cells of the mouse fetal gonad based on forward and side scattering. *Cytometry A,* 75**,** 547-53.

WOLF, P. G., CUBA RAMOS, A., KENZEL, J., NEUMANN, B. & STEMMANN, O. 2018. Studying meiotic cohesin in somatic cells reveals that Rec8-containing cohesin requires Stag3 to function and is regulated by Wapl and sororin. *J Cell Sci,* 131.

WOODS, L. M., HODGES, C. A., BAART, E., BAKER, S. M., LISKAY, M. & HUNT, P. A. 1999. Chromosomal influence on meiotic spindle assembly: abnormal meiosis I in female Mlh1 mutant mice. *J Cell Biol,* 145**,** 1395-406.

WU, N. & YU, H. 2012. The Smc complexes in DNA damage response. *Cell Biosci,* 2**,** 5.

YOKOBAYASHI, S. & WATANABE, Y. 2005. The kinetochore protein Moa1 enables cohesion-mediated monopolar attachment at meiosis I. *Cell,* 123**,** 803-17.

YUN, Y., HOLT, J. E., LANE, S. I., MCLAUGHLIN, E. A., MERRIMAN, J. A. & JONES, K. T. 2014. Reduced ability to recover from spindle disruption and loss of kinetochore spindle assembly checkpoint proteins in oocytes from aged mice. *Cell Cycle,* 13**,** 1938-47.

ZHANG, H., LIU, L., LI, X., BUSAYAVALASA, K., SHEN, Y., HOVATTA, O., GUSTAFSSON, J. A. & LIU, K. 2014. Life-long in vivo cell-lineage tracing shows that no oogenesis originates from putative germline stem cells in adult mice. *Proc Natl Acad Sci U S A,* 111**,** 17983-8.

ZHANG, H., PANULA, S., PETROPOULOS, S., EDSGARD, D., BUSAYAVALASA, K., LIU, L., LI, X., RISAL, S., SHEN, Y., SHAO, J., LIU, M., LI, S., ZHANG, D., ZHANG, X., GERNER, R. R., SHEIKHI, M., DAMDIMOPOULOU, P., SANDBERG, R., DOUAGI, I., GUSTAFSSON, J. A., LIU, L., LANNER, F., HOVATTA, O. & LIU, K. 2015. Adult human and mouse ovaries lack DDX4-expressing functional oogonial stem cells. *Nat Med,* 21**,** 1116-8.

ZHANG, J., SHI, X., LI, Y., KIM, B. J., JIA, J., HUANG, Z., YANG, T., FU, X., JUNG, S. Y., WANG, Y., ZHANG, P., KIM, S. T., PAN, X. & QIN, J. 2008. Acetylation of Smc3 by Eco1 is required for S phase sister chromatid cohesion in both human and yeast. *Mol Cell,* 31**,** 143-51.

ZIELINSKA, A. P., HOLUBCOVA, Z., BLAYNEY, M., ELDER, K. & SCHUH, M. 2015. Sister kinetochore splitting and precocious disintegration of bivalents could explain the maternal age effect. *Elife,* 4**,** e11389.

ZOU, H., MCGARRY, T. J., BERNAL, T. & KIRSCHNER, M. W. 1999. Identification of a vertebrate sister-chromatid separation inhibitor involved in transformation and tumorigenesis. *Science,* 285**,** 418-22.

ZUCKERMAN, S. 1951. The number of oocytes in the mature ovary. *Recent Prog Horm Res,* 6**,** 63-108.